Models for sound propagation in suspensions and emulsions

Thesis

Models for sound propagation in suspensions and emulsions

Thesis submitted by

Jonathan M Evans BEng

for the degree of

Doctor of Philosophy

June 1996

Engineering Mechanics Discipline

Faculty of Technology

The Open University

Milton Keynes MK7 6AA

UK

Abstract

Theoretical and experimental work on sound propagation in suspensions and emulsions is reviewed. Three theoretical approaches are identified: scattering theory, coupled phase theory and porous media theory. Coupled phase theory is extended and compared analytically and numerically to scattering and porous media theory.

Important regimes of scattering theory - the lossless and viscothermal scattering, single and multiple scattering and incoherent scattering regimes - are examined. Experimental data is used to corroborate lossless multiple scattering theory in the short wavelength, high volume fraction region.

Previous coupled phase theories have modelled sound propagation in two phase media (i) with heat transfer assuming incompressible particles and (ii) with a compressible particulate phase neglecting heat transfer. Type (i) models are examined analytically and compared to scattering theory. Types (i) and (ii) are compared and brought together in a more general coupled phase theory. The new theory provides an alternative model to scattering theory for sound propagation in emulsions. Predictions of the new theory are compared to experimental data and predictions of scattering theory.

Conditions for the equivalence of the frameless Biot porous media theory and coupled phase theory are identified. Predictions of the two approaches are compared to experimental data. New measurements of pore size distribution are used to predict measured acoustical properties of air saturated glass beads.

Other extensions to coupled phase theory are reviewed and developed. Predictions including the effect of high volume fraction on the drag and the induced mass force are compared to experimental data and predictions of porous media theory. Coupled phase theory including heat transfer is extended to include particle size distributions; predictions of this are compared to measurements. The effect of non-spherical particles is investigated. Using the theory of Culick, frequency shifts for modes in an enclosure into which a suspension has been introduced are calculated. These are compared to the predictions of an intuitive approach. The method of Margulies and Schwartz for modelling particle diffusion is discussed.

Areas where further work is required are identified.

'We must attach a higher prestige to that very creative act, the writing of serious review articles and books...'

The Quark and the Jaguar, Murray Gell-Mann
(Little, Brown and Company, UK 1994)

Acknowledgements

Thanks to: Professor Keith Attenborough for his supervision, advice and support, Simon Moss and Sabine Teuber for important contributions to this work, and everyone in the Acoustics Group and Engineering Mechanics Discipline.

Thanks to: my family, especially Jan, John, Dan and Bin. Daz, Ray and Ju.

Soundtrack: Beethoven's Fantasia in C minor for piano, chorus and orchestra, Blur, Oasis, The Smiths, Airstream, Rising High Records, Harthouse Records, The Mark Radcliffe Show, Dubstar.

Inspirational reading: the pastoral science fiction of Clifford D Simak, *Feel the fear and do it anyway* by Susan Jeffers, the Melody Maker, *The quark and the jaguar* by Murray Gell-Mann, *Complexity* by M Mitchell Waldrop, Anthony Storr, Richard Dawkins, Will Self, Andre Gide.

Funding: EPSRC.

Contents

List of figures

List of tables

Nomenclature

Symbols

a	particle radius
a_h	effective radius for conductance
a_v	effective radius for drag
a_{32}	Sauter mean radius, equation (6.28)
a_{ob}	semimajor axis of oblate spheroid
a_{pr}	semiminor axis of prolate spheroid
A_n	scattering coefficient, equation (3.30)
	(section 6. 4) equation (6.62)
A	absorption coefficient
A_n	equation (6.63)
$\mathbf{A}$	matrix e.g. equations (4.40) and (4.58)
b	equation (3.19)
	(section 5. 2) slit semi-width
	(section 6. 3) semiminor axis of oblate spheroid, semimajor axis of prolate spheroid

B	(section 6. 1. 1) constant, equation (6.2)
B_n	(section 6. 4) equation (6.62)
c	sound speed
c_1	speed of longitudinal wave in solid
c_2	speed of shear wave in solid
c_{sph}	speed of spherical wave in solid
C	induced mass coefficient
	(section 5. 1. 1) constant, equation (5.11)
C_p	specific heat at constant pressure
C_v, C	specific heat at constant volume
C_1	equation (6.6)
d	magnitude of displacement in z direction
	(section 5. 2. 4) thickness of hard backed layer
$\mathbf{d}$	displacement
D	drag correction factor
D_{ni}	equation (6.72)
e	dilation, equation (5.7)
$e(b)$	log normal distribution
E_n^2	mean square amplitude
E_{ni}	equation (6.72)
E	energy
f	frequency
	(section 6. 4) equation (6. 40)
f_{ni}	equation (6.75)
$f(0)$, $f(\pi)$	far field scattering amplitudes, equation (3.6)
F	viscosity correction function, equations (5.1) and (5.2)
F_h	equation (4.42)
F_n	forcing term
$\mathbf{F}$	momentum transfer equation (6.31)

g_{ni}	equation (6.76)
h	ratio b/a_{ob} or b/a_{pr}
	(section 6. 4) equation (6.39)
h_n	spherical Hankel function
h_{ni}	equation (6.75)
H	constant, equation (5.11)
i	$\sqrt{-1}$ in $\exp(-i\omega t)$ convention
j	$\sqrt{-1}$ in $\exp(j\omega t)$ convention
j_n	spherical Bessel function
J_n	cylindrical Bessel function
J	equation (6.95)
$k,\ k_1$	compressional wave complex wavenumber
	(section 6. 1. 1) constant equation (6.2)
k_2	thermal wave waveumber
	(section 6. 1. 1) constant, equation (6.2)
k_3	viscous wave wavenumber
k_ϕ	permeability
k_0	tortuosity factor in permeability
K	(k/ω)
K	bulk modulus κ^{-1}
l	loading
	(section 6. 3) side of cube
l_{ni}	equation (6.76)
L	acoustic depth
L_{char}	characteristic length
m	mass concentration
m_s	mass of particle
M	constant, equation (5.11)

n	integer
$\mathbf{n}$	unit normal
N	number of particles per unit volume
N_b	shear modulus
N_{Pr}	Prandtl number
p	pressure
P	coefficient in Biot theory, equations (5.1) and (5.2)
P_n, P_n^1	Legendre polynomial and associated Legendre polynomial of the first kind
P_D	frictional coefficient
q	eccentricity $\left(1-h^2\right)^{\frac{1}{2}}$
Q	coefficient in Biot theory theory, equations (5.1) and (5.2)
	heat transfer, equation (6.32)
r	radial co-ordinate
	(chapter 5) radius of circular cylinder
r_h	hydraulic radius
R	gas constant
	(chapter 5) coefficient in Biot theory, equation (5.2)
R	complex reflection coefficient
Re	Reynolds number $= \frac{\rho L_{char} u_{flow}}{\mu}$
s	specific entropy
	(section 5. 2. 5) standard deviation
s_0	steady flow shape factor
s_B	Biot shape factor, equation (5.54)
S	momentum transfer term, equation (4.12)
	(section 5. 2. 7) suction
S_h	heat transfer term, equation (4.33)
t	time

T	temperature
	(section 5. 2. 7) surface tension
$\mathbf{u}$	velocity
u	velocity in z direction
u_{flow}	flow velocity
U	specific internal energy
	(section 5. 1. 3) mean volume velocity per unit area
v	relative velocity
V	volume
x	$k_{1,2,3}a$
$X_{1,2}$	equations (6.57) and (6.58)
$\Omega_{d,t}$	equations (6.57) and (6.58)
y	dummy variable
$\mathbf{y}$	matrix e.g. equations (4.40) and (4.58)
z	rectangular co-ordinate
Z_c	characteristic impedance
Z_{surf}	normal incidence surface impedance
α	porosity $1-\phi^0$
α_∞	tortuosity
α_n	(section 6. 4. 7) temporal decay constant
β	coefficient of thermal (volume) expansion
β_C	coefficient of expansion with respect to concentration of particles
δ	thickness of viscous boundary layer
δ_h	thickness of thermal boundary layer
δ_b	equation (3.23)
δF	equation (6.33)
δQ	equation (6.34)
$\delta \mathbf{u}$	equation (6.51)

δT	equation (6.52)
δ_{ij}	Kronecker delta
δf	frequency shift
Δ	small distance
ε, ε_h	equations (3.23)
ε_{s1}, ε_{s2}	equations (3.28)
ϕ	volume fraction of particles
	scalar potential
ϕ_n	(section 6. 4) equation (6.64)
Φ	scalar potential
	(section 5. 2) logarithmic units, equation (5.59)
γ	ratio of specific heats
$\eta_i(t)$	time dependence of mode
κ	compressibility
$\kappa(\omega)$	frequency dependent effective compressibility
λ	wavelength
	(chapter 5) frequency number, equation (5.19)
λ_e	Lame constant
μ	dynamic viscosity
μ_B	bulk viscosity
μ_e	Lame constant
ν	kinematic viscosity
θ	angular co-ordinate
	(section 6. 1. 1) constant, equation (6.2)
ρ	density
$\rho(\omega)$	frequency dependent effective density
ρ_a	Biot inertial coupling term, equation (5.6)
ρ_b	equation (4.45)
σ	thermometric conductivity

	(chapter 5) flow resistivity
σ_s	scattering cross section
σ_0	total scattering cross section for a single particle
τ	thermal conductivity
	(section 6. 4) time interval
$\tilde{\tau}$	complex relaxation time
τ_d	viscous relaxation time
τ_t	thermal relaxation time
ω	angular frequency $2\pi f$
ξ	plane wave attenuation coefficient (total)
	(chapter 5) volume of fluid, equation (5.8)
ξ_a	plane wave attenuation coefficient (absorption)
ξ_s	plane wave attenuation coefficient (scattering)
Ψ_k	vector potential
$\psi_i(\mathbf{r})$	mode shape
Ψ_k	vector potential

Superscripts and other notation

y^0	equilibrium component of variable
y'	perturbation component of variable
$\bar{y}$	volume averaged variable
	(section 5. 2. 5) mean value of variable
$\dot{y}$	differentiation with respect to time
$\hat{y}$	constants defined by Culick (section 6. 4)
$\|y\|$	modulus of variable
$\langle y \rangle$	spatial average
	(section 6. 4) time average

$\Re(y)$, $\Im(y)$ real, imaginary part of variable

Subscripts

f	continuous phase
s	particulate phase
va	volume averaged constant
eq	$\omega \to 0$ limit
∞	$\omega \to \infty$ limit
i	incident plane wave

Abbreviations

EC	Epstein and Cahart [47]
AH	Allegra and Hawley [49]
WT	Waterman and Truell [73]
LB	Lloyd and Berry [74]
Ma	Ma, Varadan and Varadan [75]
TD	Temkin and Dobbins [98]
MH	Mecredy and Hamilton [101]
GIN	Gumerov, Ivandaev and Nigmatulin [102]
HT	Harker and Temple [65]
MS	Margulies and Schwartz [2] [4]

Chapter 1
Introduction

1. 1 Introduction

This thesis reviews the theoretical and experimental work on sound propagation in suspensions and emulsions. The theoretical work is extended. Areas where comparisons between theoretical predictions and experiment results are unsatisfactory and where more theoretical and experimental work is necessary are identified.

The term suspension will be used to describe a number of solid particles distributed in a continuous fluid, either liquid or gas. The term emulsion will be used to describe a number of liquid particles distributed in a continuous liquid. The continuous fluid and the particles represent separate phases and the suspension or emulsion is described as a two phase medium. For suspensions the terms continuous phase and fluid phase and the terms particulate phase and solid phase are interchangeable. For emulsions the terms continuous phase and particulate phase will be used. Solid continuous phases and gas particles in a fluid (bubbles) will not be considered.

Most of the work in this thesis depends on the condition that the size of the particles is much smaller than the wavelength, implying that compressional wave scattering is negligible. One example where the particle size is of the same order of magnitude as the wavelength, and where compressional wave scattering is important, is studied in chapter 3.

There are three theoretical approaches to modelling sound propagation in suspensions and emulsions, these may be termed scattering theory, coupled phase theory and porous media theory. The three approaches are reviewed in chapter 2. The emphasis in this thesis is on coupled phase theory. Since there has been only limited comparison between these three approaches in the literature, the relationships between coupled phase theory and the other two approaches will be investigated, both analytically and numerically.

Chapter 3 summarises single and multiple scattering theory for suspensions and emulsions. Chapter 4 reviews previous coupled phase theories. These are brought together in a new, more general coupled phase theory containing the previous results as special cases. The new coupled phase theory provides an alternative to scattering theory for modelling sound propagation in emulsions. The analytical relationship between coupled phase theory and scattering theory is examined. Chapter 5 reviews porous media theory and compares it to coupled phase theory. Conditions for the formal equivalence of porous media theory and coupled phase theory are identified. New measurements of the pore size distribution of an air saturated glass bead material are used to predict its acoustical properties. Chapter 6 considers applications for which coupled phase theory, with the necessary extensions, is particularly suited. Section 6. 1 reviews work on hydrodynamic interactions between the particles, section 6. 3 investigates non-spherical particles and section 6. 5 discusses the theory of Margulies and Schwartz [1] [2] [3] [4] for modelling the effect of particle diffusion on sound propagation. Scattering theory is not suitable for modelling these phenomena. Section 6. 2 extends the work on particle size distributions in coupled phase theory and section 6. 4 discusses the theory of Culick [5] [6] [7] [8] [9] for modes in an enclosure containing a suspension.

One of the aims of theoretical work is to enable accurate predictions of the important features of sound wave behaviour measured in experiments, within the range of error introduced by uncertainty in the model input data. Theory identifies the important variables and physics, knowledge of which can lead to further experimental research and practical developments. Disagreements between theoretical predictions and experimental results can at least be identified as uncertainty in particular physical parameters. It is important to investigate theories that include more effects than are imagined to be relevant to the problem, to then be able to say that those effects can be neglected.

Influences on the sound wave behaviour considered in this thesis are: compressional wave scattering, heat transfer between the phases, momentum

transfer between the phases (viscous and inertial), compressibility, hydrodynamic interactions between particles, particle size distributions and particle shape. A wide range of experimental data is used to compare to the theoretical predictions, so that the influence of these different phenomena on the sound propagation can be shown. The data covers a large region of 'parameter space' to show where the different theories and approximations are valid. The regions where certain effects have to be included in calculations and the regions where they can be neglected can be identified. This information can be used to choose the best theory for a particular application. Choosing the correct theory is important if it is going to be solved numerically: an efficient solution will not require the evaluation of more terms than are relevant to the problem.

All the theories make assumptions. Information about the particles in a suspension or emulsion is incomplete and usually very limited. Most work assumes the particles are spherical. This is a reasonable assumption if the particles are roughly spherical, i.e. they do not have one dimension much greater than any other dimension, and if $k_f a$, where k_f is the wavenumber in the continuous phase and a is the particle radius or effective radius, is small. If the distribution of sizes is not known it is usually assumed that the particles are all of the same size. All the theories in this thesis assume that the spatial distribution of the particles is uniformly random. It is possible that this is not true in experiments.

The theories will be used to predict the behaviour of an incident plane wave as it travels through the suspension or emulsion. If scattering is small, the sound field behaves essentially as a plane wave throughout: this is known as the coherent wave. Assuming plane wave propagation, the theories can be used to derive a complex wavenumber k for the coherent wave. k contains the attenuation and sound speed for the wave: these are the quantities usually measured in experiments. This thesis concentrates on coherent wave propagation. If the scattered, or incoherent, field is more important than the coherent wave, then the modelling is approached differently. The prototypic model for incoherent scattering presented by Morse and Ingard [10] is discussed in section 3. 1. 2.

The experimental data used in this thesis has been obtained from various sources. Attenuation and sound speed data at audio frequencies has been obtained from measurements on alumina dust in air suspensions by Moss [11] [12]. This data is used in chapter 6. Reflection coefficient data at audio

frequencies for stacked glass beads in air is used to compare to porous media theory predictions in chapter 5. Both these media have particle sizes such that $k_f a << 1$, although the alumina particles are of the order of 1 micron and the glass beads are of the order of 1 mm. The alumina suspension has a very low volume fraction (10^{-5}) while the glass beads have a near maximum (for identical spheres) volume fraction of 0.6.

Data at ultrasonic frequencies has been reproduced from the literature. The data has been obtained from measurements on oil in water emulsions for volume fractions ϕ up to 0.6 (chapters 3 and 4) and kaolinite in water suspensions for ϕ up to 0.4 (chapters 5 and 6). Again for these media $k_f a << 1$. Data for aqueous suspensions of glass beads at volume fractions up to 0.6 is used in chapter 3. This data covers the region where $k_f a \cong 1$ and compressional wave scattering is important. Because compressional wave scattering is significant and the volume fraction is high, this data exhibits the effect of multiple scattering.

Applications

An understanding of sound propagation in suspensions and emulsions is important in many areas.

Sound can be used for monitoring and characterisation of two phase media in the process, nuclear power, chemical, petrochemical, cosmetic and agrochemical industries. Atkinson and Kytomaa [13] discussed the use of ultrasound for monitoring the flow properties of highly concentrated liquid solid mixtures such as slurries (e.g. coal), drilling muds, pastes, concretes and polymer melts. It has advantages over other methods such as resistive and capacitative point probes in that it is nonintrusive. This is important because particulate media are often susceptible to blocking and bridging. It has a high frequency response and so can be used for the measurement of dynamic and transient phenomena. It can be used for highly concentrated and opaque materials where laser Doppler anenometry cannot. Other applications include the oil industry, where emulsions can be created during the separating of water and oil [14], and the pneumatic transport of powders and pulverised coal [15]. Hay [16] studied the scattering of ultrasound from turbulent two phase flows. Johnson and Plona [17] studied ultrasound propagation through superfluids (non-viscous fluids) in superleaks (packed powders). Nuclear reactor safety problems such as coolant blowdown and sodium expulsion depend in their solution on a knowledge of how pressure waves propagate through two phase media [18].

Ultrasonic particle size and concentration instrumentation already exists and is being developed. The AcoustoPhor system can provide reliable particle size

distribution data for slurries with particle diameters in the range 0.01 to 100 microns with volume fractions up to 0.5 [19]. Ultrasound scattering can be used to characterise single particles, for example biological cells, in terms of volume, density and compressibility [20]. Sound propagation can be used to measure the physico-chemical and thermostatic properties of fluids [1].

A well known medical application is the ultrasonic Doppler flowmeter which makes use of backscattering from blood. Higher frequencies have been used for blood [21] and intravascular [22] imaging. Knowledge of ultrasound propagation in inhomogeneous media is important for medical imaging and the characterisation of biological tissues and cells in suspension [23] [24].

Underwater, understanding of sound propagation in sea-bed sediments is important for the petroleum and mineral industries which use seismic soundings for geological imaging [25]. Sonar can be used for the remote sensing of suspended sediments, to study within wave and turbulent sediment transport processes [26]. Bubbles from breaking waves in the ocean are believed to affect underwater sound propagation [27].

Meteorologists are interested in the propagation of sound in clouds and fog (fog horns) [28], and air pollution such as smoke or dust.

Ultrasound measurements methods are ideal for the food industry since they are non-invasive, non-intrusive, non-destructive and non-hazardous. They can be used for non-conducting media and are low in cost compared to other techniques [29]. Pinfield *et al* [30] used ultrasound to monitor creaming and crystallisation in model foodstuffs.

Sound may prove useful in the fundamental study of classical wave propagation through strongly scattering media. Sound scattering experiments avoid some of the limitations of light scattering experiments [31]. Nagy [32] used 2D measurements of incoherent scattering for the imaging of low permeability porous solids.

Particles can be an influence on the (nonlinear) acoustics in combustion chambers like metallized propellant rocket motors and jet engine thrust augmentors [5]. Another space application is the lift-off of the US Space Shuttle where a very strong water shower is used to suppress the strength of the ground reflected waves produced by the exhaust jets. This idea is quite effective in protecting the very weak wall structure of the Orbitor from possible fracture due to the air disturbances [33].

Other areas which involve the interaction of suspended particles and sound are acoustic levitation, laser Doppler anenometry for the remote detection of sound [34], smoke precipitation in coal fired boilers and particle filtering and dewatering [35].

Other situations involving particulate materials include [36] [37]:

gas-solid suspensions: dust collectors, fluidized beds, combustion chambers with powdered fuel injection, cosmic dusts, nuclear fallout, flow of granular materials, volcanic clouds;

gas-liquid suspensions: atomisers, rocket engine injectors, factory stack effluents, evaporators, sprays, foams, sandblasting;

liquid-solid suspensions: fluidized beds, fibre suspensions in paper making, latex particles in emulsion paints, flotation and sedimentation, factory waste products, quicksand.

1. 2 Theoretical conventions

The variables of the problem - frequency f, particle radius a and volume fraction ϕ and the physical parameters of the two phases - govern characteristic lengths. The data used in this thesis tries to cover as wide a range of these as possible, to define ranges of applicability for the different models and approximations.

The wavelength λ is the characteristic length for the sound wave, this is controlled by f. Twice the radius $2a$ is the characteristic dimension for a particle. d, the particle separation, is governed by ϕ. Coupled phase and porous media theories are both continuum theories which require that $\lambda \gg 2a$. This is usually written as $k_f a \ll 1$, where $k_f = \omega/c_f$ is the wavenumber in the continuous phase and c_f is the sound speed in the continuous phase. If $k_f a \ll 1$ there is negligible compressional wave scattering. The assumption that the particulate phase is a continuum requires that its properties are uniform for distances of the order of a wavelength, this requires $\lambda \gg d$ (see section 4. 1. 2). Two more characteristic lengths are the viscous and thermal boundary layer thicknesses δ and δ_h. These are governed by the frequency ($\propto f^{-\frac{1}{2}}$) and the physical parameters. The isolated particle assumption requires that, in the continuous phase, δ and $\delta_h < \frac{1}{2}d$, so that the viscous and thermal waves do not overlap (see section 3. 2. 9). The conditions for the neglect of compressional wave scattering, the isolated particle assumption and the validity of the continuum assumption for different physical parameters are presented as regime maps in chapters 3 and 4.

Continuum theories allow the volume fraction ϕ to take any value between 0 and 1, although in practice ϕ will always be less than 1. For identical spheres the maximum volume fractions for regular packings are: $\pi/6 = 0.52$ for simple cubic packing, $\sqrt{3}\pi/8 = 0.68$ for body-centred cubic packing and $\sqrt{2}\pi/6 = 0.74$ for face-centred cubic packing or hexagonal close packing [38]. The maximum volume fractions for random packings are less, experimental studies suggest that 'random loose' packing has a maximum volume fraction of 0.60 and 'random close' packing a maximum volume fraction of 0.64 [39] [40].

The validity of single or multiple scattering theory depends on the acoustic depth $N\sigma_0 L$, where N is the number of particles per unit volume, σ_0 is the total scattering cross section of a particle, which represents the total energy removed from the incident wave by the particle, and L is the distance the incident wave travels in the two phase medium. If $N\sigma_0 L \ll 1$ single scattering is valid. If $N\sigma_0 L$ is not small then multiple scattering must be taken into account. It can be seen that when designing a propagation experiment the distance between the source and receiver L needs to be taken into account.

The condition $N\sigma_0 L \ll 1$ is also implicit in the non-scattering theories, see section 1. 3. 2 below.

For convenience here the complex representation for sinusoidal variables will be used [41]. The sinusoidal time and z direction dependence of the field variables will be represented by an exponential function of the form

$$y = y' \exp[i(kz - \omega t)]$$

where y' is a complex amplitude and ω is the angular frequency. The actual physical quantity is given by the real part of this

$$y_{\text{real}} = \Re\left(y' \exp[i(kz - \omega t)]\right).$$

The exponential forms can be used in linear equations because, if L is any linear operator [42],

$$\mathrm{L}y_{\text{real}} = \mathrm{L}\Re(y) = \Re(\mathrm{L}y).$$

k is the complex wavenumber which governs the spatial dependence of the field variables and in particular the plane acoustic wave. In general it is complex and frequency dependent and may be written

$$k(\omega) = \frac{\omega}{c(\omega)} + i\xi(\omega)$$

where $c(\omega)$ is the frequency dependent velocity and $\xi(\omega)$ is the frequency dependent plane wave attenuation coefficient. All materials have a complex

wavenumber of this form although in some cases the attenuation and the frequency dependence of the sound speed may be neglected. In this thesis, for air at audio frequencies, the attenuation is neglected and the sound speed is assumed constant. The sound speed in water at ultrasonic frequencies is assumed to be constant also. Experimental results for ultrasound attenuation are expressed in terms of excess attenuation due to the particulate phase i.e. that in addition to the attenuation in the pure continuous phase. The theoretical excess attenuation is calculated by neglecting the attenuation in the continuous phase. Thus for all cases c_f is constant and $k_f = \omega/c_f$ is real.

1. 3 Theoretical approaches

1. 3. 1 Scattering theory (chapter 3)

Scattering theories treat the problem by assuming a plane wave incident on a scatterer is converted into several 'scattered' waves. The simplest case is the scattering from a perfectly reflecting object in an inviscid, non-heat-conducting gas. Here there are two sound waves to consider: the incident and scattered wave. The scattered wave is determined by the boundary conditions at the scattering object. If the gas is viscous and heat conduction is included then there is also a viscous and thermal wave associated with any sound wave. In free field conditions the effect of these is to remove energy from the sound wave. For a plane wave the effect can be represented as an attenuation and a modified sound speed. When the sound wave encounters a scatterer new viscous and thermal waves are created which remove additional energy. The scattered viscous and thermal waves are rapidly attenuated with distance and are assumed to be confined to a 'boundary layer'. If the scatterer is fluid then the incident sound wave causes a compressional, viscous and thermal wave to be produced inside it. If it is solid then an elastic compressional wave, a shear wave and a thermal wave are produced.

The scattering theory for a single scatterer therefore involves 7 waves. These are expressed as infinite sums of spherical harmonics. The 6 unknown waves are determined by the boundary conditions at the scatterer. The series representation of the scattered compressional wave, contained in the coefficients A_n, is the only information required to determine the effect on an incident wave. The terms in the series representation depend on $k_f a$. The value of $k_f a$ determines how many terms in the series are necessary to represent the wave accurately. If $k_f a \ll 1$ only the first two terms are required.

The scattered compressional wave from a single scatterer is used to calculate the effect of a group of scatterers. In the single scattering approximation the

complex wavenumber depends on the coefficients A_n multiplied by N, the number of scatterers. This is valid if $N\sigma_0 L \ll 1$, i. e. if the effect of scattering is small and it can be assumed that the wave incident on each scatterer is the same and equal to the incident wave. This is also known as the Born approximation. The condition is satisfied if there are few scatterers per unit volume, if each scatterer has a low cross section or if the propagation distance is short.

Multiple scattering theories take account of the fact that when $N\sigma_0 L$ is not small the wave incident on each scatterer will not be the same. The fact that the scattered waves are re-scattered must be taken into account. This introduces terms into the equation for the complex wavenumber which are multiples of the A_n coefficients and are proportional to N^2 and higher powers of N.

The term coherent scattering restricts attention to the effect of scattering on the incident plane wave. The resultant plane wave is the incident plane wave plus the average of the scattered field. The term incoherent scattering refers to the fluctuations of the scattered field about its average [43]. Incoherent scattering is discussed in section 3. 1. 2.

1. 3. 2 Coupled phase theory (chapters 4 and 6)

Coupled phase theories start from the same set of equations as scattering theories i.e. the conservation or balance equations and equations of state for both of the phases. These are then 'coupled' via a momentum transfer term in the momentum equations and a heat transfer term in the energy equations. Viscous and thermal effects are usually assumed to be confined to the boundary layers around the particles and are neglected in the rest of the continuous phase. The fact that the two phases occupy the same control volume is included by means of volume averaged variables. This couples the continuity equations.

Unlike scattering theory, the space and time dependence of all the field variables - two densities, two velocities, two temperatures, pressure and volume fraction - are assumed to have the form for plane wave propagation

$$y = y^0 + y' \exp[i(kz - \omega t)]$$

where k is the unknown complex wavenumber, y^0 indicates the constant equilibrium value of the variable and y' is the unknown amplitude of the perturbation to the variable caused by the sound wave.

For the exponential term, derivatives with respect to time are replaced by $-i\omega$ and derivatives with respect to space are replaced with ik. All the exponential terms in the conservation and state equations then cancel and the equations are left in algebraic form in terms of the unknown amplitudes y', the unknown k,

the known constants y^0 and other known physical parameters. This set of equations can be written as a matrix equation

$$\mathbf{A}\mathbf{y} = 0$$

where y is a vector containing all the amplitudes y'. Non-trivial solutions of this equation require

$$\det \mathbf{A} = 0$$

which yields an equation which can be solved for *k*.

Other coupled phase methods assume the space and time dependence relevant to standing waves in an enclosure (see section 6. 4).

The expression for the momentum transfer contains terms representing the steady state Stokes drag, the Bassett history force and the induced mass. For spherical particles, the Stokes drag is dominant when $a/\delta \ll 1$, where δ is the viscous boundary layer thickness in the continuous phase, i.e. the lower frequencies for a given particle size. In this region the attenuation ξ scales with $a^2\omega^2/\mu$ where μ is the dynamic viscosity. The low frequency limit of the sound speed is independent of frequency. When $a/\delta \geq 1$ the Basset force begins to influence the momentum transfer. When $a/\delta \gg 1$ the Basset force is dominant and the attenuation scales with $\sqrt{\omega\mu}/a$. In this region the sound speed is independent of frequency and depends on the inertial effect of the induced mass force [25].

The expression for the heat transfer has terms exactly analogous to the momentum transfer terms [44]. The term corresponding to the induced mass has been neglected in this thesis.

Coupled phase theories must be subject to the same condition $N\sigma_0 L \ll 1$ as single scattering theories because they assume the pressure and the other field variables are the same for all the particles. This condition has been discussed by Leander [45] for the 'causality approach' to attenuation in clouds of bubbles.

1. 3. 3 Porous media theory (chapter 5)

Porous media theories are continuum theories, based on the same principles as coupled phase theories. The general Biot theory [46] models fluids in a 'frame' formed of solid grains. Because the individual grains may be in contact the frame can be elastic or inelastic and can support shear as well as compressional waves. As well as the bulk moduli of the fluid and solid K_f and K_s, the theory involves the, possibly complex, bulk and shear moduli of the frame as a whole

K_b and N_b. Viscous and inertial momentum transfer between the phases is included using 'rigid frame' theory (see below). The theory predicts the existence of three waves in the material - a 'slow' and 'fast' compressional wave and a shear wave - and can be used to derive wavenumbers for these three waves.

Other porous media theories assume that the frame is rigid and have concentrated on modelling the momentum and heat transfer between the frame and the fluid in the pores. The viscous force and heat transfer are obtained by solving the problem of sound propagation in a fluid in a solid tube, as a model for a pore. These are then related to the bulk properties of the porous medium: the porosity $\alpha = 1 - \phi$, flow resistivity σ and tortuosity α_∞. These properties can either be measured or obtained from theoretical expressions. The influence of pore shape is included by means of a theoretical or adjustable shape factor. A pore size distribution can be included using measured or adjustable parameters. The inertial force is obtained from the tortuosity, which can be measured or related theoretically to the porosity and the induced mass for a single grain.

Chapter 2
Literature review

This chapter contains a survey of the development of methods of modelling sound propagation in suspensions and emulsions and practical situations in which they have been applied. An outline of the methods has been given in chapter 1. Section 2. 4 reviews the Kramers-Kronig approach, although this approach has not been employed in this thesis. As well as the literature that forms the basis for the work in chapters 3 to 6, novel related work has been included to give a perspective. Particular attention has been given to the details of experimental data to indicate what is available and where more work is required. Some names are mentioned but not given a reference. The details for these can be found in the reference under which they are discussed.

2. 1 Scattering theory

2. 1. 1 Single scattering

The theory of sound scattering from a single sphere has been developed as far as is necessary to deal with suspensions and emulsions. The first treatment to include three waves in both the sphere and the surrounding continuum was that of Epstein and Cahart (EC) [47]. These three waves are compressional, thermal and viscous in a fluid and elastic compressional, thermal and shear in a solid. The EC treatment is applicable when both the continuous and particulate phases are a fluid. The plane wave attenuation of one sphere is calculated from the far field scattered compressional wave. For the long wavelength regime only the first two coefficients in the series expansion of the scattered wave are important. Explicit expressions for these may be obtained. A_0 represents

compressional wave scattering and thermal effects. A_1 represents viscous effects. A similar analysis, neglecting waves inside the sphere, can be found in Morse and Ingard's book [10]. Epstein and Cahart assumed that the attenuation from a group of spheres is *N*, the number of spheres, times the attenuation of one sphere.

Zink and Delsasso [48] used the EC expressions for viscous and thermal attenuation to derive the frequency dependent sound speed in terms of a frequency dependent complex density and heat capacity. The frequency dependent density represents the viscous effect and the frequency dependent heat capacity represents the thermal effect. It is more common to see the thermal effect represented by a frequency dependent complex *compressibility*.

Allegra and Hawley (AH) [49] presented a comprehensive review of the development of the scattering theory for a single sphere and extended the EC theory for a fluid continuous phase and a solid particulate phase. They also obtained explicit long wavelength expressions for A_0 and A_1. For comparison to experiment the first three A_n coefficients were calculated numerically. The attenuation was derived in the same manner as in the EC theory. Ultrasound attenuation was measured at frequencies between 3 and 165 MHz in suspensions of polystyrene spheres in water. The spheres had radii between 0.044 and 0.653 μm and the maximum volume fraction was 0.1. There was good agreement between the theoretical predictions and the experimental data. Another experiment measured the ultrasonic attenuation at frequencies between 3 and 75 MHz in a latex slurry with a nominal particle radius of 0.11 μm at volume fractions up to 0.5. These measurements are compared to scattering and coupled phase theory predictions in chapter 4.

Lin and Raptis [50] [51] [52] pointed out that the AH equations are only valid for isothermal deformations of a solid. Their single scatterer theory employed the correct field equations for a thermoelastic solid. The scattering and thermoviscous absorption cross sections and scattering angular dependence were calculated numerically for spheres and cylinders for $k_f a$ up to 16, where a is the sphere or cylinder radius.

Anson and Chivers [53] calculated the thermal attenuation, relative to other forms of attenuation, for a variety of suspensions and emulsions. The suspensions were all the combinations of seven different solids in 72 different liquids. The emulsions were 71 different liquids in water. The volume fraction was 0.01 and $k_f a$ was 0.01. From these results a generalised approximate curve was proposed. For selected systems the relative contributions of viscous losses,

thermal losses, compressional wave scattering losses and intrinsic attenuation in the particulate phase material were calculated for $k_f a$ up to 1.

Scattering from a viscoelastic sphere was modelled by Ayres and Gaunaurd [54]. Anson and Chivers [55] looked at scattering from spherical shells. The shell is in a fluid continuum and the shell and core material can be either solid or fluid. The analysis includes viscous and thermal effects and viscoelasticity.

Thorne *et al* [26] measured ultrasound attenuation and backscattering amplitude for dilute aqueous suspensions of spheres. Frequencies were between 2.2 and 3.5 MHz and the particles had mean radii between 101 and 1190 μm. Thus $1 < k_f a < 17$. For single sphere measurements plots versus frequency exhibit fine structure, indicating resonance phenomena. For distributions of sphere sizes this fine structure is smoothed out. Theory successfully predicts both these forms. A 'smoothed' theory may be used when there is a sphere size distribution.

Roy and Apfel [20] measured scattering from individual polystyrene spheres with diameters ranging from 4 to 15 μm. 2 μs long 30 MHz tone bursts were used. The data was used to estimate the density and compressibility of the polystyrene.

2. 1. 2 Non-spherical scatterers

In reality scatterers will not be perfectly spherical and smooth. The scattered intensity will be, in general, different in all directions. Scattering theory for these cases has concentrated on compressional wave scattering. Waterman [56] developed the theory for scattering from a smooth body of arbitrary shape. In principal the method can be applied to any shape of scatterer. For complex geometries a numerical integral will be required, analytical forms are only derivable for simple shapes e.g. spheroids. Jansson [57] applied Waterman's method to a rough sphere and obtained an analytical solution. There are numerous examples of numerical treatments, for example, the 'boundary integral' method is used in reference [58].

Attenborough and Walker [59] modified the EC theory to calculate the thermoviscous absorption of a plane wave obliquely incident on an infinite thermoelastic cylinder. Explicit expressions were given for the absorption of normally incidence plane waves in the long wavelength regime.

Stanton [60] reviewed scattering from spherical and non-spherical objects. For the sphere, prolate spheroid, straight finite cylinder and bent finite cylinder useful approximate formulas were derived. The scatterer may be solid, liquid or

gaseous. The formulae combine the low frequency (Rayleigh scattering) and high frequency (geometrical scattering) limits to obtain simple closed form solutions. These were compared with the exact results and experimental data on ideally shaped objects and non-ideally shaped marine organisms.

2. 1. 3 Multiple scattering: coherent wave

Multiple scattering has to be taken into account when the quantity $N\sigma_0 L$, the 'acoustic depth', is of the order of 1. Ishimaru [61] [62] provides a comprehensive review of the theory of multiple scattering of waves. A review up to 1962 was given by Twersky [63], who developed a generalised theory and derived the previous results as special cases. The multiple scattering theories most commonly found in the acoustics literature are the Waterman and Truell, Lloyd and Berry , Twersky, Tsang *et al* and Ma *et al* theories. These five are compared in McClements [64] (see below). Harker and Temple [65] reviewed theoretical work on multiple scattering in metals and composite materials.

Twersky [63], in the first of a series of three papers, derived the complex wavenumber in a slab region of randomly distributed scatterers in terms of the free space scattering amplitude of the scatterers. It was shown that the energy lost by the coherent wave reappears in other directions, this is the incoherent scattering. The second paper in the series [66] looked at the general problem of a scatterer characterised by one wavenumber being exciting by a wave with another wavenumber giving rise to a scattered wave with a third wavenumber. The third paper [67] applied this method to scatterers radiating into free space being excited by a wave with the effective wavenumber of the scattering medium. Javanaud and Thomas [68] gave a useful summary of Twersky's work as it applies to ultrasound propagation. Later, Twersky looked at pair-correlated random distributions [69] [70] of scatterers. The scatterers were either cylinders of various cross sectional shapes or shapes bounded in space, such as ellipsoids, aligned or averaged over orientation.

McClements *et al* [71] [72] measured ultrasound velocity and attenuation at frequencies between 1.25 and 10 MHz in a sunflower oil in water emulsion at volume fractions up to 0.5. The particles had radii between 0.14 and 0.74 μm. They calculated numerically as many AH scattered wave coefficients as were significant. These were then used in the expressions for the complex wavenumber given by the multiple scattering theories of Waterman and Truell (WT) [73] and Lloyd and Berry (LB) [74]. The theoretical predictions agreed very well with the velocity measurements. The agreement with the attenuation

measurements was not so good, the theory overpredicting the attenuation at high volume fractions.

In similar work [29] [64], McClements measured ultrasound velocity and attenuation at frequencies between 0.2 and 7 MHz in a hydrocarbon oil (hexadecane) in water emulsion at volume fractions up to 0.56. The particles had radii between 0.1 and 1.8 μm. The multiple scattering theory of Ma, Varadan and Varadan (Ma) [75] was tested. It gave similar results to the LB theory. The theory was extended to include particle size distributions. As in reference [71] the theory consistently overpredicted the measured attenuation. This may be due to interactions between the viscous and thermal waves. At these high volume fractions the separation between particles can be small so that their boundary layers overlap.

The data of McClements *et al* is compared to scattering theory predictions in chapter 3 and coupled phase theory predictions in chapter 4.

Pinfield, Povey and Dickinson [30] also performed experiments on sunflower oil and hexedecane in water emulsions. They were interested in creaming and crystallisation effects. Creaming occurs when the dispersed phase is less dense than the continuous phase and so it moves to the top of the sample. Crystallisation is the solidification of an initially liquid dispersed phase. Scattering theory was used to interpret ultrasound velocity measurements, as a means of monitoring these phenomena.

Froyse and Nesse [14] measured the ultrasound velocity and attenuation in oil-in-water and water-in-oil emulsions. The frequency range was 250 kHz to 900 kHz, the mean droplet radius was between 0.5 and 1 μm and the maximum volume fraction for both emulsions was 0.8. At a volume fraction of 0.4 the attenuation results for both emulsions agree well with predictions of the WT and Ma theories. The sound speed results agree less well with predictions. The two theories break down when the volume fraction is above 0.5. When the volume fraction is between 0.7 and 0.8 the emulsion has a foam like structure.

Holmes *et al* [76] did similar work to McClements *et al* for suspensions. They measured the ultrasound velocity and attenuation in monodisperse aqueous suspensions of polystyrene spheres. Frequencies were between 2 and 55 MHz, the particles had diameters between 200 and 615 nm and volume fractions were between 0.05 and 0.45. Single and multiple scattering models predicted similar results, which agreed well with the measurements. Similar work was carried out for aqueous suspensions of silica particles [77].

Alig and Lellinger [78] measured the ultrasound velocity and attenuation in gelatine containing glass beads. The frequency range was 2 to 50 MHz, the beads had diameters between 42 and 400 μm and the maximum volume fraction was 0.07. The results show the effect of scattering, which is well predicted by the WT theory.

Atkinson and Kytomaa [13] measured the ultrasound velocity and attenuation and the sound intensity in the axial and radial directions for aqueous suspensions of glass beads using a 1 mm diameter receiver. The frequency range was 100 kHz to 1 MHz, the beads had a diameter of 1 mm and the maximum volume fraction was 0.62. The maximum value of $k_f a$ was approximately 2. Since this is in the compressional wave scattering regime, predictions of the coupled phase theory used did not agree with the experimental data. These measurements are compared to the predictions of multiple scattering theory in chapter 3.

Wu *et al* [79] compared predictions of their multiple scattering theory, including particle size distribution, with measurements of attenuation in water saturated sand. Frequencies were between 40 and 600 kHz, the particles had a mean size of 340 μm and the volume fraction was 0.55. The measured attenuations were higher than those predicted by the theory. This disagreement could be due to particle roughness and non-sphericity.

Attenborough and Walker [80] modelled multiple scattering in dilute random arrays of parallel cylinders. Viscous and thermal effects were included and the complex wavenumber was derived by a Twersky [63] multiple scattering formulation. Predictions of the model were compared with measurements on glass fibre absorbent materials at audio frequencies. The predictions and experimental data agreed at the higher frequencies but there was large disagreement at the lower frequencies. The failure of the theory at low frequencies could be due to the neglect of viscous and thermal wave interactions or the assumption of parallel, isolated fibres.

Schwartz and Plona [81] performed experiments in the strong scattering regime. They measured the complex wavenumber in water-saturated glass spheres of mean diameter 545 μm and Plexiglass spheres of mean diameter 275 μm. The volume fraction in both cases was 0.62. Because of the large particle sizes and the high frequencies (between 300 kHz to 2 MHz) viscous effects were negligible compared to compressional wave scattering. The experimental data was compared to the predictions of two multiple scattering theories. These were the 'Quasicrystalline approximation' (QCA) and the 'Effective medium

approximation' (EMA), the latter was originally developed for the description of electronic states in metals. The EMA predictions agreed more closely with the experimental results.

Schwartz and Johnson [82] discussed multiple scattering theory for spherical solid grains in an inviscid fluid and its connections with the Biot theory for porous media. For ordered cubic suspensions the problem has the form predicted by Biot i.e. a single geometric parameter characterises the suspension. For disordered suspensions, however, the Biot theory is not rigorously applicable. Approximate schemes such as the QCA, EMA, CPA (coherent-potential approximation), the incremental IDA (iterated dilute approximation) and the ATA (average *t*-matrix approximation) were compared. Available experimental data does not have a great enough solid to fluid density ratio to distinguish between the competing approximations.

Romack and Weaver [83] discussed the QCA and CPA approximations used by Schwartz and Johnson for one dimensional scattering using the diagram method of Frisch. Three approximations were compared in a numerical 'Monte Carlo' experiment.

Ye and Ding [27] used the diagram method for monopole scatterers. They calculated the complex wavenumber for 'one-way' scattering where the sound at the receiver point has been scattered by each particle once and 'two-way' scattering where each particle scatters twice. The complex wavenumber is the pole of the spatial Fourier transform of the Green's function, which is given by a Dyson equation. The one-way result is the same as the WT result for monopoles. For bubbles the two-way scattering gives unphysical results near the bubble resonance. It may be possible to correct this by including higher order scattering.

2. 1. 4 Self-consistent scattering theories

Sayers [84] developed a 'self-consistent' (valid for volume fraction ϕ=0 and 1) theory from the WT theory. The two phases are each characterised by two Lame constants and a density. The method was applied to a medium where the densities and shear moduli of the two phases are identical. By invoking self-consistency, the WT multiple scattering expression for the complex wavenumber is 'corrected' so that it is valid for all values of volume fraction.

Sayers and Smith [85] applied the approach to porous media. They used the 'coherent potential approximation' of quantum mechanics which says that no net scattering occurs. The interpretation of this was the implication that the

volume average of the scattering coefficients is zero. The method obtains 'effective' versions of the Lame constants and the density for the two phase medium.

Berryman [86] [87] developed a self-consistent scattering theory for composite elastic media. This included spheroidal particles and attenuation. The attenuation was in the form of complex bulk and shear moduli which have to be pre-determined.

There are numerous other scattering theories for solid-solid composites which can be characterised by a density, a bulk modulus and a shear modulus [65]. Anson and Chivers [88] compared twelve of them. These were either multiple scattering, self-consistent or 'incremental'. The latter method involves introducing the particulate phase into the continuous phase in steps and recalculating the effective parameters after each step. The effective medium is used as the continuous medium for the subsequent step.

2. 1. 5 Incoherent scattering

Morse and Ingard [10] discussed coherent and incoherent scattering in the single scattering limit from a cloud of spheres which are characterised by a density and a compressibility. The 'Born approximation' for small scattering region, low volume fraction and low scattering strength was employed. This work is discussed in section 3. 1. 2.

Non-planar incident waves from a source transducer (diffraction) and measurement of incoherent scattering was reviewed and discussed by Chivers [24] [43]. When incoherent scattering is significant, the phase and amplitude of a wave emerging from an inhomogeneous medium vary from one place to another in the field. Assuming an incident plane wave, it is no longer valid to talk about the plane wave ultrasound velocity and attenuation of the medium. It is necessary to map the spatial variation of the amplitude and phase of the wavefronts with a small or focused transducer. This permits the assessment of the relative magnitudes of the coherent and incoherent scattering.

Adach *et al* [89] measured the pressure amplitude distribution in the field of a weakly focused transducer in castor oil containing polystyrene beads. The frequency range was 1 to 2.5 MHz, the beads had a mean diameter of 323 μm and the maximum volume fraction was 0.02. The beads have a resonance in this frequency range. The measured excess attenuation agreed well with predictions of the WT theory. There was no detectable defocusing of the field due to the presence of the resonating scatterers.

Twersky [90] studied long wavelength incoherent scattering from correlated distributions of arbitrarily convex particles averaged over orientation. Comparisons between Twersky's theoretical predictions and experimental measurements on scattering from blood cells can be found in reference [91]. Reference [92] extends the theory to particle size distributions.

An alternative to the Twersky approach to multiple scattering was presented by Liu [93] [94] [95]. Liu assumed that the particulate media was a discontinuous stochastic field, scattering from the individual particles is not considered explicitly. The spatial distribution of the two phases can be determined by geometrical probability and was derived for spherical particles. The method is similar to that used by Morse and Ingard. Comparisons with the experimental results of Shung [21] showed that the Liu theory is superior to that of Twersky at high volume fractions. The Shung results satisfy the 'weak fluctuation' assumption that the acoustic parameters of the two phases are close.

Scattering from blood cells reduces the clarity of ultrasound imaging of blood vessels. Intravascular imaging uses transducers which typically have a radius of 0.7 mm. Scattering becomes important above 10 MHz and is mainly caused by red blood cells. These are approximately 2 μm thick and 7 μm in diameter. Gronningsaeter *et al* [22] developed a method for filtering out the scattering noise by taking advantage of the Doppler effect.

Tolstoy [96] analysed the phenomenon of 'superresonance', which is related to multiple scattering. Superresonance refers to conditions where the resonance of single scatterers is enhanced by the presence of neighbouring scatterers and boundaries.

2. 1. 6 Ultrasound diffusion

Weaver and Sachse [97] studied the diffuse multiply scattered ultrasonic field in water saturated, disordered glass beads. The beads had diameters of about 3 mm and the volume fraction was about 0.62, corresponding to random close packing. Tone bursts were used with frequencies between 250 kHz and 1.3 MHz. The transducers used had active elements with diameters of approximately 1.3 mm. The multiple scattering attenuation is too great for coherent wave propagation and the energy density evolves in accordance with a diffusion equation. The diffusivity parameter exhibits a frequency dependence which characterises the microstructural length scale.

Page *et al* [31] performed 2.5 MHz ultrasound propagation experiments through random close packed glass beads in water. The volume fraction was

about 0.63 and the beads had a radius of 0.5 mm. Since the wavelength is 0.6 mm this is a strongly scattering system. The beads were contained a cylindrical container with thin polystyrene walls which was immersed in water. The thickness of the sample was varied, the maximum thickness being 20.5 mm and the diameter was always greater than 10 times the thickness. Two source geometries were used: either a focused transducer to approximate a point source or a 6 mm diameter transducer in the far field to obtain plane waves. The transmitted field was measured using a miniature hydrophone whose diameter was 'much less than the ultrasonic wavelength', to obtain the detailed spatial distribution or 'speckle pattern'. Pulse lengths were between 1 and 100 μs, the longest length is a good approximation to a continuous wave. The measured average transmitted intensity versus time is accurately modelled by a diffusion equation. Sound propagation is important in the study of multiply scattered classical waves because, unlike light, all the phase information can be detected.

2. 2 Coupled phase theories

Temkin and Dobbins (TD) [98] used a coupled phase approach to predict the plane wave complex wavenumber for a perfect gas containing a low volume fraction of incompressible particles. The momentum transfer was due to Stokes drag and the heat transfer was given by Newton's law of cooling. Consideration was given to a particle size distribution. Predictions of the theory were compared with the measurements of Zink and Delsasso [48] on alumina dust in air at frequencies between 0.5 and 13.6 kHz. The particles had radii between 2.5 and 7.5 μm and the volume fractions were of the order of 10^{-5}. The agreement between the predictions and measurements was satisfactory.

In another paper [99], Temkin and Dobbins obtained very good agreement between their theoretical predictions and measurements on oleic acid particles in nitrogen. The measurements were made at frequencies between 1 and 10 kHz, the mean particle radii were between 0.8 and 4.7 μm and the volume fractions were between 3×10^{-4} and 0.01.

Mednikov [100] extended the TD method to finite amplitudes of the sound wave. The drag becomes a function of Reynolds number Re.

Mecredy and Hamilton (MH) [18] [101] followed the TD method and extended it in several areas. The conservation equations were derived in terms of volume averaged variables. The theory was derived for a liquid with gas particles or a gas with liquid particles, and included condensation and evaporation, i.e. mass transfer, between the two phases. The liquid phase was assumed to be

incompressible. The momentum transfer was due to Stokes law drag and the induced mass force. The resistance to heat transfer was assumed to occur in the gas phase at the boundary of the particles. If the gas is in particulate form then the resistance to heat transfer takes place inside the particles, if the gas is the continuous phase then heat transfer takes place in the boundary layer exterior to the particle. The resultant matrix equation was solved numerically. An asymptotic sound speed was identified for the high and low frequency limits.

Gumerov, Ivandaev and Nigmatulin (GIN) [102] covered much the same ground as Mecredy and Hamilton. In addition they included the unsteady viscous (Bassett history) force and the unsteady heat transfer between the two phases. The buoyancy force, which Mecredy and Hamilton wrote in terms of pressure, was written in terms of the fluid velocity. Models of finite amplitude sound propagation in fog follow similar lines [28] [103]. The GIN and MH models are compared analytically in chapter 4, where they are also compared to scattering theory.

A different coupled phase theory was presented by Harker and Temple (HT) [65]. They neglected heat transfer between the phases and assumed that the particulate phase was compressible. Predictions of the theory agree well with the experimental results of Urick [104] [105]. Urick measured the ultrasound velocity at 1 MHz in a suspension of kaolin or kaolinite particles in water. The particles had a mean radius of 0.45 μm and the volume fraction varied between 0 and 0.4. The HT theory is extended in chapter 4 by including heat transfer.

In another paper [106] Harker and Temple extended their theory to account for particle size distributions. They measured ultrasound velocity and attenuation in suspensions of silicon carbide in water, ethylene glycol and glycerol. The highest volume fraction measured was 0.3. Agreement between theoretical predictions and experimental data was good for the velocity but not as good for the attenuation.

The coupled phase method is a special case of multi-phase continuum mechanics. Soo [107] presented a general multi-phase theory. The conservation equations were derived in an overall form for the multi-phase media and separately for the individual phases. From this the low frequency sound speed for a suspension of particles was obtained. The effect of boundaries on multi-phase flow was discussed.

A more recent general theory is that of Dobran, which was used as the basis for the work of Margulies and Schwartz [1] [2] [3] [4]. Their two phase equations were written in a total and 'diffusive' (one phase relative to the other) form.

They looked at both infinitesimal and finite amplitude sound propagation in two phase media. In a formal sense, they considered the influence of processes such as radiation, viscoelasticity, chemical reactions between the phases, the Dufour effect (where heat is transported by diffusing particles) and phoresis. Phoresis refers to the diffusion of particles by gradients of temperature (thermophoresis), by gradients of pressure (barophoresis) by gradients of concentration of particles (pcynophoresis) or by external forces e.g. electrophoresis. Viscosity and heat conduction in the continuous phase (intrinsic absorption) were also included. Other coupled phase research has tended to neglect the intrinsic absorption, thus predicting the *excess* attenuation. The Margulies and Schwartz method for modelling the effect of particle diffusion on sound propagation is discussed in section 6. 5.

Culick [5] [6] [7] [8] [9] studied reverberant modes in combustion chambers which contain particles. In its general form the theory includes non-uniform flow and sources of mass, momentum and energy. These model, for instance, combustion and chemical reactions. Explicit cases considered were the effect of particles and viscous losses and heat transfer at the surfaces. More recently Vetter and Culick [15] [108] [109] calculated the frequency shifts, due to the presence of particles, of transverse modes in a pipe containing flowing pulverised coal in air.

The Culick theory is used in section 6. 4 to predict frequency shifts for low frequency transverse modes in a pipe containing a suspension. The predictions are compared to the results of an intuitive approach for calculating the frequency shifts using the Temkin and Dobbins theory.

Ahuja [110] [111] used momentum transfer terms for prolate and oblate spheroids executing translational oscillations in a fluid to study the influence of particle shape on the complex wavenumber. The spheroids were oriented with their axis of symmetry either parallel or perpendicular to the sound field. Modified Stokes drag, history and induced mass terms were included. Momentum and heat transfer terms used in coupled phase theory are reviewed in section 2. 5. 1 below. Ahuja showed that changing the shape and orientation of the particles, while keeping their volume fixed, can significantly alter the complex wavenumber. A more general theory would include particles with a distribution of orientations. The influence of non-spherical particles on the complex wavenumber is discussed in section 6. 3.

The theory of Atkinson and Kytomaa [13] [25] [112] [113] is identical to that of Harker and Temple except for the expression for the induced mass. References

[112] and [113] review and extend work on the volume fraction dependence of the induced mass, this work is discussed in section 6. 1. 3. Reference [113] derives high and low frequency expressions for the sound speed and attenuation. The expression for the high frequency limit of the sound speed contains the induced mass term. The high and low frequency expressions for the attenuation are usually assumed to be zero.

Strout [42] developed a model for the force on a sphere in a suspension in a sound field. The model includes hydrodynamic interactions between particles and is thus valid for high volume fractions. The modified expression for the drag force was used in the HT coupled phase theory. Predictions of the new theory, and predictions of the coupled phase theory using previous results for the high volume fraction drag, were compared to the attenuation measurements of Urick (see above). Predictions of multiple scattering theory were also compared to Urick's data. The new theory gave the closest agreement with the measurements. Predictions of Strout's theory are compared to experimental data and porous media theory predictions in section 6. 1. 2.

Pendse and Sharma [19] used the coupled phase theory derived by Strout to relate attenuation to particle size. This was the basis for their particle analysis system for solid-in-liquid suspensions. The technique is based on measurements of attenuation at frequencies between 1 and 100 MHz. This data is converted to particle size information by inverting an integral equation. The system provides reliable size distribution data for distributions of arbitrary functional form, for particle diameters between 0.01 and 100 μm and for volume fractions up to 0.5.

2. 3 Porous media theory

The development of porous media theories is described in detail in Allard's book [46].

2. 3. 1 Rigid frame theory

Kirchoff [114] provided the general theory for sound propagation in tubes including viscous and thermal effects. Weston [115] used the results of Kirchoff to define three main types of propagation in tubes. The tube is 'narrow' when the tube radius is much less than the boundary layer thickness. In a 'wide' tube the propagation approximates to that of an unbounded medium in the centre of the tube and viscous and thermal effects are confined to boundary layers near the walls. In a 'very wide' tube the sound energy is concentrated near the walls. Zwikker and Kosten [116] simplified the Kirchoff theory for circular tubes.

Stinson [117] showed how the viscous and thermal effects are related and generalised the work of Zwicker and Kosten to arbitrary tube cross-sections.

Craggs and Hildebrandt [118] [119] calculated the effective density (i.e. the viscous effect) for slits and tubes with circular, triangular, rectangular and hexagonal cross-sections using a finite element method. The effective density and bulk modulus (i.e. thermal effects) for a material containing a number of tubes (i.e. pores) can be derived from the definition of the flow resistivity and the porosity [46].

Biot [120] demonstrated that changing the frequency dependent parameter in the exact result for the effective density in cylindrical pores, via a shape factor, gives a good approximation to the exact result for slit shaped pores. It was assumed that this result extends to all cross-sectional shapes. Allard applied this result to the frequency dependence of the bulk modulus. The complex wavenumber for a porous media is given by $\omega\sqrt{\rho/K}$ where ρ and K are the frequency dependent effective density and bulk modulus respectively. Oblique pores can be accounted for by including a 'tortuosity' factor in the frequency parameter and the expressions for effective density and bulk modulus.

Attenborough [121] reviewed theoretical work and considered the effect of pore size distribution. The pore size distribution method of Yamamoto and Turgut [122] was extended via the method of Stinson to include thermal effects. For certain practical applications, pore size distribution has a more important influence on acoustical parameters than pore shape. The Attenborough theory is used in section 5. 2, with new measurements of pore size distribution, to predict the complex reflection coefficient of air saturated glass beads.

Permeability, or the related flow resistivity, is one of the bulk properties of a porous medium that can be measured. This can be done by measuring the pressure drop of air flowing through a sample of the medium. Heijs and Lowe [123] used a 'computed tomograph' image of the internal geometry of a clay soil in a numerical model of flow through the soil, to determine the permeability. The young marine clay was sampled in the field in 150 layers 1 mm apart. Each cylindrical layer had a radius of 12.3 cm. The spatial resolution in the horizontal plane was 0.27×0.27 mm. With the resolution used the data showed only one continuous pore from the top to the bottom of the sample. Flow occurring at a smaller scale was assumed negligible. Work on numerical modelling of flow through porous media was reviewed. The data was used in a 'lattice-Boltzmann' model of flow through the soil to determine the permeability and the 'Kozeny' constant in the Carman-Kozeny equation. These

quantities were also determined for a random array of spheres. For the spheres the Carman-Kozeny equation gave a good estimate of the permeability. For the soil the estimates were not so good. It was concluded that the specific surface area used in the Carman-Kozeny relation is not an appropriate length scale for all porous media.

2. 3. 2 Poroelastic theory

The general theory for propagation in poroelastic media, the Biot formalism, is also described in Allard's book [46]. This models the solid phase (the 'frame') as an elastic continuum. The frame can be 'consolidated', where the grains are welded together, or 'unconsolidated', where they are not joined together. The theory treats both the individual and coupled behaviour of the two phases. The general theory contains 13 parameters including the dynamic permeability, a pore size parameter, a structure factor (related to tortuosity) and the complex bulk and shear moduli of the frame. The latter two are defined for the frame, not the material making up the frame. The theory predicts three waves propagating in the porous medium. There are two compressional waves (the 'fast' and 'slow' wave) and a shear wave. Complex wavenumbers for these three waves can be obtained from the theory.

When the coupling between the two phases is small, such as in an air saturated solid, the fast wave is similar to an airborne wave propagating in a rigid frame. The slow wave and the shear wave are frame-borne and are similar to those that would occur if the frame was in a vacuum.

Berryman [124] compared predictions of the general Biot theory to the measurements of Plona on water-saturated consolidated glass beads. The frequency was 500 kHz, the grains had sizes between 210 and 290 μm and the porosity went up to 0.3. The theory successfully predicted the measured values of the speeds of the three types of wave.

Johnson and Plona [17] repeated the Plona experiments for both consolidated and unconsolidated glass beads. Consolidation can be achieved either by bonding or subjecting the material to a confining stress. Two compressional waves were observed in the consolidated medium. Only one is observed in the unconsolidated medium. This behaviour is successfully predicted by the Biot theory and is due to a change in the frame moduli. The unconsolidated medium corresponds very nearly to the frameless approximation and the consolidated medium is close to the rigid frame approximation.

Yamamoto and Turgut [122] included the effect of pore size distribution in the general Biot theory. The complex wavenumbers are independent of the effects of pore size distribution at the low and high frequency limits but strongly dependent in the intermediate region.

Leclaire *et al* [125] extended the Biot theory to frozen media, where there are three phases: water, ice particles and a solid frame. The theory predicts three compressional and two transverse modes. Velocities for the fastest longitudinal and transverse modes were measured for various samples as they were heated from -30°C to ambient temperature. The samples were (i) consolidated bronze beads with a grain size of approximately 160 μm, (ii) an unconsolidated glass powder with a grain size of approximately 100 μm and (iii) an unconsolidated silt with a grain size of approximately 30 μm. The glass powder showed a slight dispersion (change of velocity with frequency) between 100 and 800 kHz. Attenuation measurements showed the low and high frequency regimes predicted by the theory. The characteristic frequency where the two regimes meet shifts to lower frequencies with increasing temperature.

Nagy [126] measured the slow wave speed and attenuation in air-saturated porous ceramics and natural rocks. The frequencies were between 10 and 500 kHz and the samples were between 1 and 5 mm thick. For these conditions there is no fast wave transmission, it is reflected by the sample. The measurement technique is sensitive for materials with permeabilities as low as 100 mDarcy. The measured velocities agreed well with predictions of Attenborough's porous media theory [127] [128]. The measured attenuation agreed with the theoretical predictions at the low frequencies. At the high frequencies, however, the measurements were much higher than those predicted. The theoretical attenuation approaches a linear asymptote at high frequencies.

In a subsequent paper, Nagy [32] described measurements of the coherent and incoherent components of the waves transmitted through the samples. The work, similar to that of Page *et al* (see above), used a sharply focused receiver with a resolution of 1 mm at 250 kHz, which measured the field over a 2″×1.4″ area. Both incoherent and viscous losses account for the attenuation. The incoherent component of the wave cannot, however, account for the all of disagreement between the experiment and porous media theory which seems to be due to additional viscous losses.

2. 3. 3 Frameless theory

For suspensions, where the grains are isolated, the frame bulk and shear moduli in the general Biot theory go to zero and the theory is much simplified. This approximation will be called the frameless Biot theory. The frameless Biot theory predicts only one compressional wave. Kosten and Janssen [129] [116] developed a similar theory including elasticity in the solid phase of a porous material.

Ogushwitz [130] [131] used the frameless Biot theory. The permeability and pore size parameter were calculated in terms of the theoretical hydraulic radius for a material comprised of uniform spherical grains. These expressions were also used by Hovem [132]. The hydraulic radius is a function of grain diameter and porosity. The permeability is derived from the hydraulic radius by the Kozeny-Carman relation and involves a constant accounting for the tortuosity and shape of the pores. The pore size parameter is given by twice the hydraulic radius.

For the tortuosity, Ogushwitz used the expression derived by Berryman [124] in terms of the porosity and the induced mass of a sphere. For porosities near 1 the tortuosity may be assumed to be unity.

Ogushwitz compared his theoretical predictions with Hampton's measurements on kaolinite (aluminium silicate) particles in water. The frequency range was 4 to 600 kHz, the particles had a mean radius 1.2 μm and the volume fraction went up to 0.37. Good fits to the data were obtained with a permeability factor of 5. Hovem compared predictions of the same theory to the same data assuming the particle mean radius was 1 μm and the tortuosity was 1. A good fit was achieved with a permeability factor of 10. He also tested a single scattering theory, which severely overpredicted the attenuation. This is because, except at very low volume fractions, the viscous losses do not increase linearly with volume fraction as the scattering theory predicts. Predictions of the Biot theory also agree well with the measurements of Urick on aqueous kaolinite suspensions [131].

Hovem and Ingram [133] compared the frameless Biot theory with measurements in water saturated glass beads. The frequencies were between 10 and 300 kHz, the particles had a mean diameter of 180 μm and the porosity was 0.365. There was acceptable agreement between the experimental results and theoretical predictions.

Gibson and Toksoz [134] derived a coupled phase theory for suspensions which, excepting the expression for the viscous force, is equivalent to the

frameless Biot theory when the tortuosity is 1. Their expression for the viscous force uses the Biot relation, with the resistance to fluid flow derived from the Stokes drag of a single sphere. This is then modified for high volume fractions by the volume fraction dependent correction factor of Hasimoto (see section 6. 1. 2). Predictions of the theory agreed well with the data of Hampton and Urick and are close to the Biot theory predictions of Ogushwitz (see above). The relationship between the frameless Biot theory and coupled phase theory is investigated in chapter 5.

2. 4 Kramers-Kronig approach

Kramers-Kronig (K-K) theories make use of the Kramers-Kronig relations which state that, for a medium which is causal, linear and passive, the real and imaginary parts of the complex wavenumber are related by a pair of Hilbert transforms [23] [135]. Thus, in a given situation where the relations are applicable, the attenuation may be derived from a independent measurement of the velocity or vice versa.

O'Donnell *et al* [23] [136] derived approximate 'local' forms of the Kramers-Kronig relations valid when the attenuation and velocity are slowly varying functions of frequency. These were tested by comparison with the results of experiments in liquid solutions and polyethylene. The velocity predicted from the measured attenuation agreed well with the measured velocity.

Temkin [137] applied the method to dilute bubbly liquids. The sound speed was calculated from a formula for the attenuation. This agreed with expressions derived from other models. Approximate K-K relations can only be used in the regions away from resonance. Brauner and Beltzer [138] calculated the sound speed for bubbles in the resonance region from the scattering cross-section of the breathing mode.

Morfey and Howell [139] calculated the sound speed in air from the absorption due to vibrational relaxation. The results compared favourably with experimental data.

Nachman *et al* [140] derived a wave equation for a medium with relaxation losses. This equation verified the K-K conditions. The wave equation was then used for a scattering problem to determine the effects of relaxation on scattering.

The causality requirements of the K-K relations prompted Weaver [141] to investigate which multiple scattering theories obey causality.

Leander [45] showed that K-K and other theories implicitly require the non-interacting particles condition $\xi L \ll 1$, where ξ is the total plane wave attenuation coefficient. This is analogous to the condition for the validity of single scattering theories $N\sigma_0 L \ll 1$, where $N\sigma_0 L$ is the acoustic depth (see section 1. 2).

2. 5 Fluid dynamics

The implications for acoustics of the latest developments in the fluid dynamics of particulate media have yet to be explored. This section discusses work on the building blocks of the theories of the previous sections. The book 'Bubbles, Drops and Particles,' by Clift *et al* [142] is an invaluable review of work on flow, heat transfer and mass transfer for particles of all shapes, sizes and constitutions.

2. 5. 1 Momentum and heat transfer for a single particle

Most scattering and coupled phase theories assume that the viscous forces and heat transfer on a single particle in a suspension are the same as those on an isolated particle. This is strictly true only for low volume fractions.

The expression derived by Stokes for the force on an oscillating sphere in an incompressible viscous fluid which is at rest at infinity (i.e. it is at rest in the absence of the sphere) can be found in Landau and Lifshitz [143]. Mazur and Bedeaux [144] reviewed work on the force on a sphere and extended it to the case of a sphere with a time dependent velocity in a nonstationary and nonhomogeneous fluid flow.

Brenner [37] [145] [146] derived the low Reynolds number drag on an arbitrarily shaped body at any angle to a steady flow. Kanwal [147] derived the drag on an axially symmetric body slowly oscillating parallel to its axis. The result remains true for a body of arbitrary shape. Lai and Mockros [148] obtained equations of motion for oblate and prolate spheroids with a general acceleration time history in the axial direction. The force on the spheroids involves a steady-state drag, an induced mass effect and an effect due to the history of the motion. A coupled phase theory with spheroidal and cubic particles is developed in section 6. 3.

Achenbach [149] measured the drag on a rough sphere for Reynolds number Re between 5×10^4 and 2×10^6. The roughness is characterised by a roughness parameter, the ratio of the height of the roughnesses to the sphere diameter. This parameter varied between 2.5×10^{-4} and 1.25×10^{-2}. For the Reynolds numbers encountered in sound propagation through particulate media the effect of roughness should be negligible.

Michaelides and Feng [44] derived the energy equation for a rigid sphere in a viscous fluid subject to an unsteady flow and temperature field. There are three terms which control the rate of change of the temperature of the sphere. The first is analogous to the added mass term in the corresponding momentum equation. This represents the rate of flow of heat that would have entered the volume occupied by the sphere in its absence. The second accounts for the conduction from the sphere to the fluid due to temperature difference and the curvature of the temperature field. The temperature difference term is the usual steady state term analogous to the Stokes drag. The third term is a history integral which appears because of the temporal and spatial variation of the temperature field. This is analogous to the Bassett history term in the momentum equation.

2. 5. 2 Group of particles

A review of work up to 1965 on the fluid dynamics of suspensions can be found in the book 'Low Reynolds Number Hydrodynamics' by Happel and Brenner [37].

Kuwabara [150] calculated the low Reynolds number drag on an individual member of a random array of spheres or cylinders as a function of volume fraction. The Stokes approximation to the fluid dynamics equations was solved using boundary conditions on effective fluid spheres or cylinders concentric to the actual spheres or cylinders.

Sangani and Acrivos [38] did the same but more accurately for simple cubic, body-centred cubic and face-centred cubic arrays of spheres and periodic arrays of cylinders. The numerically derived expressions for the spheres (up to the order of ϕ^{10}) are valid up to the maximum volume fraction corresponding to the limit of a particular packing. Acrivos *et al* [151] [152] looked at the analogous heat transfer problem for regular and random arrays of spheres and periodic arrays of cylinders. The work assumed small Reynolds and Peclet numbers. The Peclet number Pe is given by $u_{\text{flow}} L_{\text{char}} \rho C_p / \tau$, where u_{flow} is the flow velocity and L_{char} is the characteristic dimension.

Kytomaa [25] [111] [112] reviewed volume fraction dependent drag and virtual mass terms.

The above workers assumed viscosity was independent of volume fraction. Zuber [153], who was looking at sedimentation, used expressions for volume fraction dependent viscosity and virtual mass. Work on viscosity was reviewed. The viscosity dependence on volume fraction at high volume fractions is due to

hydrodynamic interactions and collisions between the particles. In addition the viscosity can depend on the particle size distribution. Zuber briefly discussed the turbulent regime where the drag depends on Reynolds number. The Reynolds number will depend on the relative velocity between the two phases and the volume fraction dependent viscosity.

Batchelor [154] reviewed and advanced work on the volume fraction dependence of transport properties including viscosity. Mo and Sangani [155] included Stokes flow hydrodynamic interactions in a numerical scheme. Through particle boundary conditions this was applied to bubbles, drops and porous particles. The permeability, sedimentation velocity and viscosity were calculated for high volume fractions.

Strout [42] reviewed methods of calculating the drag on a sphere in a high volume fraction suspension. Previous 'cell' models were derived in the steady-state regime. Strout developed a new cell model allowing the spheres to oscillate. This model is valid at higher frequencies or, more specifically, at higher values of a/δ , where a is the sphere radius and δ is the viscous skin depth.

The above results for volume fraction dependent viscosity and drag are compared in section 6. 1.

2. 5. 3 Flow of particles

In many practical applications suspensions of particles are formed by flow of the suspending fluid. This section describes some examples of work in this field and work on scattering from flowing particles.

Hinze [156] worked out the conservation equations for a flowing homogeneous suspension. These were extended to the turbulent regime by applying Reynold's procedure. The equations were applied to vertical upward flow through a cylindrical tube. The velocity distribution was assumed uniform over the cross-section except near the walls.

Cox and Mason [157] reviewed theoretical and experimental work on the flow of particles in tubes, including non-spherical particles and the effect of volume fraction on the velocity distribution.

Crowe [158] defined the difference between 'dilute' and 'dense' gas-particle flows. The aerodynamic response time τ_A of a particle represents the time it takes a particle released from rest in a uniform gas flow field to achieve 63% of the gas velocity. The collision time τ_C is the time between collisions. This will be a representative value for all the particles and will depend on the particle

size distribution and the flow regime. If $\tau_A/\tau_C < 1$ the flow is dilute. In the dilute regime particles have time to respond to the local flow field, their motion can be said to be aerodynamically controlled. If $\tau_C/\tau_A < 1$ the flow is dense: the particle motion is governed by collisions.

The prediction of flow parameters for realistic situations will require numerical solution of the fluid dynamics equations. Crowe [159] reviewed numerical models for gas-particle flows. Giacinto *et al* [160] developed a numerical model for dilute gas-particle flows. This was applied to a duct with a sudden restriction, simulating a flow metering device. The coupling between the phases, the increase in pressure drop in the duct and the energy dissipation due to the drag of the particles were calculated.

Choi and Chung [161] developed a model for turbulent flow. τ_A was assumed to be much smaller than the time scale of the eddies. Predicted velocity profiles and friction factors were in good agreement with experimental data. The data included measurements on zinc powder flowing in a 5 cm diameter pipe at Re=53000. The particles had an average size of 15 μm and the maximum volume fraction was of the order of 10^{-2}.

Kumeran and Koch [162] [163] studied the low Reynolds number flow of a dilute bidisperse gas-particle suspension. The velocity distribution was obtained for high St. St is the Stokes number $=\tau_A/\tau_S$ where τ_S is the flow system time. The drag is given by Stokes law and particles interact only by solid body collisions, hydrodynamic interactions are neglected. The effect of hydrodynamic interactions is small compared to that of collisions in polydisperse suspensions at sufficiently high Stokes number. The study highlights the effects of particle collisions on velocity fluctuations. The regimes $\tau_C \ll \tau_A$ and $\tau_A \ll \tau_C$ were considered.

Atkinson and Kytomaa [13] developed an 'ultrasonic Doppler velocimeter'. It was shown that this instrument could measure the flow speed of aqueous suspensions of glass beads at near maximum volume fraction. A 200-500 kHz tone burst is emitted from a transducer at one side of a 10 cm diameter pipe. A receiver at the other side of the pipe detects a signal shifted in frequency due to the velocity of the scattering particles with respect to the incident ultrasound. The frequency shift is related to the flow velocity.

Hay [16] measured ultrasound attenuation and backscattering amplitude as functions of volume fraction, frequency and particle size for a particle-laden turbulent jet with a Reynolds number Re of about 1.8×10^4. Frequencies were

between 1 and 5 MHz and the particles had sizes between 100 and 500 μm. Two-point correlation estimates of jet velocity and measurements of the time averaged jet width as a function of particle size were related to the mean and turbulent structure of the jet.

Chapter 3
Scattering theory

Compressional wave scattering becomes significant for sound propagation in suspensions and emulsions when $k_f a \cong 1$, in this region continuum theories are not valid. This chapter begins by looking at lossless scattering, where only compressional waves in the two phases are considered. The general six wave scattering problem is presented in section 3. 2, for fluid or solid particles in a fluid. The $k_f a << 1$ 'long wavelength' solution to this problem is considered in detail. This is the region where both scattering theory and the coupled phase theories described in chapter 4 are applicable and can be compared.

The first step in the scattering approach calculates the scattering coefficients for a single particle. These coefficients have to be transformed into the complex wavenumber k for a plane wave in a fluid containing a number of these particles. This transformation is in the form of a single scattering or multiple scattering equation. The most often cited multiple scattering theories are compared in sections 3. 1. 1 and 3. 2. 11. Both the single and multiple scattering theories assume that for an incident plane wave the scattering medium can be replaced by a continuum. The attenuation and modified sound speed of k for the continuum represent the effect of scattering. This interpretation is only valid when the coherent wave is dominant. A basic treatment of incoherent scattering for particulate media, from Morse and Ingard [10], is discussed in section 3. 1. 2. Incoherent scattering is an important area of current research [24] [31] [32] [97].

3. 1 Lossless scattering

3. 1. 1 Long wavelength lossless scattering

A plane wave incident on a sphere will lose energy to scattering. This is commonly given in terms of the *scattering cross-section* σ_s, which is the total power scattered by the sphere divided by the incident plane wave's intensity. For a sphere of material with density ρ_s and compressibility κ_s in the long wavelength limit this is given by [10]

$$\sigma_s = \tfrac{4}{3}(\pi a^2)(k_f a)^4 \left[\tfrac{1}{3}\left(\frac{\kappa_s - \kappa_f}{\kappa_f} \right)^2 + \left(\frac{\rho_s - \rho_f}{2\rho_s - \rho_f} \right)^2 \right]. \tag{3.1}$$

The *plane wave attenuation coefficient* ξ_s of a plane wave propagating in a region containing a number N of these spheres for low volume fraction ϕ is given by

$$\xi_s = \frac{N\sigma_s}{2} = \frac{\phi k_f{}^4 a^3}{2} \left[\tfrac{1}{3}\left(\frac{\kappa_s - \kappa_f}{\kappa_f} \right)^2 + \left(\frac{\rho_s - \rho_f}{2\rho_s - \rho_f} \right)^2 \right]. \tag{3.2}$$

This is the single scattering result where the energies scattered by each sphere are summed.

σ_s is derived from the first two coefficients in the series representation of the scattered wave,

$$A_0 = \frac{i}{3}(k_f a)^3 \left(\frac{\kappa_s - \kappa_f}{\kappa_f} \right) \text{ and} \tag{3.3}$$

$$A_1 = \frac{i}{3}(k_f a)^3 \left(\frac{\rho_s - \rho_f}{2\rho_s + \rho_f} \right). \tag{3.4}$$

Equation (3.2) can be obtained from (3.3) and (3.4) using the expression for the *scattering* attenuation coefficient derived by Epstein and Cahart [47] (see section 3. 2. 7)

$$\xi_s = \tfrac{3}{2} \frac{\phi}{k_f{}^2 a^3} \sum_{n=0}^{\infty} (2n+1) |A_n|^2 . \tag{3.5}$$

The complex wavenumber

$$k = \omega/c + i\xi$$

gives the attenuation and modified sound speed (dispersion). Single and multiple scattering expressions for k in a medium containing a number of spheres have been reviewed by Twersky [63]. A commonly used expression is that originally derived by Urick and Ament

$$k^2 = k_f{}^2 + 4\pi N f(0) + \frac{4\pi^2 N^2}{k_f{}^2}\left[f^2(0) - f^2(\pi)\right] \tag{3.6}$$

$$f(0) = \frac{1}{ik_f}\sum_{n=0}^{\infty}(2n+1)A_n$$

$$f(\pi) = \frac{1}{ik_f}\sum_{n=0}^{\infty}(-1)^n(2n+1)A_n\,.$$

This is a multiple scattering theory in that it accounts for the fact that the wave scattered from each sphere will be re-scattered. The multiple scattering results in the N^2 term. Equations (3.6) have also been derived by Twersky and Waterman and Truell [73]. They will be referred to here as the Waterman and Truell (WT) theory.

Using just the first two terms A_0 and A_1 (3.6) becomes

$$k^2 = k_f{}^2 + \frac{4\pi N}{ik_f}(A_0 + 3A_1) - \frac{48\pi^2 N^2}{k_f{}^4}A_0A_1. \tag{3.7}$$

In this approximation the terms in $|A_n|^2$ or $A_nA_n^*$, where the asterisk indicates complex conjugate, disappear. Multiple scattering is represented by the A_0A_1 term. Equation (3.7) neglects the scattering attenuation represented by (3.5) or (3.2). Since A_0 and A_1 are purely imaginary ξ is 0 in (3.7). The modified sound speed given by (3.7) is

$$c^{-2} = c_f{}^{-2}\left[1+\phi\left(\frac{\kappa_s-\kappa_f}{\kappa_f}\right)\right]\left[1+3\phi\left(\frac{\rho_s-\rho_f}{2\rho_s+\rho_f}\right)\right]. \tag{3.8}$$

Assuming $\rho_s \to \rho_f$ (3.8) becomes

$$c^{-2} = \kappa_{va}\rho_{va}\,.$$

This expression was originally used by Urick [104]. It is a low frequency limiting case for the coupled phase theories of chapter 4.

The long wavelength limit of the multiple scattering theory of Ma *et al* (Ma) [75] does predict an attenuation. Their expressions for the sound speed and attenuation are

$$c^{-2} = c_f{}^{-2}\frac{(1+\phi\lambda_\kappa)(1-\phi\lambda_\rho)}{1+2\phi\lambda_\rho} \tag{3.9}$$

$$\xi = \frac{k_f{}^4a^3\phi}{6}\frac{(1-\phi)^4}{(1+2\phi)^2}\left[\frac{(1+\phi\lambda_\kappa)(1-\phi\lambda_\rho)}{1+2\phi\lambda_\rho}\right]^{\frac{1}{2}}\left(\frac{\lambda_\kappa{}^2}{1+\phi\lambda_\kappa}+\frac{3\lambda_\rho{}^2}{1+2\phi\lambda_\rho(1-\phi\lambda_\rho)}\right)$$

$$\lambda_\kappa = \frac{\kappa_s - \kappa_f}{\kappa_f} \qquad \lambda_\rho = \frac{\rho_f - \rho_s}{2\rho_s + \rho_f}.$$

The Ma expression for the attenuation reduces to (3.2) in the low ϕ limit i.e. if $2\phi, \kappa\phi, 2\phi\rho \ll 1$.

The attenuations predicted by (3.2) and (3.9) are compared to the experimental data of Atkinson and Kytomaa [13] in figure 3. 1. Atkinson and Kytomaa measured the attenuation and sound speed for 1 mm diameter glass beads in water for frequencies between 100 kHz and 1 MHz, and volume fractions up to 0.62. The density ratio (glass to water) is 2.5 and the compressibility ratio is 0.11. Figure 3. 1 shows the theoretical attenuation per wavelength ξ/k_f and the data at 200 kHz and 400 kHz; these are plotted versus volume fraction. The attenuation given by expression (3.2) is proportional to volume fraction and is only valid at low volume fractions. The attenuation given by the Ma expression reaches a maximum and falls off at the higher volume fractions. The two theoretical expressions agree when $\phi \ll 1$. The Ma theory is closest to the data but it is only satisfactory at the low volume fractions.

Figure 3. 2 shows the sound speed relative to that in water versus volume fraction predicted by the WT (3.8) and Ma (3.9) theories, and the Atkinson and Kytomaa data. Again, the Ma theory is closest to the data; the agreement is reasonably good.

Atkinson and Kytomaa compared their measurements to the predictions of a coupled phase theory that only included viscous losses. There was a complete lack of agreement between the experimental data and theoretical predictions. The attenuation prediction was approximately two orders of magnitude below the measured attenuation over the whole range of ϕ. The sound speed prediction showed a minimum, with $c < c_f$, while the data shows $c > c_f$ for all ϕ.

Better agreement with the data could be obtained by using the multiple scattering theory with the full series representation of the scattered wave. This is valid for higher $k_f a$. The numerical solution of this has been discussed by Tsang *et al* [164]. The full solution predicts, as the volume fraction increases, a higher attenuation and a lower sound speed than those predicted by the long wavelength solution. These corrections will give better agreement with the data shown in figures 3. 1 and 3. 2.

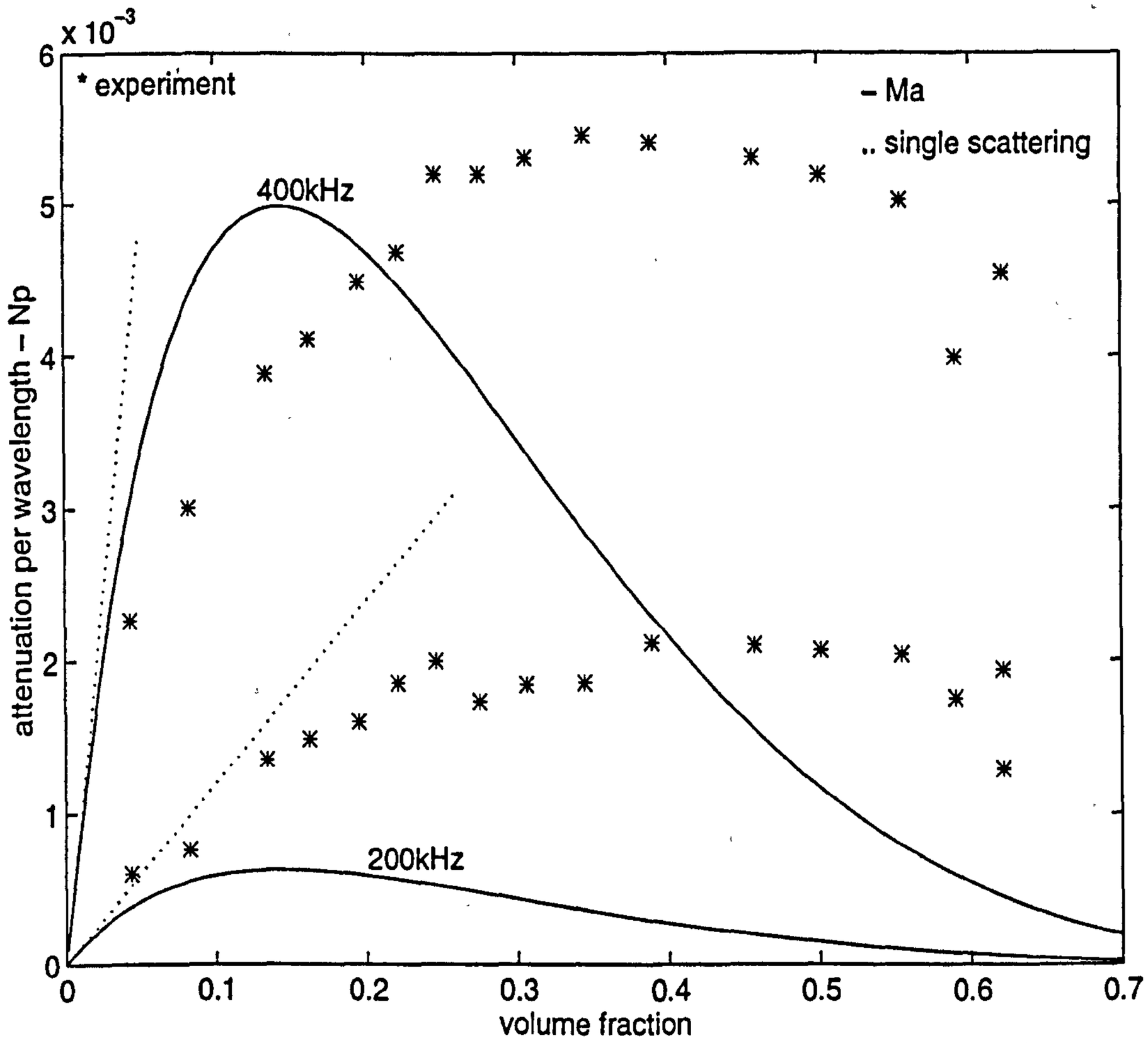

Figure 3. 1 Attenuation per wavelength versus volume fraction for 1 mm diameter glass beads in water. Comparison of data of Atkinson and Kytomaa and predictions of single and multiple scattering theories.

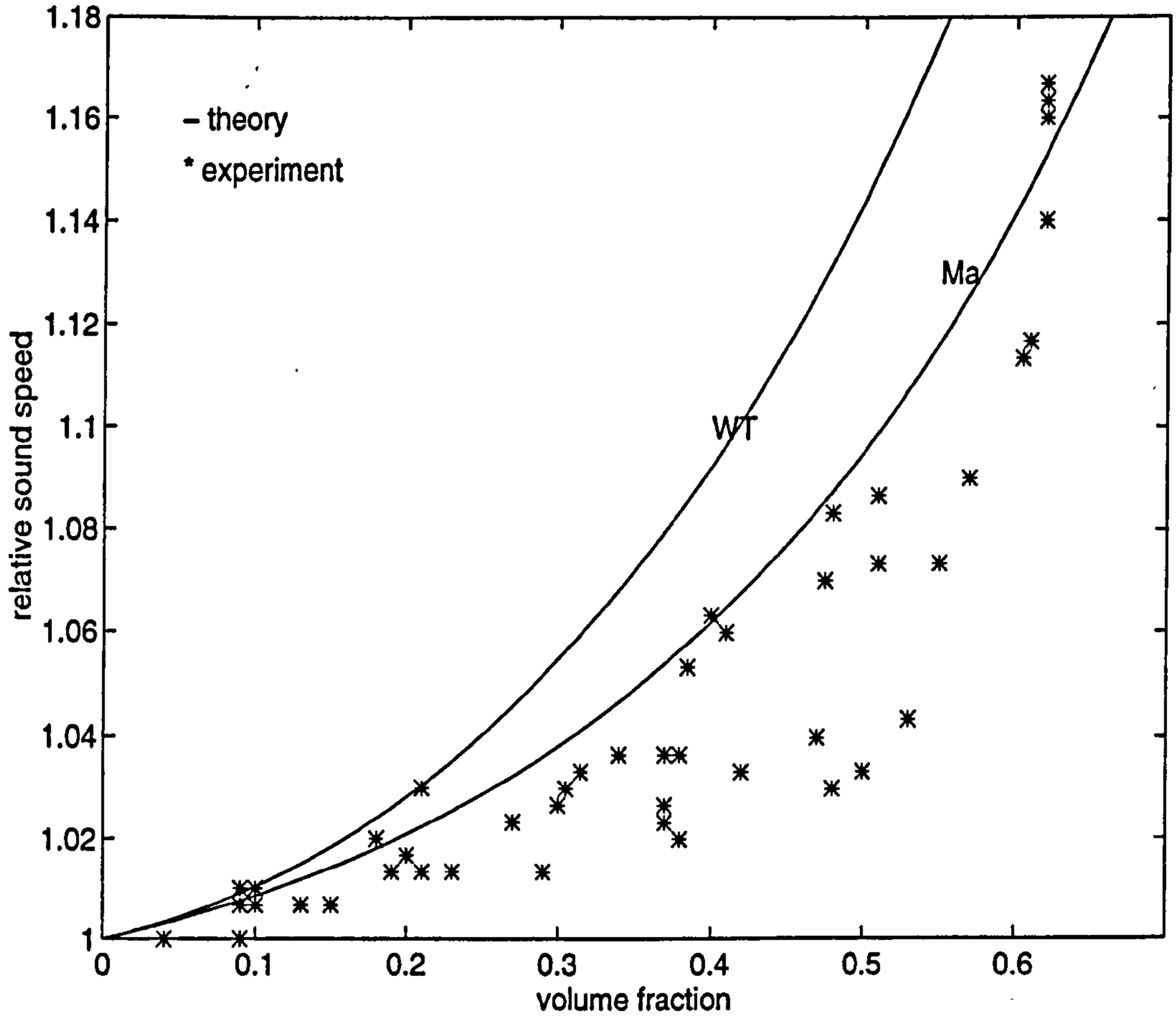

Figure 3. 2 Relative sound speed versus volume fraction for 1 mm diameter glass beads in water, frequencies 100 kHz to 1 MHz. Comparison of data of Atkinson and Kytomaa and predictions of multiple scattering theories.

3. 1. 2 Incoherent scattering

The above work concerns that part of the scattered field that combines coherently with the incident plane wave to form a new plane wave. The remainder of the scattered field combines incoherently i.e. as if the separate contributions have a random phase relationship to each other.

Twersky [63] [67] applied energy considerations to the multiple scattering problem to evaluate the incoherent energy flux. It was confirmed that for lossless scatterers the energy lost by the coherent wave equals the energy in the incoherent field.

In this section the emphasis is on the incoherently scattered field rather than the plane wave coherent field. The quantity of interest is the angular dependence of the scattered intensity, particularly in the forward and backward directions. The Born approximation is used so multiple scattering is neglected.

Morse and Ingard [10] discuss scattering from a region R containing a number of spherical scatterers with varying properties. The scatterers occupy the region S. The nth sphere has radius a_n, compressibility κ_n and density ρ_n and its centre is at $\mathbf{r}_n$.

The wave equation inside and outside R is

$$\nabla^2 p - \frac{1}{c_f^{\,2}}\frac{\partial^2 p}{\partial t^2} = \frac{1}{c_f^{\,2}}\frac{\partial^2 p}{\partial t^2}\gamma_\kappa(\mathbf{r},t) + \nabla\cdot\left[\gamma_\rho(\mathbf{r},t)\nabla p\right] \tag{3.10}$$

where

$$\gamma_\kappa(\mathbf{r}) = \begin{cases} \dfrac{\kappa_n - \kappa_f}{\kappa_f} & \mathbf{r}\in S \\ 0 & \mathbf{r}\notin S \end{cases} \text{ and } \gamma_\rho(\mathbf{r}) = \begin{cases} \dfrac{\rho_n - \rho_f}{\rho_n} & \mathbf{r}\in S \\ 0 & \mathbf{r}\notin S \end{cases}$$

The equation for the scattering of a single frequency incident plane wave $p_i(\mathbf{r})$ from R is

$$p(\mathbf{r}) = p_i(\mathbf{r}) + \int_R \left(k_f^{\,2}\gamma_\kappa(\mathbf{r}_0)p(\mathbf{r}_0)g(\mathbf{r}|\mathbf{r}_0) + \gamma_\rho(\mathbf{r})\nabla_0 p(\mathbf{r}_0)\cdot\nabla_0 g(\mathbf{r}|\mathbf{r}_0)\right)dV_0$$

where $p(\mathbf{r})$ is the total pressure and g is the Green's function for an unbounded medium

$$g(\mathbf{r}|\mathbf{r}_0) = \frac{\exp\left(ik_f|\mathbf{r}-\mathbf{r}_0|\right)}{4\pi|\mathbf{r}-\mathbf{r}_0|}.$$

Subscript zeros indicate quantities inside R.

The mean values of γ_κ and γ_ρ are

$$\sum_n \tfrac{4}{3}\pi a_n{}^3\left(\frac{\kappa_n}{\kappa_f}-1\right) \text{ and } \sum_n \tfrac{4}{3}\pi a_n{}^3\left(1-\frac{\rho_f}{\rho_n}\right)$$

respectively. Inserting these in (3.10) and rearranging gives an homogeneous wave equation for sound waves in R with an effective density and compressibility

$$\rho_R=\left[\frac{1}{\rho_f}+\sum_{n=1}^{N}\tfrac{4}{3}\pi a_n{}^3\left(\frac{1}{\rho_n}-\frac{1}{\rho_f}\right)\right]^{-1} \quad \kappa_R=\kappa_f+\sum_{n=1}^{N}\tfrac{4}{3}\pi a_n{}^3\left(\kappa_n-\kappa_f\right). \tag{3.11}$$

The effective compressibility is the volume averaged compressibility and the effective density is the reciprocal of the volume averaged specific volume.

These quantities are responsible for the coherent scattering. The coherent scattered wave is that which would be scattered from the region R if it had uniform properties ρ_R and κ_R.

The angle distribution function $\Phi(\theta)$ from a spherical scatterer in the long wavelength regime is given by

$$\Phi(\theta)=\tfrac{1}{3}k_f{}^2a^3\left(\frac{\kappa_s-\kappa_f}{\kappa_f}+3\frac{\rho_s-\rho_f}{2\rho_s+\rho_f}\cos\theta\right)$$

and the far-field pressure is given by

$$p(r,\theta)=A_i\frac{e^{ik_f r}}{r}\Phi(\theta).$$

For the nth scatterer in R, the scattered wave at a position $\mathbf{r}$ a large distance from R can be written as

$$\tfrac{4}{3}\pi a_n{}^3\left(\lambda_{\kappa n}+\lambda_{\rho n}\cos\theta\right)k_R{}^2p(\mathbf{r}_n)\frac{e^{ik_R R_n}}{4\pi R_n} \tag{3.12}$$

where

$$\lambda_{\kappa n}=\frac{\kappa_n-\kappa_R}{\kappa_R},\ \lambda_{\rho n}=3\frac{\rho_n-\rho_R}{2\rho_n+\rho_R},$$

$k_R=\omega\sqrt{\rho_R\kappa_R}$ and $R_n=|\mathbf{r}-\mathbf{r}_n|$. p is the pressure amplitude at the scatterer. The factors $\lambda_{\kappa n}$ and $\lambda_{\rho n}$ can be incorporated into the function

$$\delta(\mathbf{r})=\lambda_\kappa(\mathbf{r})+\lambda_\rho(\mathbf{r})\cos\theta$$

where

$$\lambda_\kappa(\mathbf{r})=\frac{\kappa_n-\kappa_R}{\kappa_R},\lambda_\rho(\mathbf{r})=3\frac{\rho_n-\rho_R}{2\rho_n+\rho_R}\quad \mathbf{r}\in S$$
$$\lambda_\kappa(\mathbf{r})=\frac{\kappa_f-\kappa_R}{\kappa_R},\lambda_\rho(\mathbf{r})=3\frac{\rho_f-\rho_R}{2\rho_f+\rho_R}\quad \mathbf{r}\notin S$$

which has an average value of zero in R. $\delta(\mathbf{r})$ has a correlation function

$$\chi(\mathbf{d})=\frac{1}{V_R}\int_R\delta(\mathbf{r})\delta(\mathbf{r}+\mathbf{d})dV,$$

where V_R is the volume of R. $\chi(0)$ is the mean square value of $\delta(\mathbf{r})$ which can be approximated by

$$\langle\delta^2\rangle\cong\langle N\rangle\left(\tfrac{4}{3}\pi\right)\langle a\rangle^3\left|\langle\lambda_{\kappa nf}\rangle+\langle\lambda_{\rho nf}\rangle\cos\theta\right|^2 \tag{3.13}$$

where the angle brackets indicate mean values in R and

$$\lambda_{\kappa nf}=\frac{\kappa_n-\kappa_f}{\kappa_n},\quad \lambda_{\rho nf}=3\frac{\rho_n-\rho_f}{2\rho_n+\rho_f}.$$

Since $\langle\delta\rangle=0$ the integral of χ over R must be zero. This means it must have a negative portion. With an exponential decay, a simple form for $\chi(\mathbf{d})$ is

$$\chi(\mathbf{d})=\langle\delta^2\rangle\left(1-\frac{d^2}{3\langle a\rangle^2}\right)\exp\left(-\tfrac{1}{2}\frac{d^2}{\langle a\rangle^2}\right).$$

If $N\sigma_0 L$ is small, multiple scattering is negligible and the Born approximation may be applied. The amplitude of the wave incident on the scatterers, $p(\mathbf{r}_n)$ in (3.12), is assumed to be the incident wave amplitude A_i and is the same for all the scatterers. This condition will be satisfied if the volume fraction is low or if the volume of R is small.

The sum of all the terms (3.12) can be transformed to give an integral for the incoherently scattered far-field pressure

$$p_s(\mathbf{r})=\frac{A_i e^{ik_f r}}{4\pi r}\int_R\delta(\mathbf{r}_0)e^{-i\mathbf{m}\cdot\mathbf{r}_0}dV$$

where $\mathbf{m}=\mathbf{k}_s-\mathbf{k}_i$. $\mathbf{k}_s$ is a vector in the direction of the scattered wave with magnitude k_R and $\mathbf{k}_i$ is a vector in the direction of the incident wave with the same magnitude. It has been assumed $R_n\cong r$, the magnitude of $\mathbf{r}$. The magnitude of $\mathbf{m}$ is given by

$$m=2k_R\sin\frac{\theta}{2} \tag{3.14}$$

where θ is the angle between $\mathbf{k}_s$ and $\mathbf{k}_i$.

The incoherently scattered intensity divided by the incident intensity $|A_i|^2/\rho_f c_f$ is

$$\frac{I_s}{I_i}=\frac{4\pi^4 k_R{}^2}{r^2}|\Delta(\mathbf{m})|^2$$

where $\Delta(\mathbf{K})$ is the Fourier transform defined by

$$\Delta(\mathbf{K})=\frac{1}{8\pi^3}\int_R \delta(\mathbf{r})e^{-i\mathbf{K}\cdot\mathbf{r}}dV\,.$$

It can be shown that

$$|\Delta(\mathbf{K})|^2=\frac{V_R}{64\pi^6}\int_R \delta(\mathbf{d})e^{-i\mathbf{K}\cdot\mathbf{d}}dV=\langle\delta^2\rangle\frac{V_R K^2 a^5}{3(2\pi)^{\frac{9}{2}}}e^{-\frac{1}{2}K^2a^2}$$

and thus

$$\frac{I_s}{I_i}=\frac{V_R k_R{}^4 m^2 a^5}{12\sqrt{2\pi}r^2}\langle\delta^2\rangle e^{-\frac{1}{2}m^2a^2} \qquad (3.15)$$

where m is given by (3.14) and $\langle\delta^2\rangle$ is given by (3.13). Here a is the mean radius.

From (3.13) the incoherently scattered intensity is proportional to N. This distinguishes it from the coherent scattering where the intensity is proportional to N^2.

The angular dependence of (3.15) is contained in the terms

$$\left|1+\frac{\langle\lambda_{\rho nf}\rangle}{\langle\lambda_{\kappa nf}\rangle}\cos\theta\right|^2\sin^2\left(\frac{\theta}{2}\right)\exp\left(-2k_R{}^2a^2\sin^2\frac{\theta}{2}\right),$$

this expression is plotted versus θ in figure 3. 3 for

$$\frac{\langle\lambda_{\rho nf}\rangle}{\langle\lambda_{\kappa nf}\rangle}=2 \text{ and } 0.5\,.$$

It has been assumed that $k_R a=1$.

If the intensities of the wavelets given by (3.12) are summed, i.e. the effect of their relative positions is neglected, the scattered intensity is given by

$$\frac{I_s}{I_i}\cong\tfrac{1}{9}NV\frac{k_f{}^4a^6}{r^2}\left|\langle\lambda_{\kappa nf}\rangle+\langle\lambda_{\rho nf}\rangle\cos\theta\right|^2.$$

Here N is the mean number of scatterers per unit volume.

The angular dependence of this expression is also shown in figure 3. 3. This is not to scale. It is seen that the interference between the wavelets reduces the intensity of the scattered wave in the forward direction.

A similar method to the one presented by Morse and Ingard is the basis for the multiple scattering theory of Liu [93] [94] [95]. First, an homogeneous wave equation is derived for the mean properties of the scattering region. Liu spatially averaged the sound speed *c*, rather than the density and compressibility as in equations (3.11). The fluctuating part is represented by a discontinuous stochastic field $\beta(\mathbf{r})$ analogous to $\delta(\mathbf{r})$ above. The mean square value of the scattered field is obtained in terms of the spatial correlation function of $\beta(\mathbf{r})$. Instead of assuming an expression for this, as Morse and Ingard did for $\chi(\mathbf{d})$ above, Liu used geometrical probability. The spatial correlation function is derived in terms of the volume fraction, the particle radius and the sound speeds of the two phases. Analytical results were obtained for the scattering of impulsive sound when $|c_f - c_s| \ll c_f$ and c_s.

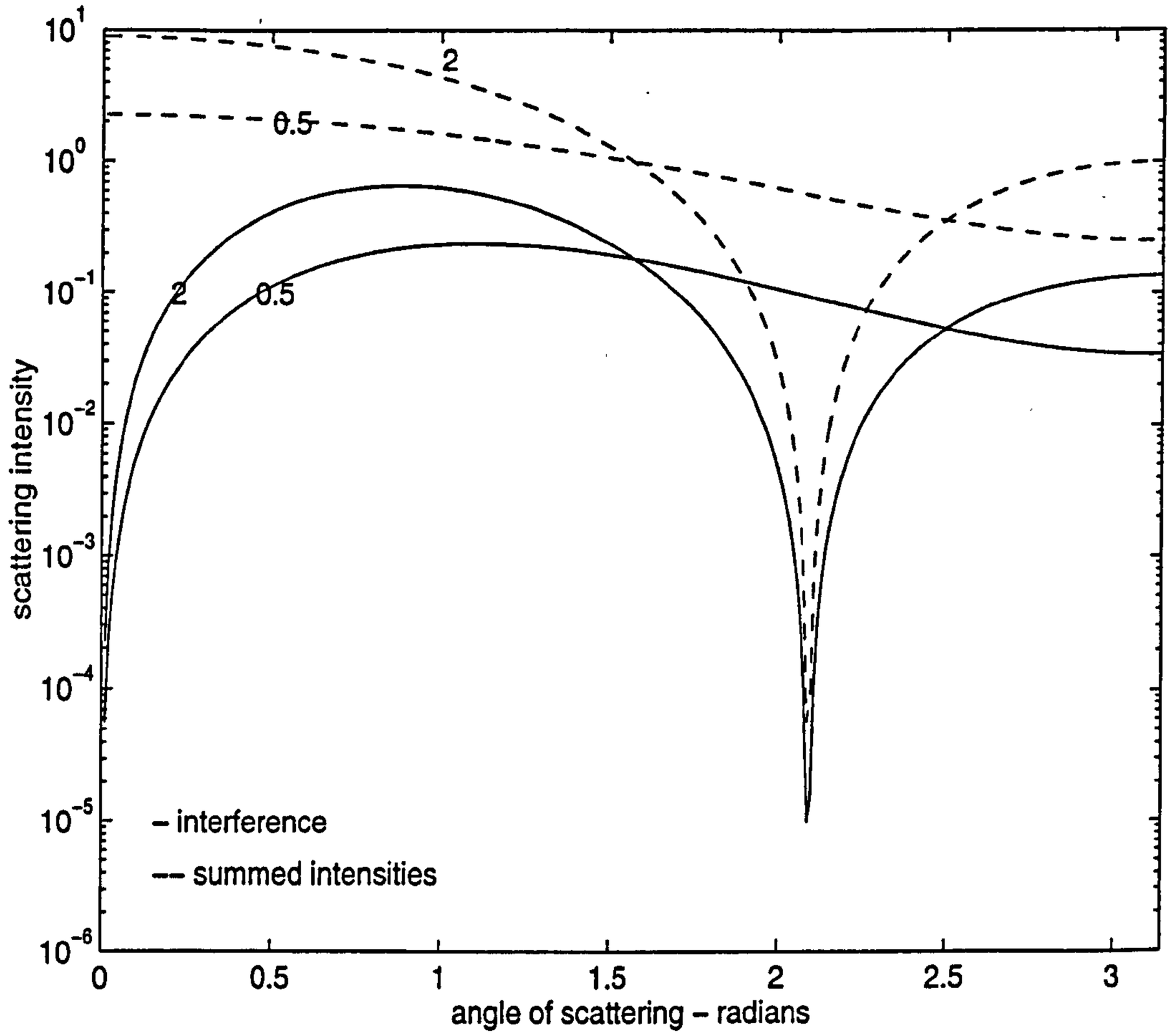

Figure 3. 3 Angular dependence of scattered intensity from region containing spherical scatterers with ratio of mean λ factors 2 and 0.5. Comparison of angular dependence when interference is included and when individual scatterer intensities are summed.

3. 2 Viscothermal scattering

3. 2. 1 Viscothermal fluid

The linear acoustic equations for a viscothermal fluid including bulk viscosity are (from Pierce, Chapter 10 [41])

$$\frac{\partial \rho}{\partial t} + \rho^0 \nabla \cdot \mathbf{u} = 0, \tag{3.16}$$

$$\rho^0 \frac{\partial \mathbf{u}}{\partial t} = -\nabla p + \mu_B \nabla(\nabla \cdot \mathbf{u}) + \mu\left[\nabla^2 \mathbf{u} + \tfrac{1}{3}\nabla(\nabla \cdot \mathbf{u})\right] \text{ and} \tag{3.17}$$

$$\rho^0 T^0 \frac{\partial s}{\partial t} = \tau \nabla^2 T. \tag{3.18}$$

Using the relations

$$\rho' = \frac{1}{c^2} p' - \left(\frac{\rho \beta T}{C_p}\right)_0 s' \text{ and}$$

$$T' = \left(\frac{T\beta}{\rho C_p}\right)_0 p' + \left(\frac{T}{C_p}\right)_0 s'$$

to eliminate ρ and s from equations (3.16) to (3.18) and representing $\mathbf{u}$ in terms of a scalar velocity potential ϕ and a vector potential ψ_k

$$\mathbf{u} = -\nabla\phi + \nabla \times \psi_k \text{ with } \nabla \cdot \psi_k = 0,$$

equations (3.16) to (3.18) can be expressed as the field equations given by Lin and Raptis [52]:

$$\frac{\partial^2 \phi}{\partial t^2} - \frac{\beta c^2}{\gamma}\frac{\partial T}{\partial t} = \left[\frac{c^2}{\gamma} + b\frac{\partial}{\partial t}\right]\nabla^2 \phi \tag{3.19}$$

$$\frac{\partial T}{\partial t} = \frac{\tau}{\rho^0 C_v}\nabla^2 T + \frac{\gamma - 1}{\beta}\nabla^2 \phi \text{ and} \tag{3.20}$$

$$\frac{\partial \psi_k}{\partial t} = \nu \nabla^2 \psi_k. \tag{3.21}$$

These are also the equations used by Epstein and Cahart [47] (their equations 5.15).

The constant b is given by

$$b = \tfrac{4}{3}\nu + \mu_B/\rho.$$

Eliminating ϕ or T between equations (3.19) and (3.20) shows that the scalar velocity potential and the temperature satisfy the same field equation

$$c^2\left(\sigma\nabla^2-\frac{\partial}{\partial t}\right)\nabla^2\left\{\begin{matrix}\phi\\T\end{matrix}\right\}+\left[b\frac{\partial}{\partial t}\nabla^2-\frac{\partial^2}{\partial t^2}\right]\left(\gamma\sigma\nabla^2-\frac{\partial}{\partial t}\right)\left\{\begin{matrix}\phi\\T\end{matrix}\right\}=0. \qquad (3.22)$$

3. 2. 2 Fluid Helmholtz equations

Assuming $\exp(-i\omega t)$ harmonic time dependence for ψ_k (3.21) can be rewritten as

$$\left(\nabla^2+{k_{f3}}^2\right)\psi_k=0$$

where k_{f3}, the wavenumber for the viscous shear wave is given by

$$k_{f3}=\frac{1+i}{\delta}.$$

δ is the viscous skin depth or viscous boundary layer thickness and is given by

$$\delta=\sqrt{\frac{2\mu}{\rho\omega}}.$$

Helmholtz equations for the compressional and thermal waves can be obtained from (3.22) by putting $\phi=\phi_c+\phi_t$ where ϕ_c is the velocity potential of the compressional wave and ϕ_t is the velocity potential of the thermal wave. The wavenumber of the compressional wave k_{f1} and the wavenumber of the thermal wave k_{f2} are given by [52]

$$k_{f1}=\frac{c}{2\omega}\left[\left(1-\varepsilon_h-\gamma\varepsilon_h+2i\sqrt{\varepsilon_h+\gamma\varepsilon_h\varepsilon}\right)^{\frac{1}{2}}+\left(1-\varepsilon-\gamma\varepsilon_h-2i\sqrt{\varepsilon_h+\gamma\varepsilon_h\varepsilon}\right)^{\frac{1}{2}}\right]$$

$$k_{f2}=\frac{c}{2\omega}\left[\left(1-\varepsilon_h-\gamma\varepsilon_h+2i\sqrt{\varepsilon_h+\gamma\varepsilon_h\varepsilon}\right)^{\frac{1}{2}}-\left(1-\varepsilon-\gamma\varepsilon_h-2i\sqrt{\varepsilon_h+\gamma\varepsilon_h\varepsilon}\right)^{\frac{1}{2}}\right] \qquad (3.23)$$

$$\varepsilon=\frac{2i\omega^2}{3c^2}{\delta_b}^2 \qquad \varepsilon_h=\frac{i\omega^2}{2c^2}{\delta_h}^2$$

where δ_b is δ with μ replaced with $\mu+\frac{3}{4}\mu_B$ and δ_h is the thermal skin depth or thermal boundary layer thickness

$$\delta_h=\sqrt{\frac{2\tau}{\rho\omega C_p}}.$$

Usually ε and ε_h are small and equations (3.23) are approximated by

$$k_{f1}=\frac{\omega}{c}+\frac{i\omega^3}{c^3}\left(\frac{{\delta_b}^2}{3}+\frac{(\gamma-1){\delta_h}^2}{4}\right)$$

$$k_{f2}=\frac{1+i}{\delta_h}.$$

The imaginary part of k_{f1} is the 'classical' absorption of a fluid.

3. 2. 3 Thermoelastic solid

Wave propagation in thermoelastic solids is discussed in Thurston [165]. Allegra and Hawley [49] extended the EC theory for a fluid continuous phase and a solid particulate phase. Their solid phase field equations can be written as

$$\frac{\partial^2\Phi}{\partial^2 t}-\frac{\beta c_{sph}{}^2}{\gamma}T=\left[\frac{c_{sph}{}^2}{\gamma}+\tfrac{4}{3}\frac{\mu_e}{\rho^0}\right]\nabla^2\Phi, \tag{3.24}$$

$$\frac{\partial T}{\partial t}=\gamma\sigma\nabla^2 T+\frac{\gamma-1}{\beta}\nabla^2\frac{\partial\Phi}{\partial t} \text{ and} \tag{3.25}$$

$$\frac{\partial^2\Psi_k}{\partial t^2}=c_2{}^2\nabla^2\Psi_k. \tag{3.26}$$

Here the solid element displacement **d** has been written in terms of a scalar potential Φ and a vector potential Ψ_k via the expressions

$$\mathbf{d}=-\nabla\Phi+\nabla\times\Psi_k \text{ and } \nabla\cdot\Psi_k=0.$$

The constant c_{sph} is the speed of sound for a spherical compressional wave in an elastic isotropic solid and is given by

$$c_{sph}{}^2=\left(\lambda_e+\tfrac{2}{3}\mu_e\right)/\rho=K/\rho$$

where K is the bulk modulus. c_2, the speed of shear waves in the solid, is given by

$$c_2{}^2=\mu_e/\rho.$$

Equations (3.24) to (3.26) can be obtained from the fluid versions (3.19) to (3.21). This is achieved by replacing μ with $\mu_e/-i\omega$, c with c_{sph}, ϕ with $\partial\Phi/\partial t$, neglecting μ_B and employing the equation

$$\frac{\partial}{\partial t}=-i\omega$$

which is valid for harmonic variations of the field variables with time.

Lin and Raptis [52] point out that the AH equations are only valid for isothermal deformations of a solid and replace equation (3.24) with

$$\frac{\partial^2\Phi}{\partial^2 t}-\beta c_{sph}{}^2T=c_1{}^2\nabla^2\Phi. \tag{3.27}$$

c_1, the speed of longitudinal waves, is given by

$$c_1{}^2=\left(\lambda_e+2\mu_e\right)/\rho.$$

3. 2. 4 Solid Helmholtz equations

The Helmholtz equation for the elastic shear wave from (3.26) is

$$\left(\nabla^2 + {k_{s3}}^2\right)\Psi_k = 0$$

where k_{s3}, the wavenumber of the elastic shear wave, is given by

$k_{s3} = \omega / c_2$.

As for the fluid, the temperature and displacement potentials in the solid satisfy the same equation. This is derived from (3.25) and (3.27):

$$\left(\gamma\sigma\nabla^2 - \frac{\partial}{\partial t}\right)\left(\frac{\partial^2}{\partial t^2} - {c_1}^2\nabla^2\right)\begin{Bmatrix}\Phi\\ T\end{Bmatrix} + (\gamma - 1){c_{\text{sph}}}^2\frac{\partial}{\partial t}\nabla^2\begin{Bmatrix}\Phi\\ T\end{Bmatrix} = 0.$$

Putting $\Phi = \Phi_c + \Phi_t$, where Φ_c is the displacement potential of the elastic compressional wave and Φ_t is the displacement potential of the thermal wave, and assuming harmonic time dependence obtains

$$\left(\nabla^2 + {k_{s1}}^2\right)\Phi_c = 0$$

$$\left(\nabla^2 + {k_{s2}}^2\right)\Phi_t = 0.$$

Here k_{s1} and k_{s2} are the wavenumbers for the elastic compressional and thermal waves respectively. They are given by [52]

$$k_{s1} = \frac{\omega}{2c_1}\left\{\left[1 + i\varepsilon_{s1}(1+\varepsilon_{s2}) + (1+i)\sqrt{2\varepsilon_{s1}}\right]^{\frac{1}{2}} + \left[1 + i\varepsilon_{s1}(1+\varepsilon_{s2}) - (1+i)\sqrt{2\varepsilon_{s1}}\right]^{\frac{1}{2}}\right\}$$

$$k_{s1} = \frac{\omega}{2c_1}\left\{\left[1 + i\varepsilon_{s1}(1+\varepsilon_{s2}) + (1+i)\sqrt{2\varepsilon_{s1}}\right]^{\frac{1}{2}} - \left[1 + i\varepsilon_{s1}(1+\varepsilon_{s2}) - (1+i)\sqrt{2\varepsilon_{s1}}\right]^{\frac{1}{2}}\right\}$$

$$\varepsilon_{s1} = \frac{\rho\gamma {c_1}^2}{\omega\tau} \qquad \varepsilon_{s2} = \frac{(\gamma - 1){c_{\text{sph}}}^2}{\rho {c_1}^2}.$$

(3.28)

For most solids $\gamma \approx 1$ so $\varepsilon_{s2} \to 0$ and equations (3.28) can be approximated by

$$k_{s1} = \frac{\omega}{c_1} \qquad k_{s2} = \frac{1+i}{\delta_h}.$$

3. 2. 5 Scattering from a single sphere

The scattering problem will be studied for a fluid continuum and a fluid particle. This is simpler than a solid particle in a fluid continuum. The experimental data used later to compare to the theoretical predictions are either for emulsions, which are fluid-fluid, or for suspensions at low $k_f a$. For the suspensions the particles may be assumed to be incompressible so the description of the sound propagation in the material of the particle is not important and the fluid-fluid model will suffice. In the following Φ will represent the scalar potential and Ψ_k will represent the vector potential of the **velocity** in the particle.

For the scattering calculation spherical co-ordinates (r,θ,ϕ) are employed. The incident plane wave travels in the z-direction and has a velocity potential ϕ_{inc}. The problem is consequently independent of the angle ϕ. The only non-zero components of the vector potentials are the ϕ components. The velocity potential of the incident wave and the potentials of the six scattered waves (three in the continuum and three in the particle) can be expressed as infinite sums. The r dependence for the incident plane wave and the inward travelling scattered waves in the particle is a circular Bessel function. The r dependence for the outward travelling scattered waves in the continuum is a spherical Hankel function. The θ dependence for the waves is a Legendre polynomial. The potentials are

$$\phi_{inc} = \sum_{n=0}^{\infty} i^n (2n+1) j_n(k_{f1} r) P_n(\cos\theta), \tag{3.29}$$

$$\phi_c = \sum_{n=0}^{\infty} i^n (2n+1) A_n h_n(k_{f1} r) P_n(\cos\theta), \tag{3.30}$$

$$\phi_t = \sum_{n=0}^{\infty} i^n (2n+1) B_n h_n(k_{f2} r) P_n(\cos\theta), \tag{3.31}$$

$$\psi_\phi = \sum_{n=0}^{\infty} i^n (2n+1) C_n h_n(k_{f3} r) P_n^{\,1}(\cos\theta), \tag{3.32}$$

$$\Phi_c = \sum_{n=0}^{\infty} i^n (2n+1) a_n j_n(k_{s1} r) P_n(\cos\theta), \tag{3.33}$$

$$\Phi_t = \sum_{n=0}^{\infty} i^n (2n+1) b_n j_n(k_{s2} r) P_n(\cos\theta), \tag{3.34}$$

$$\Psi_\phi = \sum_{n=0}^{\infty} i^n (2n+1) c_n h_n(k_{s3} r) P_n^{\,1}(\cos\theta). \tag{3.35}$$

Here j_n is the spherical Bessel function of order n, h_n is the spherical Hankel function of the first kind of order n, P_n is the Legendre polynomial of order n and $P_n^{\,1}$ is the associated Legendre polynomial of the first kind. Only the ϕ components of the vector potentials ψ_k and Ψ_k exist because the field is axially symmetric. The unknown coefficients $A_n, B_n, C_n, a_n, b_n,$ and c_n can be found using the boundary conditions.

The boundary condition at the surface of the sphere is the requirement that the velocity, stress, temperature and heat flow are continuous across this surface. For axial symmetry this means

$$
\begin{aligned}
u_{fr} &= u_{sr} \\
u_{f\theta} &= u_{s\theta} \\
T_f &= T_s \\
\tau_f \partial T_f/\partial r &= \tau_s \partial T_s/\partial r \\
P_{frr} &= P_{srr} \\
P_{fr\theta} &= P_{sr\theta}.
\end{aligned}
\tag{3.36}
$$

Here r indicates the radial component of the variable and θ indicates the component in the θ direction. P_{ij} is the total stress tensor, the viscous stress tensor plus the hydrostatic pressure and is given by

$$P_{ij} = \mu\sigma_{ij} - \left(\tfrac{2}{3}\mu - \mu_B\right)\nabla\cdot\mathbf{u}\delta_{ij} - p\delta_{ij}.$$

Here σ_{ij} is the stress tensor

$$\frac{\partial u_i}{\partial x_j} + \frac{\partial u_j}{\partial x_i},$$

δ_{ij} is the Kronecker delta and μ_B is the bulk viscosity. In polar co-ordinates

$$P_{rr} = -p + \left(\mu_B - \tfrac{2}{3}\mu\right)\nabla\cdot\mathbf{u} + 2\mu\sigma_{rr} \text{ and} \tag{3.37}$$

$$P_{r\theta} = 2\mu\sigma_{r\theta}. \tag{3.38}$$

The variables in the boundary conditions can be expressed in terms of the six potentials. The components of the velocity are obtained from its definition $\mathbf{u} = -\nabla\phi + \nabla\times\psi_k$ expressed in polar co-ordinates

$$u_{fr} = -\frac{\partial\phi}{\partial r} + \frac{1}{r\sin\theta}\frac{\partial}{\partial\theta}\left(\psi_\phi \sin\theta\right) \tag{3.39}$$

$$u_{sr} = -\frac{\partial\Phi}{\partial r} + \frac{1}{r\sin\theta}\frac{\partial}{\partial\theta}\left(\Psi_\phi \sin\theta\right) \tag{3.40}$$

$$u_{f\theta} = -\frac{1}{r}\frac{\partial\phi}{\partial\theta} - \frac{1}{r}\frac{\partial}{\partial r}\left(r\psi_\phi\right) \tag{3.41}$$

$$u_{s\theta} = -\frac{1}{r}\frac{\partial\Phi}{\partial\theta} - \frac{1}{r}\frac{\partial}{\partial r}\left(r\Psi_\phi\right). \tag{3.42}$$

The temperature is written in terms of the scalar potentials using equation (3.19) and the Helmholtz equations

$$\left(\nabla^2 + {k_{f1}}^2\right)\phi_c = 0$$

$$\left(\nabla^2 + {k_{f2}}^2\right)\phi_t = 0$$

$$\left(\nabla^2 + {k_{s1}}^2\right)\Phi_c = 0$$

$$\left(\nabla^2 + {k_{s2}}^2\right)\Phi_t = 0$$

to give

$$T_f = \frac{\gamma_f}{i\omega\beta_f c_f^{\,2}}\left[\left(\omega^2 - \Gamma_f k_{f1}^{\,2}\right)\phi_c + \left(\omega^2 - \Gamma_f k_{f2}^{\,2}\right)\phi_t\right]$$

$$T_s = \frac{\gamma_s}{i\omega\beta_s c_s^{\,2}}\left[\left(\omega^2 - \Gamma_s k_{s1}^{\,2}\right)\Phi_c + \left(\omega^2 - \Gamma_s k_{s2}^{\,2}\right)\Phi_t\right]$$

where $\Gamma = \frac{c^2}{\dot{\gamma}} - i\omega b$.

If the imaginary part of k_{f1} is neglected, b is assumed zero in (3.19) and the quantity $\omega\tau/c^2\rho C_p$ is neglected compared to 1 then the simplified expressions

$$T_f = \frac{-i\omega\left(\gamma_f - 1\right)}{\beta_f c_f^{\,2}}\phi_c - \frac{\rho_f C_{pf}}{\beta_f \tau_f}\phi_t \tag{3.43}$$

$$T_s = \frac{-i\omega\left(\gamma_s - 1\right)}{\beta_s c_s^{\,2}}\Phi_c - \frac{\rho_s C_{ps}}{\beta_s \tau_s}\Phi_t \tag{3.44}$$

are obtained.

The components of the stress tensor are given by the definitions (3.37) and (3.38). The components σ_{rr} and $\sigma_{r\theta}$ in terms of the velocity are from Landau and Lifshitz [143]

$$\sigma_{rr} = \frac{\partial u_r}{\partial r}$$

$$2\sigma_{r\theta} = \frac{1}{r}\frac{\partial u_r}{\partial \theta} + \frac{\partial u_\theta}{\partial r} - \frac{u_\theta}{r}.$$

The pressure in terms of the scalar potential ϕ can be obtained from the momentum equation (3.17)

$$p = \rho\frac{\partial \phi}{\partial t} - \rho b\nabla^2\phi.$$

Thus the total stress tensor components P_{rr} are

$$P_{frr} = \left(i\omega\rho_f + 2\mu_f\nabla^2\right)\phi + 2\mu_f\left\{\frac{\partial^2\phi}{\partial r^2} + \frac{1}{\sin\theta}\frac{\partial}{\partial\theta}\left[\sin\theta\left(\frac{\psi_\phi}{r^2} - \frac{1}{r}\frac{\partial\psi_\phi}{\partial r}\right)\right]\right\} \tag{3.45}$$

$$P_{srr} = \left(i\omega\rho_s + 2\mu_s\nabla^2\right)\Phi + 2\mu_s\left\{\frac{\partial^2\Phi}{\partial r^2} + \frac{1}{\sin\theta}\frac{\partial}{\partial\theta}\left[\sin\theta\left(\frac{\Psi_\phi}{r^2} - \frac{1}{r}\frac{\partial\Psi_\phi}{\partial r}\right)\right]\right\}. \tag{3.46}$$

Epstein and Cahart neglected the $\nabla^2\phi_c$ term in (3.45) and used

$$P_{frr} = i\omega\rho_f\left(\phi_c + \phi_t - \frac{2\mu_f C_{pf}}{\tau_f}\phi_t\right) + 2\mu_f\left\{\frac{\partial^2\phi}{\partial r^2} + \frac{1}{\sin\theta}\frac{\partial}{\partial\theta}\left[\sin\theta\left(\frac{\psi_\phi}{r^2} - \frac{1}{r}\frac{\partial\psi_\phi}{\partial r}\right)\right]\right\} \tag{3.47}$$

and the corresponding expression for (3.46) is

$$P_{srr} = i\omega\rho_s\left(\Phi_c + \Phi_t - \frac{2\mu_s C_{ps}}{\tau_s}\Phi_t\right) + 2\mu_s\left\{\frac{\partial^2\Phi}{\partial r^2} + \frac{1}{\sin\theta}\frac{\partial}{\partial\theta}\left[\sin\theta\left(\frac{\Psi_\phi}{r^2} - \frac{1}{r}\frac{\partial\Psi_\phi}{\partial r}\right)\right]\right\}. \tag{3.48}$$

The (r,θ) components are

$$P_{fr\theta} = -\mu_f\left\{-2\frac{\partial}{\partial\theta}\left(\frac{1}{r}\frac{\partial\phi}{\partial r} - \frac{\phi}{r^2}\right) - \left(\frac{\partial^2\psi_\phi}{\partial r^2} - \frac{2\psi_\phi}{r^2}\right) + \frac{1}{r^2}\frac{\partial}{\partial\theta}\left[\frac{1}{\sin\theta}\frac{\partial}{\partial\theta}\left(\psi_\phi\sin\theta\right)\right]\right\} \tag{3.49}$$

$$P_{sr\theta} = -\mu_s\left\{-2\frac{\partial}{\partial\theta}\left(\frac{1}{r}\frac{\partial\Phi}{\partial r} - \frac{\Phi}{r^2}\right) - \left(\frac{\partial^2\Psi_\phi}{\partial r^2} - \frac{2\Psi_\phi}{r^2}\right) + \frac{1}{r^2}\frac{\partial}{\partial\theta}\left[\frac{1}{\sin\theta}\frac{\partial}{\partial\theta}\left(\Psi_\phi\sin\theta\right)\right]\right\}. \tag{3.50}$$

Equations (3.39) to (3.44) and (3.47) to (3.50) are substituted into the boundary conditions (3.36). The series representations of the potentials (equations (3.29) to (3.35)) are then substituted into the resulting expressions, noting that $\phi = \phi_{inc} + \phi_c + \phi_t$. The Legendre functions disappear and a 6×6 matrix equation for the coefficients A_n, B_n, C_n, a_n, b_n, and c_n results

$$\mathbf{Ta} = \mathbf{c}, \tag{3.51}$$

where

$$\mathbf{a} = \{A_n \;\; B_n \;\; C_n \;\; a_n \;\; b_n \;\; c_n\}^T.$$

T is a 6×6 matrix and **c** is a 6×1 matrix, their elements are functions of the Bessel and Hankel functions.

3. 2. 6 Allegra and Hawley (AH) long wavelength result

From equation (3.51) the coefficients A_n of the series representation of the scattered compressional wave can be found. The plane wave attenuation and complex wavenumber in a continuum containing a number of these scatterers can be obtained using just these coefficients. At a given frequency the magnitude of A_n decreases with increasing n and in the low frequency or long wavelength limit good approximations can be obtained by using just A_0 and A_1. Allegra and Hawley (AH) [49] obtained explicit expressions for A_0 and A_1 in the long wavelength limit. The result for A_0 is given by their equation (13)

$$A_0 = -i\frac{x_{f1}}{3}\left(x_{f1}^{\,2} - \frac{\rho_f}{\rho_s}x_{s1}^{\,2}\right)$$
$$+ ix_{f1}\frac{b_{cf}}{b_{tf}}\left(1-\frac{\rho_f b_{cs}}{\rho_s b_{cf}}\right)x_{f2}^{\,2}h_1(x_{f2})\left(1-\frac{\tau_f b_{tf}}{\tau_s b_{ts}}\right)\left(h_0(x_{f2})-\frac{\tau_f x_{f2}h_1(x_{f2})}{\tau_s x_{s2}j_1(x_{s2})}j_0(x_{s2})\right)$$

where x is the wavenumber indicated by the subscript multiplied by a the sphere radius. b_c is the coefficient of the compressional wave potential in (3.43) or (3.44) and b_t is the coefficient of the thermal wave potential.

Using the explicit expressions for the spherical Hankel and Bessel functions

$$j_0(z) = \frac{\sin z}{z}$$

$$j_1(z) = \frac{\sin z}{z^2} - \frac{\cos z}{z}$$

$$h_0(z) = \frac{e^{iz}}{iz}$$

$$h_1(z) = -\frac{e^{iz}}{z} + \frac{e^{iz}}{iz^2}$$

A_0 becomes

$$A_0 = \frac{i(k_f a)^3}{3}\left(\frac{\rho_f c_f^{\,2}}{\rho_s c_s^{\,2}} - 1\right)$$
$$+ k_f^{\,2} a c_f T_f \rho_f \tau_f \left(\frac{\beta_f}{\rho_f C_{pf}} - \frac{\beta_s}{\rho_s C_{ps}}\right)^2 \left[\frac{1}{1-ix_{f2}} - \frac{\tau_f}{\tau_s}\frac{\tan x_{s2}}{\tan x_{s2} - x_{s2}}\right]^{-1}. \qquad (3.52)$$

The AH expression for A_1 is

$$A_1 = \frac{-\frac{ix_{f1}^3}{3}\left(\frac{\rho_f}{\rho_s}-1\right)\left(h_2(x_{f3})Q(x_{s3}) - \frac{\mu_f}{\mu_s}x_{f3}h_1(x_{f3})j_2(x_{s3})\right)}{\left(\frac{3\rho_f}{\rho_s}h_2(x_{f3}) + 2\left(\frac{\rho_f}{\rho_s}-1\right)h_0(x_{f3})\right)Q(x_{s3}) - \frac{\mu_f}{\mu_s}x_{f3}h_1(x_{f3})j_2(x_{s3})\left(\frac{\rho_f}{\rho_s}+2\right)}$$

$$Q(x_{s3}) = x_{s3}j_1(x_{s3}) - 2\left(1-\frac{\mu_f}{\mu_s}\right)j_2(x_{s3}).$$

From this an expression, Allegra and Hawley obtained a result for solid particles by letting $\mu_s \to \infty$

$$A_1 = \frac{\frac{ix_{f1}^3}{3}\left(1-\frac{\rho_f}{\rho_s}\right)h_2(x_{f3})}{2\left(\frac{\rho_f}{\rho_s}-1\right)h_0(x_{f3}) + \frac{3\rho_f}{\rho_s}h_2(x_{f3})}. \tag{3.53}$$

This assumes that there is no shear wave in the particle. McClements [64] has shown that (3.53) also works well for fluid-fluid systems in the long wavelength regime, this is because the viscous wave inside the particle is not important and can be neglected. Substituting for the Hankel functions and for x_{f3} gives

$$A_1 = \frac{ix_{f1}^3}{3}\left[\frac{3\rho_f}{\rho_s-\rho_f} + 2\left[1 + \frac{3(1+i)\delta_f}{2a} + \frac{3i\delta_f^2}{2a^2}\right]^{-1}\right]^{-1}. \tag{3.54}$$

3. 2. 7 Plane wave attenuation

Epstein and Cahart obtained the attenuation due to viscous and thermal effects. This may be named the absorption attenuation after the related absorption cross-section which includes all the attenuation mechanisms except scattering. The total (or extinction) attenuation, the sum of the absorption and scattering attenuations, was obtained by Allegra and Hawley.

The dissipation of energy in a viscothermal fluid per unit volume per unit time D can be obtained from equations (3.16) to (3.18) and is given by

$$\mathrm{D} = P_{ij}\frac{\partial u_j}{\partial x_i} + p\nabla\cdot\mathbf{u} + \frac{\tau}{T^0}(\nabla T')^2.$$

A method for calculating the absorption attenuation ξ_a from D is shown in the Epstein and Cahart paper. D is time averaged and then integrated over the whole of space surrounding the sphere and the space inside the sphere. As in the boundary conditions, the field variables are written in terms of the potentials and then the series representations substituted. The energy absorbed in the vicinity of a single sphere per unit time is

$$D_{single} = -\frac{2\pi\rho_f\omega}{k_f}\sum_n (2n+1)\left(\Re(A_n)+|A_n|^2\right).$$

For N spheres per unit volume, where N is related to the volume fraction by

$$N = \frac{3\phi}{4\pi a^3},$$

the total energy loss per unit time per unit volume is N times the loss from a single sphere ND_{single}. This additive or single scattering assumption assumes that the wave incident on all the scatterers is the same. Thus as the incident wave progresses through the medium its attenuation must be small i.e.

$$N\sigma_0 L \ll 1$$

where σ_0 is the total scattering cross section of a single particle, the power the particle removes from the incident wave divided by the incident wave's intensity.

The energy loss of the incident plane wave per unit distance is then ND_{single} divided by the time averaged energy the plane wave carries through a normal unit area in unit time $\frac{1}{2}k_f\omega\rho_f$.

The plane wave attenuation coefficient, which describes the amplitude of the plane wave not the energy, is half of the energy loss per unit distance and thus is given by

$$\xi_a = -\tfrac{3}{2}\frac{\phi}{k_f{}^2a^3}\sum_n (2n+1)\left(\Re(A_n)+|A_n|^2\right). \qquad (3.55)$$

The energy in the scattered wave from a single sphere can be shown to be

$$\frac{2\pi\rho_f\omega}{k_f}\sum_n (2n+1)|A_n|^2$$

and thus the scattering plane wave attenuation for N spheres is

$$\xi_s = \tfrac{3}{2}\frac{\phi}{k_f{}^2a^3}\sum_{n=0}^{\infty}(2n+1)|A_n|^2. \qquad (3.56)$$

The single scattering total or extinction plane wave attenuation is $\xi_a + \xi_s$ i.e.

$$\xi = -\tfrac{3}{2}\frac{\phi}{k_f{}^2a^3}\sum_{n=0}^{\infty}(2n+1)\Re(A_n). \qquad (3.57)$$

This can also be obtained from the low ϕ or low N approximation of the WT multiple scattering formula. From (3.6)

$$k = k_f\left[1+\frac{4\pi N}{k_f^{\,2}}f(0)+\frac{4\pi^2N^2}{k_f^{\,4}}\left(f^2(0)-f^2(\pi)\right)\right]^{\frac{1}{2}}.$$

Taking only the first two terms in the series expansion of the bracket and neglecting terms in N^2 gives

$$k \cong k_f\left[1+\frac{2\pi N}{k_f^{\,2}}f(0)\right]. \tag{3.58}$$

The plane wave attenuation is the imaginary part of k so substituting for f gives

$$\xi = -\frac{2\pi N}{k_f^{\,2}}\sum_n (2n+1)\Re(A_n)$$

which is identical to (3.57). This is the single scattering limit of the multiple scattering theory which also requires the condition $N\sigma_0 L \ll 1$.

3. 2. 8 Effective sound speed

The effective sound speed in a fluid containing a number of spherical scatterers can be obtained from the real part of the complex wavenumber given by a multiple scattering formula. The low ϕ or single scattering sound speed corresponding to the attenuation given by (3.57) can be obtained from (3.58)

$$c = \frac{\omega}{\Re(k)} = \omega\left[k_f + \frac{3\phi}{2k_f^{\,2}a^3}\sum_n (2n+1)\,\mathrm{Im}\,A_n\right]^{-1}.$$

3. 2. 9 Isolated particle assumption

The scattering coefficients are calculated for an isolated sphere. For a number of particles it is possible the viscous and thermal waves in the continuous phase will overlap. The boundary layer thicknesses in the continuous phase δ_f and δ_{hf} measure the distance over which these waves are significant. The thermal or shear wave amplitude will decay by the factor $1/e$ in this thickness. If $\delta_f \geq d/2$ or $\delta_{hf} \geq d/2$, where d is the distance between neighbouring particles, then the waves will overlap and the theory may be invalid. The average particle separation can be estimated from the volume fraction. For the average centre to centre spacing in a suspension with a uniform concentration, Zuber [153] gives

$$d_{cc} = 2a\phi^{-\frac{1}{3}}. \tag{3.59}$$

Thus the distance between the particles is given by

$$d = d_{cc} - 2a = 2a\left(\phi^{-\frac{1}{3}} - 1\right). \tag{3.60}$$

McClements [64] used

$$d = 2a\left(\left(\frac{6\phi}{\pi}\right)^{-\frac{1}{3}} - 1\right). \tag{3.61}$$

The maximum volume fraction for packing of spheres, which is a regular packing, is $\pi\sqrt{2}/6 = 0.74$. The maximum volume fraction for random packing must be less than this value (see Scott [39] and Bernal and Mason [40]). For this value of ϕ d should be zero. The value of d given by equation (3.60) is nearer to zero than that given by (3.61) so the Zuber expression will be used in the following calculations. The equations $\delta_f = d/2$ and $\delta_{hf} = d/2$ can be rewritten as

$$\phi = \left[\left(\frac{\rho_f \pi f a^2}{\mu_f}\right)^{-\frac{1}{2}} + 1\right]^{-\frac{1}{3}} \text{ and} \tag{3.62}$$

$$\phi = \left[\left(\frac{\rho_f C_{pf} \pi f a^2}{\tau_f}\right)^{-\frac{1}{2}} + 1\right]^{-\frac{1}{3}}. \tag{3.63}$$

3. 2. 10 Thermal and viscous effects

The A_0 coefficient given by equation (3.52) consists of a scattering term and a thermal term. The scattering term is the same as the lossless scattering A_0 given by (3.3). The A_1 term includes the viscous effect. The viscous effect becomes negligible when $\omega \to \infty$ because $\delta \to 0$ and then (3.54) is identical to the lossless result (3.4).

The relative effects of the viscous and thermal terms on the complex wavenumber are shown in figure 3. 4 for alumina dust in air. Here the attenuation and sound speed are calculated from (3.58) using the expressions for A_0 and A_1 given by equations (3.52) and (3.54) respectively. The viscous curve is obtained by using only A_1 and the thermal curve is obtained using only A_0. The scattering contribution to the thermal curve is negligible. The viscous curve also contains the inertial effect and it would be more accurate to describe this as the visco-inertial curve.

The physical properties of the two phases are given in appendix 1. The coefficient of thermal expansion β_s of the particulate phase is not known, nor is the sound speed. Thus in equation (3.52) the expression $\beta_s/\rho_s C_{ps}$ is assumed to be negligible compared to $\beta_f/\rho_f C_{pf}$. This is a valid assumption since the solid expansion coefficient will be much less than that of the fluid and the solid density is three orders of magnitude greater than that of the fluid. It is also assumed that

$$\frac{\rho_f c_f^2}{\rho_s c_s^2} = 0$$

in (3.52) which is the limit for a perfectly hard scatterer.

The particle radius is 2 μm and the volume fraction is 10^{-5}, which is in the low ϕ 'dilute' region. At $f = 10^7$ Hz, $k_f a = 0.4$, this is near to the limit of the long wavelength assumption. Figure 3. 5 shows the curves corresponding to equations (3.62) and (3.63) which indicate for which values of f and ϕ the viscous and thermal waves overlap. For the volume fraction of 10^{-5}, this occurs for frequencies below 1000 Hz.

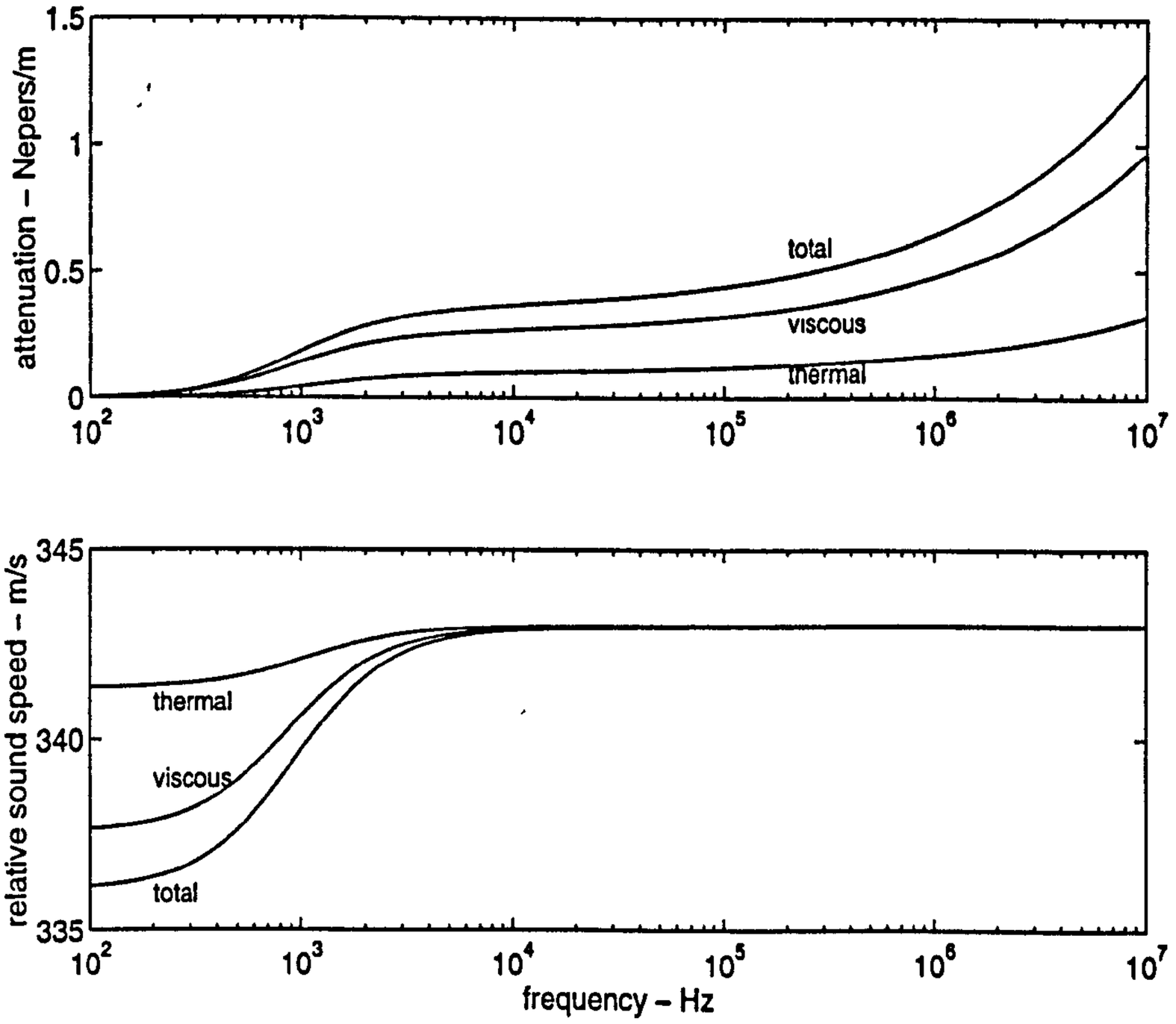

Figure 3. 4 Attenuation and sound speed versus frequency for 2 μm radius alumina particles in air, volume fraction 10^{-5}. Comparison of viscous and thermal effects.

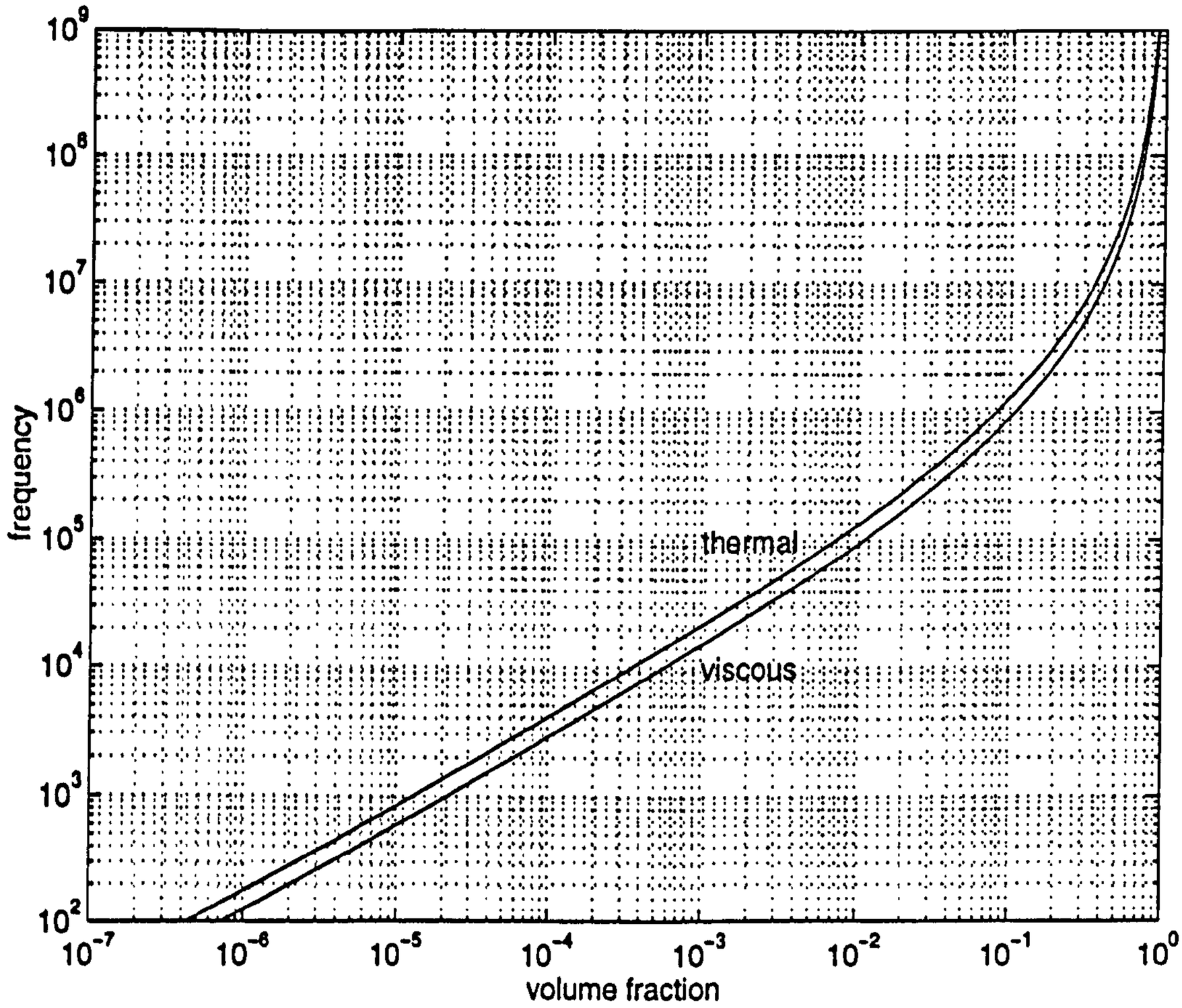

Figure 3. 5 Curves indicating the values of frequency and volume fraction for which the viscous and thermal boundary layer thicknesses equal half the particle separation, in an air suspension of 2 μm radius particles. The boundary layers overlap in the regions to the right of the curves.

3. 2. 11 Multiple scattering

In this section the work of McClements and Povey [71] is extended. They compared the predictions of the Lloyd and Berry multiple scattering theory and the low ϕ 'single scattering' theory with their measurements on a sunflower oil in water emulsion. Here, predictions of the WT and Ma *et al* multiple scattering theories, described in McClements [64], are also compared with the measurements. The expressions for the complex wavenumber in terms of A_0 and A_1 are given in table 3. 1.

Single scattering	$k^2 = k_f^{\,2} - \frac{3i\phi}{k_f a^3}(A_0 + 3A_1)$
WT	$k^2 = k_f^{\,2} - \frac{3i\phi}{k_f a^3}(A_o + 3A_1) - \frac{27\phi^2}{k_f^{\,4} a^6} A_0 A_1$
LB	$k^2 = k_f^{\,2} - \frac{3i\phi}{k_f a^3}(A_o + 3A_1) - \frac{27\phi^2}{k_f^{\,4} a^6}(A_0 A_1 + 2A_1^{\,2})$
Ma	$k^2 = \frac{k_f^{\,2} - \frac{3i\phi}{k_f a^3}(A_0 + A_1) - \frac{9\phi^2}{k_f^{\,4} a^6} A_0 A_1}{1 + \frac{6i\phi}{k_f^{\,3} a^3} A_1}$

Table 3. 1 Single and multiple scattering expressions for the complex wavenumber k in the long wavelength limit.

The Ma expression is the simplified long wavelength expression given by McClements' equation (5). Figure 3. 6 compares predictions of the four theories and the experimental data. The physical properties are given in appendix 1, the frequency is 1.25 MHz and the particles are all assumed to have a radius equal to the mean radius of 0.27 μm. McClements and Povey [71] solved an equation like (3.51) to obtain as many A_n coefficients as were significant. In the present work only the expressions (3.52) and (3.54) for A_0 and A_1 were used. The results are close to those shown in reference [71]. This is because the long wavelength criterion $k_f a \ll 1$ is satisfied; here $k_f a \approx 10^{-3}$.

Since the attenuation predictions of the three multiple scattering theories are almost identical only one line is shown in figure 3. 6. For the same reason one line represents the velocity predictions of the LB and Ma theories. The figure shows that the multiple scattering theories predict less attenuation and

dispersion than the single scattering theory. Single scattering is valid when $N\sigma_0 L \ll 1$. $N\sigma_0$ is the single scattering attenuation, which at $\phi = 0.4$ is 49 Npm^{-1}. Thus for $N\sigma_0 L < 0.5$, the path length L must be less than 10 mm for single scattering to be valid. This is actually the value of L used in the experiments in reference [71]. The WT theory seems to be valid for the range of ϕ in figure 3. 6 because the corrections of the LB and Ma theories make little difference to the prediction.

The theoretical predictions agree well with the sound speed measurements. For the attenuation at the higher volume fractions the theory predicts a larger attenuation than is shown by the measurements. Although an experimental error of ± 30 dB m^{-1} is quoted this does not account for the observed discrepancy.

Figure 3. 7 plots the overlap conditions (3.62) and (3.63) for the sunflower oil in water emulsion. At 1.25 MHz the thermal boundary layer begins to overlap when $\phi > 0.2$. Reference [71] shows that the viscous effect is very small compared to the thermal effect, so it is not necessary to consider the viscous boundary layer condition as well. Figure 3. 7 suggests that for the higher volume fractions the isolated particle assumption is not valid. This may explain why the theoretical predictions do not agree with the measurements in figure 3. 6.

Figure 3. 8 shows the differences between the scattering theories. The physical parameters used in the equations are those of the alumina dust in air suspension described in the previous section. The frequency is 10^5 Hz. Experimental data for this suspension is only available at $\phi \approx 10^{-5}$ and will be shown in chapter 6. The differences between the predictions are due to the viscous contribution to the A_1 term. Unlike the predictions for the emulsion shown in figure 3. 6, the multiple scattering theories predict more attenuation than the single scattering theory. Figure 3. 8 also shows the sound speed prediction of the lossless Ma theory from equations (3.9), the attenuation prediction of the lossless theory is negligibly small.

At $\phi = 0.01$, $N\sigma_0 = 438$ Npm^{-1} for this suspension, which is very large. The condition $N\sigma_0 L \ll 1$ will only be valid if L is less than 1 mm. In experiments L will be at least 10 mm and so multiple scattering will be significant. For volume fractions above 0.01 the attenuation will be too great for coherent wave propagation.

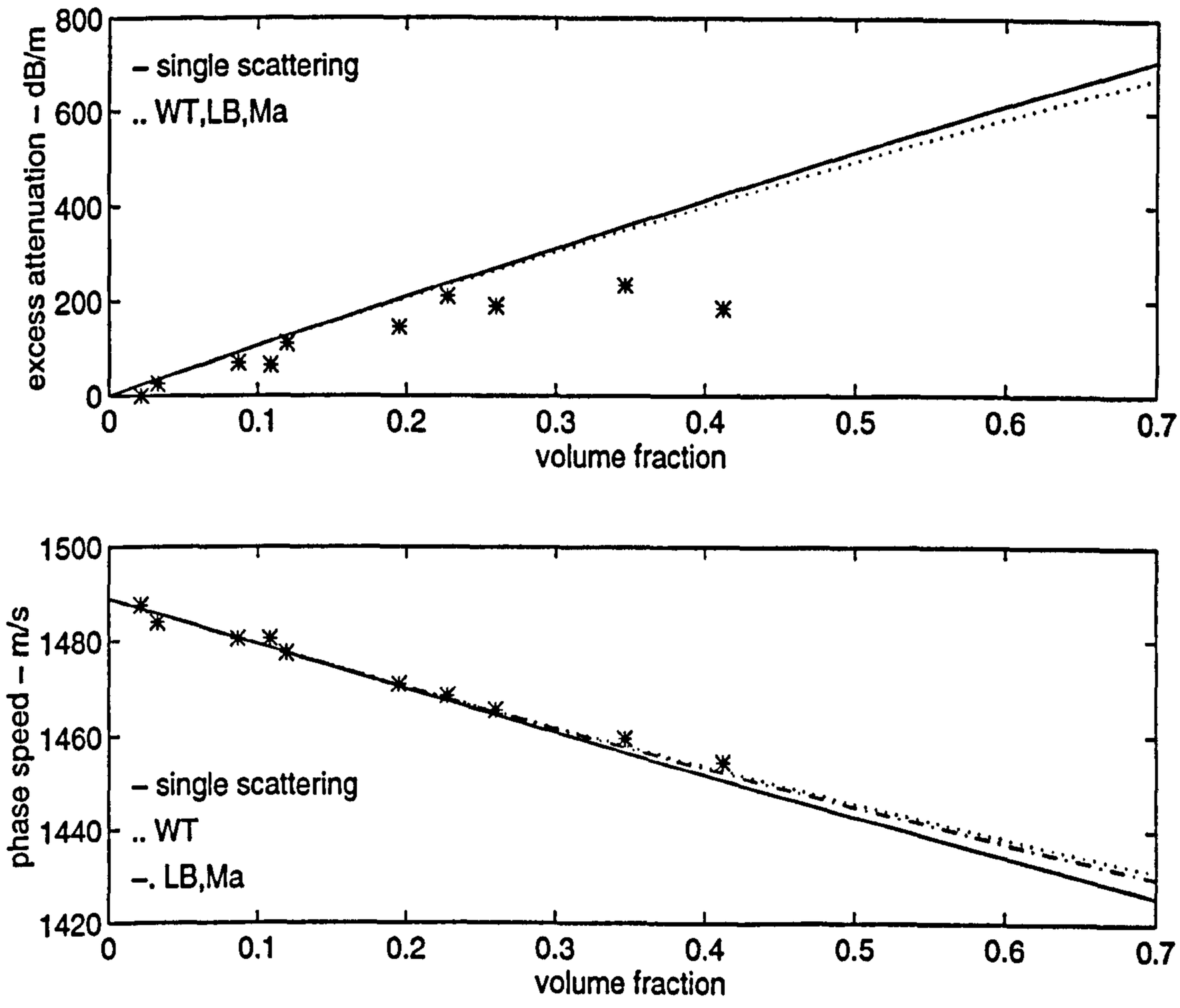

Figure 3. 6 Excess attenuation and sound speed versus volume fraction for a sunflower oil in water emulsion with particles of mean radius 0.27 μm at 1.25 MHz. Comparison of data of McClements and Povey and predictions of single and multiple scattering theories.

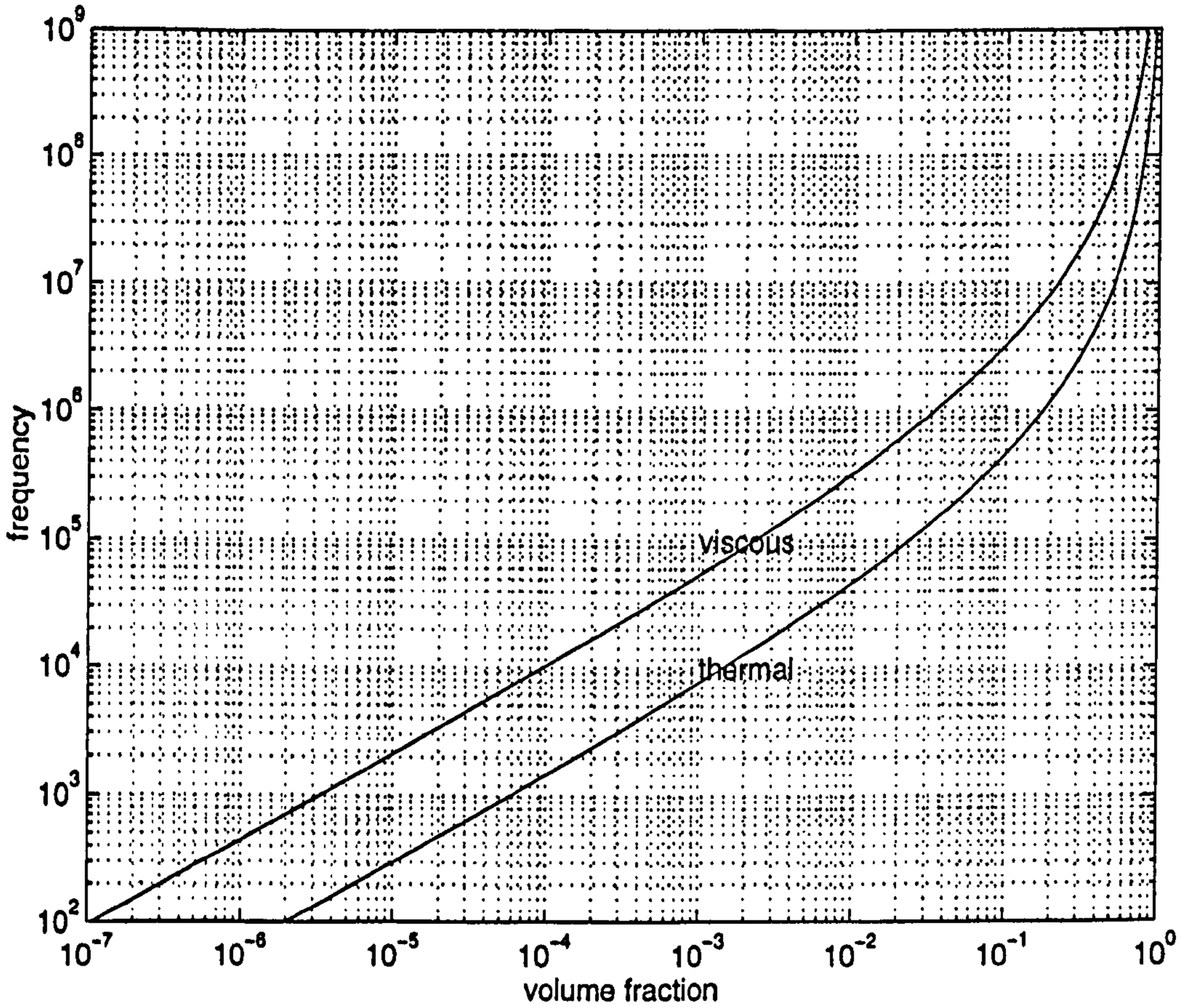

Figure 3. 7 Curves indicating the values of frequency and volume fraction for which the viscous and thermal boundary layer thicknesses equal half the particle separation for particles of mean radius 0.27 μm in water. The boundary layers overlap in the regions to the right of the curves.

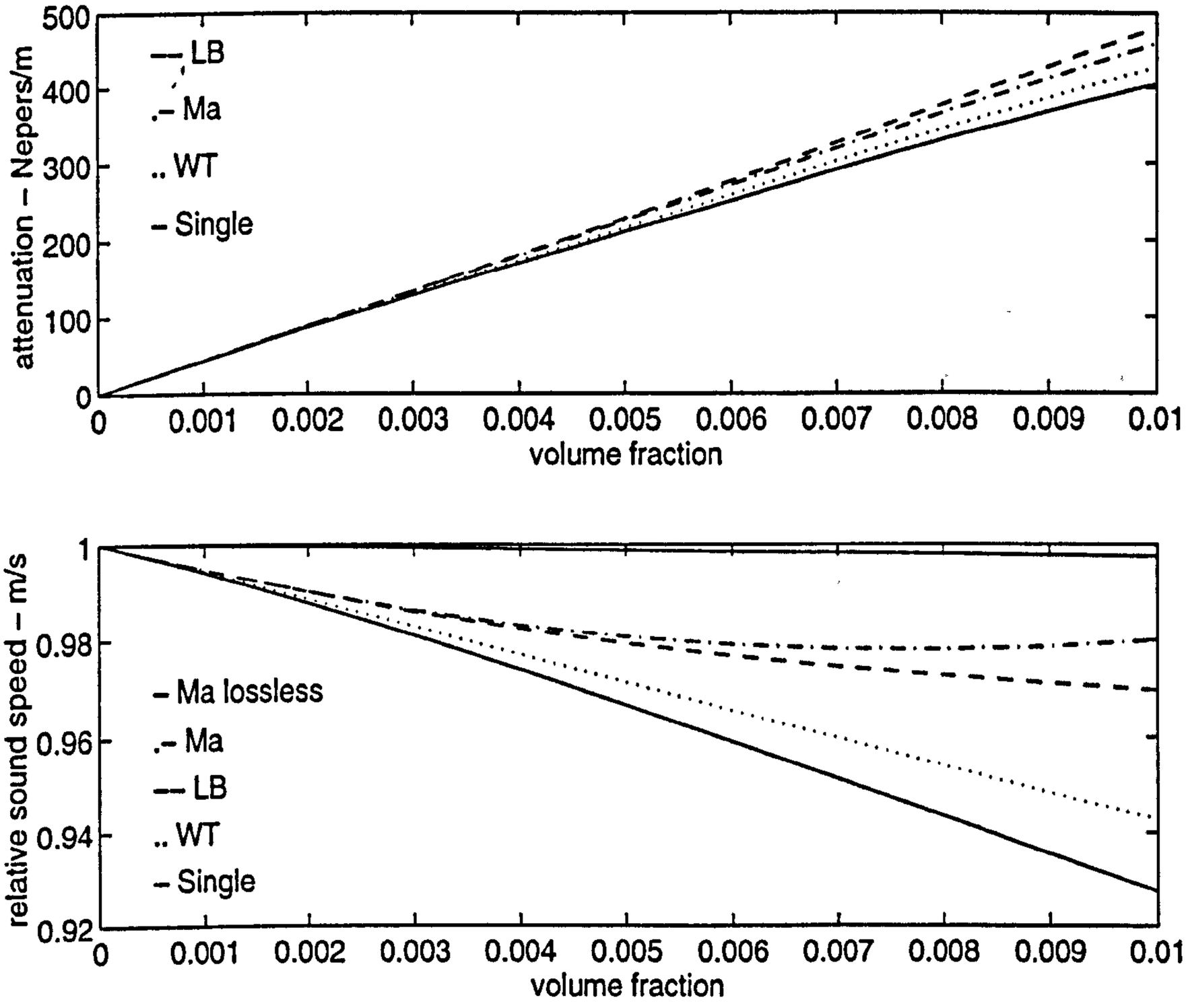

Figure 3. 8 Attenuation and sound speed versus volume fraction for an air suspension of alumina particles with radius 2 μm at 10^5 Hz. Comparison of predictions of single and multiple scattering theories.

Chapter 4
Coupled phase theories

Coupled phase theories are continuum theories, they are valid when $k_f a \ll 1$. In this region compressional wave scattering is negligible and the coherent wave is dominant. Coupled phase theories only consider the coherent wave, which is usually a plane wave, and take no account of scattering. Both the fluid and particulate phases are considered to be continua; their presence in the same control volume is accounted for by volume averaging. The plane wave is assumed to propagate in both phases simultaneously so coupled phase theories can be described as single wave theories. The resulting complex wavenumber dependence on volume fraction is different to that obtained from scattering theory. Comparison of theoretical predictions and experimental data at high volume fractions (but low $k_f a$) highlights this difference between the two approaches.

This chapter is divided into three main sections. The first two describe the two existing types of coupled phase theory. Section 4. 1 describes those theories that include heat transfer and assume that the particulate phase is incompressible. The closely related methods of Gumerov, Ivandaev and Nigmatulin (GIN) [102] and Mecredy and Hamilton (MH) [18] are discussed. Section 4. 2 describes the theory that has a compressible particulate phase but neglects heat transfer. This theory has been derived by Harker and Temple (HT) [65] and Atkinson and Kytomaa [13] [25] [112] [113]. Section 4. 3 derives a new coupled phase theory which combines the theories described in sections 4. 1 and 4. 2 i.e. it incorporates a compressible particulate phase and heat transfer.

4. 1 Incompressible coupled phase theory with heat transfer

4. 1. 1 Acoustic perturbation

In this chapter the sound wave is assumed to be a small amplitude single frequency plane wave propagating parallel to the z axis. All the field variables can be represented by their constant ambient value, which will be indicated by a superscript zero, plus a small perturbation dependent on space and time. This is caused by the sound wave and thus varies in time and space in an harmonic fashion. The general field variable y is thus given by

$$y = y^0 + y' \exp[i(kz - \omega t)] \tag{4.1}$$

where y' is a small complex amplitude and k is the complex wavenumber.

The relations

$$\frac{\partial y}{\partial t} = -i\omega y' \exp[i(kz - \omega t)] \text{ and } \frac{\partial y}{\partial z} = iky' \exp[i(kz - \omega t)] \tag{4.2}$$

are useful.

4. 1. 2 Volume averaged densities

Coupled phase theory is a special case of two phase continuum mechanics. From multiphase continuum mechanics it takes the concept of volume averaged variables. A suspension or emulsion is a two phase medium with a continuous phase, indicated by the subscript f, and a discrete particulate phase indicated by the subscript s. These phases have densities ρ_f and ρ_s. In the theory the particulate phase is assumed to be a continuum. This requires that the characteristic length scale, the wavelength of the sound wave, must be much greater than the distance (say centre to centre) between the particles. This gives from equation (3.59)

$$\frac{c_f}{f} \gg 2a\phi^{-\frac{1}{3}} \text{ or}$$

$$\phi \gg \left(\frac{2af}{c_f}\right)^3 .$$

Gumerov *et al* quoted this inequality neglecting the 2, giving a less strict condition. They suggested that the continuum theory should be applicable as long as the wavelength λ satisfies $\lambda \gg a$. This is the usual long wavelength criterion which continuum theories must satisfy.

Crowe [159] drew comparisons with molecules in a gas. The continuum assumption is valid for volumes over which the average density is statistically

stationary. For gases a volume containing 10^4 molecules is sufficient. The condition for the wavelength to be greater than the side of a cube containing 10^4 particles is

$$\frac{c_f}{f} > \left(\frac{4\pi a^3 \times 10^4}{3\phi}\right)^{\frac{1}{3}} \text{ or}$$

$$\phi > \frac{4\pi \times 10^4}{3}\left(\frac{af}{c_f}\right)^3.$$

This permits a more limited range of f and ϕ than the GIN condition.

If the particles are uniformly randomly distributed then the suspension or emulsion can be defined using just the volume fraction of particulate phase in the continuous phase ϕ. The three independent variables ρ_f, ρ_s and ϕ are used to form two dependent variables, the volume averaged densities of the two phases

$$\overline{\rho}_f = (1-\phi)\rho_f \text{ and} \tag{4.3}$$

$$\overline{\rho}_s = \phi\rho_s. \tag{4.4}$$

The densities are of the form (4.1), thus from equations (4.3) and (4.4)

$$\overline{\rho}_f{}^0 = (1-\phi^0)\rho_f{}^0$$
$$\overline{\rho}_s{}^0 = \phi^0\rho_s{}^0$$
$$\overline{\rho}_f' = (1-\phi^0)\rho_f' - \rho_f{}^0\phi'$$
$$\overline{\rho}_s' = \phi^0\rho_s' + \rho_s{}^0\phi'$$

to first order in the small quantities.

4. 1. 3 Mass balance equations

The conservation of mass or mass balance equation for each phase is obtained from the usual linear equation

$$\frac{\partial\rho}{\partial t} + \rho^0\nabla\cdot\mathbf{u} = 0$$

by replacing the density with its volume averaged counterpart

$$\frac{\partial\overline{\rho}_s}{\partial t} + \overline{\rho}_s{}^0\frac{\partial u_s}{\partial z} = 0 \tag{4.5}$$

$$\frac{\partial\overline{\rho}_f}{\partial t} + \overline{\rho}_f{}^0\frac{\partial u_f}{\partial z} = 0. \tag{4.6}$$

Here the mass balance equation has been reduced to its one dimensional form because the velocity u varies only in the z direction.

These are the mass balance equations of the MH and GIN theories when mass transfer is neglected.

The volume averaged densities can be used throughout the analysis, as in the work of Gumerov *et al* and Mecredy and Hamilton. Here, however, the real densities will be used. Substituting for $\overline{\rho}_s$ and $\overline{\rho}_f$ in (4.5) and (4.6) gives

$$\phi^0 \frac{\partial \rho_s}{\partial t} + \rho_s{}^0 \frac{\partial \phi}{\partial t} + \phi^0 \rho_s{}^0 \frac{\partial u_s}{\partial z} = 0 \qquad (4.7)$$

$$\alpha \frac{\partial \rho_f}{\partial t} - \rho_f{}^0 \frac{\partial \phi}{\partial t} + \alpha \rho_f{}^0 \frac{\partial u_f}{\partial z} = 0 \qquad (4.8)$$

where $\alpha = 1 - \phi^0$.

These are also the continuity equations used by Harker and Temple (see section 4. 2).

A useful equation can be obtained if $\partial\phi/\partial t$ is eliminated between (4.7) and (4.8):

$$\frac{\phi^0}{\rho_s{}^0} \frac{\partial \rho_s}{\partial t} + \frac{\alpha}{\rho_f{}^0} \frac{\partial \rho_f}{\partial t} = -\frac{\partial}{\partial z}\left(\phi^0 u_s + \alpha u_f\right). \qquad (4.9)$$

This is valid because the variable part of ϕ does not appear in any other equations. This will be called the continuity equation.

4. 1. 4 Incompressible particulate phase

If the material of which the particles are comprised is incompressible then

$$\rho_s' = 0$$

and

$$\overline{\rho}_s' = \rho_s{}^0 \phi' .$$

Although the actual density of the particulate phase does not vary, the volume averaged density does. The first term of equations (4.7) and (4.9) disappears:

$$\rho_s{}^0 \frac{\partial \phi}{\partial t} + \phi^0 \rho_s{}^0 \frac{\partial u_s}{\partial z} = 0 \qquad (4.10)$$

$$\frac{\alpha}{\rho_f{}^0} \frac{\partial \rho_f}{\partial t} = -\frac{\partial}{\partial z}\left(\phi^0 u_s + \alpha u_f\right). \qquad (4.11)$$

The incompressible particle assumption has been shown to work when the compressibility of the particulate phase is much less than that of the continuous phase. This is true for solid particles in gases or liquids and liquid particles in gases. It will not be valid for liquid-liquid emulsions or gas particles in a liquid.

4. 1. 5 Momentum balance equations

The conservation of momentum or momentum balance equation for each phase is obtained from the linear Euler equation

$$\rho^0 \frac{\partial u}{\partial t} = -\frac{\partial p}{\partial z}$$

by replacing the density with its volume averaged counterpart and taking account of momentum transfer between the phases.

From this point on it is assumed that the continuous phase is a fluid; this is true for all suspensions and emulsions. The momentum transfer between the phases is due to Stokes drag, the Bassett history force, the virtual or induced mass effect and the buoyancy force. It is assumed that the particles are spheres, non-spherical particles will be discussed in section 6. 3. The velocity of the particles and the fluid phase are of the form of equation (4.1) with equilibrium values equal to zero.

Mazur and Bedeaux [144] have obtained the force on a sphere oscillating in an oscillating fluid flow; this is given by

$$\left(-i\rho_f{}^0\omega\right)\left(\tfrac{4}{3}\pi a^3\right)\left[\left(\tfrac{9}{4}i\frac{\delta^2}{a^2}+\tfrac{9}{4}(1+i)\frac{\delta}{a}+\tfrac{3}{2}\right)u_f-\left(\tfrac{9}{4}i\frac{\delta^2}{a^2}+\tfrac{9}{4}(1+i)\frac{\delta}{a}+\tfrac{1}{2}\right)u_s\right].$$

Rewriting the terms inside the square brackets gives

$$\left(-i\rho_f{}^0\omega\right)\left(\tfrac{4}{3}\pi a^3\right)\left[\left(\tfrac{9}{4}i\frac{\delta^2}{a^2}+\tfrac{9}{4}(1+i)\frac{\delta}{a}+\tfrac{1}{2}\right)\left(u_f-u_s\right)+u_f\right].$$

The force is comprised of terms dependent on the relative velocity and one term that depends only on the fluid velocity. The latter term is the buoyancy force. The δ^2 term is the Stokes drag term, the δ term is the Bassett history term and the $\frac{1}{2}$ is the induced mass term.

For a number of spheres the total force on the particulate phase is N times that for a single sphere

$$-i\rho_f{}^0\omega\phi^0\left[S\left(u_f-u_s\right)+u_f\right] \tag{4.12}$$

where S, the momentum transfer term, is given by

$$S=\tfrac{9}{4}i\frac{\delta^2}{a^2}+\tfrac{9}{4}(1+i)\frac{\delta}{a}+C. \tag{4.13}$$

C is the induced mass coefficient for a single sphere.

Equation (4.12) assumes the force on each particle is not altered by the presence of the others. As in scattering theory this is true if the distance between

neighbouring particles is greater than $2\delta_f$, see section 3. 2. 9. The more commonly quoted condition is $\phi \ll 1$. Hydrodynamic interaction between particles is discussed in section 6. 1.

The coefficient $C = \frac{1}{2}$ for isolated spheres i.e. when $\phi \ll 1$. For high volume fractions, expressions for S and C that depend on ϕ have been obtained. These are discussed in chapter 6.

The LHS of the Euler equation for the particulate phase is

$$\phi^0 \rho_s{}^0 \frac{\partial u_s}{\partial t}.$$

The RHS will be the force on the particulate phase given by (4.12); the $\partial p/\partial z$ term is zero because of the incompressibility assumption. The particulate phase momentum equation is

$$\phi^0 \rho_s{}^0 \frac{\partial u_s}{\partial t} = -i\omega\phi^0 \rho_f{}^0 S\left(u_f - u_s\right) - i\omega\phi^0 \rho_f{}^0 u_f. \tag{4.14}$$

The corresponding fluid phase equation is, including the pressure gradient term,

$$\alpha\rho_f{}^0 \frac{\partial u_f}{\partial t} = i\omega\phi^0 \rho_f{}^0 S\left(u_f - u_s\right) + i\omega\phi^0 \rho_f{}^0 u_f - \frac{\partial p}{\partial z} \tag{4.15}$$

because the amount of momentum gained by the particulate phase must be equal to that lost by the fluid phase. These are the momentum equations of the GIN theory. The MH momentum equations can be obtained from these by substituting for u_f in the buoyancy force terms using the single fluid Euler equation

$$-i\omega\rho_f{}^0 u_f = -\frac{\partial p}{\partial z}.$$

(4.14) and (4.15) become

$$\phi^0 \rho_s{}^0 \frac{\partial u_s}{\partial t} = -i\omega\phi^0 \rho_f{}^0 S\left(u_f - u_s\right) - \phi^0 \frac{\partial p}{\partial z} \tag{4.16}$$

$$\alpha\rho_f{}^0 \frac{\partial u_f}{\partial t} = i\omega\phi^0 \rho_f{}^0 S\left(u_f - u_s\right) - \alpha \frac{\partial p}{\partial z}. \tag{4.17}$$

These are the momentum equations of the MH theory neglecting the mass transfer terms. (4.16) and (4.17) are also the momentum equations of the Harker and Temple theory discussed in section 4. 2.

4. 1. 6 Alternative forms

If the relations (4.2) are used in equations (4.16) and (4.17) the exponential function may be cancelled in all the terms. The equilibrium terms $u_s{}^0$ and $u_f{}^0$ are zero. Eliminating u_f' or u_s' between the equations gives

$$u_s' = \frac{kp'}{\omega}\frac{\rho_f + S(\rho_f/\alpha)}{\rho_f\rho_s + S(\rho_f/\alpha)\rho_{va}} \text{ and} \tag{4.18}$$

$$u_f' = \frac{kp'}{\omega}\frac{\rho_s + S(\rho_f/\alpha)}{\rho_f\rho_s + S(\rho_f/\alpha)\rho_{va}}. \tag{4.19}$$

Here ρ_{va} is the total volume averaged density which is given by

$$\rho_{va} = \phi^0\rho_s{}^0 + \alpha\rho_f{}^0.$$

In the subsequent work a constant with the subscript va indicates volume averaging i.e.

$$(y)_{va} = \phi^0 y_s + \alpha y_f.$$

In (4.18) and (4.19) the densities are the constant equilibrium values but the superscript 0 has been omitted.

The corresponding expressions from the GIN momentum equations are similar:

$$u_s' = \frac{kp'}{\omega}\frac{\rho_f + S\rho_f}{\rho_f\rho_s + S\rho_f\rho_{va}} \tag{4.20}$$

$$u_f' = \frac{kp'}{\omega}\frac{\rho_s + S\rho_f}{\rho_f\rho_s + S\rho_f\rho_{va}}. \tag{4.21}$$

From these equations it is seen that as $\omega \to 0$ and $S \to \infty$

$$u_s' \to u_f' \to \frac{kp'}{\omega\rho_{va}},$$

this is the equilibrium state where the two phases move in phase.

In the limit $\omega \to \infty$, $S \to C$, but if it is assumed $S \to 0$, i.e. no momentum transfer, then

$$u_s' = \frac{kp'}{\omega\rho_s} \text{ and } u_f' = \frac{kp'}{\omega\rho_f}.$$

These are the results that would be obtained from the single fluid Euler equation.

4. 1. 7 Comparison with long wavelength scattering theory

The momentum transfer term S appearing in the momentum equations (4.14) and (4.15) or (4.16) and (4.17) can be used to rewrite the expression for the A_1 scattering coefficient given by equation (3.54):

$$A_1 = \frac{ix_{f1}^{\,2}}{9}\left[\frac{\rho_f^{\,0}}{\rho_s^{\,0}-\rho_f^{\,0}}+(S+1)^{-1}\right]^{-1}.$$

4. 1. 8 Thermodynamics

Following Epstein and Cahart [47] the general form for the equations of state of a liquid are

$p = p(\rho, T)$ and $U = U(\rho, T)$

where U is the specific internal energy. Differentiating the first equation with respect to space and the second with respect to time gives

$$\nabla p = \left(\frac{\partial p}{\partial \rho}\right)_T \nabla\rho + \left(\frac{\partial p}{\partial T}\right)_\rho \nabla T \text{ and} \tag{4.22}$$

$$\dot{U} = \left(\frac{\partial U}{\partial \rho}\right)_T \dot{\rho} + \left(\frac{\partial U}{\partial T}\right)_\rho \dot{T}. \tag{4.23}$$

Here the dot indicates differentiation with respect to time. The subscripts on the coefficients indicate that either T or ρ is kept constant. The coefficients in (4.22) and (4.23) are given by

$$\left(\frac{\partial p}{\partial \rho}\right)_T = \frac{c^2}{\gamma}$$

$$\left(\frac{\partial p}{\partial T}\right)_\rho = \frac{\rho^0(\gamma-1)C_v}{T^0} = \frac{\rho^0 c^2 \beta}{\gamma}$$

$$\left(\frac{\partial U}{\partial \rho}\right)_T = \frac{1}{(\rho^0)^2}\left(p^0 - \frac{\rho^0(\gamma-1)C_v}{\beta}\right)$$

$$\left(\frac{\partial U}{\partial t}\right)_\rho = C_v.$$

Using the single fluid continuity equation

$$\frac{\partial \rho}{\partial t} = -\rho^0 \nabla \cdot \mathbf{u}$$

to eliminate ρ in (4.23) gives

$$\frac{\partial U}{\partial t} = -\frac{1}{\rho^0}\left(p^0 - \frac{\rho^0(\gamma-1)C_v}{\beta}\right)\nabla\cdot\mathbf{u} + C_v\frac{\partial T}{\partial t}.$$

Eliminating U with the energy equation

$$\rho^0 \frac{\partial U}{\partial t} = -p^0 \nabla \cdot \mathbf{u}$$

gives

$$C_v \frac{\partial T}{\partial t} + \frac{(\gamma - 1)C_v}{\beta} \nabla \cdot \mathbf{u} = 0. \tag{4.24}$$

for the energy equation in terms of temperature and particle velocity.

(4.22) with (4.2) gives

$$\frac{\gamma}{c^2} p' = \rho' + \rho^0 \beta T', \tag{4.25}$$

which will be called the equation of state.

The energy equation (4.24) can also be obtained in terms of temperature and pressure. Eliminating ρ between (4.22) and the single fluid continuity equation gives

$$\nabla \cdot \mathbf{u} = -\frac{\gamma}{\rho^0 c^2} \frac{\partial p}{\partial t} + \beta \frac{\partial T}{\partial t}$$

and using this to eliminate the velocity in (4.24) gives

$$\rho^0 C_p \frac{\partial T}{\partial t} = T^0 \beta \frac{\partial p}{\partial t}. \tag{4.26}$$

Here use has been made of the identity

$$c^2 = \frac{(\gamma - 1)\gamma C_v}{T\beta^2}.$$

4. 1. 9 Perfect gas

Gumerov *et al* and Mecredy and Hamilton assumed that the fluid phase was a perfect gas. In this case β, the coefficient of thermal volume expansion, $= 1/T^0$. Using the relations

$$C_v(\gamma - 1) = R$$

and $p^0 = \rho^0 R T^0$

(4.24) becomes

$$\rho^0 C_v \frac{\partial T}{\partial t} + p^0 \nabla \cdot \mathbf{u} = 0.$$

Also (4.25) becomes

$$p' = RT^0 \rho' + R\rho^0 T'$$

and (4.26) becomes

$$\rho^0 C_p \frac{\partial T}{\partial t} = \frac{\partial p}{\partial t}.$$

4. 1. 10 Two phase energy equations

The GIN theory uses equation (4.26) for each phase with the density replaced by the volume averaged density. Since the particulate phase is incompressible its energy equation has no pressure term. Gumerov *et al* multiplied the pressure term for the fluid phase by α, i.e. it is volume averaged, but there is no explanation for this. The two equations are

$$\phi^0 \rho_s{}^0 C_{vs} \frac{\partial T_s}{\partial t} = 0 \tag{4.27}$$

$$\alpha \rho_f{}^0 C_{pf} \frac{\partial T_f}{\partial t} = \alpha T_f{}^0 \beta_f \frac{\partial p}{\partial t}. \tag{4.28}$$

It was shown in the previous section that (4.28) is identical to (4.24). To transform (4.28) back into (4.24) requires the use of the state equation (4.25) and the single fluid continuity-equation. Substituting for the pressure using the state equation gives

$$\alpha \rho_f{}^0 C_{vf} \frac{\partial T_f}{\partial t} = \frac{\alpha(\gamma_f - 1) C_{vf}}{\beta_f} \frac{\partial \rho_f}{\partial t}.$$

Substituting for ρ_f using equation (4.11) instead of the single fluid continuity equation gives

$$\alpha \rho_f{}^0 C_{vf} \frac{\partial T_f}{\partial t} = -\frac{(\gamma_f - 1)\rho_f{}^0 C_{vf}}{\beta_f} \frac{\partial}{\partial z}\left(\phi^0 u_s + \alpha u_f\right). \tag{4.29}$$

Equation (4.29) shows the influence of the particulate phase. This is the equation quoted by Mecredy and Hamilton, neglecting the mass transfer terms. Equation (4.28) is the same equation in a more concise form.

4. 1. 11 Heat transfer

Heat transfer between the phases is modelled with source terms in the energy equations.

Michaelides and Feng [44] derived the energy equation of a rigid sphere in a viscothermal fluid with an unsteady flow and temperature field. This is given by their equation (36). Neglecting the spatial derivatives of T_f gives

$$m_s C_{ps}\frac{\partial T_s}{\partial t} = m_s C_{pf}\frac{\partial T_f}{\partial t} - 4\pi a\tau_f\left(T_s - T_f\right) - 4a^2\sqrt{\rho_f{}^0 C_{pf}\pi\tau_f}\int_0^t \frac{d\left(T_s(t') - T_f(t')\right)}{dt'}(t-t')^{-\frac{1}{2}}dt'. \tag{4.30}$$

Here m_s is the mass of the sphere.

For harmonic time dependence the final term, the history term, becomes

$4a^2\sqrt{\rho_f{}^0 C_{pf}\pi\tau_f}(-i\omega)\sqrt{\frac{\pi}{2\omega}}(1+i)\left(T_f - T_s\right)$ or

$$4a^2\sqrt{\rho_f{}^0 C_{pf}\pi\tau_f}\sqrt{\frac{\pi}{2\omega}}\left(\omega + \frac{d}{dt}\right)\left(T_f - T_s\right).$$

The $\partial T_f/\partial t$ term on the RHS is analogous to the induced mass term in the momentum equation. Numerical tests show that this term can be neglected compared to the other terms for the range of frequencies of interest here.

The second term on the right hand side is analogous to the Stokes drag term in the momentum equation.

The terms on the RHS of equation (4.30) represent the energy supply to the sphere. For N particles per unit volume in the fluid, the energy supply to the particulate phase is

$$\left[\frac{3\kappa_f\phi}{a^2} + \frac{3\phi}{a}\sqrt{\frac{\rho_f' C_{pf}\kappa_f\omega}{2}}(1-i)\right]\left(T_f - T_s\right)$$

or

$$-i\omega\rho_f{}^0\phi\left[\tfrac{3}{2}iC_{pf}\frac{\delta_{hf}{}^2}{a^2} + \tfrac{3}{2}(1+i)C_{pf}\frac{\delta_{hf}}{a}\right]\left(T_f - T_s\right). \tag{4.31}$$

This form has also been obtained by Gumerov *et al*. In addition they included the effect of the thermal boundary layer inside the particle. The temperature of the particulate phase is governed by their equation (22)

$$\frac{\partial T_s}{\partial t} = \frac{T_f - T_s}{\tilde{\tau}_T}. \tag{4.32}$$

$\tilde{\tau}_T$ is a complex relaxation time given by

$$\tilde{\tau}_T = \frac{\rho_s C_s}{\rho_f C_{pf}}\left(\tilde{\tau}_f + \tilde{\tau}_s\right).$$

Here C_s stands for either C_{vs} or C_{ps} because for an incompressible medium they are the same.

$\tilde{\tau}_f$ is the complex relaxation time for the heat flow in the fluid

$$\tilde{\tau}_f = \frac{a^2 \rho_f{}^0 C_{pf}}{3\tau_f} \frac{1}{1 - i x_{f2}}$$

and $\tilde{\tau}_s$ is that for the heat flow inside the particle

$$\tilde{\tau}_s = -\frac{a^2 \rho_f{}^0 C_{pf}}{3\tau_s} \frac{\tan x_{s2} + 3/x_{s2} - 3\tan x_{s2}/x_{s2}{}^2}{\tan x_{s2} - x_{s2}}.$$

Multiplying (4.30) by $\phi^0 \rho_s{}^0 C_s$ gives a LHS equivalent to (4.27)

$$\phi^0 \rho_s{}^0 C_s \frac{\partial T_s}{\partial t} = \phi^0 \rho_f{}^0 C_{pf} \left(\tilde{\tau}_f + \tilde{\tau}_s\right)^{-1} \left(T_f - T_s\right).$$

This is the energy equation for the particulate phase. Writing the energy equation in the form

$$\phi^0 \rho_s{}^0 C_s \frac{\partial T_s}{\partial t} = -i\omega \phi^0 \rho_f{}^0 S_h \left(T_f - T_s\right) \tag{4.33}$$

defines a heat transfer term S_h analogous to the S momentum transfer term. This is related to the GIN relaxation times by

$$S_h = \frac{C_{pf}}{-i\omega} \left(\tilde{\tau}_f + \tilde{\tau}_s\right)^{-1}$$

$$= \frac{3\tau_f}{-i\omega a^2 \rho_f{}^0} \left[\frac{1}{1 - i x_{f2}} - \frac{\tau_f}{\tau_s} \frac{\tan x_{s2} + 3/x_{s2} - 3\tan x_{s2}/x_{s2}{}^2}{\tan x_{s2} - x_{s2}} \right]^{-1}. \tag{4.34}$$

If $\tau_f / \tau_s \to 0$ the second term in the brackets can be neglected and the RHS of (4.33) is equivalent to (4.31).

The fluid energy equation including heat transfer is

$$\alpha \rho_f{}^0 C_{vf} \frac{\partial T_f}{\partial t} = i\omega \phi^0 \rho_f{}^0 S_h \left(T_f - T_s\right) - \frac{\left(\gamma_f - 1\right) \rho_f{}^0 C_{vf}}{\beta_f} \frac{\partial}{\partial z} \left(\phi^0 u_s + \alpha u_f\right). \tag{4.35}$$

because, neglecting mass transfer, the amount of heat energy gained by the particulate phase must be equal to that lost by the fluid phase.

4. 1. 12 Comparison with long wavelength scattering theory

The term in square brackets in equation (4.32) for the heat transfer is similar to the term in square brackets in equation (3.52) for the A_0 coefficient. The $\tilde{\tau}_f$ dependence on frequency in both cases is

$$\frac{1}{1-ix_{f2}}. \tag{4.36}$$

The $\tilde{\tau}_s$ dependence on frequency is different in the two expressions. The long wavelength scattering theory gives

$$\frac{\tau_f}{\tau_s}\frac{\tan x_{s2}}{\tan x_{s2}-x_{sx}}. \tag{4.37}$$

The GIN expression is also derived from long wavelength scattering but the temperature distribution inside the particle has then been volume averaged to give an effective single temperature for the whole particle. This results in $\tilde{\tau}_s$ having the frequency dependence

$$\frac{\tau_f}{\tau_s}\frac{\tan x_{s2}+\frac{3}{x_{s2}}-\frac{3\tan x_{s2}}{x_{s2}^{\,2}}}{\tan x_{s2}-x_{s2}}. \tag{4.38}$$

For low frequencies the fluid expression (4.36) tends to a steady state value of 1. The coupled phase expression for the particulate phase (4.38) has a steady state value of

$$\frac{\tau_f}{5\tau_s}.$$

In figure 4. 1 the magnitudes of the expressions (4.36) to (4.38) are plotted versus frequency, the steady state values are plotted as dashed lines. The physical properties used are for alumina dust in air, these are given in appendix 1. The particles have a radius of 2 μm.

For low frequencies the square brackets term in S_h has a constant steady state value. The scattering theory expression for $\tilde{\tau}_s$ grows indefinitely as $\omega \to 0$ so the heat transfer part of A_0 tends to zero.

Figure 4. 1 shows that for this type of suspension it is possible to neglect the internal heat transfer compared to the external heat transfer in the GIN expression. The same cannot be said for the scattering theory, except at high frequencies.

The scattering theory is not valid in the low frequency limit. It is known from observations that heat transfer does have a steady state at low rates of temperature change. This behaviour is modelled by the GIN expression.

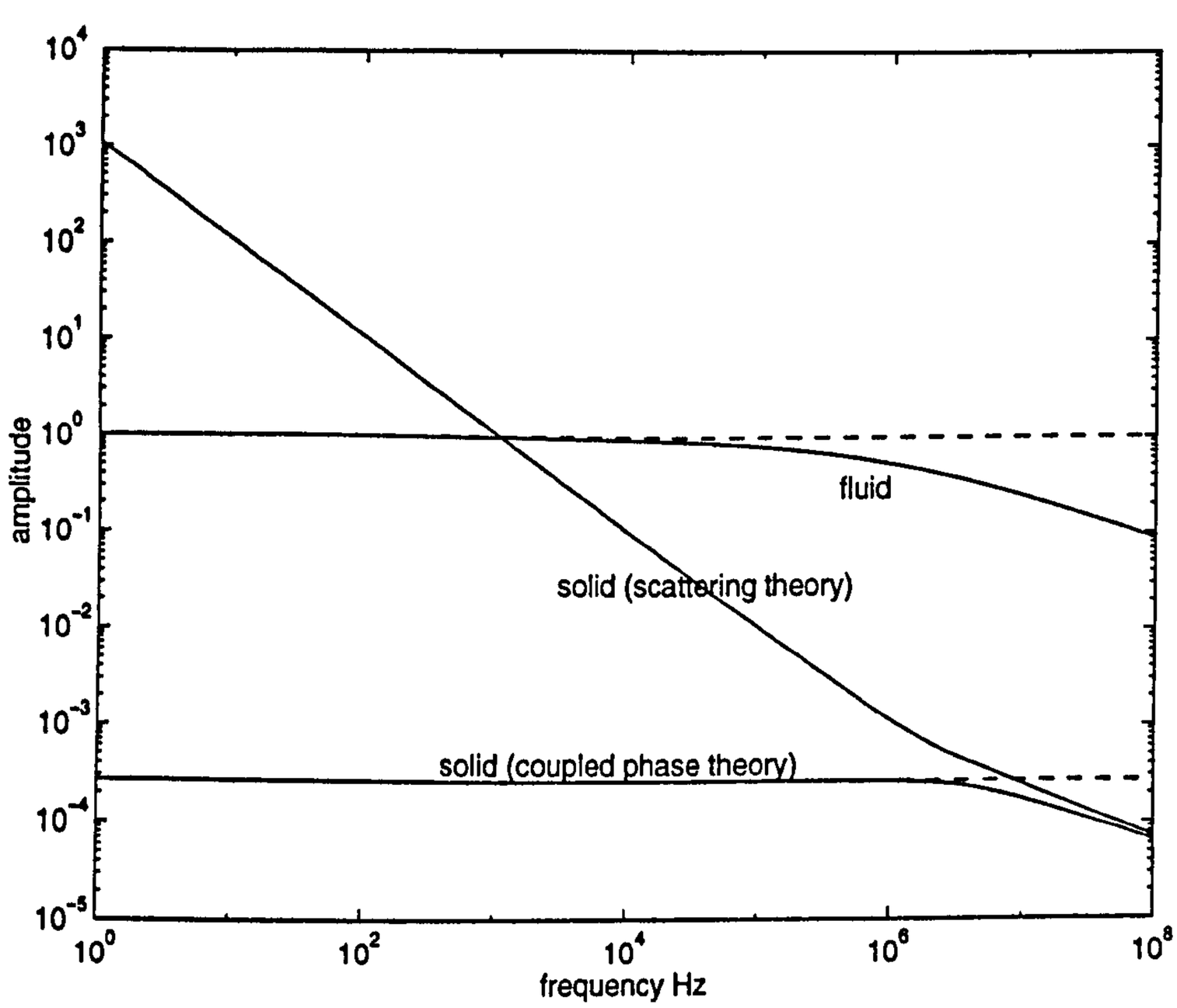

Figure 4. 1 Frequency dependence of the magnitudes of the complex relaxation times for heat transfer in the air and particles of an air suspension of 2 μm radius alumina particles. Comparison of the expressions given by the GIN and scattering theories. Dashed lines indicate steady state values.

4. 1. 13 The complex wavenumber

The set of linear equations defining the medium with an incompressible particulate phase and with heat transfer between the phases are the continuity equation (4.11), the momentum equations of either GIN ((4.14) and (4.15)) or MH ((4.16) and (4.17)), the state equation (4.25) and the energy equations (4.33) and (4.35). The momentum transfer term is given by (4.13) and the heat transfer term by (4.34). The MH version (neglecting mass transfer) is given below.

The set of six equations

$$\frac{\alpha}{\rho_f{}^0}\frac{\partial \rho_f}{\partial t} = -\frac{\partial}{\partial z}\left(\phi^0 u_s + \alpha u_f\right) \tag{4.39a}$$

$$\phi^0 \rho_s{}^0 \frac{\partial u_s}{\partial t} = -i\omega\phi^0 \rho_f{}^0 S\left(u_f - u_s\right) - \phi^0 \frac{\partial p}{\partial z} \tag{4.39b}$$

$$\alpha\rho_f{}^0 \frac{\partial u_f}{\partial t} = i\omega\phi^0 \rho_f{}^0 S\left(u_f - u_s\right) - \alpha \frac{\partial p}{\partial z} \tag{4.39c}$$

$$\frac{\gamma_f}{c_f{}^2} p' = \rho_f' + \rho_f{}^0 \beta_f T_f' \tag{4.39d}$$

$$\phi^0 \rho_s{}^0 C_s \frac{\partial T_s}{\partial t} = -i\omega\phi^0 \rho_f{}^0 S_h \left(T_f - T_s\right) \tag{4.39e}$$

$$\alpha\rho_f{}^0 C_{pf} \frac{\partial T_f}{\partial t} = i\omega\phi^0 \rho_f{}^0 S_h \left(T_f - T_s\right) + \alpha T_f{}^0 \beta_f \frac{\partial p}{\partial t} \tag{4.39f}$$

in the six unknowns ρ_f', u_s', u_f', T_s', T_f' and p' can be solved to obtain k the complex wavenumber.

Since all the variables are of the form (4.1) the derivatives can be transformed using the relations (4.2) and the exponential terms cancel in all the equations. Since $T_f{}^0 = T_s{}^0$ these terms disappear in the relative temperature terms.

The six equations may be written as a 6×6 matrix equation

$$\mathbf{A}\mathbf{y} = 0 \tag{4.40}$$

where

$$\mathbf{y} = \left(\rho_f' \;\; u_f' \;\; u_s' \;\; T_f' \;\; T_s' \;\; p'\right).$$

y has a non trivial solution if and only if

$$\det \mathbf{A} = 0. \tag{4.41}$$

A is a matrix in terms of physical constants, ϕ, S and S_h and k so equation (4.41) can be solved to obtain an expression for k.

4. 1. 14 Perfect gas

After simplifying and assuming a perfect gas, equations (4.39) become

$$\alpha\rho_f' = K\rho_f{}^0\left(\phi^0 u_s' + \alpha u_f'\right)$$

$$\left(\rho_s{}^0 + \rho_f{}^0 S\right)u_s' = \rho_f{}^0 S u_f' + Kp'$$

$$\rho_f{}^0\left(\alpha + \phi^0 S\right)u_f' = \phi^0\rho_f{}^0 S u_s' + \alpha K p'$$

$$p' = RT\rho_f' + \rho_f{}^0 RT_f'$$

$$T_s' = T_f'\left(1 + \frac{\rho_s{}^0 C_s}{\rho_f{}^0 S_h}\right)^{-1}$$

$$\phi^0\rho_f{}^0 S_h T_s' = \rho_f{}^0\left(\alpha C_{pf} + \phi^0 S_h\right)T_f' - \alpha p'$$

where $T = T_f{}^0 = T_s{}^0$ and $K = k/\omega$.

Eliminating T_s' between the last two equations gives

$$\rho_f{}^0 C_{vf}\left(\gamma_f + F_h\right)T_f' - p' = 0$$

where

$$F_h = \frac{\phi^0\rho_s{}^0 C_s S_h}{\alpha C_{vf}\left(\rho_s{}^0 C_s + \rho_f{}^0 S_h\right)}. \tag{4.42}$$

Eliminating the density between the continuity and state equations gives

$$\alpha p' = RTK\rho_f{}^0\left(\phi^0 u_s' + \alpha u_f'\right) + \alpha R\rho_f{}^0 T_f'.$$

The set of equations can then be written as the matrix equation

$$\begin{pmatrix} \rho_f S & -\left(\rho_s + \rho_f S\right) & K & 0 \\ -\rho_f(\alpha + \phi S) & \phi\rho_f S & \alpha K & 0 \\ 0 & 0 & -\left(\gamma_f - 1\right) & \rho_f R\left(\gamma_f + F_h\right) \\ \alpha RTK\rho_f & \phi RTK\rho_f & -\alpha & \alpha R\rho_f \end{pmatrix}\begin{pmatrix} u_f' \\ u_s' \\ p' \\ T_f' \end{pmatrix} = 0. \tag{4.43}$$

Here the superscript zeros have been dropped but the equilibrium values of the respective quantities are understood. This notation will be used for the remainder of this section.

Equation (4.43) has been solved symbolically using Mathcad. Some of the expressions produced by Mathcad as steps in the calculation are shown in mecred.ma in appendix 2. The MH expression for the square of the complex wavenumber is

$$K^2 = \left(\frac{k}{\omega}\right)^2 = \frac{(\alpha\kappa_f)(S\rho_{va} + \alpha\rho_s)}{S + \alpha\rho_s\rho_b} \frac{1 + F_h}{1 + F_h/\gamma_f} \tag{4.44}$$

where ρ_{va} is the total volume averaged density discussed in section 4.1.6 and

$$\rho_b = \frac{\alpha}{\rho_f} + \frac{\phi}{\rho_s}. \tag{4.45}$$

κ_f is the compressibility of the fluid phase given by

$$\kappa_f = \frac{1}{c_f^2 \rho_f}. \tag{4.46}$$

For a perfect gas

$$\kappa_f = \frac{1}{p^0 \gamma_f}.$$

Because Mecredy and Hamilton included mass transfer in their theory, the six balance equations contained terms in addition to those presented here. For this reason they were not able to derive an analytical result and solved the matrix equation corresponding to (4.43) numerically.

If the GIN momentum equations (4.14) and (4.15) are used the result is

$$K^2 = \left(\frac{k}{\omega}\right)^2 = \frac{(\alpha\kappa_f)(S\rho_{va} + \rho_s)}{S + \rho_s\rho_b} \frac{1 + F_h}{1 + F_h/\gamma_f}. \tag{4.47}$$

This is identical to the complex wavenumber given by equations (24) in Gumerov *et al* [102] with the heat transfer term given by their equations (26).

4. 1. 15 Limiting sound speeds

It is useful to check the limiting behaviour of the theoretical expressions for low and high frequencies. The high frequency limit of the sound speed is known as the frozen sound speed and the low frequency limit of the sound speed is known as the equilibrium sound speed.

In the limit $\omega \to 0$, equations (4.13) and (4.34) show that S and $S_h \to \infty$. The heat transfer term

$$\frac{1 + F_h}{1 + F_h/\gamma_f}$$

can be rewritten in terms of S_h as

$$\frac{S_h(\rho C_v)_{va} + \alpha\rho_s C_s C_{vf}}{S_h\gamma_f^{-1}(\rho C_v\gamma)_{va} + \alpha\rho_s C_s C_{vf}}.$$

Thus in the limit $\omega \to 0$

$$\left(\frac{k}{\omega}\right)^2 = \alpha\kappa_f\rho_{va}\frac{\gamma_f(\rho C_v)_{va}}{(\rho C_v\gamma)_{va}}.$$

The quantity on the right is real so the attenuation ξ is zero, the equilibrium sound speed is given by

$$c_{eq}^{-2} = \alpha\kappa_f\rho_{va}\frac{\gamma_f(\rho C_v)_{va}}{(\rho C_v\gamma)_{va}}. \tag{4.48}$$

In the limit $\omega \to \infty$, $S_h \to 0$ and $S \to C = \frac{1}{2}$. In the high frequency limit the inertial momentum transfer is important. The MH frozen sound speed is given by

$$c_\infty^{-2} = \frac{\alpha\kappa_f(C_v\rho_{va} + \alpha\rho_s)}{C + \alpha\rho_s\rho_b}. \tag{4.49}$$

If no momentum transfer is assumed i.e. $S \to 0$ then the frozen sound speed is given by

$$c_\infty^{-2} = \alpha\kappa_f/\rho_b. \tag{4.50}$$

4. 1. 16 Alumina dust in air

For the alumina dust in air suspension from section 3. 2. 10, with a volume fraction of 10^{-5}, the attenuation and sound speed were calculated from the MH and GIN models given by equations (4.44) and (4.47) respectively. The results were almost identical to the scattering theory predictions shown in figure 3. 4.

Figure 4. 2 plots the predictions of the two coupled phase theories, and the single scattering theory from figure 3. 8, at 10^5 Hz for volume fractions up to 0.01. Again, the predictions of the two coupled phase theories are almost identical to the prediction of the single scattering theory. The small difference between the two coupled phase theories is not important.

Figure 4. 3 plots the conditions for the validity of the isolated particle assumption from figure 3. 5 and the conditions for a continuum from section 4. 1. 1. The long wavelength line has been obtained by plotting $\lambda = a$ or $f = c/a$. The long wavelength assumption is valid in the region below this line. The GIN curve is

$$\phi = \left(\frac{fa}{c_f}\right)^3$$

and the Crowe curve is

$$\phi = \left(\frac{4\pi \times 10^4}{3}\right)\left(\frac{fa}{c_f}\right)^3 .$$

The continuum assumption is valid in the regions below these curves. The isolated particle and continuum conditions give upper and lower bounds for both the frequency and the volume fraction. Figure 4. 3 suggests that the continuum assumption is not valid at frequencies above 10^6 when the volume fraction is as low as 10^{-5}. For frequencies below 10^6 the boundary layers are overlapping if the volume fraction is greater than 0.1 and thus the isolated particle assumption is not strictly valid.

Figure 4. 4 compares the sound speed at 10^5 Hz and the limiting sound speeds from the previous section. Also shown is Urick's formula [104]

$$c^{-2} = \kappa_{va}\rho_{va} .$$

The equilibrium sound speed is close to Urick's formula showing that the large difference between the densities of the two phases is the dominant influence on the sound speed. Because the particulate phase is incompressible, the sound speed tends to zero as the volume fraction increases.

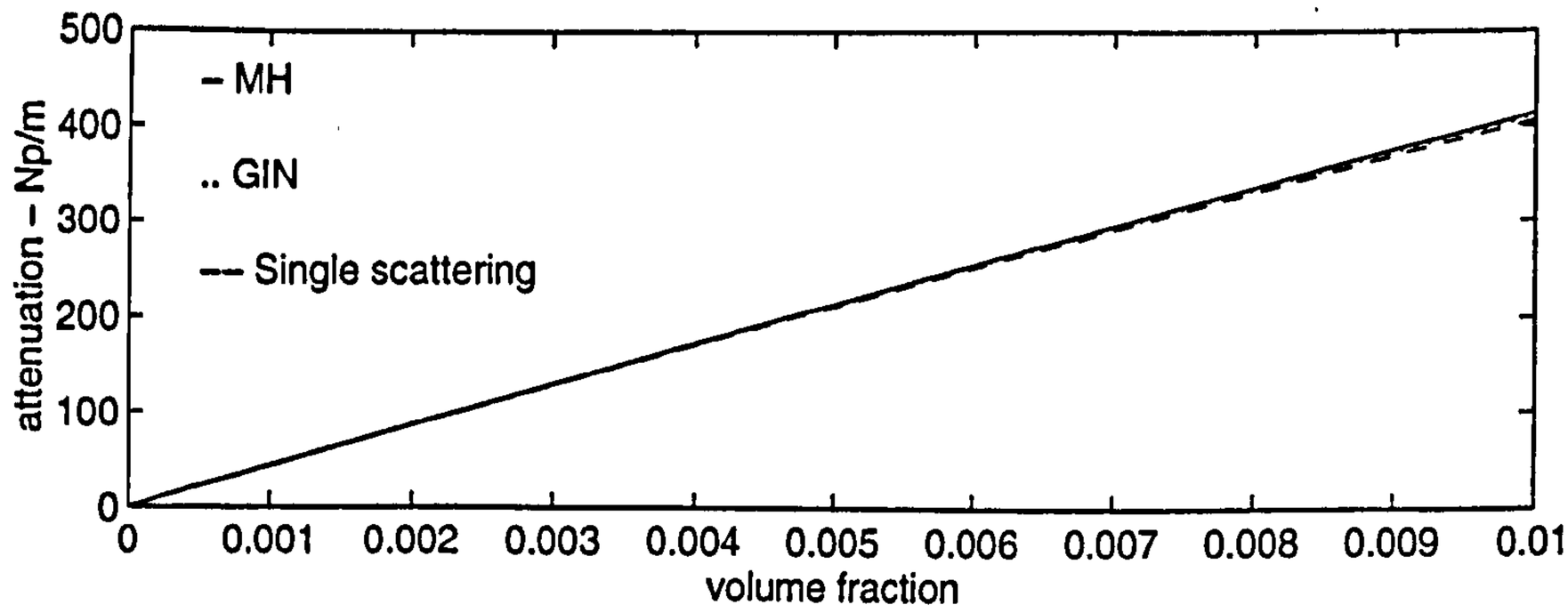

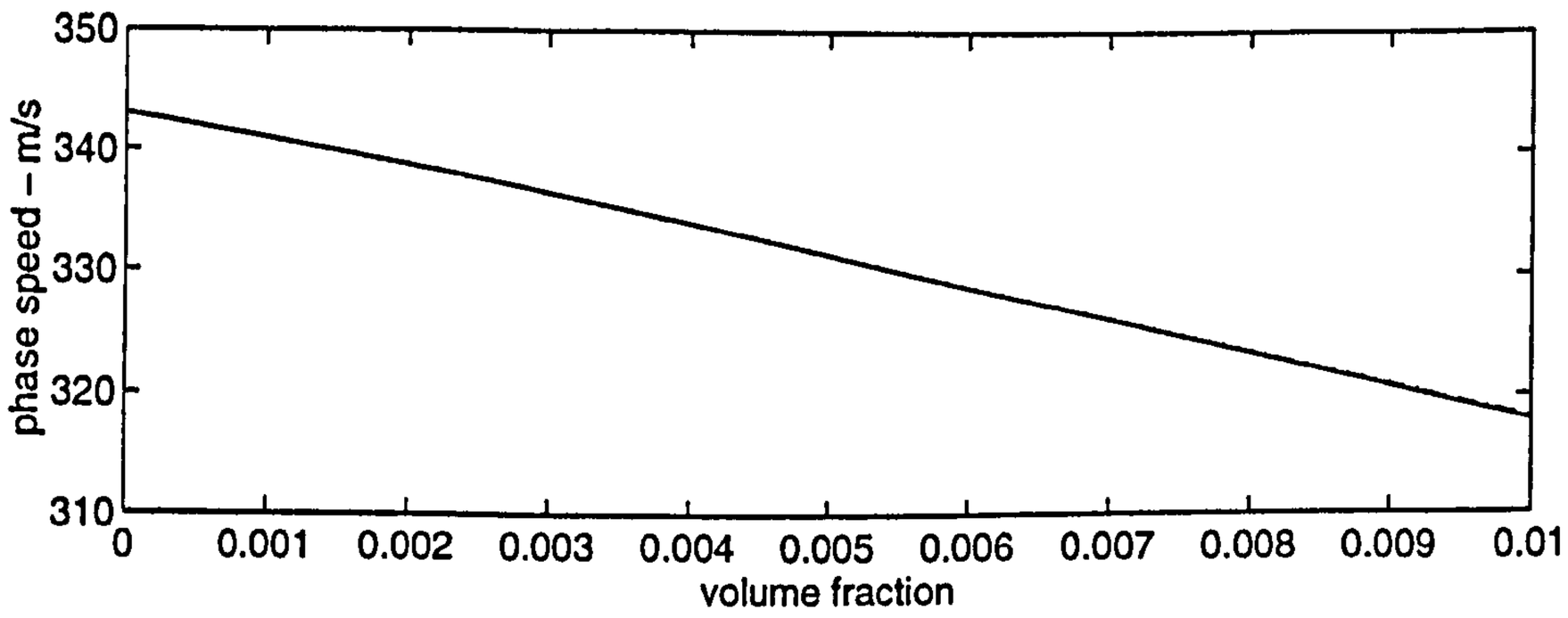

Figure 4. 2 Attenuation and sound speed versus volume fraction for an air suspension of alumina particles of radius 2 μm at 10^5 Hz. Comparison of predictions of MH and GIN coupled phase theories and single scattering theory.

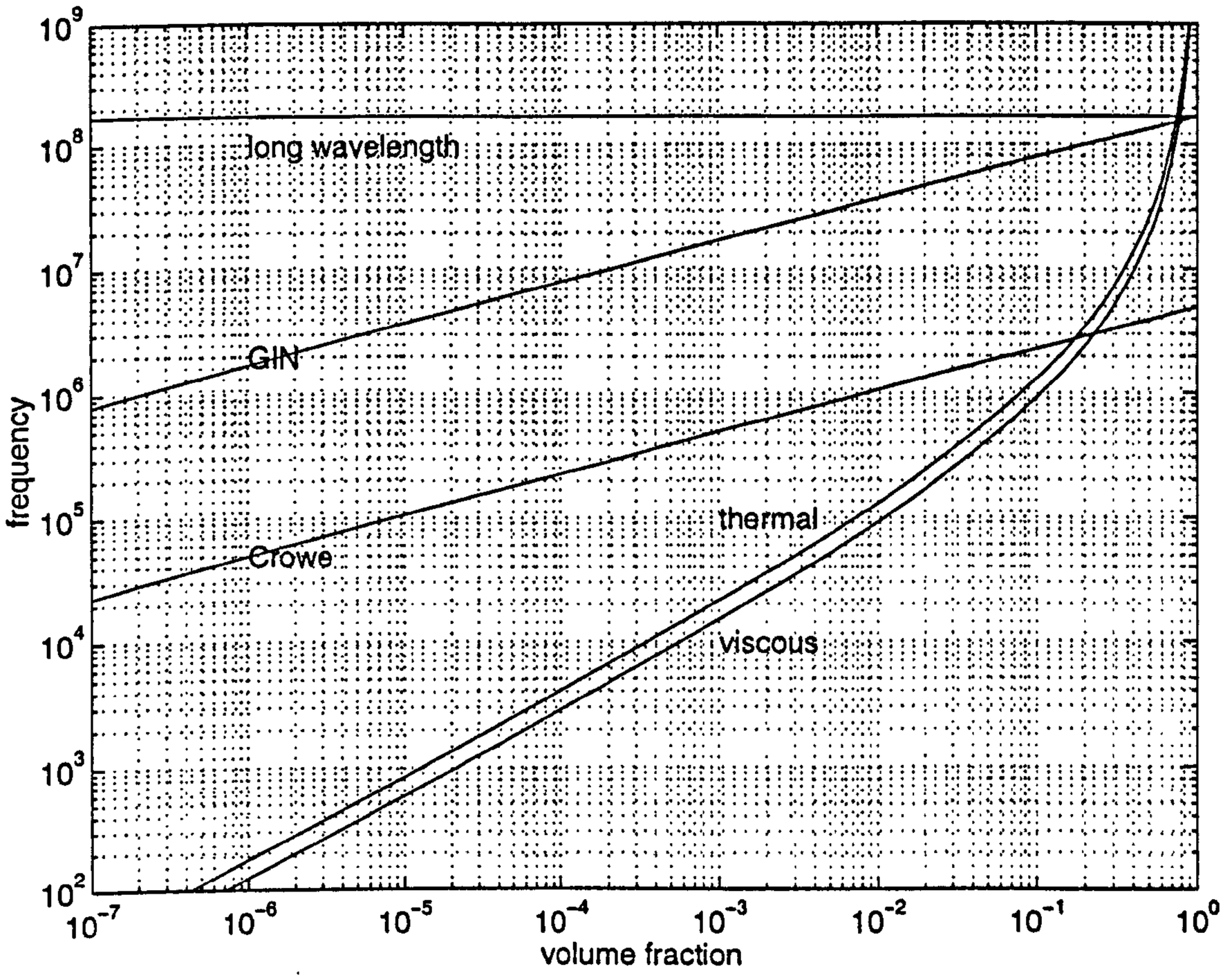

Figure 4. 3 Curves indicating regions where the continuum, long wavelength and isolated particle assumptions are valid, for an air suspension of particles of radius 2 μm. The long wavelength assumption is valid in the region below the 'long wavelength' line. The continuum assumption is valid in the region below the GIN and Crowe lines. The boundary layers overlap in the regions to the right of the 'thermal' and 'viscous' curves.

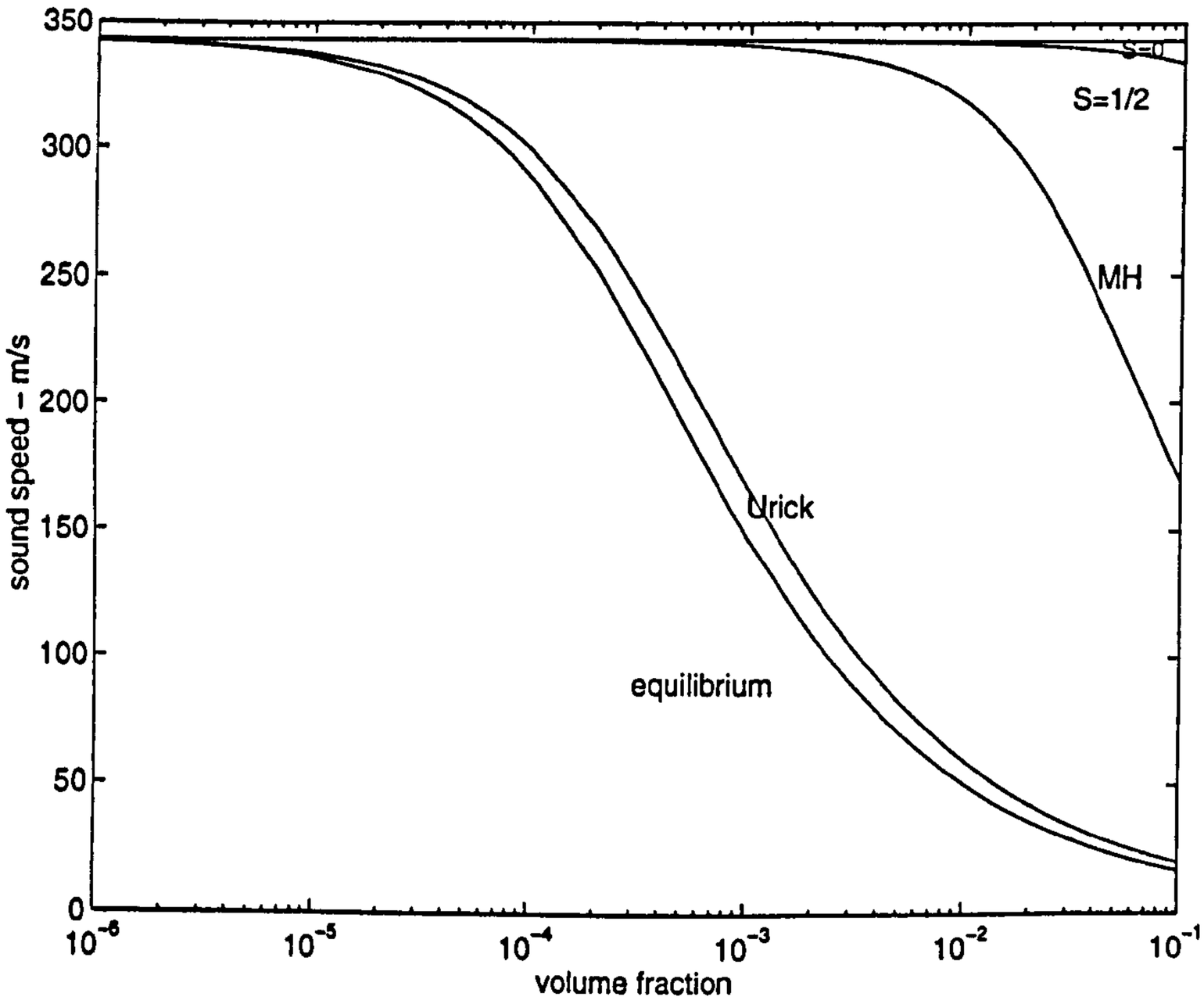

Figure 4. 4 Sound speed versus volume fraction for an air suspension of 2 μm alumina particles at 10^5 Hz. Comparison of predictions of MH theory and limiting sound speeds.

4. 2 Compressible particulate phase

This section follows the work of Harker and Temple (HT) [65] and Atkinson and Kytomaa [113]. The conservation of mass and momentum equations are identical to those used in the previous section.

Since the particulate phase is compressible it requires a state equation. The energy and state equations for each phase are obtained by assuming both phases behave isothermally when perturbed by the sound wave. Thus energy equations are not necessary and the state equations for the two phases are from (4.25)

$$p_s' = c_s^2 \rho_s' \tag{4.51}$$

$$p_f' = c_f^2 \rho_f' \tag{4.52}$$

because $\gamma \equiv 1$ for the isothermal approximation.

Another assumption made here and in the following section is that

$$p_s = p_f = p$$

so

$$p_s^0 = p_f^0 = p^0$$

and

$$p_s' = p_f' = p' .$$

This assumption can only be valid when the particulate phase behaves as a continuum.

Substituting equations (4.51) and (4.52) into (4.9) after the rule (4.1) has been applied gives

$$\left(\phi^0 \kappa_s + \alpha \kappa_f\right) p' = \kappa_{va} p' = K\left(\phi^0 u_s' + \alpha u_f'\right)$$

because $c^{-2} = \kappa\rho$.

The momentum equations are from section 4. 1. 13

$$\left(\rho_s^0 + \rho_f^0 S\right) u_s' = \rho_f^0 S u_f' + K p'$$

$$\rho_f^0 \left(\alpha + \phi^0 S\right) u_f' = \phi^0 \rho_f^0 S u_s' + \alpha K p'$$

and a 3×3 matrix equation can be formed:

$$\begin{pmatrix} \alpha K & \phi K & -\kappa_{va} \\ \rho_f S & -\left(\rho_s + \rho_f S\right) & K \\ -\rho_f(\alpha + \phi S) & \phi \rho_f S & \alpha K \end{pmatrix} \begin{pmatrix} u_f' \\ u_s' \\ p' \end{pmatrix} = 0 .$$

Here the superscript zeros have been omitted. As in section 4. 1. 13 this matrix has been solved symbolically using Mathcad to give

$$K^2 = \left(\frac{k}{\omega}\right)^2 = \frac{\kappa_{va}\left(S\rho_{va} + \alpha\rho_s\right)}{S + \alpha\rho_s\rho_b}. \tag{4.53}$$

If $\kappa_s = 0$ equation (4.53) gives the MH expression (4.42) assuming $F_h = 0$, i.e. no heat transfer. The limiting sound speeds of (4.53) are Urick's formula in the low frequency limit

$$c_{eq}^{-2} = \kappa_{va}\rho_{va},$$

$$c_\infty^{-2} = \frac{\kappa_{va}\left(C\rho_{va} + \alpha\rho_s\right)}{C + \alpha\rho_s\rho_b}$$

when $S = C$

and

$$c_\infty^{-2} = \frac{\kappa_{va}}{\rho_b}$$

when $S = 0$.

Equation (4.53) and its limiting sound speeds are 'self consistent' i.e. they are valid for $0 \le \phi \le 1$. When $\phi = 0$ (4.53) gives

$$c = \left(\rho_f\kappa_f\right)^{-\frac{1}{2}} = c_f$$

and when $\phi = 1$ gives

$$c = \left(\rho_s\kappa_s\right)^{-\frac{1}{2}} = c_s.$$

If the GIN version of the momentum equations are used to obtain the matrix equation then, as for equations (4.44) and (4.47), the factor of α multiplying the ρ_s in equation (4.53) disappears

$$K^2 = \left(\frac{k}{\omega}\right)^2 = \frac{\kappa_{va}\left(S\rho_{va} + \rho_s\right)}{S + \rho_s\rho_b}.$$

Equation (4.53) is used in chapter 5. Its predictions are compared to measurements of the complex wavenumber in suspensions of solid (kaolinite) particles in water and predictions of porous media theory.

4. 3 Coupled phase theory with compressible particulate phase and heat transfer

In emulsions sound propagation is influenced by momentum transfer, heat transfer and compressibility in the particulate phase. To model this, a new

coupled phase theory is derived by combining the theories derived in sections 4. 1 and 4. 2. This is shown to be the only coupled phase theory that successfully models sound propagation in emulsions, and it provides an alternative to scattering theory.

4. 3. 1 Energy and state equations

For liquids the general energy equation (4.24) and state equation (4.25) are required. Multiplying (4.24) by $\phi^0\rho_s{}^0$ for the particulate phase and by $\alpha\rho_f{}^0$ for the continuous phase and adding the heat transfer from equations (4.33) and (4.35) gives

$$\phi^0\rho_s{}^0C_s\frac{\partial T_s}{\partial t}+\frac{\rho_s{}^0(\gamma_s-1)C_s}{\beta_s}\frac{\partial u_s}{\partial z}=-i\omega\rho_f{}^0S_h\left(T_f-T_s\right) \tag{4.54}$$

$$\alpha\rho_f{}^0C_{vf}\frac{\partial T_f}{\partial t}+\frac{\alpha\rho_f{}^0\left(\gamma_f-1\right)C_{vf}}{\beta_f}\frac{\partial u_f}{\partial z}=i\omega\phi^0\rho_f{}^0S_h\left(T_f-T_s\right). \tag{4.55}$$

The state equations for the two phases are

$$\gamma_s\rho_s{}^0\kappa_s p'=\rho_s'+\rho_s{}^0\beta_s T' \tag{4.56}$$

$$\gamma_f\rho_f{}^0\kappa_f p'=\rho_f'+\rho_f{}^0\beta_f T_f'. \tag{4.57}$$

4. 3. 2 Alternative energy equations

Alternative energy equations can be obtained by the same method that yielded the MH and GIN equation (4.35). The method will be described for the continuous phase only, as it is identical for the particulate phase. Starting from the $\left(p,T_f\right)$ energy equation (4.28) p is replaced using the state equation to give an equation in $\left(\rho_f,T_f\right)$. If ρ_f is replaced using the single phase continuity equation

$$\frac{\partial\rho_f}{\partial t}+\rho_f{}^0\frac{\partial u_f}{\partial z}=0$$

then (4.55) is obtained. If ρ_f is replaced using (4.8) then an equation similar to (4.55) is obtained but with a $\partial\phi/\partial t$ term in it. A similar term appears in the equation for the solid phase.

This method will be termed the two phase method and the method described in section 4. 3. 1, leading to equations (4.54) and (4.55), will be termed the single phase method. As discussed below the two methods have been tested against data for a sunflower oil in water emulsion. While the one phase method closely predicts the measured attenuation and agrees with scattering theory the

attenuation predicted by the two phase method is a negligible fraction of the measured value: consequently this method is rejected.

The two phase method is, however, used in the GIN and MH theories for incompressible particles in section 4. 1. To test the importance of the particulate phase term

$$-\phi^0 p^0 \frac{\partial u_s}{\partial z}$$

in the fluid energy equation (4.29), which results from the two phase method, both theories were re-formulated neglecting this term. The revised expressions for the complex wavenumber are

$$K^2 = \left(\frac{k}{\omega}\right)^2 = \frac{(\alpha\kappa_f)(S\rho_{va} + \alpha\rho_s)(1+F_h)}{(S+\alpha\rho_s\rho_b)(1+F_h/\gamma_f)+\phi(1-\gamma_f)\gamma_f^{-1}(S+\alpha)}$$

for the MH theory and

$$K^2 = \left(\frac{k}{\omega}\right)^2 = \frac{(\alpha\kappa_f)(S\rho_{va} + \rho_s)(1+F_h)}{(S+\rho_s\rho_b)(1+F_h/\gamma_f)+\phi(1-\gamma_f)\gamma_f^{-1}(S+1)}$$

for the GIN theory. Comparison with equations (4.44) and (4.47) shows that an extra term proportional to ϕ has been introduced. Numerical tests for alumina dust in air at 10^5 Hz have shown that the difference between the equations derived from the two methods is negligible even at $\phi = 0.74$. It can be concluded that for a high impedance contrast the two phase method is not necessary. It does, however, produce a simpler final expression for the complex wavenumber.

The two methods have been tested against data for two media: a high impedance contrast suspension and a low impedance contrast emulsion. The results for both media support the one phase method. Although the results for the suspension do not prove that the two phase method is wrong, they do not support it either because it has been shown that the extra term it introduces is not required. The two phase method was shown to give very poor predictions for the emulsion. What is required is data for propagation in a medium with properties between these two extremes as further evidence.

4. 3. 3 Complex wavenumber

The governing equations of the coupled phase theory for emulsions are

$$\phi^0 \frac{\partial \rho_s}{\partial t} + \rho_s{}^0 \frac{\partial \phi}{\partial t} + \phi^0 \rho_s{}^0 \frac{\partial u_s}{\partial z} = 0$$

$$\alpha\frac{\partial \rho_f}{\partial t}-\rho_f{}^0\frac{\partial \phi}{\partial t}+\alpha\rho_f{}^0\frac{\partial u_f}{\partial z}=0$$

$$\phi^0\rho_s{}^0\frac{\partial u_s}{\partial t}=-i\omega\phi^0\rho_f{}^0S\left(u_f-u_s\right)-\phi^0\frac{\partial p}{\partial z}$$

$$\alpha\rho_f{}^0\frac{\partial u_f}{\partial t}=i\omega\phi^0\rho_f{}^0S\left(u_f-u_s\right)-\alpha\frac{\partial p}{\partial z}$$

$$\phi^0\rho_s{}^0C_s\frac{\partial T_s}{\partial t}+\frac{\phi^0\rho_s{}^0(\gamma_s-1)C_s}{\beta_s}\frac{\partial u_s}{\partial z}=-i\omega\phi^0\rho_f{}^0S_h\left(T_f-T_s\right)$$

$$\alpha\rho_f{}^0C_{vf}\frac{\partial T_f}{\partial t}+\frac{\alpha\rho_f{}^0\left(\gamma_f-1\right)C_{vf}}{\beta_f}\frac{\partial u_f}{\partial z}=i\omega\phi^0\rho_f{}^0S_h\left(T_f-T_s\right)$$

$$\gamma_s\rho_s{}^0\kappa_s p'=\rho_s'+\rho_s{}^0\beta_s T'$$

$$\gamma_f\rho_f{}^0\kappa_f p'=\rho_f'+\rho_f{}^0\beta_f T_f'.$$

These lead to a matrix equation

$$\mathbf{A}\mathbf{y}=0 \tag{4.58}$$

where

$$\mathbf{y}=\left(\rho_f'\ \ \rho_s'\ \ u_f'\ \ u_s'\ \ T_f'\ \ T_s'\ \ p'\ \ \phi'\right)^T$$

and

$$\mathbf{A}=\begin{pmatrix}
0 & \phi & 0 & -K\phi\rho_s & 0 & 0 & 0 & \rho_s \\
-\alpha & 0 & K\alpha\rho_f & 0 & 0 & 0 & 0 & \rho_f \\
0 & 0 & \rho_f S & -\left(\rho_s+\rho_f S\right) & 0 & 0 & K & 0 \\
0 & 0 & -\rho_f(\alpha+\phi S) & \phi\rho_f S & 0 & 0 & \alpha K & 0 \\
0 & 0 & 0 & K\dfrac{\rho_s C_s(\gamma_s-1)}{\beta_s} & \rho_f S_h & -\left(\rho_s C_s+\rho_f S_h\right) & 0 & 0 \\
0 & 0 & K\dfrac{\alpha\rho_f C_{vf}\left(\gamma_f-1\right)}{\beta_f} & 0 & -\rho_f\left[\alpha C_{vf}+\phi S_h\right] & \phi\rho_f S_h & 0 & 0 \\
0 & 1 & 0 & 0 & 0 & \rho_s\beta_s & -\gamma_s\rho_s\kappa_s & 0 \\
1 & 0 & 0 & 0 & \rho_f\beta_f & 0 & -\gamma_f\rho_f\kappa_f & 0
\end{pmatrix}$$

The equation

$$\det\mathbf{A}=0 \tag{4.59}$$

has been solved partially symbolically using Mathematica. The notebooks used are given in appendix 2.

The notebook couple.ma solves the equation at a single frequency to obtain K at various values of ϕ. All the quantities in (4.59) are entered numerically except for ϕ, and K which is unknown. Mathematica then solves (4.59) to give an

equation for K in terms of ϕ. In another step this equation is rearranged to find the attenuation and sound speed in terms of ϕ. Finally these expressions can be evaluated for a series of values of ϕ.

The notebook couplf.ma solves at a single value of ϕ to obtain K at various values of $a\sqrt{f}$. The variables here are S and S_h. Expressions are obtained for $\alpha\lambda$ and c in terms of S and S_h. Then S and S_h are evaluated for values of $a\sqrt{f}$ and these numbers are substituted into the expressions for $\alpha\lambda$ and c.

4. 3. 4 High frequency limit

In the limit $\omega \to \infty$, $S_h \to 0$, i.e. no heat transfer, and (4.59) can be solved symbolically to give

$$\left(\frac{k}{\omega}\right)^2 = \frac{(\kappa\gamma)_{va}(S\rho_{va} + \alpha\rho_s)}{S\gamma_{va} + \alpha\rho_s\rho_\infty} \text{ where} \tag{4.60}$$

$$\rho_\infty = \left(\frac{\gamma}{\rho}\right)_{va} = \frac{\alpha\gamma_f}{\rho_f} + \frac{\phi\gamma_s}{\rho_s}.$$

If $\gamma_f = \gamma_s = 1$, which is a good approximation for liquids, (4.60) is identical to the Harker and Temple result (4.53).

In the limit $\omega \to \infty$, $S \to C$. Assuming $S \to 0$, i.e. neglecting momentum transfer, (4.59) gives

$$K^2 = \frac{(\kappa\gamma)_{va}\left(S_h(\rho C_v)_{va} + C_{vf}C_s\rho_s\alpha\right)}{S_h A + C_{vf}C_s\rho_s\alpha\rho_\infty},$$

$$A = \phi\alpha\left(C_{vf}\left(\frac{\rho_f}{\rho_s} + (\gamma_f - 1)\frac{\beta_s}{\beta_f} + \gamma_f\frac{\alpha}{\phi}\right) + C_s\left(\frac{\rho_s}{\rho_f} + (\gamma_s - 1)\frac{\beta_f}{\beta_s} + \gamma_s\frac{\phi}{\alpha}\right)\right). \tag{4.61}$$

This result, obtained from the new coupled phase theory neglecting momentum transfer, is a good approximation for the emulsions discussed below.

In the limit $S \to 0$ equation (4.60) gives the frozen sound speed

$$c_\infty^{-2} = \frac{(\kappa\gamma)_{va}}{\rho_\infty} \tag{4.62}$$

which is also given by equation (4.61) in the limit $S_h \to 0$. This is of the same form as the MH frozen sound speed (4.50).

4. 3. 5 Low frequency limit

Using equations (4.18) and (4.19) or (4.20) and (4.21) in the limit $S \to \infty$, the velocities are given by

$$u_s' \to u_f' \to \frac{kp'}{\omega \rho_{va}}.$$

Equation (4.59) may then be solved symbolically to give

$$\left(\frac{k}{\omega}\right)^2 = \frac{(\kappa\gamma)_{va}\rho_{va}\left(S_h(\rho C_v)_{va} + C_{vf}C_s\rho_s\alpha\right)}{S_h A_{eq} + C_{vf}C_s\rho_s\alpha\gamma_{va}},$$

$$A_{eq} = \phi\alpha\left(\rho_f C_{vf}\left(1+(\gamma_f-1)\frac{\beta_s}{\beta_f}+\gamma_f\frac{\alpha}{\phi}\right)+\rho_s C_s\left(1+(\gamma_s-1)\frac{\beta_f}{\beta_s}+\gamma_s\frac{\phi}{\alpha}\right)\right). \quad (4.63)$$

In the limit $\omega \to 0, S_h \to \infty$, equation (4.63) gives for the equilibrium sound speed c_{eq}

$$c_{eq}^{-2} = \frac{(\kappa\gamma)_{va}\rho_{va}(\rho C_v)_{va}}{A_{eq}}. \quad (4.64)$$

If $\beta_f = \beta_s$ (4.64) becomes

$$c_{eq}^{-2} = \frac{(\kappa\gamma)_{va}\rho_{va}(\rho C_v)_{va}}{(\rho C_v \gamma)_{va}}$$

which, with $\kappa_s = 0$, for an incompressible particulate phase, is exactly the MH equilibrium sound speed (4.48).

4. 3. 6 Sunflower oil in water emulsion

Figures 4. 5 and 4. 6 compare the measurements on a sunflower oil in water emulsion, discussed earlier in section 3. 2. 11, with predictions of the coupled phase theory. The frequency is 1.25 MHz and the particle radius is 0.74 μm for the data in figure 4. 5 and 0.27 μm for the data in figure 4. 6. These radii are mean values for the emulsion particles. Shown are the predictions of the full solution of equation (4.59), the $S = 0$ equation (4.61) and the $S = \infty$ equation (4.63) and the equilibrium and frozen sound speeds (equations (4.64) and (4.62) respectively).

Both approximate curves agree well with the data. In figure 4. 5 the full solution attenuation is nearer to the $S = 0$ attenuation while in figure 4. 6 it is nearer to the $S = \infty$ attenuation. This is as would be expected as a is lower in figure 4. 6. The full solution velocity is nearer to the $S = \infty$ velocity for both values of a. In figure 4. 5 the measured and predicted velocities are nearer to the frozen sound speed while in figure 4. 6 they are nearer to the equilibrium sound speed.

Figures 4. 7 and 4. 8 compare the data to the predictions of both the full coupled phase theory and multiple scattering theory. Predictions of the $S = 0$ coupled phase theory have been compared to the McClements data and predictions of

the WT multiple scattering theory in reference [166]. The particle radius is 0.74 μm in figure 4. 7 and 0.27 μm in figure 4. 8. The scattering theory is the WT theory from table 3. 1 with the AH long wavelength scattering coefficients given by equations (3.52) and (3.54). At the higher volume fractions the attenuation predicted by the coupled phase theory is smaller than that predicted by the scattering theory and is closer to the measurements. The velocity predictions of both theories are close to the measurements. In figure 4. 7 the coupled phase theory predicts a lower velocity than the scattering theory and does not agree as well with the measurements. These figures suggest that the coupled phase theory could be a better model for the volume fraction dependence of the complex wavenumber than the scattering theory.

Figure 4. 9 plots the predictions of the two theories versus the frequency number $a\sqrt{f}$ for $\phi = 0.108$. For both theories it is straightforward to show that c and $\alpha\lambda$, where λ is the wavelength, are functions of $a\sqrt{f}$. Both theories predict a lower sound speed than that shown by the data over the whole range of $a\sqrt{f}$. The full scattering solution used in reference [71] does agree with the sound speed data; this indicates that higher A_n terms are necessary. The coupled phase theory may not be valid for the higher values of $a\sqrt{f}$. The predictions of the coupled phase theory are closer to the attenuation data than the predictions of the WT theory shown or the full scattering theory used in reference [71].

Figure 4. 10 shows the overlapping boundary layer conditions and the continuum conditions for the emulsion. These conditions were discussed in section 4. 1. 16 for the alumina suspension. The particle radius is 0.27 μm. At the frequency of 1.25 MHz the range of volume fractions used in the sunflower oil emulsion experiments satisfy the Crowe condition. This indicates that the continuum assumption is valid. The higher volume fractions do not satisfy the thermal condition, this means that the thermal boundary layers are overlapping. There may be interactions between the thermal waves around the particles.

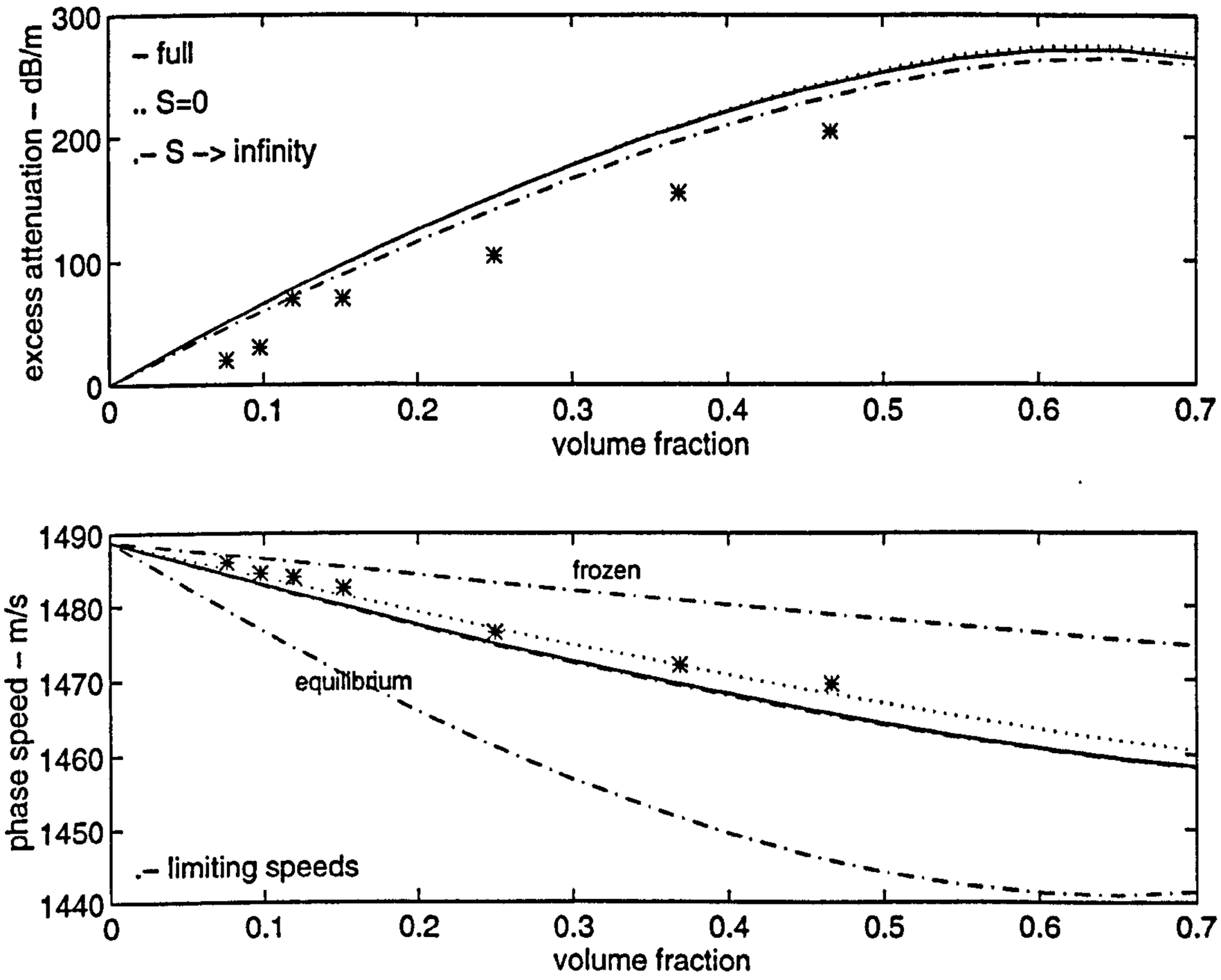

Figure 4. 5 Excess attenuation in dB and ultrasonic velocity versus oil volume fraction for a sunflower oil in water emulsion at 1.25 MHz with mean particle radius 0.74 μm. Comparison of data of McClements and Povey and predictions of full coupled phase theory, theory with S=0 and theory with $S \rightarrow \infty$. Also shown are the limiting sound speeds.

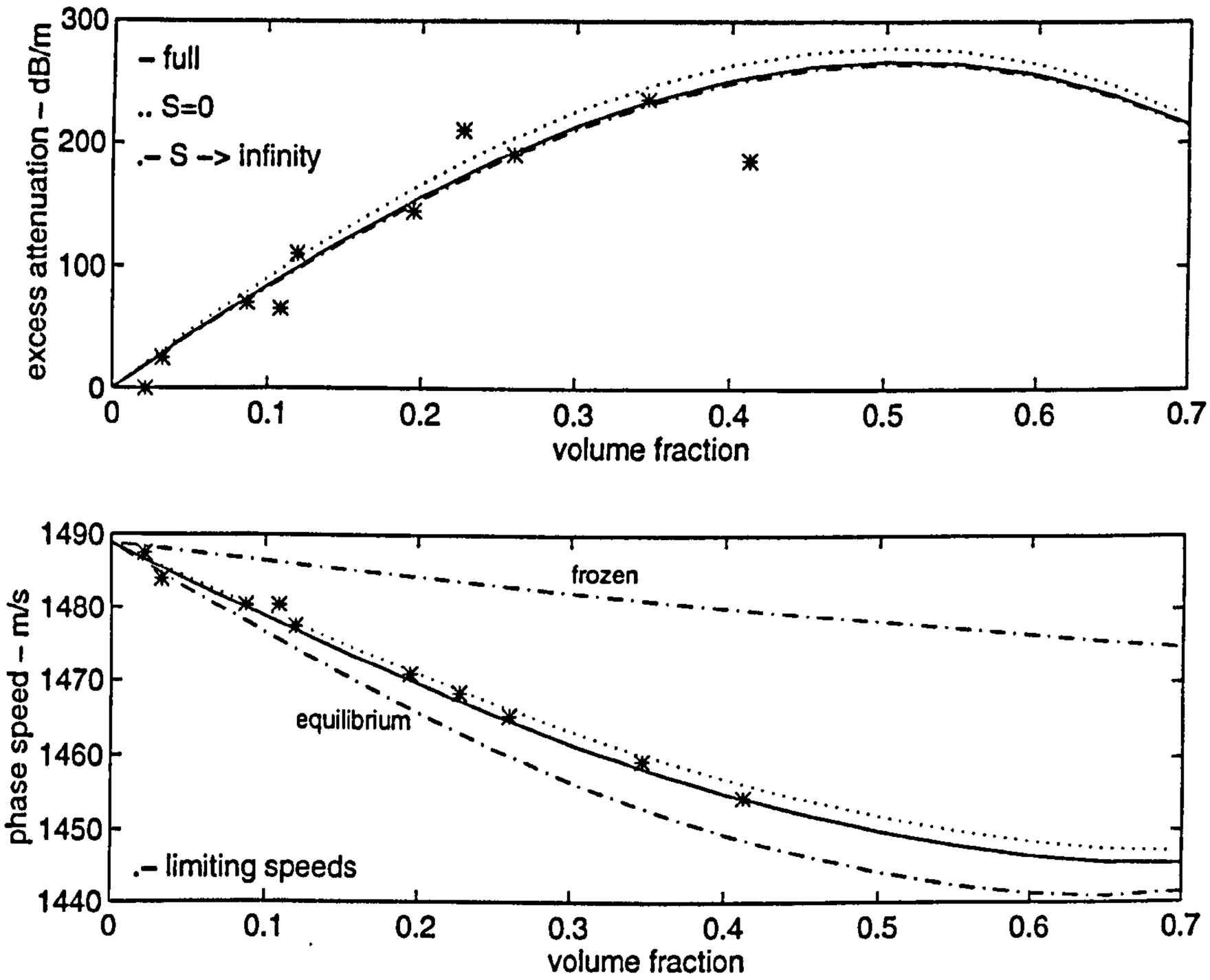

Figure 4. 6 Excess attenuation in dB and ultrasonic velocity versus oil volume fraction for a sunflower oil in water emulsion at 1.25 MHz with mean particle radius 0.27 μm. Comparison of data of McClements and Povey and predictions of full coupled phase theory, theory with S=0 and theory with $S \rightarrow \infty$. Also shown are the limiting sound speeds.

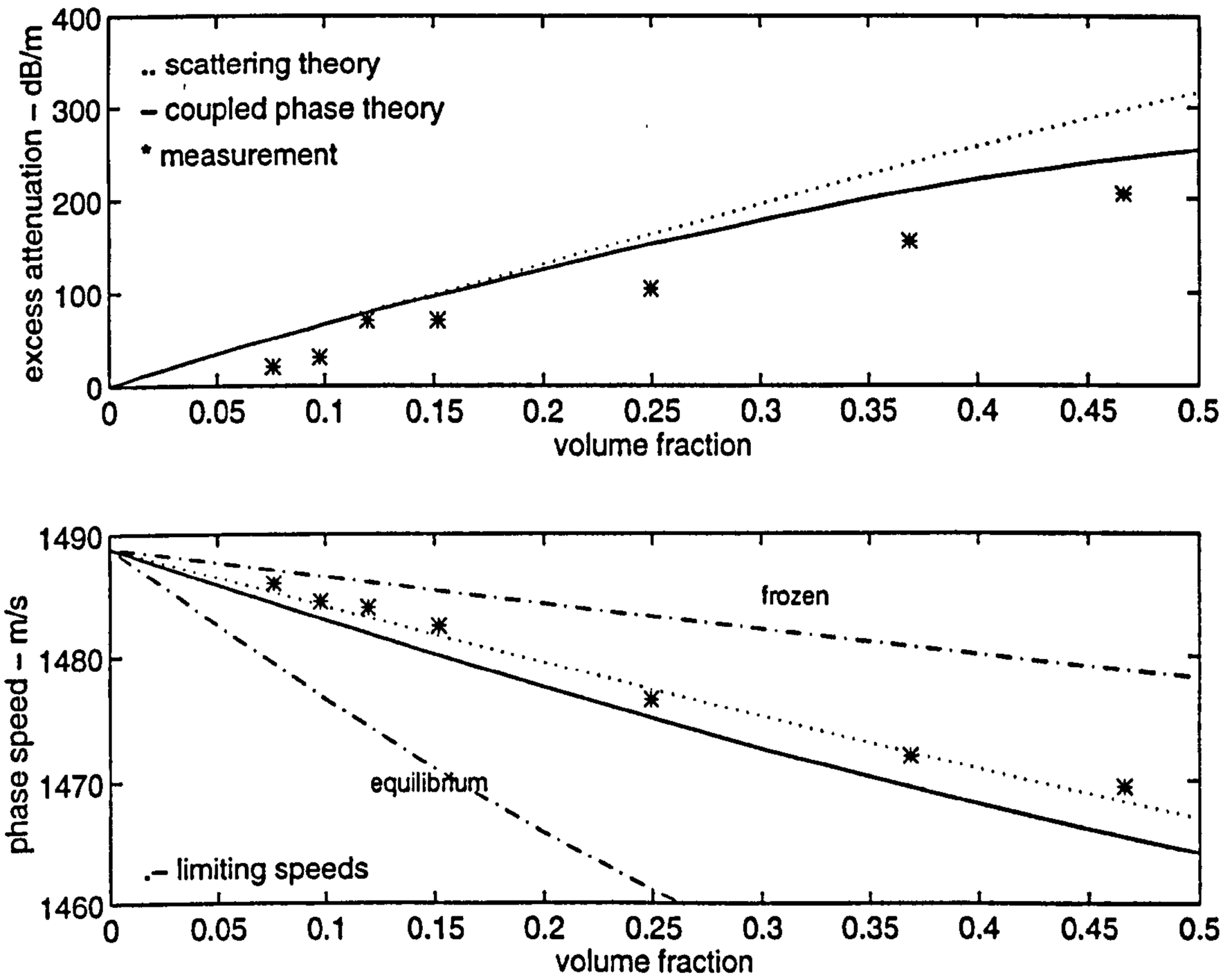

Figure 4. 7 Excess attenuation in dB and ultrasonic velocity versus oil volume fraction for a sunflower oil in water emulsion at 1.25 MHz with mean particle radius 0.74 μm. Comparison of data of McClements and Povey and predictions of coupled phase theory and WT multiple scattering theory. Also shown are the limiting sound speeds.

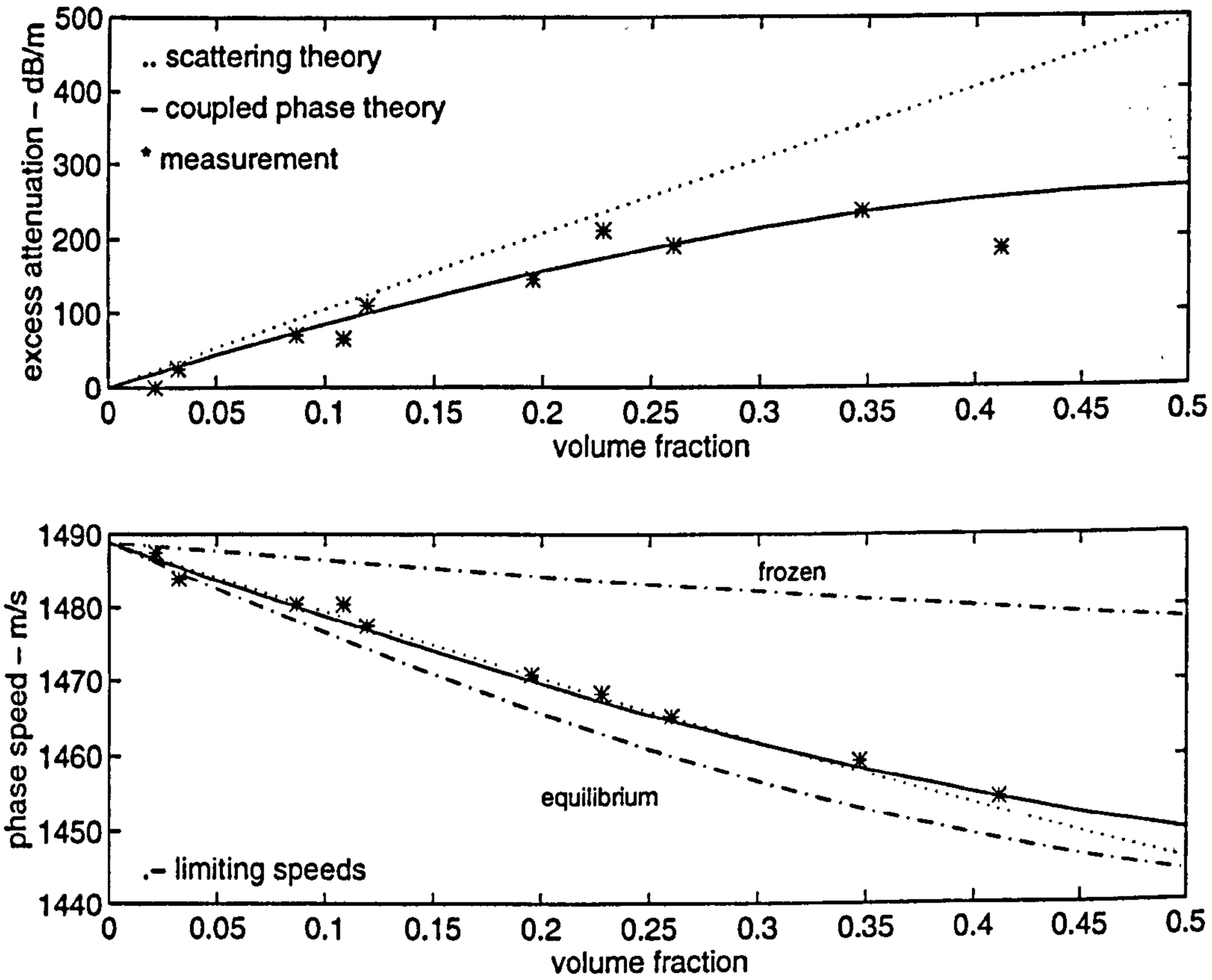

Figure 4. 8 Excess attenuation in dB and ultrasonic velocity versus oil volume fraction for a sunflower oil in water emulsion at 1.25 MHz with mean particle radius 0.27 μm. Comparison of data of McClements and Povey and predictions of coupled phase theory and WT multiple scattering theory. Also shown are the limiting sound speeds.

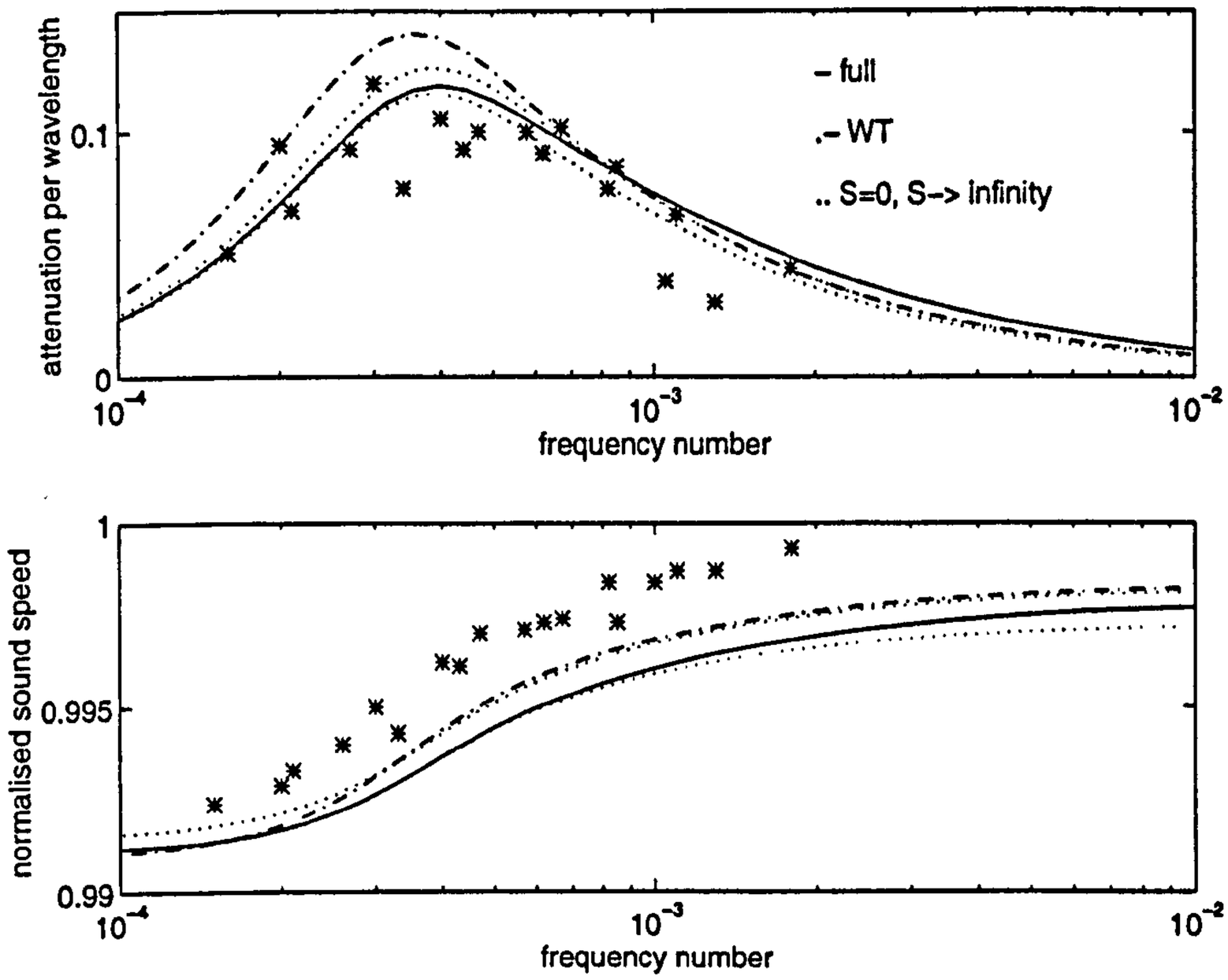

Figure 4. 9 Excess attenuation per wavelength and normalised sound speed versus non-dimensional frequency for a sunflower oil in water emulsion with volume fraction 0.108. Comparison of data of McClements and Povey and predictions of full coupled phase theory, coupled phase theory with $S=0$, coupled phase theory with $S\rightarrow\infty$ and WT multiple scattering theory.

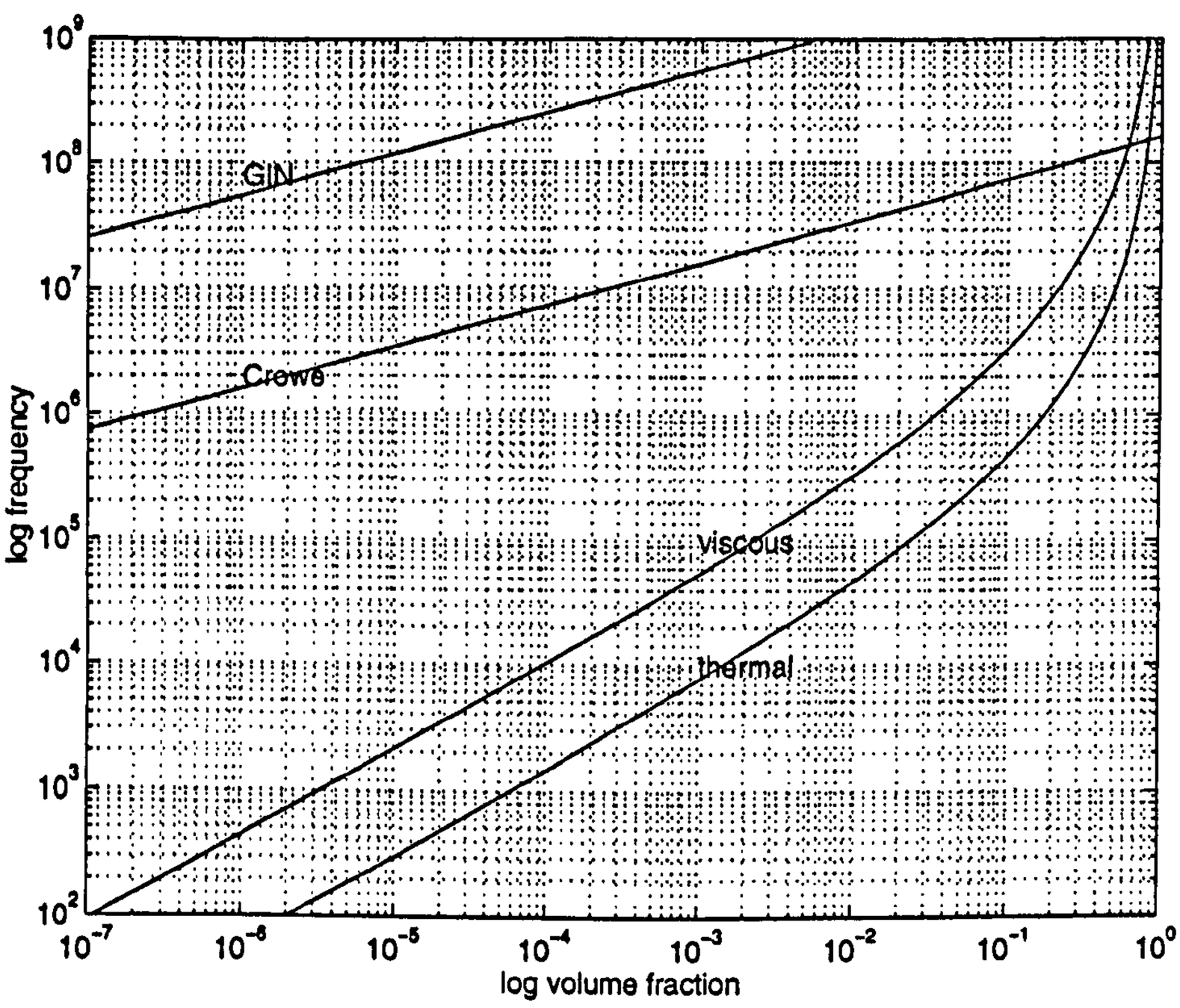

Figure 4. 10 Curves indicating regions where the continuum and isolated particle assumptions are valid, for particles of mean radius 0.27 μm in water. The continuum assumption is valid in the region below the GIN and Crowe lines. The boundary layers overlap in the regions to the right of the 'thermal' and 'viscous' curves.

4. 3. 7 Hexadecane in water emulsion

McClements [29] [64] measured the ultrasound velocity and attenuation in a hydrocarbon oil (hexadecane) in water emulsion. The frequencies were between 0.2 and 7 MHz and the particles had radii between 0.1 and 1.8 μm. Measurements were made at three volume fractions, the maximum being 0.56. The physical properties of the two phases are given in appendix 1. The non dimensional number $k_f a$ is less than 0.053 so long wavelength theories should be valid.

The long wavelength WT, LB and Ma theories used by McClements consistently overpredicted the measured attenuation, the discrepancy increasing with volume fraction. Figures 4. 11 and 4. 12 compare predictions of the full coupled phase theory and the $S=0$ and $S=\infty$ approximations with experimental data from reference [64]. In figure 4. 11 the volume fraction is 0.126 and in figure 4. 12 $\phi=0.564$. In reference [64] a distribution of particle sizes was incorporated into the scattering theory by volume averaging the scattering coefficients. The particle size distribution was obtained by measurements. For the coupled phase theory shown here the particles were assumed to be monodisperse i.e. with equal radii.

The coupled phase theory predictions for the attenuation are closer to the data than the scattering theory predictions shown in reference [64]. The scattering theory predictions are not shown here because the particle radii were not published. The full coupled phase theory gives a worse prediction than the scattering theory for the phase speed, being lower than the data for the whole range of the frequency number $a\sqrt{f}$. The prediction of the $S=0$ theory, however, is very close to the data, being as close or even slightly closer than the scattering theory prediction. Taking both attenuation and velocity into account, the $S=0$ or high frequency theory gives the best agreement with the data.

This result suggests that each phase obeys its own single fluid momentum equation, as in section 4. 1. 6, with no interaction. This formulation is more akin to the scattering theory and explains why the $S=0$ prediction is closer to the scattering prediction.

4. 3. 8 Aqueous suspension of polystyrene particles

Allegra and Hawley measured the ultrasonic attenuation at frequencies between 3 and 75 MHz in a suspension of polystyrene particles in water with a 'nominal' particle radius of 0.11 μm at volume fractions up to 0.5. The physical properties are given in appendix 1. Figure 4. 13 compares the measured

attenuation at 9 MHz with the predictions of the WT multiple scattering theory and the full coupled phase theory. At 9 MHz $k_f a = 4 \times 10^{-3}$ so the long wavelength assumption is valid. Neither theory can be described as being a close fit to the data. This may be due to the unknown distribution of particle sizes.

4. 3. 9 Attenuation at high volume fractions

Other examples where scattering theory overpredicts attenuation at high volume fractions can be found in the literature. Urick [104] [105] and Hampton [131] measured the ultrasound attenuation in a suspension of kaolin particles in water at 1 MHz and 100 kHz respectively at volume fractions up to 0.4. The data shows a maximum in the attenuation at $\phi \cong 0.2$. This data has previously been used to test porous media theories. Strout [42] compared the predictions of coupled phase theory and scattering theory with the Urick data. The coupled phase theory was the HT version modified for high volume fractions by including the effect of hydrodynamic interactions between the particles. This method is discussed in chapter 6. The coupled phase theory prediction was close to the measurements while the scattering theory was unsatisfactory.

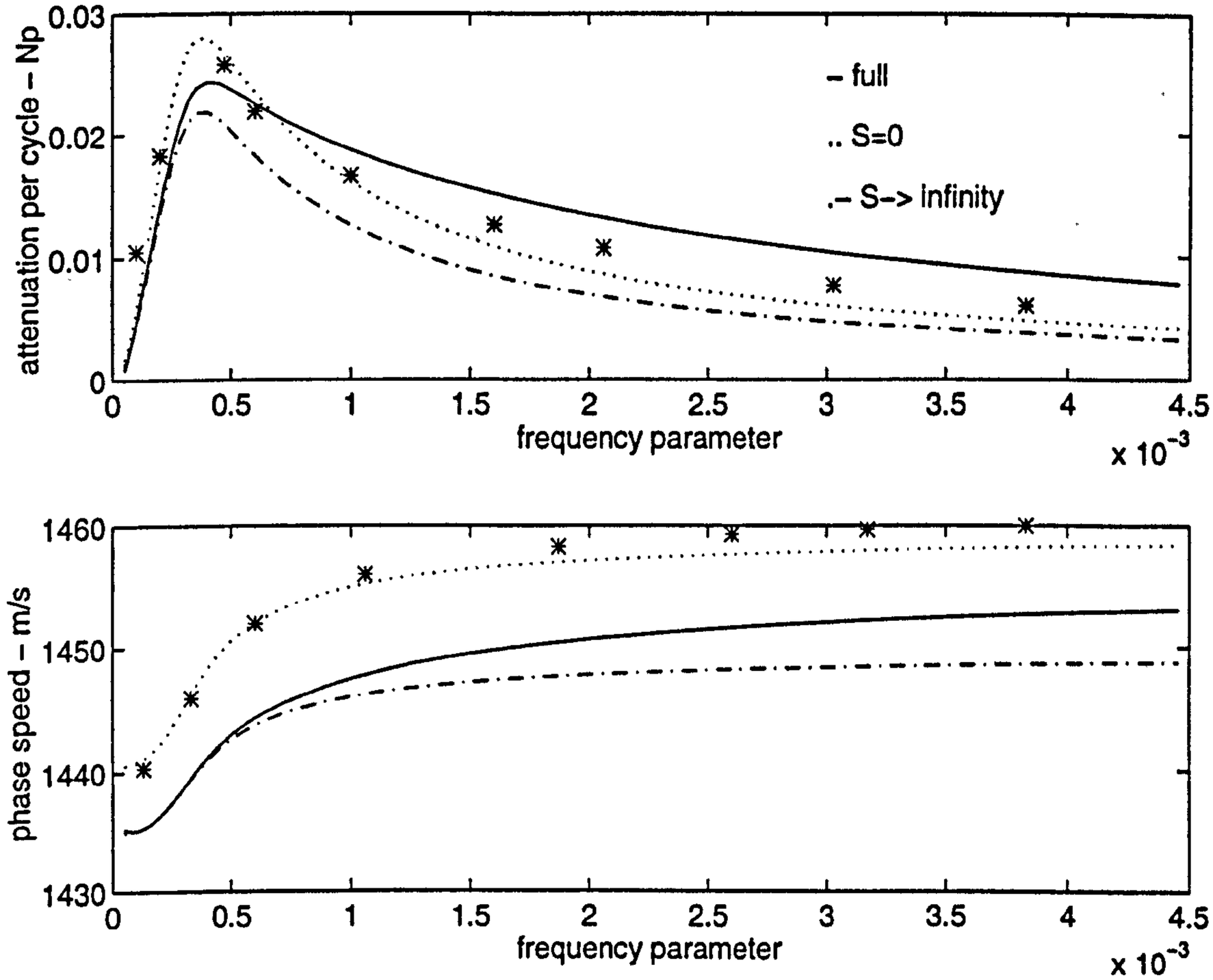

Figure 4. 11 Excess attenuation per cycle and sound speed versus non-dimensional frequency for a hexadecane in water emulsion with volume fraction 0.126. Comparison of data of McClements and predictions of full coupled phase theory, coupled phase theory with S=0 and coupled phase theory with $S \rightarrow \infty$.

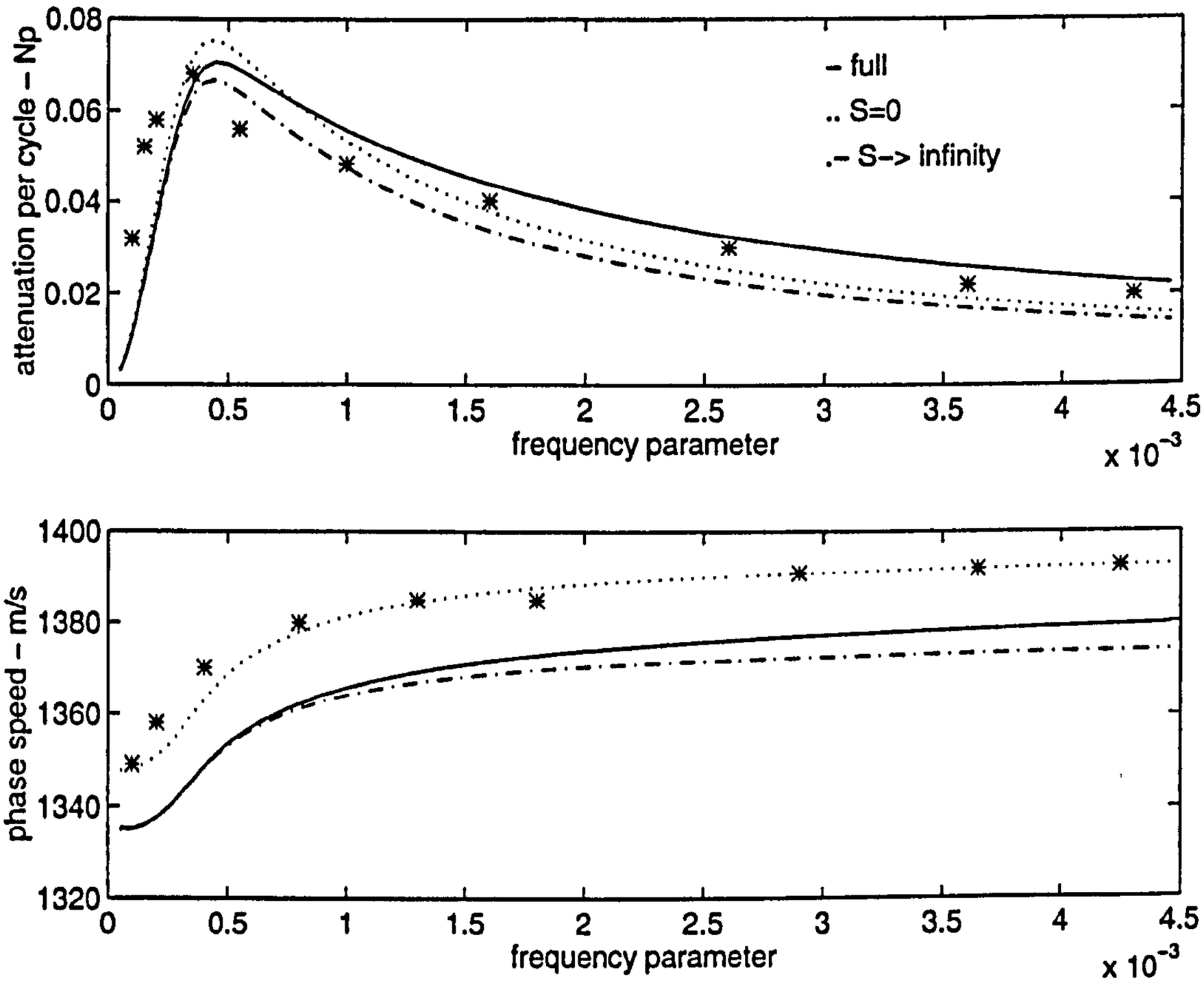

Figure 4. 12 Excess attenuation per cycle and sound speed versus non-dimensional frequency for a hexadecane in water emulsion with volume fraction 0.564. Comparison of data of McClements and predictions of full coupled phase theory, coupled phase theory with S=0 and coupled phase theory with $S \rightarrow \infty$.

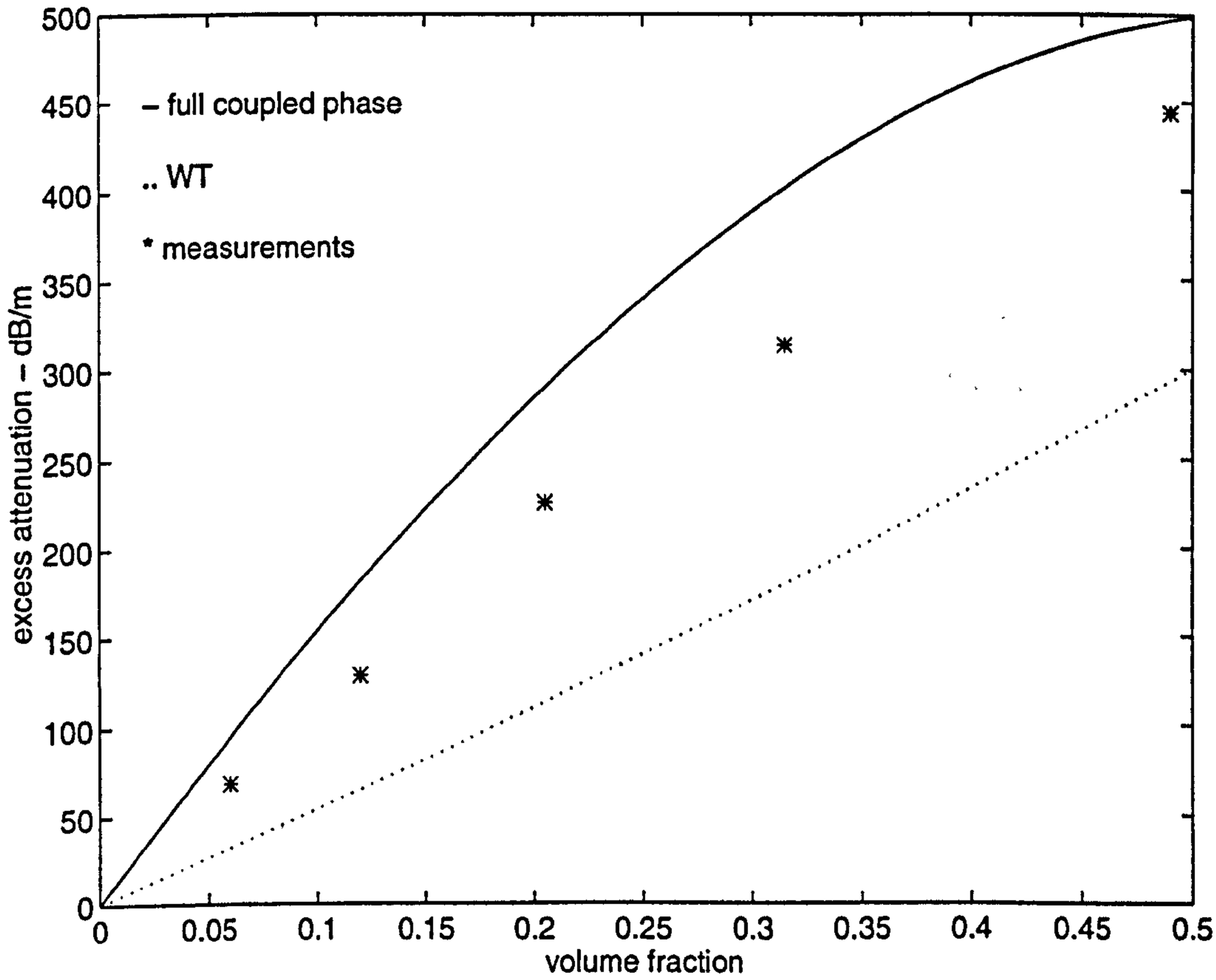

Figure 4. 13 Excess attenuation versus volume fraction for an aqueous suspension of polystyrene particles with nominal radius 0.11 μm at 9 MHz. Comparison of data of Allegra and Hawley and predictions of full coupled phase theory and WT multiple scattering theory.

Chapter 5
Porous media theory

The Biot porous theory models sound propagation in solid-fluid two phase media where the solid phase is composed of particles or grains. Both phases are assumed to be continuous, as in coupled phase theory. Unlike coupled phase theory, the solid phase grains are in contact and form the 'frame'. The theory results in wave equations which predict two compressional waves and one shear wave in the medium. From the wave equations, complex wavenumbers for these three waves can be obtained.

The Biot theory can be applied to suspensions by neglecting the frame. This special case has only one wave equation and predicts only one compressional wave. Its general form is identical to the Harker and Temple result from section 4. 2. The two theories differ only in their expressions for the viscous force between the phases. The expression usually used in the Biot theory is one based on a pore model of the material. The expression used in coupled phase theories is based on isolated spherical particles. In this chapter, predictions of the two models are compared to measurements of the ultrasound complex wavenumber in high volume fraction suspensions. The pore model predictions gives better agreement with the data than the particle model.

Another special case is the rigid frame theory where the solid phase velocity is set to zero. This is valid when the coupling between the two phases is negligible. This occurs when the impedance contrast between the phases is large, for example if the phases were glass and air. Measurements of the

acoustical properties of air saturated stacked glass beads are compared to predictions of the rigid frame theory in section 5. 2.

5. 1 Biot theory

5. 1. 1 Wave equations

The derivation of the three wavenumbers from first principles can be found in Allard [46]. The whole derivation will not be presented here, the starting point is the equations of motion for the two phases. It is easier to write these in terms of the displacements of the phases $\mathbf{d}_s$ and $\mathbf{d}_f$ i.e. the integrals with respect to time of their velocities $\mathbf{u}_s$ and $\mathbf{u}_f$. These are Allard's equations (6.54) and (6.55)

$$(\phi\rho_s+\rho_a)\frac{\partial^2\mathbf{d}_s}{\partial t^2}-\rho_a\frac{\partial^2\mathbf{d}_f}{\partial t^2}= \\ (P-N_b)\nabla\nabla\cdot\mathbf{d}_s+Q\nabla\nabla\cdot\mathbf{d}_f+N_b\nabla^2\mathbf{d}_s-\alpha^2\sigma F\frac{\partial}{\partial t}(\mathbf{d}_s-\mathbf{d}_f) \tag{5.1}$$

$$(\alpha\rho_f+\rho_a)\frac{\partial^2\mathbf{d}_f}{\partial t^2}-\rho_a\frac{\partial^2\mathbf{d}_s}{\partial t^2}= \\ R\nabla\nabla\cdot\mathbf{d}_f+Q\nabla\nabla\cdot\mathbf{d}_s+\alpha^2\sigma F\frac{\partial}{\partial t}(\mathbf{d}_s-\mathbf{d}_f). \tag{5.2}$$

ϕ, the volume fraction of the solid phase, is assumed to be constant. $\alpha=1-\phi^0$ (chapter 4) is the 'porosity' in porous media theories. It is the volume of space in the frame that is filled by fluid.

The constants P, Q and R depend on the bulk moduli of the fluid and solid K_f and K_s and the bulk and shear moduli of the frame K_b and N_b. The bulk modulus is the inverse of the compressibility. K_s is the usual property of the solid material of which the grains are comprised. K_b and N_b are properties of the collection of grains as a whole and represent the fact that they are in contact. If the grains are isolated then K_b and N_b are zero. K_b and N_b can be complex to represent inelasticity of the frame. If the grains are joined together, the frame is said to be consolidated. The constants are given by [46]

$$P=\frac{(1-\alpha)^2K_s-(1-\alpha)K_b+\alpha\dfrac{K_fK_b}{K_s}}{1-\alpha-\dfrac{K_b}{K_s}+\alpha\dfrac{K_s}{K_f}}+\tfrac{4}{3}N_b \tag{5.3}$$

$$Q=\alpha\frac{(1-\alpha)K_s-K_b}{1-\alpha-\dfrac{K_b}{K_s}+\alpha\dfrac{K_s}{K_f}} \tag{5.4}$$

$$R = \frac{\alpha^2 K_s}{1 - \alpha - \frac{K_b}{K_s} + \alpha \frac{K_s}{K_f}}. \tag{5.5}$$

The constant ρ_a is given by

$$\rho_a = \alpha \rho_f (\alpha_\infty - 1). \tag{5.6}$$

α_∞ is the tortuosity which will be discussed in greater detail below. For a single pore the tortuosity accounts for the increase in path length through the pore if it is not straight. For a granular material this will be an effective tortuosity for the material as a whole. This can be obtained from measurements or theory, for instance by relating it to the induced mass coefficient C.

The term σF accounts for viscous momentum transfer. F is the viscosity correction function and σ is the flow resistivity. In terms of the permeability k_ϕ

$$\sigma = \frac{\mu}{k_\phi}.$$

The viscosity correction function and the permeability will be discussed later.

For compressional waves

$$\mathbf{d}_s = \nabla \phi_s$$

where ϕ_s is a scalar potential. This means that

$$\nabla \nabla \cdot \mathbf{d}_s = \nabla^2 \mathbf{d}_s$$

because

$$\nabla \nabla^2 \phi_s = \nabla^2 \nabla \phi_s$$

and so the terms in N_b in (5.1) cancel out.

Equations (5.1) and (5.2) can now be recast in terms of the quantities

$$e = \nabla \cdot \mathbf{d}_s \tag{5.7}$$

$$\xi = \alpha \nabla \cdot (\mathbf{d}_s - \mathbf{d}_f) \tag{5.8}$$

to obtain wave equations for the compressional waves. e is the dilation of a volume element attached to the frame and ξ is the volume of fluid that has flowed into or out of that element.

The wave equations for the compressional waves are [130]

$$\nabla^2 (He - C\xi) = \frac{\partial^2}{\partial t^2} (\rho_{va} e - \rho_f \xi) \tag{5.9}$$

$$\nabla^2(Ce - M\xi) = \frac{\partial^2}{\partial t^2}\left(\rho_f e - \frac{\alpha_\infty \rho_f}{\alpha}\xi\right) - \sigma F \frac{\partial}{\partial t}\xi . \tag{5.10}$$

The constants H, C and M are formed from P, Q and R as

$$H = P + 2Q + R$$

$$C = \frac{Q+R}{2} \tag{5.11}$$

$$M = \frac{R}{\alpha^2} .$$

5. 1. 2 Frameless Biot theory

For suspensions it can be assumed that the particles are isolated and thus $K_b = N_b = 0$. Equations (5.3) to (5.5) then give

$$P = (1-\alpha)^2 \kappa_{va}^{-1}$$

$$Q = \alpha(1-\alpha)\kappa_{va}^{-1}$$

$$R = \alpha^2 \kappa_{va}^{-1}$$

where

$$\kappa_{va} = (1-\alpha)\kappa_s + \alpha\kappa_f = K_{va}^{-1} = (1-\alpha)K_s^{-1} + \alpha K_f^{-1} .$$

Also

$$H = C = M = \kappa_{va}^{-1} .$$

For the frameless medium there will be no shear wave so

$$\nabla\nabla\cdot\mathbf{d} = \nabla^2\mathbf{d}$$

and equations (5.1) and (5.2) become

$$(\phi\rho_s + \rho_a)\frac{\partial^2 \mathbf{d}_s}{\partial t^2} - \rho_a \frac{\partial^2 \mathbf{d}_f}{\partial t^2} = \phi\kappa_{va}^{-1}\nabla^2(\phi\mathbf{d}_s + \alpha\mathbf{d}_f) - \alpha^2\sigma F\frac{\partial}{\partial t}(\mathbf{d}_s - \mathbf{d}_f) \tag{5.12}$$

$$(\alpha\rho_f + \rho_a)\frac{\partial^2 \mathbf{d}_f}{\partial t^2} - \rho_a \frac{\partial^2 \mathbf{d}_s}{\partial t^2} = \alpha\kappa_{va}^{-1}\nabla^2(\phi\mathbf{d}_s + \alpha\mathbf{d}_f) + \alpha^2\sigma F\frac{\partial}{\partial t}(\mathbf{d}_s - \mathbf{d}_f) . \tag{5.13}$$

Equations (5.9) and (5.10) become

$$\kappa_{va}^{-1}\nabla^2(e-\xi) = \frac{\partial^2}{\partial t^2}(\rho_{va}e - \rho_f\xi) \tag{5.14}$$

$$\kappa_{va}^{-1}\nabla^2(e-\xi) = \frac{\partial^2}{\partial t^2}\left(\rho_f e - \frac{\alpha_\infty \rho_f}{\alpha}\xi\right) - \sigma F\frac{\partial}{\partial t}\xi . \tag{5.15}$$

The displacements are of the form of equation (4.1)

$$\mathbf{d}_s = d_s \exp[j(kz + \omega t)]$$

$$\mathbf{d}_f = d_f \exp[j(kz+\omega t)].$$

Here the $+j\omega t$ convention has been used to be consistent with the derivation of equations (5.1) and (5.2). Substituting these expressions into (5.14) and (5.15) gives the matrix equation

$$\begin{pmatrix} -\phi\rho_s + \phi\kappa_{va}{}^{-1}K^2 & -\alpha\rho_f + \alpha\kappa_{va}{}^{-1}K^2 \\ \rho_f(1-\alpha_\infty) + \dfrac{j\alpha\sigma F}{\omega} - \phi\kappa_{va}{}^{-1}K^2 & \rho_f\alpha_\infty - \dfrac{j\alpha\sigma F}{\omega} - \alpha\kappa_{va}{}^{-1}K^2 \end{pmatrix} \begin{pmatrix} d_s \\ d_f \end{pmatrix} = 0$$

with

$$K = \frac{k}{\omega}.$$

Setting the determinant to zero gives

$$K^2 = \left(\frac{k}{\omega}\right)^2 = \rho_{va}\kappa_{va} \frac{\rho_f\left(\dfrac{\alpha_\infty}{\alpha} - \dfrac{\rho_f}{\rho_{va}}\right) - \dfrac{j\sigma F}{\omega}}{\rho_f\left(\dfrac{\alpha_\infty}{\alpha} - 2\right) + \rho_{va} - \dfrac{j\sigma F}{\omega}}. \tag{5.16}$$

This is the frameless Biot theory expression for the complex wavenumber.

5. 1. 3 Viscosity correction function and flow resistivity

F, the viscosity correction function, represents the viscous forces acting between the two phases. It performs the same function as the Stokes drag and Bassett history terms in the coupled phase theory. These terms were derived assuming the particles were spherical. F is derived assuming the fluid phase is situated in tubes or pores in the solid phase. The solid phase is assumed to be incompressible and of infinite mass. This is the rigid frame assumption.

The momentum equation for a fluid with mean velocity

$$u_f = u_f' \exp[j(kz+\omega t)]$$

in a circular pore parallel to the z axis is (Allard equation (4.15))

$$-\frac{\partial p}{\partial z} = j\omega\rho u_f \tag{5.17}$$

where ρ is the effective density given by

$$\rho = \rho_f\left(1 + \frac{\dfrac{2}{\lambda\sqrt{-j}}\dfrac{J_1(\lambda\sqrt{-j})}{J_0(\lambda\sqrt{-j})}}{1 - \dfrac{2}{\lambda\sqrt{-j}}\dfrac{J_1(\lambda\sqrt{-j})}{J_0(\lambda\sqrt{-j})}}\right) \tag{5.18}$$

and

$$\lambda = r\left(\frac{\omega\rho_f}{\mu}\right)^{\frac{1}{2}}. \tag{5.19}$$

J_n is the cylindrical Bessel function of order n.

As $\omega \to 0$ it can be shown that

$$\frac{\frac{2}{\lambda\sqrt{-j}}\frac{J_1\left(\lambda\sqrt{-j}\right)}{J_0\left(\lambda\sqrt{-j}\right)}}{1-\frac{2}{\lambda\sqrt{-j}}\frac{J_1\left(\lambda\sqrt{-j}\right)}{J_0\left(\lambda\sqrt{-j}\right)}} \to \frac{1}{3} - \frac{8j}{\lambda^2}$$

and so (5.18) gives

$$\rho \to \rho_f\left(\frac{4}{3} - \frac{8j}{\lambda^2}\right) \tag{5.20}$$

and as $\omega \to \infty$

$$\frac{\frac{2}{\lambda\sqrt{-j}}\frac{J_1\left(\lambda\sqrt{-j}\right)}{J_0\left(\lambda\sqrt{-j}\right)}}{1-\frac{2}{\lambda\sqrt{-j}}\frac{J_1\left(\lambda\sqrt{-j}\right)}{J_0\left(\lambda\sqrt{-j}\right)}} \to \frac{\sqrt{2}(1-j)}{\lambda}$$

so

$$\rho \to \rho_f\left(1 + \frac{\sqrt{2}(1-j)}{\lambda}\right). \tag{5.21}$$

If the fluid is in a material with N of these pores per unit area of cross section, the effective density can be obtained from the effective density of a single pore using the flow resistivity concept.

The flow resistivity σ is defined for steady state flows from point 1 to point 2 by

$$\sigma = \frac{p_2 - p_1}{U\Delta},$$

where p_1 is the pressure at point 1 and p_2 is the pressure at point 2 and $p_2 > p_1$. Δ is the distance between 1 and 2 and U is the mean flow per unit area.

For N pores of radius r per unit area of cross section the flow resistivity is given by

$$\sigma = \frac{p_2 - p_1}{u_{f,\omega\to 0} N\pi r^2 \Delta}.$$

$u_{f,\omega\to 0}$, the steady state velocity, can be obtained from (5.17) with (5.20)

$$u_{f,\omega\to 0} = -\frac{r^2}{8\mu}\frac{\partial p}{\partial z}.$$

Since

$$\frac{p_2 - p_1}{\Delta} = -\frac{\partial p}{\partial z}$$

and $N\pi r^2 = \alpha$, the porosity, the flow resistivity is given by

$$\sigma = \frac{8\mu}{r^2\alpha}.$$

Substituting for r in λ gives

$$\lambda = \left(\frac{8\omega\rho_f}{\sigma\alpha}\right)^{\frac{1}{2}} \tag{5.22}$$

and

$$\rho = \rho_f\left(1 - j\frac{\sigma\alpha}{\omega\rho_f}F(\lambda)\right) \tag{5.23}$$

where

$$F(\lambda) = \frac{-\frac{\lambda\sqrt{-j}}{4}\frac{J_1\left(\lambda\sqrt{-j}\right)}{J_0\left(\lambda\sqrt{-j}\right)}}{1 - \frac{2}{\lambda\sqrt{-j}}\frac{J_1\left(\lambda\sqrt{-j}\right)}{J_0\left(\lambda\sqrt{-j}\right)}}. \tag{5.24}$$

Zwikker and Kosten [116] derived their rigid frame complex density in terms of the volume velocity in the pores. Their complex density is a factor of $1/\alpha$ times the ρ used here.

5. 1. 4 Tortuosity

A simple example of the tortuosity factor is allowing the pores, which in the previous subsection were parallel to the z axis, to now be inclined at an angle θ to the z axis. Allard shows that (5.22) and (5.23) must be modified to

$$\lambda = \left(\frac{8\omega\rho_f\alpha_\infty}{\sigma\alpha}\right)^{\frac{1}{2}} \text{ and} \tag{5.25}$$

$$\rho = \rho_f\alpha_\infty\left(1 - j\frac{\sigma\Omega}{\omega\rho_f\alpha_\infty}F(\lambda)\right) \tag{5.26}$$

where

$$\alpha_\infty = \frac{1}{\cos^2\theta}.$$

The tortuosity is denoted α_∞ because as $\omega \to \infty$ (5.26) gives

$$\rho \to \rho_f \alpha_\infty$$

and the momentum equation (5.17) is

$$-\frac{\partial p}{\partial z} = j\omega\rho_f \alpha_\infty u_f .$$

This shows that α_∞ controls the inertial force. In the Biot theory α_∞ appears in the inertial coupling term ρ_a.

5. 1. 5 Spherical grains

If the solid phase is assumed to be comprised of spherical grains the induced mass coefficient $C = \frac{1}{2}$. Berryman [124] has shown that from the definition of

ρ_a

$$\alpha_\infty = 1 - C\left(\frac{\alpha - 1}{\alpha}\right) \tag{5.27}$$

or

$$\rho_a = \phi\rho_f C . \tag{5.28}$$

Another expression for the tortuosity is

$$\alpha_\infty = \alpha^{-\frac{1}{2}}. \tag{5.29}$$

This was derived by Brown [167] by analogy with electrical conduction through porous media. The Brown and Berryman tortuosities are compared in figure 5. 1.

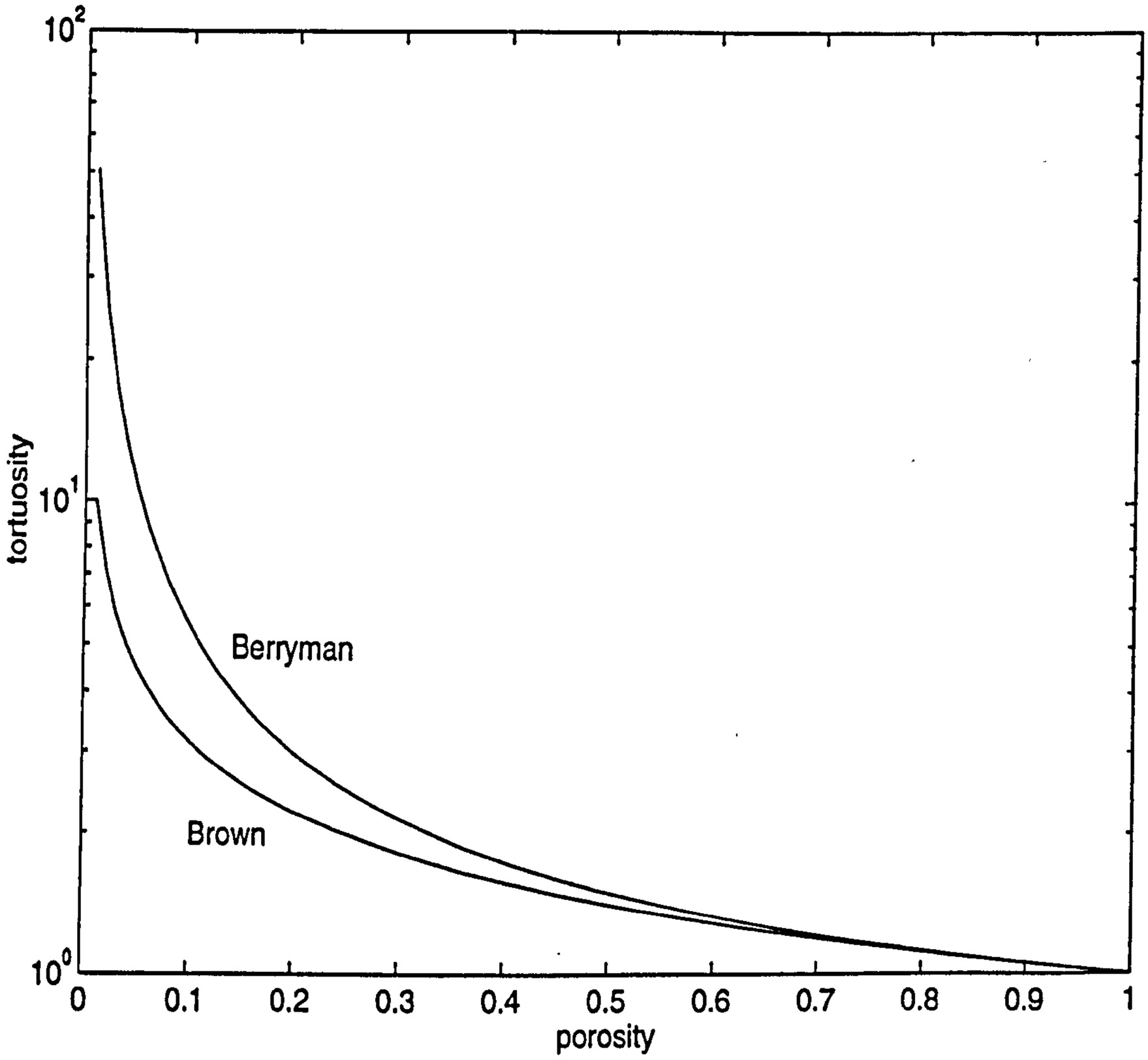

Figure 5. 1 Tortuosity versus porosity. Comparison of Brown and Berryman expressions.

The flow resistivity for spherical grains can be obtained from the Kozeny-Carman expression for the permeability [133]

$$k_\phi = \frac{a^2}{9k_0}\frac{\alpha^3}{(1-\alpha)^2}. \tag{5.30}$$

Here a is the grain radius and k_0 is an empirically determined constant which accounts for pore shape and tortuosity. For tubular pores

$$k_0 \cong 2\alpha_\infty s_0 . \tag{5.31}$$

s_0 is the steady flow shape factor which is 1 for cylindrical pores.

λ and $F(\lambda)$ have to be modified for spherical grains. The equivalent to r for spherical grains r_{sph} can be obtained via the hydraulic radius. The hydraulic radius r_h of a tube is the surface area of a unit length divided by the volume of a unit length, which for cylindrical tubes is $r/2$. For pores in a material consisting of spherical grains the hydraulic radius is given by [133]

$$r_h = \frac{a}{3}\frac{\alpha}{1-\alpha}.$$

Equating the two hydraulic radii gives

$$r_{sph} = \frac{2a}{3}\frac{\alpha}{1-\alpha} \tag{5.32}$$

and thus

$$\lambda_{sph} = r_{sph}\left(\frac{\omega\rho_f}{\mu}\right)^{\frac{1}{2}}. \tag{5.33}$$

To show the consistency between the cylindrical and spherical grain models of the pores this form can also be obtained using the form of λ given by (5.25).

Substituting for the flow resistivity in (5.25) using $\sigma = \mu/k_\phi$ and (5.30) gives

$$\lambda = \sqrt{\frac{8\alpha_\infty k_\phi}{\alpha}}\sqrt{\frac{\rho_f\omega}{\mu}}. \tag{5.34}$$

But from (5.31) and (5.32), with $s_0 = 1$,

$$k_\phi = \frac{\alpha}{8\alpha_\infty} r_{sph}^{\,2}$$

which when substituted in (5.34) gives (5.33).

5. 1. 6 Comparison with coupled phase theory

For spherical grains using equations (5.27) and (5.28) it can be shown that, apart from the expression for the viscous momentum transfer, the frameless Biot

theory is identical to the Harker and Temple (HT) coupled phase theory given in section 4. 2.

Substituting (5.28) into (5.12) and (5.13) gives

$$\phi\rho_s\frac{\partial^2\mathbf{d}_s}{\partial t^2}=\phi\kappa_{va}{}^{-1}\nabla^2\left(\phi\mathbf{d}_s+\alpha\mathbf{d}_f\right)+j\omega\rho_f\phi\left(-\frac{j\alpha^2\sigma F}{\omega\rho_f\phi}+C\right)\frac{\partial}{\partial t}\left(\mathbf{d}_f-\mathbf{d}_s\right) \tag{5.35}$$

$$\alpha\rho_f\frac{\partial^2\mathbf{d}_f}{\partial t^2}=\alpha\kappa_{va}{}^{-1}\nabla^2\left(\phi\mathbf{d}_s+\alpha\mathbf{d}_f\right)-j\omega\rho_f\phi\left(-\frac{j\alpha^2\sigma F}{\omega\rho_f\phi}+C\right)\frac{\partial}{\partial t}\left(\mathbf{d}_f-\mathbf{d}_s\right). \tag{5.36}$$

Eliminating the densities in the continuity equation (4.9)

$$\frac{\phi}{\rho_s{}^0}\frac{\partial\rho_s}{\partial t}+\frac{\alpha}{\rho_f{}^0}\frac{\partial\rho_f}{\partial t}=-\nabla\cdot\left(\phi\mathbf{u}_s+\alpha\mathbf{u}_f\right)$$

with the isothermal equations of state (4.51) and (4.52)

$$p_s'=c_s{}^2\rho_s'$$

$$p_f'=c_f{}^2\rho_f'$$

gives

$$\left(\phi\kappa_s+\alpha\kappa_f\right)\frac{\partial p}{\partial t}=\kappa_{va}\frac{\partial p}{\partial t}=-\nabla\cdot\left(\phi\mathbf{u}_s+\alpha\mathbf{u}_f\right)$$

because $c^{-2}=\kappa\rho$.

So

$$\nabla p=-\kappa_{va}{}^{-1}\nabla^2\left(\phi\mathbf{d}_s+\alpha\mathbf{d}_f\right). \tag{5.37}$$

Substituting (5.37) into (5.35) and (5.36) gives

$$\phi\rho_s\frac{\partial\mathbf{u}_s}{\partial t}=-\phi\nabla p+j\omega\rho_f\phi\left(-\frac{j\alpha^2\sigma F}{\omega\rho_f\phi}+C\right)\left(\mathbf{u}_f-\mathbf{u}_s\right) \tag{5.38}$$

$$\alpha\rho_f\frac{\partial\mathbf{u}_f}{\partial t}=-\alpha\nabla p-j\omega\rho_f\phi\left(-\frac{j\alpha^2\sigma F}{\omega\rho_f\phi}+C\right)\left(\mathbf{u}_f-\mathbf{u}_s\right). \tag{5.39}$$

Equations (5.38) and (5.39) are identical to the coupled phase momentum equations (4.16) and (4.17) if S is replaced by

$$-\frac{j\alpha^2\sigma F}{\omega\rho_f\phi}+C \tag{5.40}$$

and i with $-j$ because of the change in sign convention. The only difference between the two theories is the way in which the viscous force is modelled.

The coupled phase theory expression for the complex wavenumber (4.53) with S given by (5.40) can be obtained from the frameless Biot expression (5.16) by substituting (5.27).

5. 1. 7 Aqueous suspension of kaolinite particles

The complex wavenumber predictions of the frameless Biot and coupled phase theory will be compared to the measurements of Hampton [131] on suspensions of kaolinite particles in water. Since these two theories are identical except for the viscous force expression, it would be more correct to name them with reference to the model of the viscous force. What is here is called Biot theory would be called the 'pore based theory' and the coupled phase theory would be called the 'particle based theory'. For simplicity here, however, the two viscous force models will still be referred to by the theories they have previously been associated with.

The physical properties of kaolinite and water are given in appendix 1. Figure 5. 2 plots the real and imaginary parts of the F function from equations (5.24) and (5.33). The particle radius is 1.2 μm, the value given by Hampton, the porosity is 0.7 and $k_0 = 10$. Also shown are the high and low frequency limits

$$F_{\omega\to\infty} = \tfrac{1}{4} j\sqrt{-j}\lambda$$

$$F_{\omega\to 0} = 1 + j\frac{\lambda^2}{24}.$$

Figure 5. 3 compares the real and imaginary parts of

$$-\frac{j\alpha^2\sigma F}{\omega\rho_f\phi}$$

from (5.40) with the real and imaginary parts of S from (4.13). For the usual frequencies of interest ($<10^7$ Hz) the difference between the two predictions for the viscous force is large.

Figure 5. 4 compares the attenuation and normalised sound speed c/c_f predicted by (5.16) and the Hampton data. The attenuation shown is for a frequency of 100 kHz. The sound speed data covers the range 40 kHz to 600 kHz. The sound speed prediction is shown at 40 kHz and 600 kHz. k_0 is 10. The agreement with the data is good.

Figure 5.5 shows the effect of varying k_0. The sound speed is for a frequency of 600 kHz. k_0 could be determined using (5.31) and (5.27) but here it is varied to obtain the best fit with the data. Experiments have shown that k_0 is between 3 and 7 for spherical grains at medium porosities. For porosities above 0.8 k_0 can

exceed 10. 10 here is a satisfactory value but it has not been fitted in the numerical sense.

Figure 5. 6 shows the effect the difference between the two viscous terms shown in 5. 3 has on the complex wavenumber. The coupled phase theory prediction is not satisfactory. It will be shown in chapter 6 that, using the theory of Strout [42], the inclusion of hydrodynamic interactions between the particles can correct the coupled phase theory.

The porous media theory is a continuum theory. From section 4. 1. 2 the Crowe condition for the validity of the continuum assumption requires that the wavelength be greater than the side of a cube containing 10^4 grains, or

$$\phi > \frac{4\pi \times 10^4}{3}\left(\frac{af}{c_f}\right)^3 .$$

For the kaolinite suspension the maximum frequency is 600 kHz, so ϕ should be greater than 5×10^{-6}. Unlike the coupled phase theory expression for the viscous force S, which requires that the viscous boundary layers around the particles do not overlap and thus has a low frequency limit, the porous media theory expression F is valid for all frequencies.

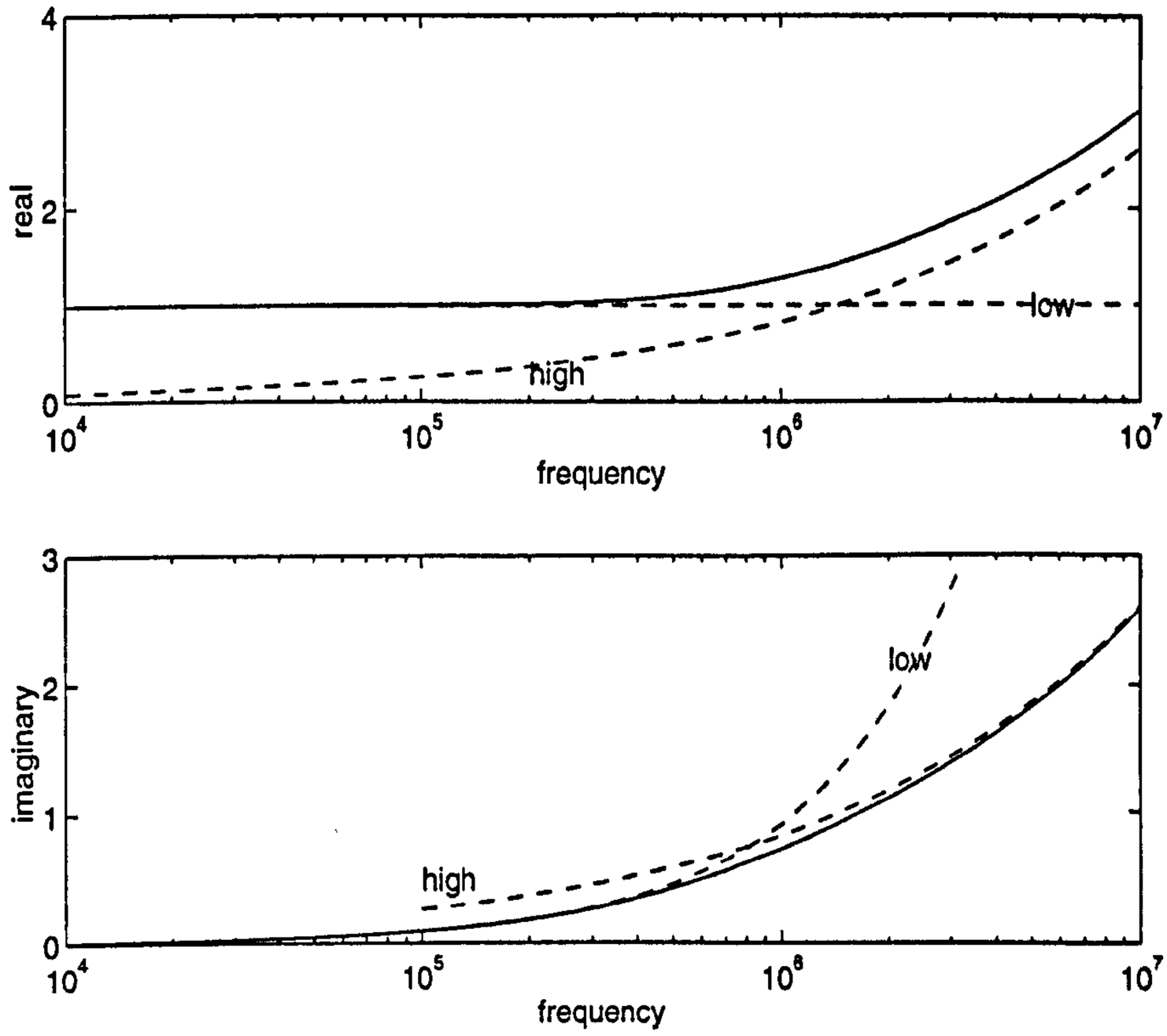

Figure 5. 2 Real and imaginary parts of *F* viscosity correction function versus frequency for an aqueous suspension of kaolinite particles of radius 1.2 μm with porosity 0.7. Curves indicated by dashed lines are the high and low frequency limits.

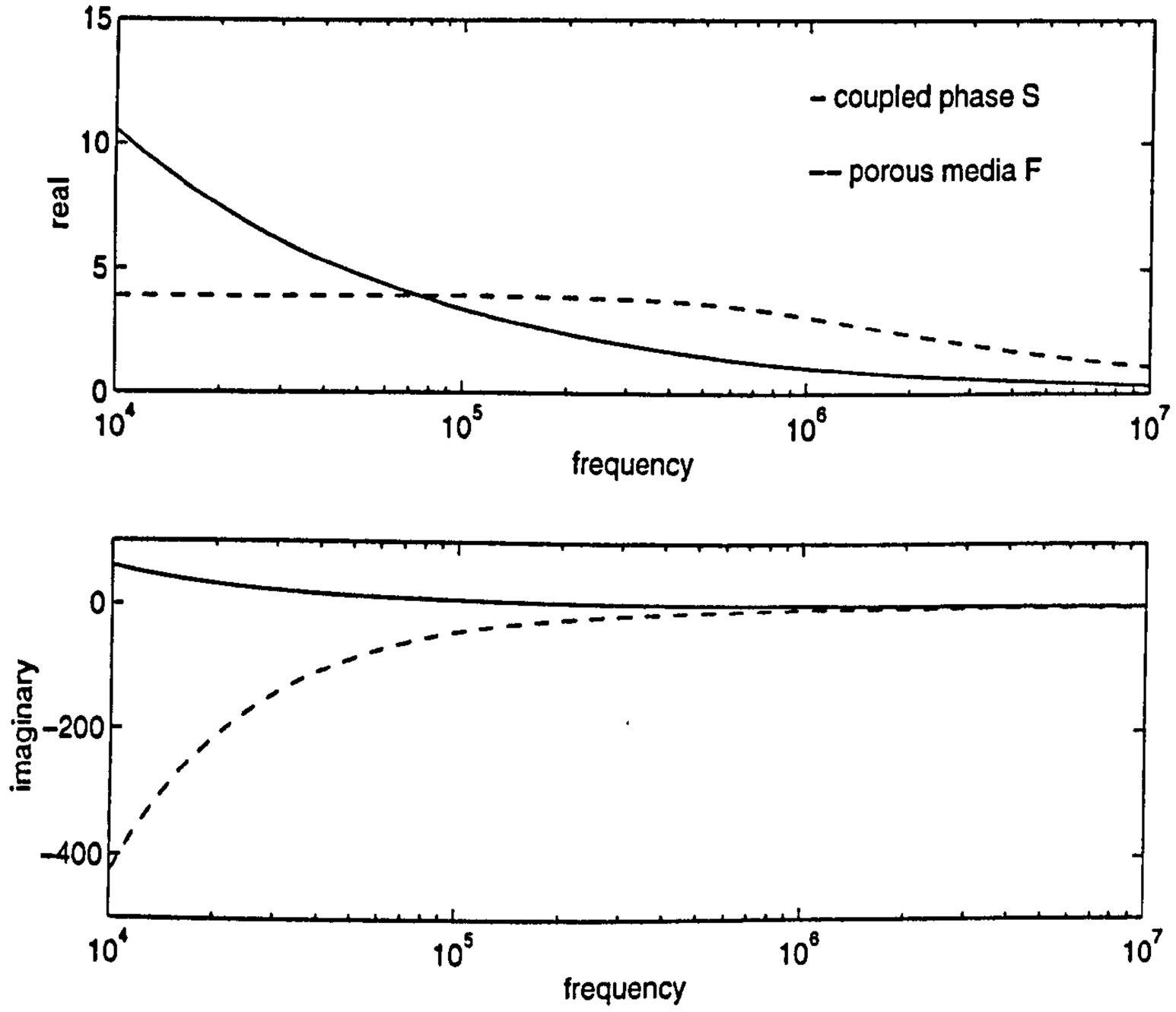

Figure 5. 3 Comparison of *S* coupled phase theory viscous force function and *F* porous media theory viscous force function. Real and imaginary parts versus frequency for an aqueous suspension of kaolinite particles of radius 1.2 μm with porosity 0.7.

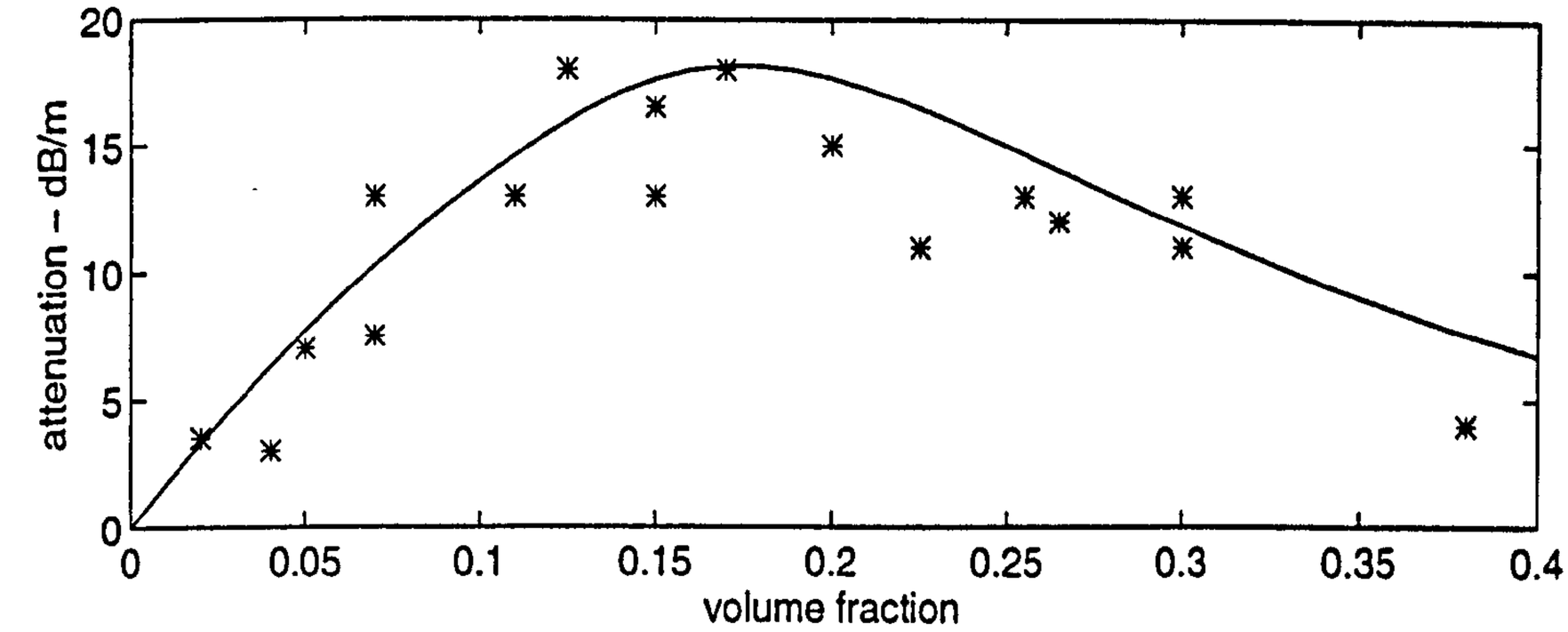

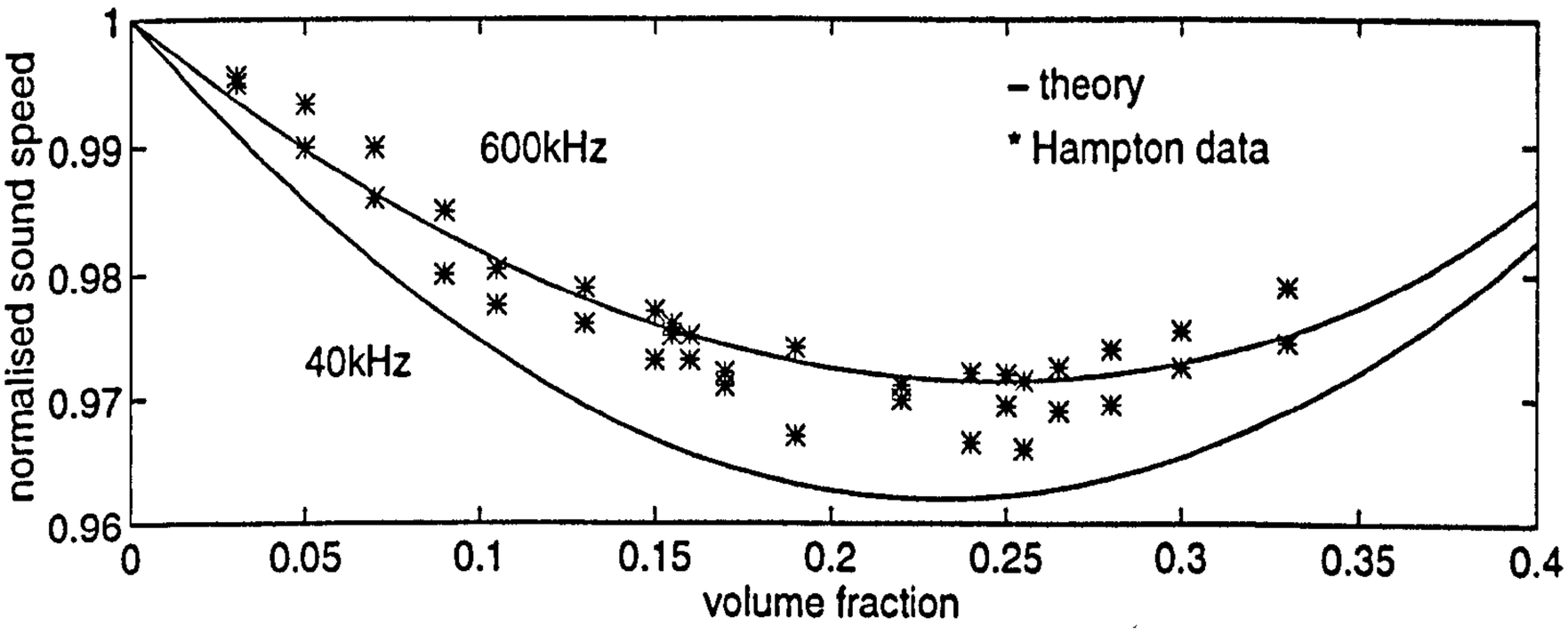

Figure 5. 4 Attenuation at 100 kHz and sound speed between 40 and 600 kHz versus volume fraction for an aqueous suspension of kaolinite particles of radius 1.2 μm. Comparison of prediction of frameless Biot theory and data of Hampton.

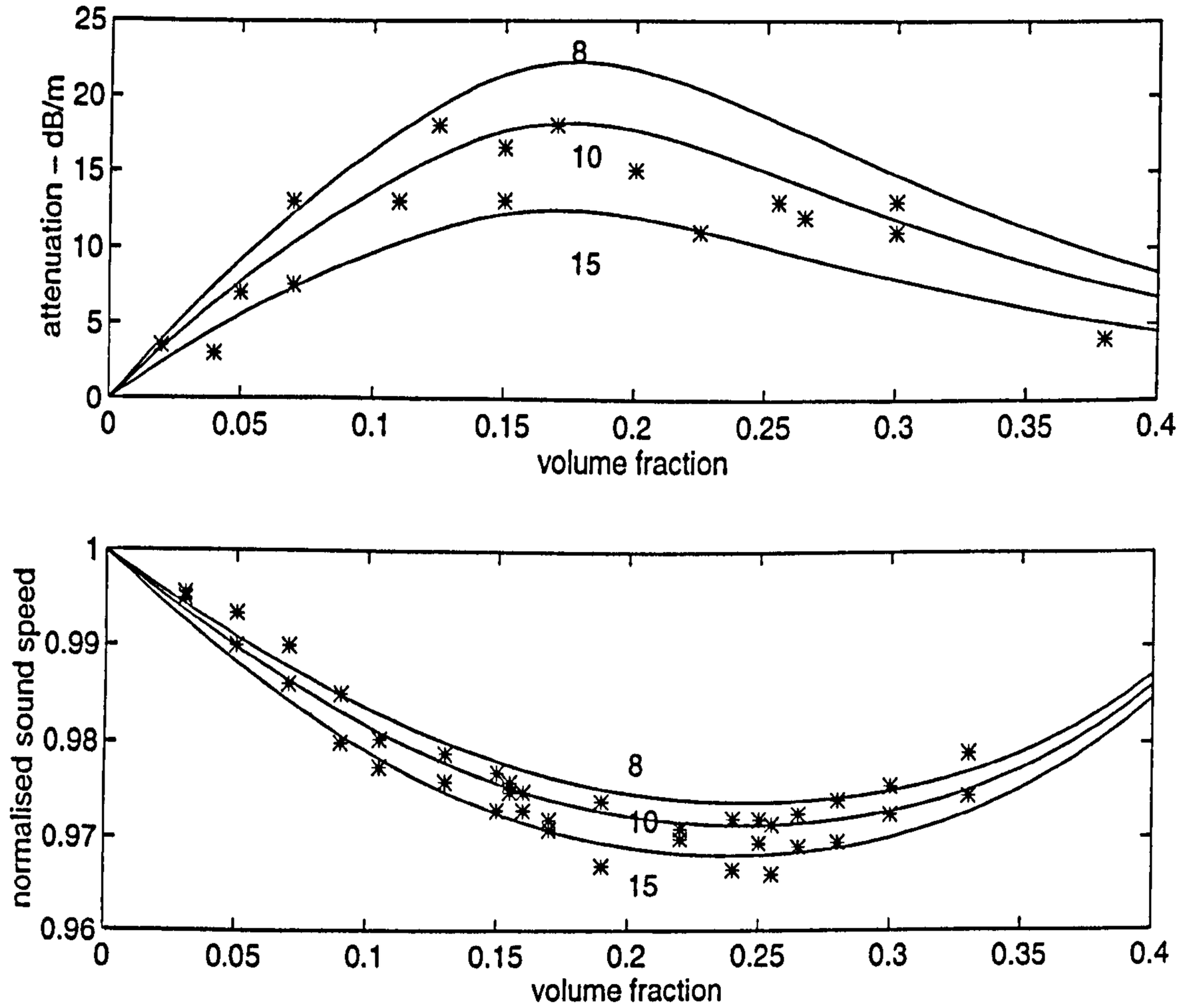

Figure 5. 5 Attenuation at 100 kHz and sound speed at 600 kHz versus volume fraction for an aqueous suspension of kaolinite particles of radius 1.2 μm. Comparison of data of Hampton and predictions of frameless Biot theory with permeability factor 8, 10 and 15.

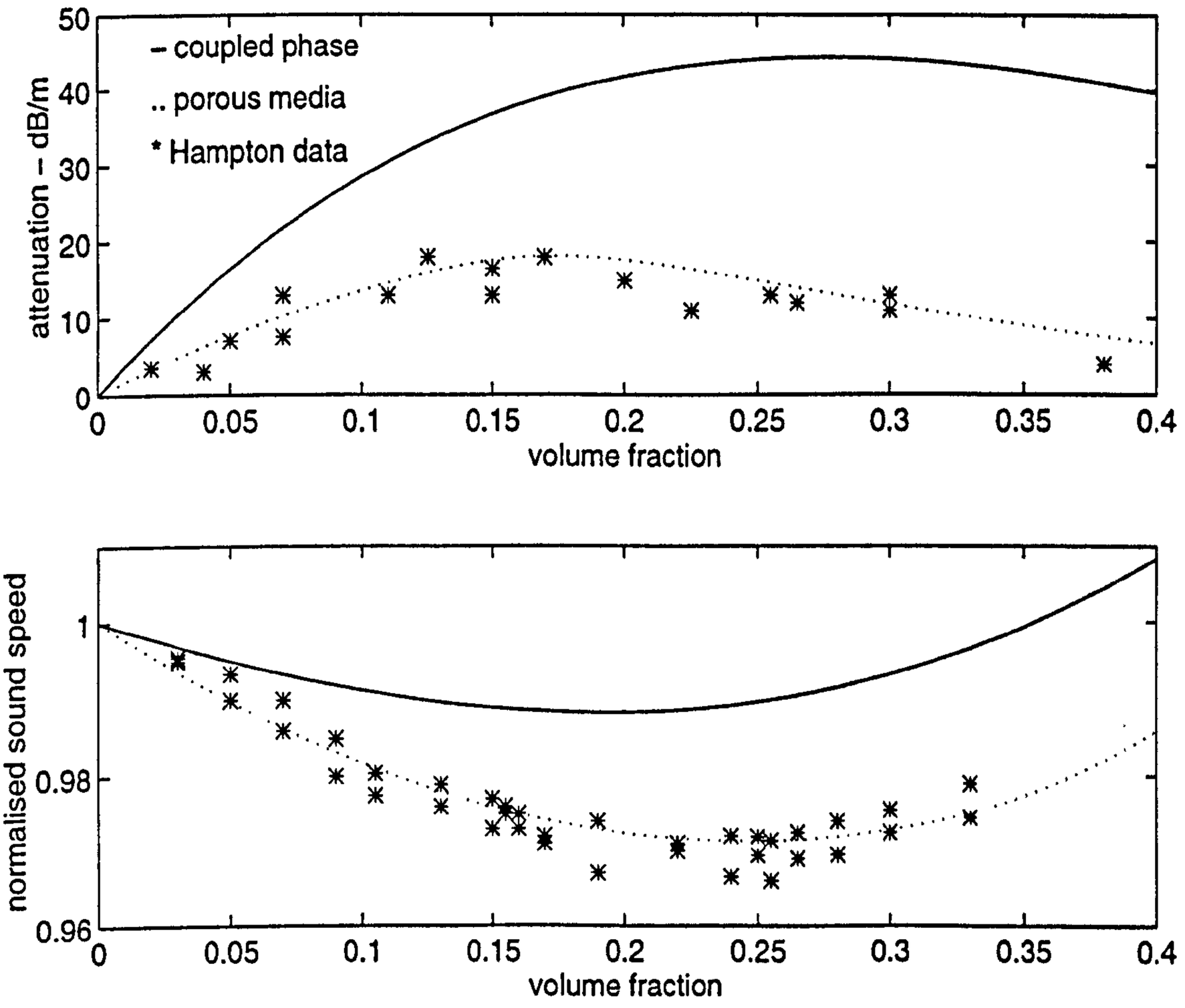

Figure 5. 6 Attenuation at 100 kHz and sound speed at 600 kHz versus volume fraction for an aqueous suspension of kaolinite particles of radius 1.2 μm. Comparison of data of Hampton and predictions of frameless Biot theory and coupled phase theory.

5. 1. 8 Rigid frame theory

The expression for the complex wavenumber which results from the rigid frame theory can be obtained as a special case of the general Biot theory or the frameless theory. The rigid frame theory expression for the effective density has been used in section 5. 1. 3 to obtain the viscous term *F*. If the solid phase is rigid then $\mathbf{d}_s = 0$ and $\kappa_s = 0$ so

$$\kappa_{va} = \alpha\kappa_f$$

and the fluid equation of motion (5.13) becomes

$$\alpha\alpha_\infty\rho_f\frac{\partial^2\mathbf{d}_f}{\partial t^2} = \alpha\kappa_f^{-1}\nabla^2\mathbf{d}_f - \alpha^2\sigma F\frac{\partial\mathbf{d}_f}{\partial t}. \tag{5.41}$$

Because

$$\mathbf{d}_f = d_f\exp[j(kz+\omega t)]$$

(5.41) gives

$$-\alpha_\infty\rho_f\omega^2 = -\kappa_f^{-1}k^2 - j\alpha\sigma F\omega$$

or

$$\left(\frac{k}{\omega}\right)^2 = \rho_f\alpha_\infty\kappa_f\left(1-j\frac{\sigma\alpha}{\omega\rho_f\alpha_\infty}F\right). \tag{5.42}$$

(5.42) is the rigid frame porous media theory which has been derived from first principles by Allard.

The expression

$$\rho_f\alpha_\infty\left(1-j\frac{\sigma\alpha}{\omega\rho_f\alpha_\infty}F\right) \tag{5.43}$$

is $\rho(\omega)$, the frequency dependent effective density. Equation (5.42) can then be written as

$$\left(\frac{k}{\omega}\right)^2 = \kappa_f\rho(\omega). \tag{5.44}$$

5. 2 Heat transfer

5. 2. 1 Frequency dependent compressibility

The effect of heat transfer has been included in the rigid frame porous media theory. The fluid compressibility κ_f in (5.44) is replaced with the frequency dependent effective compressibility $\kappa(\omega)$:

$$\left(\frac{k}{\omega}\right)^2 = \rho(\omega)\kappa(\omega)\,. \tag{5.45}$$

$\kappa(\omega)$ is derived from the expression for a single cylindrical tube in the same way as the effective density was in section 5. 1. 3. This gives [46]

$$\kappa(\omega)=\kappa_f\left(1+\frac{2(\gamma_f-1)}{\lambda\sqrt{-iN_{\mathrm{Pr}}}}\frac{J_1\left(\lambda\sqrt{-jN_{\mathrm{Pr}}}\right)}{J_0\left(\lambda\sqrt{-jN_{\mathrm{Pr}}}\right)}\right) \tag{5.46}$$

with λ from equation (5.25). κ_f is the fluid adiabatic compressibility and N_{Pr} is the fluid Prandtl number given by

$$N_{\mathrm{Pr}}=\frac{\mu C_p}{\tau}\,.$$

The effective compressibility has the high and low frequency limits

$$\kappa(\omega)_{\omega\to\infty}=\kappa_f\left(1-\frac{2j(\gamma_f-1)}{\lambda\sqrt{-jN_{\mathrm{Pr}}}}\right) \tag{5.47}$$

$$\kappa(\omega)_{\omega\to 0}=\kappa_f\left(\gamma_f-\frac{j(\gamma_f-1)N_{\mathrm{Pr}}}{8}\lambda^2\right). \tag{5.48}$$

5. 2. 2 Air saturated stacked glass beads

The rigid frame theory will be used to predict the complex reflection coefficient of a layer of air saturated stacked glass beads. The physical properties of air have already been used and are shown in appendix 1. Figure 5. 7 shows the effective density given by (5.43) and its high and low frequency limits

$$\rho(\omega)_{\omega\to\infty}=\alpha_\infty\rho_f\left(1+\frac{\sqrt{2}(1-j)}{\lambda}\right)$$

$$\rho(\omega)_{\omega\to 0}=\alpha_\infty\rho_f\left(\tfrac{4}{3}-\frac{8j}{\lambda^2}\right)$$

versus frequency. The parameters used in the equations are $\sigma=10^4\ \mathrm{kgm^{-3}s^{-1}}$, $\alpha=0.3$ and $\alpha_\infty=1$. The real part varies between $\frac{4}{3}\alpha_\infty\rho_f$ and $\alpha_\infty\rho_f$.

Figure 5. 8 shows the normalised effective bulk modulus

$$\frac{1}{\kappa(\omega)p^0} = \frac{\gamma_f}{\kappa(\omega)c_f{}^2\rho_f}$$

from equation (5.46), and the limits from (5.47) and (5.48). At low frequencies the effective compressibility tends to the isothermal compressibility of air given by $1/p^0$ and its imaginary part is zero. At high frequencies the effective compressibility tends to the adiabatic compressibility of air.

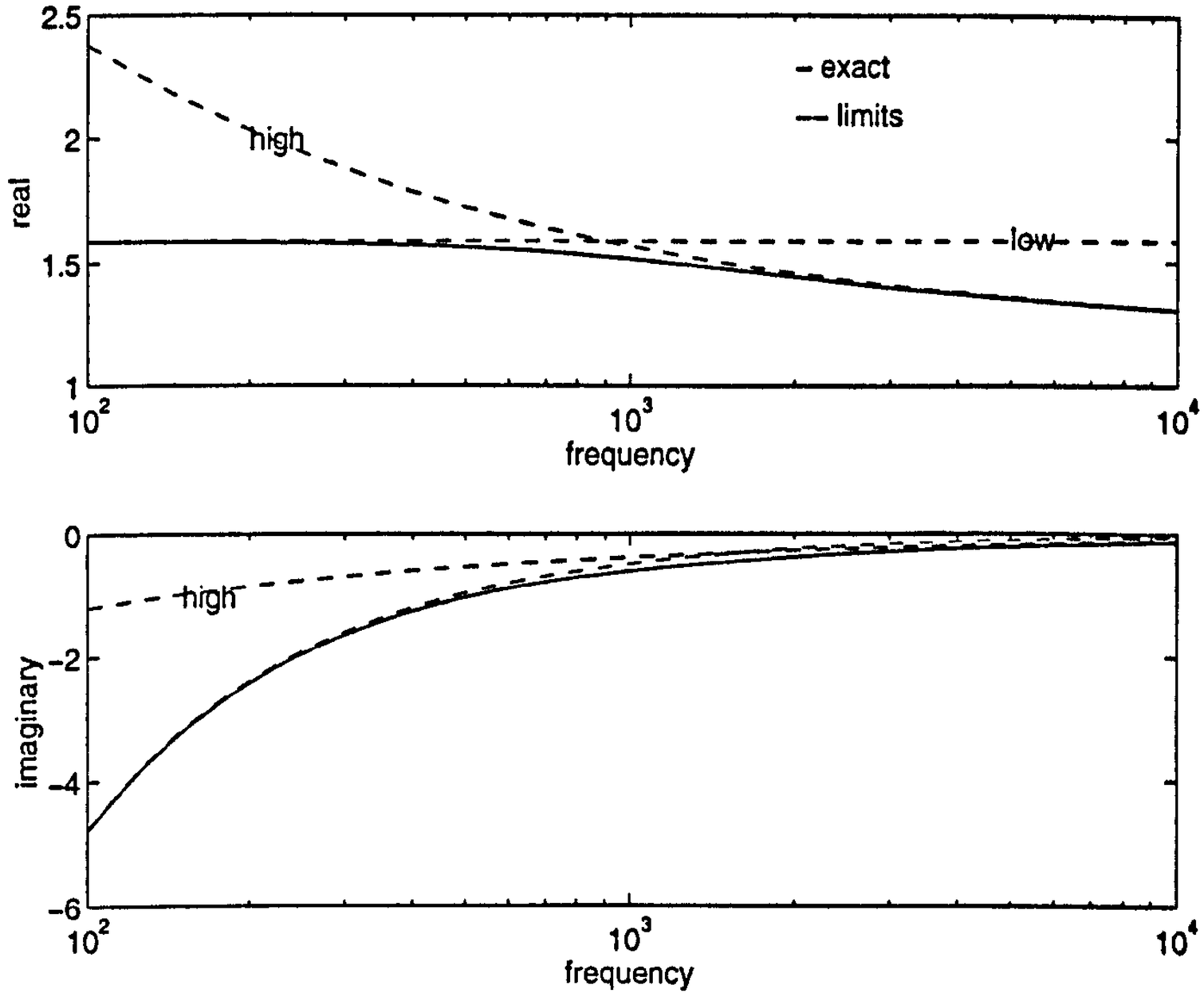

Figure 5. 7 Real and imaginary parts of effective density versus frequency for glass beads in air with flow resistivity 10^4, porosity 0.3 and tortuosity 1. Curves indicated by dashed lines are the high and low frequency limits.

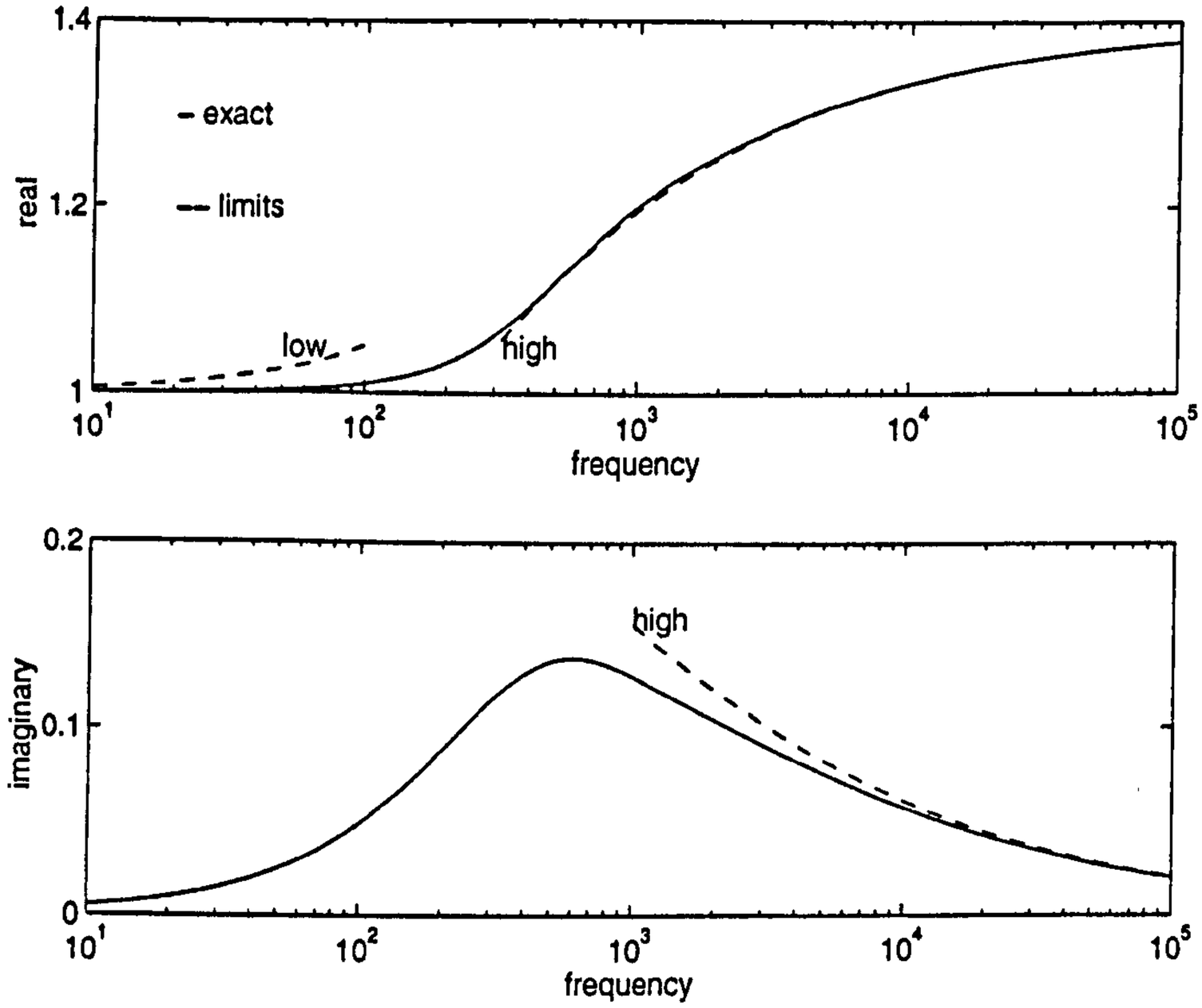

Figure 5. 8 Real and imaginary parts of normalised effective bulk modulus versus frequency for glass beads in air with flow resistivity 10^4, porosity 0.3 and tortuosity 1. Curves indicated by dashed lines are the high and low frequency limits.

5. 2. 3 Comparison with coupled phase theory

A 'rigid' coupled phase theory can be obtained from the MH coupled phase theory in section 4. 1. 14. If u_s' and $T_s' \rightarrow 0$ in the set of governing equations at the start of section 4. 1. 14 then the solution for the complex wavenumber is

$$k^2 = \omega^2 \rho(\omega) \kappa(\omega)$$

where

$$\rho(\omega) = \rho_f \left(1 + \frac{\phi}{\alpha} S \right)$$

and

$$\kappa(\omega) = \gamma_f \kappa_f \frac{\phi S_h + \alpha C_{vf}}{\phi S_h + \alpha C_{pf}}.$$

Thus

$$\rho(\omega)_{\omega \rightarrow \infty} = \rho_f \left(1 + \frac{\phi}{\alpha} C \right)$$

$$\kappa(\omega)_{\omega \rightarrow \infty} = \kappa_f$$

$$\kappa(\omega)_{\omega \rightarrow 0} = \gamma_f \kappa_f .$$

These limits are the same as those in the rigid frame porous media theory if the tortuosity is given by (5.27). However, due to the viscous terms in S, as $\omega \rightarrow 0$ the effective density becomes infinitely large. Numerical tests have shown that the predictions of the rigid coupled phase theory are very different from those of the porous media theory. Since it is already known that the rigid framed porous media theory is a good model for a variety of media (sections 5. 2. 4 and 5. 2. 6), it can be concluded that the coupled phase theory as it stands is not a satisfactory model for this type of material. This is due to the expressions for the viscous force and the heat transfer which are derived assuming isolated spherical particles. The expression for the viscous force used in coupled phase theory has already been discussed in section 5. 1. 7.

5. 2. 4 Complex reflection coefficient

The characteristic impedance Z_c of the air in the pores of a rigid frame porous material, normalised by the characteristic impedance of air $\rho_f c_f$, is, from Allard [46]

$$\frac{Z_c}{\rho_f c_f} = \frac{\sqrt{\rho(\omega)\kappa(\omega)}}{\rho_f c_f}. \qquad (5.49)$$

If the porous material is of thickness d, and is backed by a hard surface, the impedance in the pores (pressure/volume velocity) is given by [46]

$$Z_{\text{pore}} = -j\frac{Z_c}{A_{\text{pore}}}\cot kd \tag{5.50}$$

where A_{pore} is the cross sectional area of each of the pores.

The derivation of the surface impedance here follows Pierce [41]. The pressure in the free air just outside the porous material will be denoted p_{air} and the volume velocity normal to the material V_{air}. Because p_{air} must equal the pressure in the pores, for an area A

$$\frac{V_{\text{air}}}{A} = \frac{Np_{\text{air}}}{Z_{\text{pore}}}$$

where N is the number of pores per unit volume. This gives

$$\frac{p_{\text{air}}A}{V_{\text{air}}} = \frac{Z_{\text{pore}}}{N}. \tag{5.51}$$

The quantity $p_{\text{air}}/(V_{\text{air}}/A)$ is the usual (pressure/velocity) impedance for a sound wave normal to the porous material and is called the (normal) surface impedance of the material Z_{surf}. Thus from (5.50) and (5.51)

$$Z_{\text{surf}} = -j\frac{Z_c}{\alpha}\cot kd\,. \tag{5.52}$$

The complex reflection coefficient R is given by

$$\mathrm{R} = \frac{Z_{\text{surf}} - 1}{Z_{\text{surf}} + 1}. \tag{5.53}$$

The more common absorption coefficient can be obtained from R by

$$\mathrm{A} = 1 - |\mathrm{R}|^2\,.$$

The complex reflection coefficient R for a 0.05 m thick layer of air saturated glass beads of mean diameter 0.335 mm has been measured. The results were obtained with the two microphone impedance tube technique using equipment at Oldenburg University, Germany. Details of the method can be found in Teuber [168]. Figure 5. 9 compares the measurements of R with predictions of the rigid frame theory using equations (5.42), (5.45), (5.48), (5.49) and (5.52). The figure shows two measurements from a set of 8. All the other measurements lie between these two lines and are not shown. 4 of the measurements were taken with the glass beads settled by shaking while the other 4 were not shaken and were thus more loosely packed.

The 'spikes' of the measured data shown in figure 5. 9 are caused by the measurement system and are not characteristic of the stacked glass beads. This is discussed in more detail in reference [168].

The porosity and flow resistivity of the stacked beads were measured by Teuber [168]. The porosity is 0.396 and the flow resistivity is 2.4×10^{5} $kgm^{-3}s^{-1}$. The tortuosity is calculated from the porosity using equation (5.29) and is 1.59. This value could be checked by measuring the tortuosity independently. The measurement method is based on the principle that the tortuosity is related to the conductivity of the stacked beads saturated with a conducting fluid [169].

Because the pores are not cylindrical λ in (5.25) is modified to

$$\lambda = s_B\sqrt{\frac{8\alpha_\infty\rho_f\omega}{\alpha\sigma}} \tag{5.54}$$

[46] where s_B is the Biot shape factor. For cylindrical pores $s_B=1$. For pores with simple cross sections s_B can be calculated. There are different methods of obtaining s_B. Allard [46] matched the values of $\mathrm{Re}\,\rho(\omega)$ in the low frequency limit and obtained $s_B=1.07$ for square pores, $s_B=1.14$ for equilateral triangles and $s_B=0.78$ for rectangular slit shaped pores. For general pores of unknown shape s_B can be used to fit the theoretical predictions to measured data.

Figure 5. 9 shows the theoretical predictions when $s_B=0.5,\ 1.5$ and 2. It is seen that varying s_B only has an effect at the higher frequencies. At the higher frequencies all the data falls within the region bounded by the $s_B=0.5$ and $s_B=2$ theoretical curves.

The Crowe condition for the validity of the continuum assumption from section 4. 1. 2 can be applied to the present regime. The particle radius is 1.68×10^{-4} m and the maximum frequency is 10 kHz, so the Crowe condition requires $\phi>5\times10^{-3}$. This is satisfied here as $\phi=0.604$. If the particle radius is increased to 8.8×10^{-4} m, the largest beads studied in section 5. 2. 7 below, the condition is $\phi>0.7$. The volume fraction for these beads is still approximately 0.6 so the Crowe condition is not satisfied. The less strict condition $ka\ll1$ is still satisfied since $ka=0.2$.

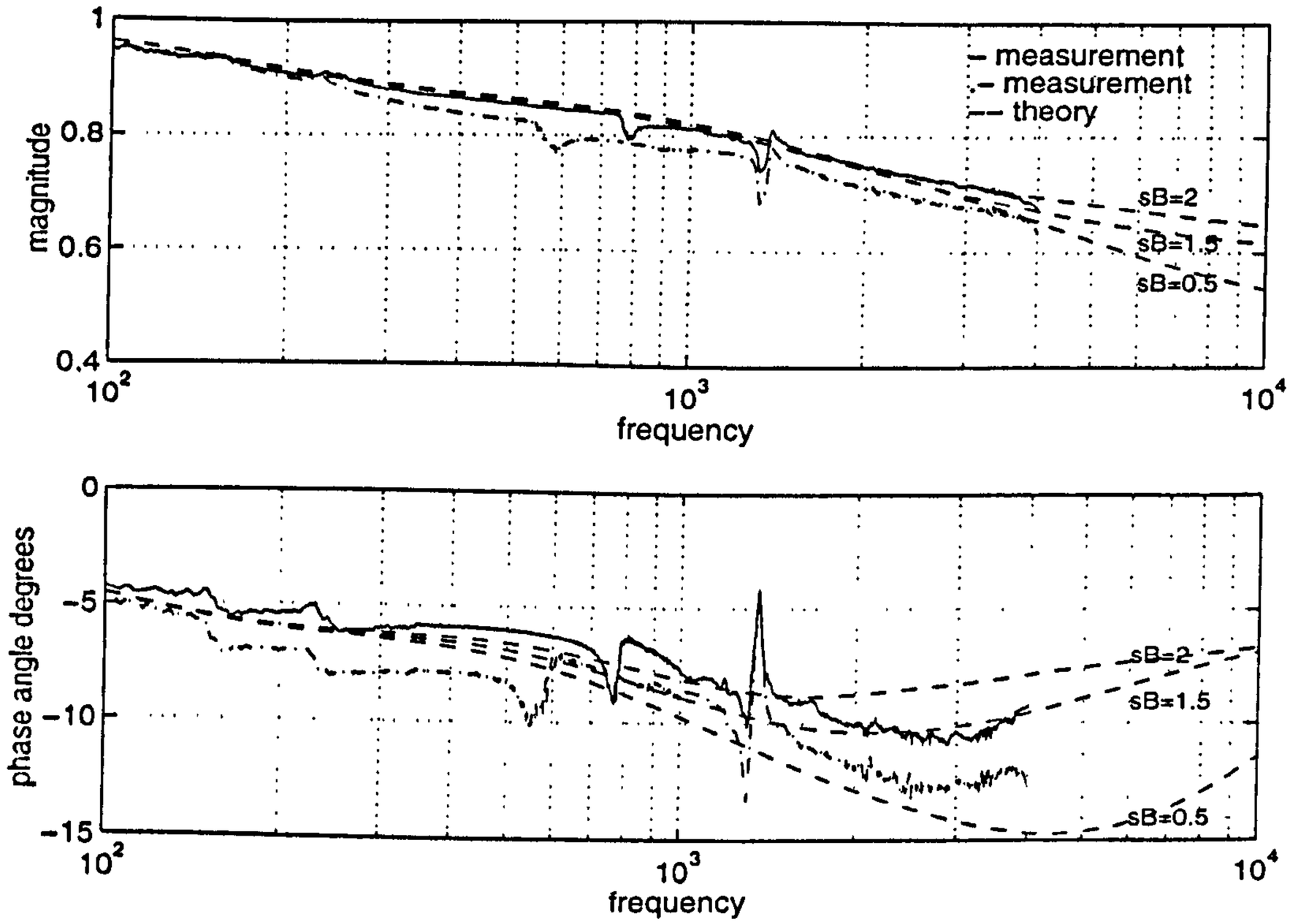

Figure 5. 9 Magnitude and phase angle of complex reflection coefficient versus frequency for glass beads in air with flow resistivity 2.4×10^5, porosity 0.396 and tortuosity 1.59. Comparison of data and predictions of rigid frame theory with Biot shape factor 0.5, 1 and 1.5.

5. 2. 5 Pore size distribution

Attenborough [121] has developed an alternative model for granular materials. All the pores are slit shaped so there is no adjustable shape factor like s_B from the previous section. The semi-widths b of the slits are assumed to have a log normal probability distribution.

The effective density and compressibility are given by

$$\rho_d(\lambda_d)=\alpha_\infty\rho_f\left(1+i\frac{\sigma\alpha}{\rho_f\omega\alpha_\infty}F_d(\lambda_d)\right) \tag{5.55}$$

$$\kappa_d(\lambda_d)=\kappa_f\left(\gamma-\frac{(\gamma-1)\alpha_\infty\rho_f}{\rho_d\left(\lambda_d\sqrt{N_{\mathrm{Pr}}}\right)}\right) \tag{5.56}$$

where

$$F_d(\lambda_d)=\frac{\left(-i\mu\omega\rho_f\right)^{\frac{1}{2}}\alpha_\infty}{\alpha\sigma}\frac{\int_0^\infty b^{-1}e(b)\tanh\left(\lambda_d\sqrt{-i}\right)db}{\int_0^\infty e(b)\left(1-\frac{\tanh\left(\lambda_d\sqrt{-i}\right)}{\lambda_d\sqrt{-i}}\right)db} \tag{5.57}$$

$$\lambda_d=b\sqrt{\frac{\omega\rho_f}{\mu}}. \tag{5.58}$$

$e(b)$ is the log normal probability distribution. This is better discussed in terms of the variable Φ where

$$\Phi=-\frac{\ln b}{\ln 2}. \tag{5.59}$$

Then

$$\int_0^\infty e(b)db=\int_{-\infty}^\infty f(\Phi)d\Phi \tag{5.60}$$

where

$$f(\Phi)=\frac{1}{s\sqrt{2\pi}}\exp\left(-\frac{\left(\Phi-\overline{\Phi}\right)^2}{2s^2}\right). \tag{5.61}$$

$\overline{\Phi}$ is the mean value of Φ given by

$$\overline{\Phi}=-\frac{\ln\overline{b}}{\ln 2} \tag{5.62}$$

where $\overline{b}$ is the mean slit semi-width. $\overline{b}$ is related to the other parameters according to the relation [122]

$$\sigma = \frac{3\mu\alpha_\infty}{\alpha\bar{b}^2}\exp\left(-2(s\ln 2)^2\right). \tag{5.63}$$

s is the standard deviation of Φ.

5. 2. 6 Comparison with reflection coefficient measurements

Figure 5. 10 compares predictions of the pore size distribution theory with the data from section 5. 2. 4. The integrals in equation (5.57) were calculated numerically using Mathematica. The Mathematica notebook porous.ma, which calculates the complex reflection coefficient, is given in appendix 2.

Figure 5. 10 shows the reflection coefficient predictions when the standard deviation $s = 0.05,\ 0.8$ and 1.5. The effect of varying s is greater at the higher frequencies. The data at the higher frequencies is contained within the region bounded by the $s = 0.05$ and $s = 0.8$ theoretical curves. These theoretical curves are very similar to the $s_B = 0.5$ and $s_B = 2$ Biot theory curves shown in figure 5. 9.

The porosity of this material is 0.396 and its flow resistivity is 2.4×10^5 $kgm^{-3}s^{-1}$. Its tortuosity can be calculated from equation (5.29). Using these values in equation (5.63) with $s = 0.8$ gives a mean slit semi-width of 22 μm. Because the pores in the stacked bead material are not really slits this value is the mean size for an effective pore size distribution.

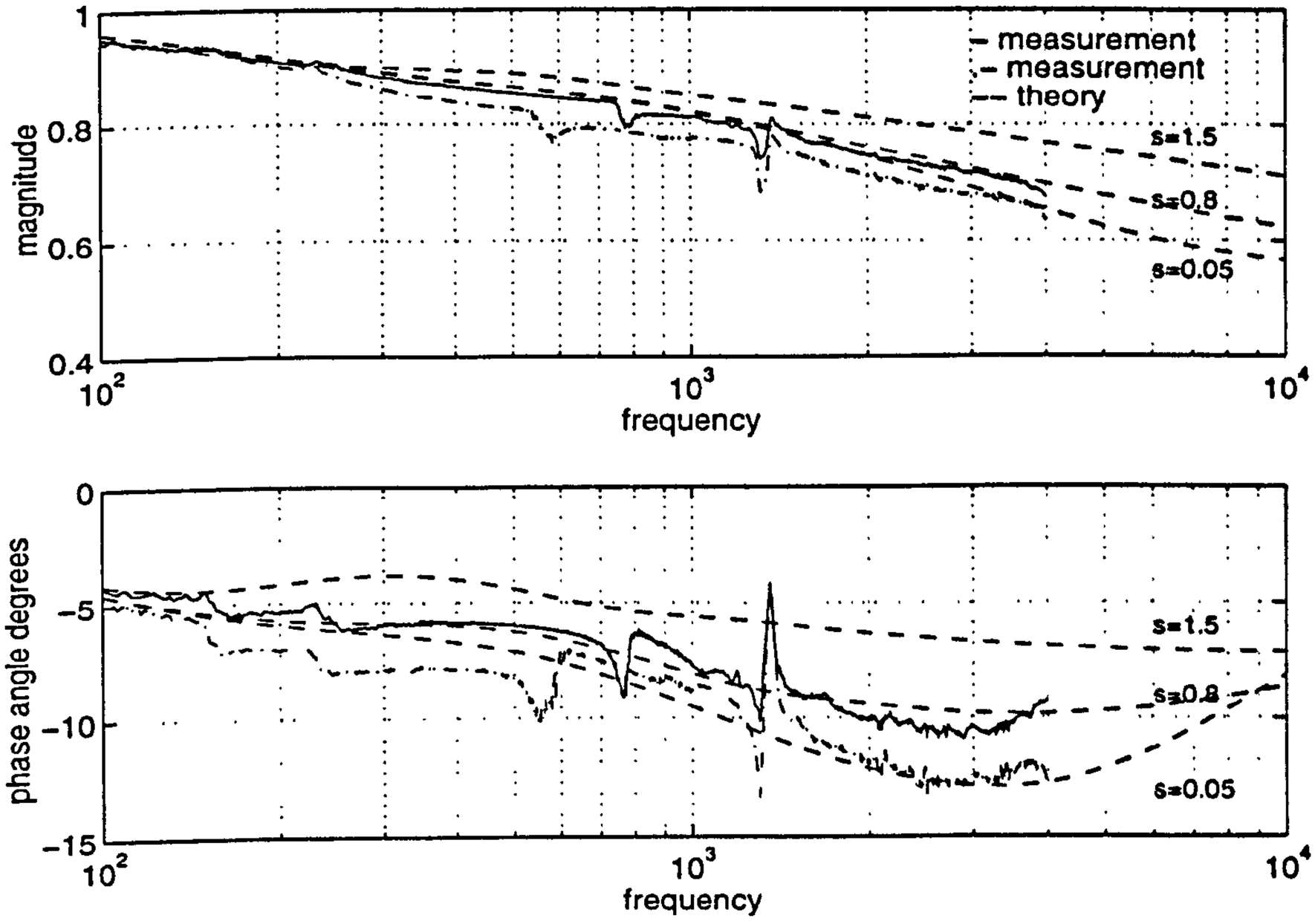

Figure 5. 10 Magnitude and phase angle of complex reflection coefficient versus frequency for glass beads in air with flow resistivity 2.4×10^5, porosity 0.396 and tortuosity 1.59. Comparison of data and predictions of Attenborough pore size distribution theory with standard deviation 0.05, 0.8 and 1.5.

5. 2. 7 Pore size distribution measurements

A simple experimental method has been used to measure an effective pore size distribution for sets of stacked glass beads. The 4 sets of beads tested had diameter ranges 0.25-0.42 mm, 0.36-0.49 mm, 0.42-0.84 mm, 0.75-1.5 mm and 1.5-2 mm. For convenience these will be referred to by the arithmetic mean of the two limits i.e. 0.335 mm, 0.43 mm, 0.63 mm, 1.125 mm and 1.75 mm. This will be called the mean diameter.

The method is based on the phenomenon of capillarity, the rising of a liquid in a small tube due to surface tension. In a cylindrical tube of radius r, the liquid rises by an amount h given by [36]

$$h = \frac{2\sigma \cos\theta}{\rho_f g r}.$$

Here σ is the surface tension. For water at 20°C $\sigma = 0.07275\ \mathrm{Jm^{-2}}$ [170]. θ is the 'contact angle' between the liquid and the surface of the tube. If the surface is clean glass then θ is said to be zero [170], this condition will be assumed here. g is the acceleration due to gravity.

For a liquid between two vertical parallel walls i.e. a slit [36]

$$h = \frac{\sigma \cos\theta}{\rho_f g b}$$

where b is the semi-width of the slit. Thus for water

$$h = 7.42 \times 10^{-6} b^{-1}. \tag{5.64}$$

h is also the suction pressure in metres of water that needs to be applied to the tube to bring the water back to the level of the free water or, in other words, to empty it of water.

If a suction h is applied to a porous material with pores of a range of sizes that has been saturated with water through capillarity, the pores with

$$b > b_{min} = 7.42 \times 10^{-6} h^{-1}$$

will be emptied of water. The volume of water removed is the volume of pores with semi-widths greater than b_{min}. If the suction is applied in increasing steps and is plotted against the volume of water removed at each step V, a water retention curve is obtained. Dividing each volume by the total volume of water removed V_{total} will give the (cumulative) volume distribution of pore sizes. If, after the test, most of the water has been removed then V_{total} will be close to the porosity α.

Figure 5. 11 shows the apparatus used for the size distribution tests. The porous plate and the sample are saturated. The burette applies a suction to the sample due to the difference in the level of the water in the burette and in the sample. The burette also measures the volume of water removed from the sample at each value of suction. The maximum suction that can be applied to the porous plate is the maximum suction that can be applied to the sample. At higher suctions the porous plate will be emptied of water first. The maximum suction in this experiment was determined by the height of the burette (0.5 m) which limits the level difference that can be produced.

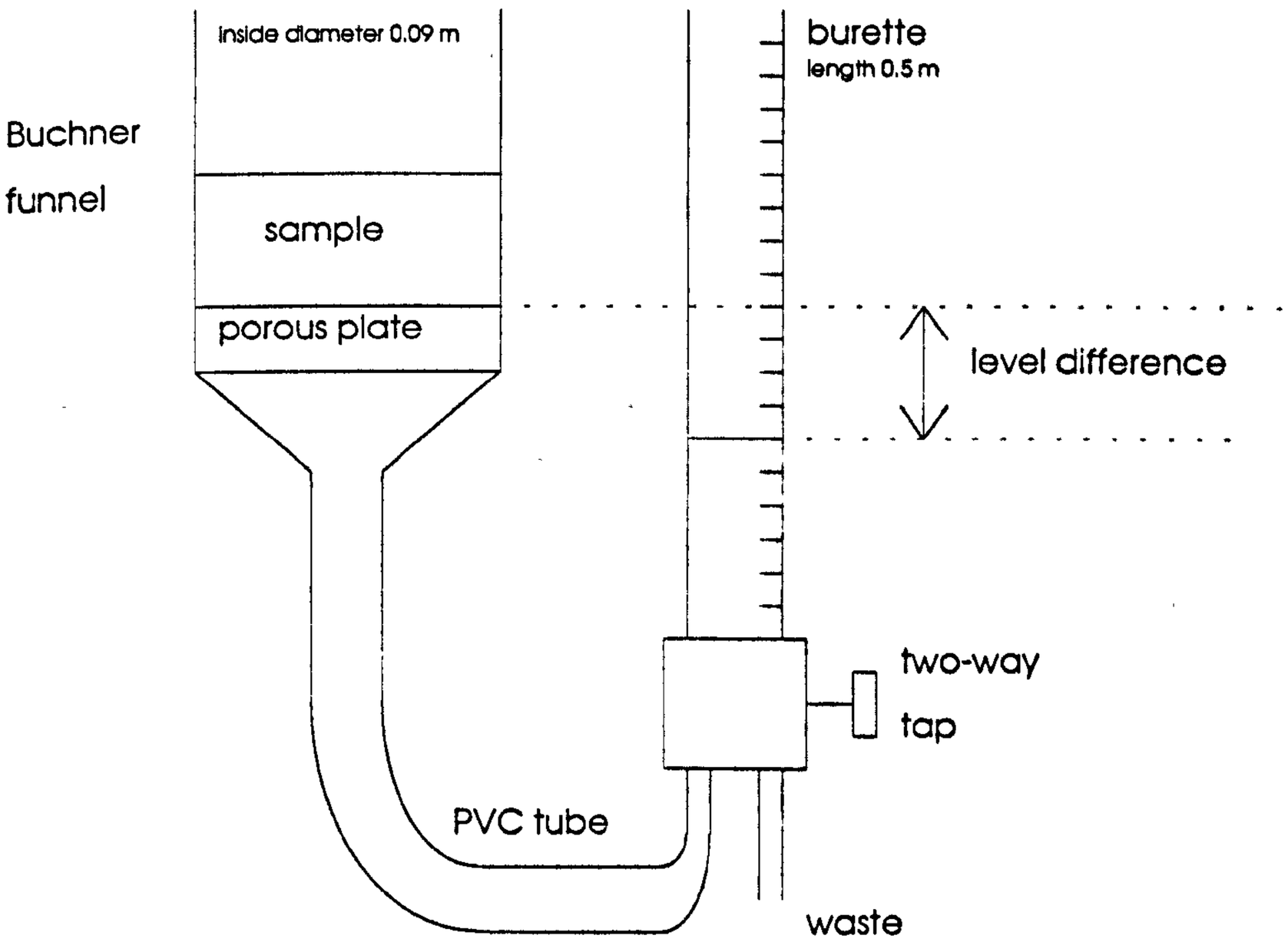

Figure 5. 11 Apparatus for effective pore size distribution measurement.

For each of the tests about 7% volume of the water remained after the maximum suction had been applied. This was determined by measuring the difference in the weight of the samples before and after oven drying. Interpreted within the present assumptions, this water is in pores that have semi-widths smaller than

$$b_{\min} = 7.42 \times 10^{-6} h_{\max}{}^{-1}.$$

This method assumes that all the pores travel from the lower surface of the sample, where the suction is applied, to the upper surface which is free to air pressure. It also assumes that the pores are not interconnected. It is clear that the pores in stacked glass beads are not arranged in this way. Therefore it is

possible that some of the remaining water is contained in pores such as side branches that do not have a direct connection to the lower surface of the sample.

Figure 5. 12 shows the measured cumulative volume distribution for the 1.125 mm beads. It must be remembered that this is an effective pore size distribution assuming that the pores are slit shaped. The data are from 3 independent tests. The water remaining after the test has been neglected. The abscissa is in Φ units where

$$\Phi = -\frac{\ln(b \text{ in mm})}{\ln 2}.$$

The solid curves are integrated log normal distributions with a mean of 2.05 Φ units and with standard deviations 0.4 and 1.1 respectively.

Also shown is the van Genuchten equation [171] [172]

$$\text{volume fraction} = \left[1 + (\alpha_1 h)^{(1-m)^{-1}}\right]^{-m}$$

where α_1 and m are empirical parameters. In figure 5. 12 $\alpha_1 = 36$ and $m = 0.75$. The resulting curve is slightly asymmetric with respect to the mean. For these beads the van Genuchten curve does not appear to be significantly different from a log normal curve with a mean of 2.05 and a standard deviation of 0.65.

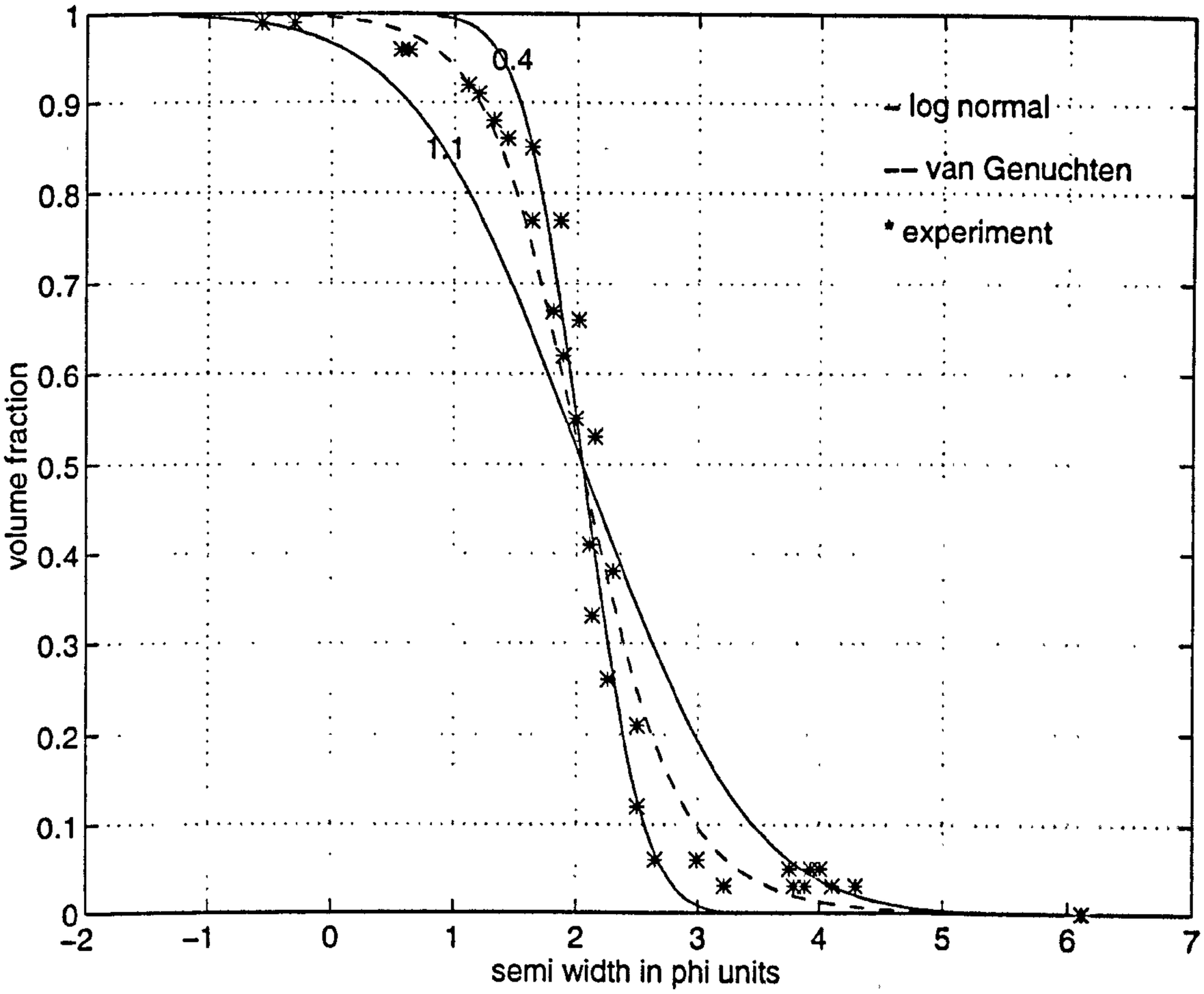

Figure 5. 12 Effective pore size distribution for stacked glass beads with mean diameter 1.125 mm. Comparison of data, van Genuchten distribution and log normal distributions with mean 2.05 and standard deviations 0.4 and 1.1.

Table 5. 1 gives the mean and standard deviation of the curves fitted (by eye) for all the bead tests. The mean pore size increases as the bead size increases, as would be expected. There are a range of standard deviations but the general trend is that the standard deviation also increases as the bead size increases.

mean bead diameter (mm)	mean of distribution (Φ units)	standard deviation
0.335	5	0.2-0.4
0.43	4.5	0.2-0.7
0.63	4.05	0.2-0.7
1.125	2.05	0.4-1.1
1.75	2	0.2-1.1

Table 5. 1 Mean and standard deviation of log normal fit to measured pore size distributions for stacked glass beads.

Teuber [168] has measured the flow resistivity and porosity of the 0.335 mm and 1.125 mm beads. Using equation (5.63) with the s used to fit to the impedance data, the effective mean pore radius can be calculated from these parameters. Because there is a range of s there will be a range of $\bar{b}$. The $\bar{b}$ obtained from the pore size distribution measurements can then be compared to that obtained from equation (5.63).

The s from the pore size distribution measurements can be compared with that used in the Attenborough theory in the preceding section to fit to the reflection coefficient data.

The two estimates for $\bar{b}$ and s are compared in Table 5. 2 for the 0.335 mm beads and in Table 5. 3 for the 1.125 mm beads.

parameter	theory and measurement	direct measurement
$\bar{b}$ μm	30-22	31
s	0.05-0.8	0.2-0.4

Table 5. 2 Mean slit semi-width and standard deviation for 0.335 mm beads. Comparison of pore size distribution measurement and estimates from porosity, flow resistivity and reflection coefficient measurements.

parameter	theory and measurement	direct measurement
$\bar{b}$ μm	134-119	241
s	0.05-0.5	0.4-1.1

Table 5. 3 Mean slit semi-width and standard deviation for 1.125 mm beads. Comparison of pore size distribution measurement and estimates from porosity, flow resistivity and reflection coefficient measurements.

The measured parameters for the 1.125 mm beads are $\alpha = 0.378$ and $\sigma = 1.3 \times 10^4$ kgm^{-3}s^{-1}.

The two methods of estimating $\bar{b}$ agree well for the 0.335 mm beads but not very well for the 1.125 mm beads. Because the standard deviation has a relatively small influence on the calculation of $\bar{b}$ this means that the direct size distribution measurement does not agree with the reflection coefficient and flow resistivity measurements for these beads. This may be because the size distribution is obtained from a static experiment using water while the reflection coefficient and flow resistivity are obtained from dynamic experiments using air.

Chapter 6
Extensions to coupled phase theory

Section 6. 1 reviews theoretical modifications to the momentum transfer term when the volume fraction is too high for the isolated particle assumption to be valid. Predictions of the modified theory are compared to experimental results and predictions of the Biot theory from chapter 5. Section 6. 2 discusses including a distribution of particle sizes in the scattering and coupled phase theories. A new coupled phase theory including a particle size distribution, based on the MH theory from chapter 4, is derived. Predictions of coupled phase theory including a size distribution are compared to complex wavenumber measurements on an alumina dust in air suspension where the particle size distribution is known. Section 6. 3 studies the effect of non-spherical particles on the complex wavenumber of the alumina dust suspension. Section 6. 4 looks at modes in an enclosure into which a suspension is introduced. The change in the modal frequencies due to the presence of the particles may be an alternative method of characterising suspensions. The frequency shifts for low frequency modes are calculated following the method of Culick [5] [6] [7] [8] [9]. These calculations are compared to the predictions of an intuitive approach. Section 6. 5 introduces the coupled phase formalism of Margulies and Schwartz [1] [2] [3] [4]. Their method of writing a total and diffusive (relative) momentum equation enables diffusion and phoresis effects to be modelled.

6. 1 High volume fractions

6. 1. 1 Effective viscosity

The drag on a spherical particle in a suspension is not the same as the drag it would experience alone in an infinite fluid. Einstein calculated the effective viscosity μ_{eff} of a suspension of rigid spheres, his calculation can be found in Landau and Lifshitz [143]. μ_{eff} is given by

$$\mu_{eff} = \mu\left(1+\tfrac{5}{2}\phi\right). \tag{6.1}$$

Equation (6.1) is only valid for $\phi < 0.05$ because mutual hydrodynamic interactions between the particles are neglected. These interactions become important at higher volume fractions.

Expressions for $\mu(\phi)$ which account for hydrodynamic interactions and particle collisions were reviewed by Zuber [153].

Vand [173] obtained

$$\mu_{eff} = \mu \exp\left[\frac{k_1\phi + \theta(k_2 - k_1)\phi^2}{1 - B\phi}\right] \tag{6.2}$$

where k_1 is the Einstein shape factor for spheres (= 2.5), k_2 is the 'shape factor of collision doublets' (= 3.175), θ is the 'collision time constant' (= 4) and B is the 'hydrodynamic interaction constant' (=39/64). If there are no collisions θ is set to zero.

Figure 6. 1 compares the HT coupled phase theory prediction of equation (4.53) with and without the effective viscosity given by equation (6.2). The figure also shows the Hampton measurements of aqueous suspensions of kaolinite which were discussed in section 5. 1. 7 and shown in figures 5. 4 to 5. 6. The prediction of the modified theory is slightly closer to the measurements.

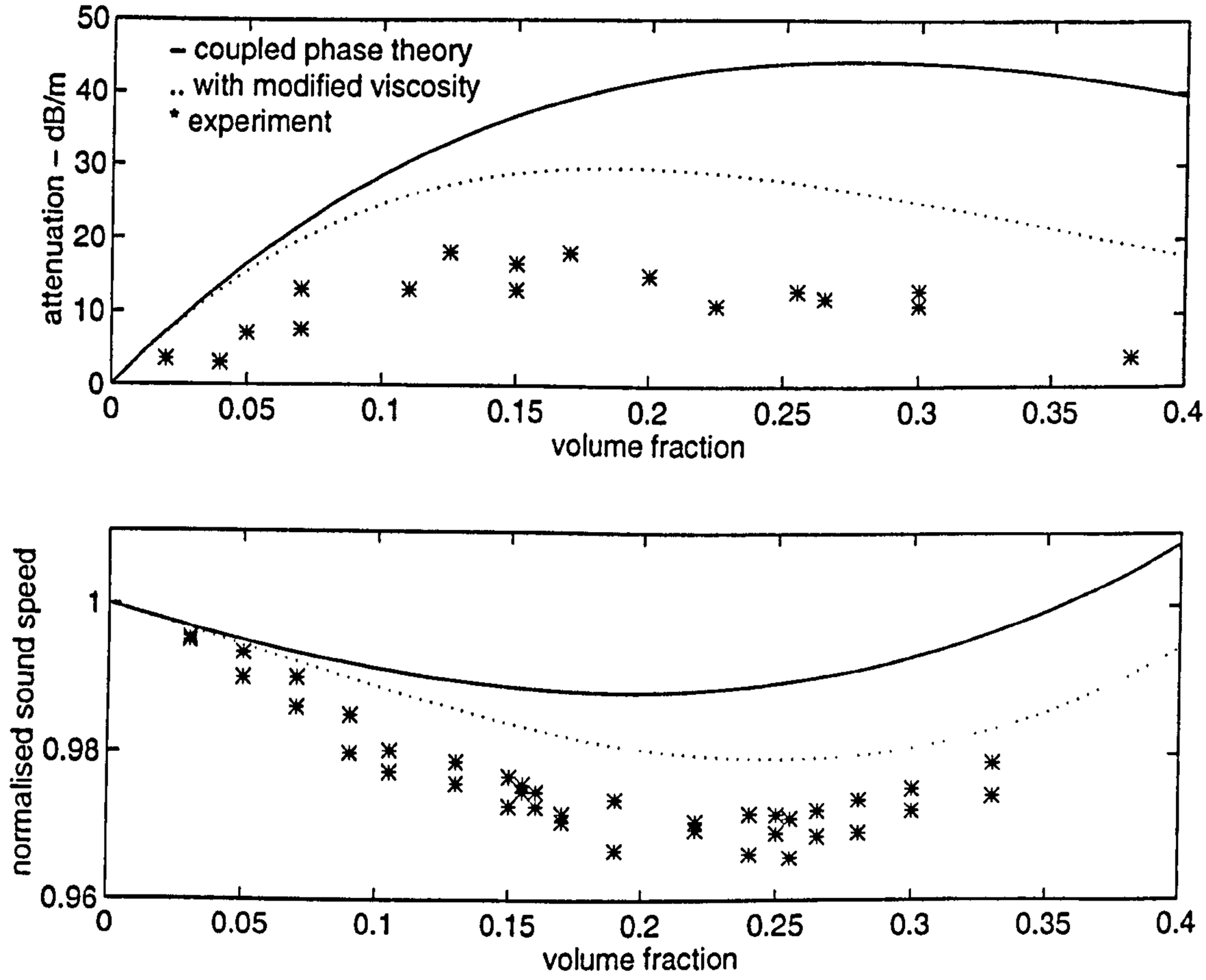

Figure 6. 1 Attenuation at 100 kHz and normalised sound speed at 600 kHz versus volume fraction for an aqueous suspension of kaolinite particles of radius 1.2 μm. Comparison of data of Hampton and predictions of HT theory with and without modified viscosity.

6. 1. 2 Hydrodynamic interactions

The effective viscosity approach seems to have been superseded by 'cell' models for the hydrodynamic interactions. Strout [42] reviewed and extended the cell model approach. The analysis results in a 'drag correction factor' D which multiplies the isolated particle Stokes drag. The product is the drag on a spherical particle in the presence of other particles, and depends on ϕ. Before Strout, only the steady state drag was considered. Hasimoto [174] obtained the factor for cubic arrays of spheres

$$D_{\text{Has}} = \left[1 - 1.1791\phi^{\frac{1}{3}} + \phi - .329\phi^{2}\right]^{-1}. \tag{6.3}$$

Happel [37] [175] obtained the corresponding expression for random arrays of spheres

$$D_{\text{Hap}} = \frac{2 + \frac{4}{3}\phi^{\frac{5}{3}}}{2 - 3\phi^{\frac{1}{3}} + 3\phi^{\frac{5}{3}} - 2\phi^{2}}. \tag{6.4}$$

Kuwabara [150] used a slightly different method for random arrays and obtained

$$D_{\text{Kuw}} = \frac{5}{5 - 9\phi^{\frac{1}{3}} + 5\phi - \phi^{2}}. \tag{6.5}$$

These three steady state correction factors are compared in figure 6. 2. The Hasimoto expression is only valid for $\phi < 0.4$.

The Hasimoto expression was used by Gibson and Toksoz [134] in a coupled phase theory. The expression for the complex wavenumber is identical to the HT result (equation (4.53)) except for the form of the S momentum transfer term. The Stokes drag term is multiplied by $\alpha^{2} D_{\text{Has}}$ and the history and induced mass terms are neglected.

Strout extended the Happel and Kuwabara methods to oscillating particles. The result takes account of both the history effect (due to the acceleration) and the induced mass effect. The correction factor from the Happel method is given by

$$D_{\text{Strout}} = -\tfrac{2}{9} k_{f3}{}^{2}\left(1 - \tfrac{3}{2} C_{1}\right) \tag{6.6}$$

where k_{f3} is the viscous wavenumber from section 3. 2. 2.

The coefficient C_1 is given by

$$\frac{\left[k^5+3\left(1-\phi^{\frac{1}{3}}\right)k^4+3\left(2\phi^{\frac{2}{3}}-3\phi^{\frac{1}{3}}+1\right)k^3+3\left(-2\phi+6\phi^{\frac{2}{3}}-3\phi^{\frac{1}{3}}\right)k^2+18\left(\phi^{\frac{2}{3}}-\phi\right)k-18\phi\right]+\exp\left[2k\left(1-\phi^{-\frac{1}{3}}\right)\right]\left[\begin{array}{c}k^5+3\left(1-\phi^{\frac{1}{3}}\right)k^4+3\left(2\phi^{\frac{2}{3}}-3\phi^{\frac{1}{3}}+1\right)k^3+3\left(-2\phi+6\phi^{\frac{2}{3}}-3\phi^{\frac{1}{3}}\right)k^2\\+18\left(\phi^{\frac{2}{3}}-\phi\right)k-18\phi\end{array}\right]}{\left[(1-\phi)k^3+3\left(\phi^{\frac{4}{3}}-\phi-\phi^{\frac{1}{3}}\right)k^2+\left(9\phi^{\frac{4}{3}}-3\phi+6\phi^{\frac{2}{3}}\right)k+\left(9\phi^{\frac{4}{3}}-6\phi\right)\right]+\exp\left[2k\left(1-\phi^{-\frac{1}{3}}\right)\right]\left[(1-\phi)k^3+3\left(\phi^{\frac{4}{3}}-\phi-\phi^{\frac{1}{3}}\right)k^2+\left(9\phi^{\frac{4}{3}}-3\phi+6\phi^{\frac{2}{3}}\right)k+\left(9\phi^{\frac{4}{3}}-6\phi\right)\right]-\exp\left[k\left(1-\phi^{-\frac{1}{3}}\right)\right][24\phi k]}$$

where k stands for k_{f3}.

Strout also used a coupled phase theory identical to equation (4.53).

D_{Strout} was derived using the time dependence $\exp(j\omega t)$. Since the S term in equation (4.53) was derived using the $\exp(-i\omega t)$ time dependence it is necessary to take the complex conjugate of D_{Strout}

$$(D_{\text{Strout}})^* = -\tfrac{2}{9}\left(k_{2f}{}^2\right)^*\left(1-\tfrac{3}{2}C_1{}^*\right) \tag{6.7}$$

to use these results in equation (4.53).

The new S term is given by

$$S = \tfrac{9}{4}i\frac{\delta^2}{a^2}(D_{\text{Strout}})^*. \tag{6.8}$$

This includes the history and induced mass terms.

For low frequencies, i.e. $k_{f3}\to 0$, D_{Strout} gives the Happel expression (6.4).

When $\phi \to 0$ the force on a single sphere predicted by (6.7) is

$$i\omega\rho_f\left(\tfrac{4}{3}\pi a^3\right)\left[\tfrac{9}{4}i\frac{\delta^2}{a^2}+\tfrac{9}{4}(1+i)\frac{\delta}{a}+\tfrac{1}{2}\right]$$

which is the usual expression including the steady state Stokes drag, the unsteady Bassett history term and the induced mass given by equation (4.13) and discussed in section 4. 1. 5.

Figure 6. 3 plots $|D_{\text{Strout}}|$ versus a/δ for a number of volume fractions. For a wide range of a/δ, the low frequency Happel result is valid. The range of validity increases with increasing ϕ.

Figure 6. 4 compares the predictions of the coupled phase theory with the S term given by equation (6.8) with Hampton's data for aqueous suspensions of kaolinite. The relevant parameters have been given in section 5. 1. 7. Also

shown is the Happel result and the Biot theory prediction from equations (5.16), (5.24), (5.27), (5.30), (5.32) and (5.33), with $k_0 = 10$. Comparing this figure with figure 5. 6 shows that the coupled phase theory prediction is in better agreement with the data when the modified S term is included, but it does not agree as well as the Biot theory prediction. Comparison with figure 6. 1 shows that the Strout cell model gives better agreement than the Vand model.

Urick [104] [105] and Greenwood *et al* [176] also performed experiments on aqueous suspensions of kaolinite. Figure 6. 5 compares predictions of the Strout theory and the Biot theory with Urick's measurements. The parameter in the Biot theory, k_0, is again 10. The frequency is 1 MHz, the particle radius is 0.45 μm and the physical parameters are given in appendix 1. These are the same as the Hampton parameters, except for the bulk modulus of kaolinite.

As in figure 6. 4, the Biot theory prediction is closer to the measurements than the Strout theory prediction. This is partly because the Biot theory has the adjustable parameter k_0.

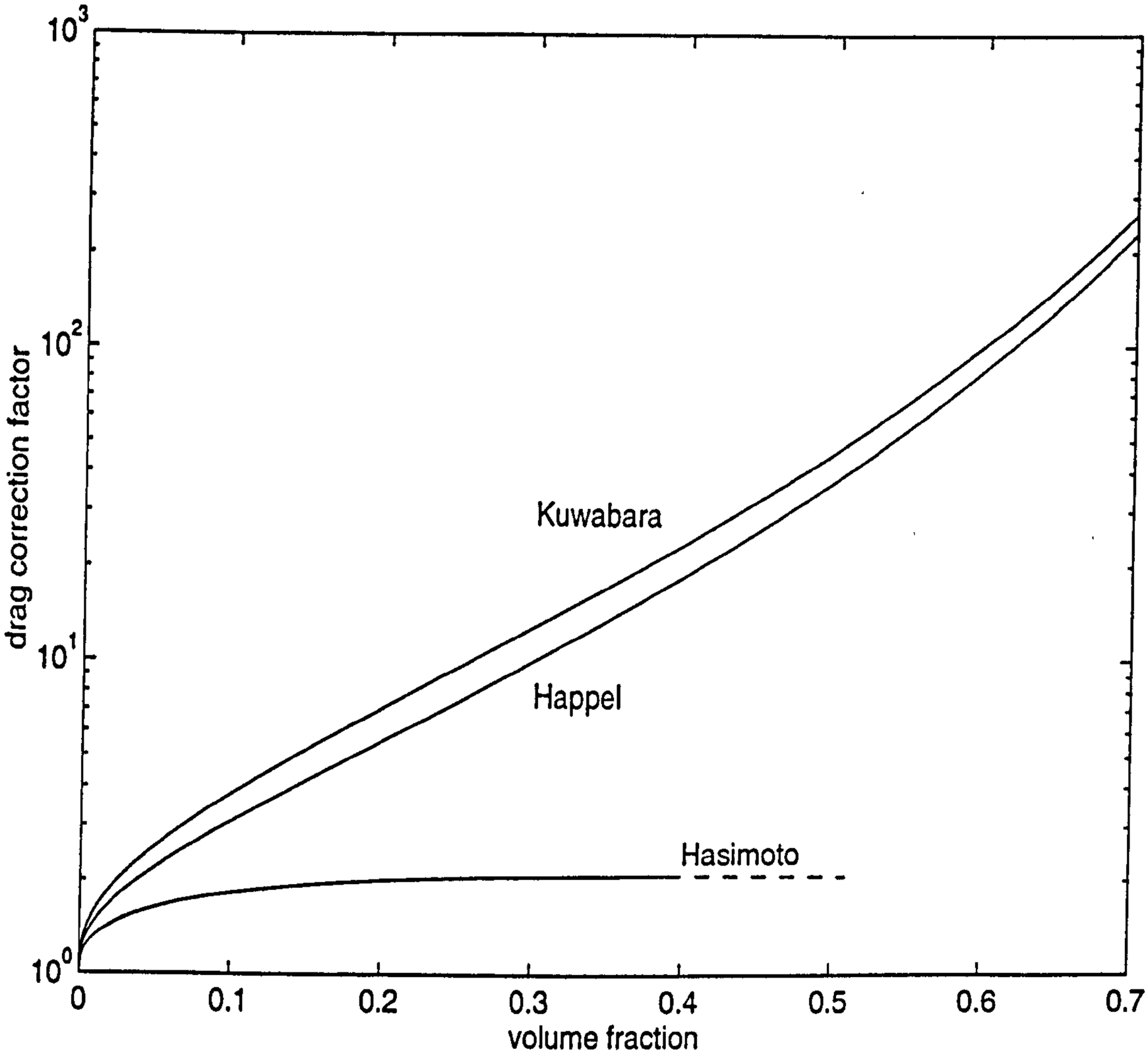

Figure 6. 2 Drag correction factor versus volume fraction. Comparison of Kuwabara, Happel and Hasimoto expressions.

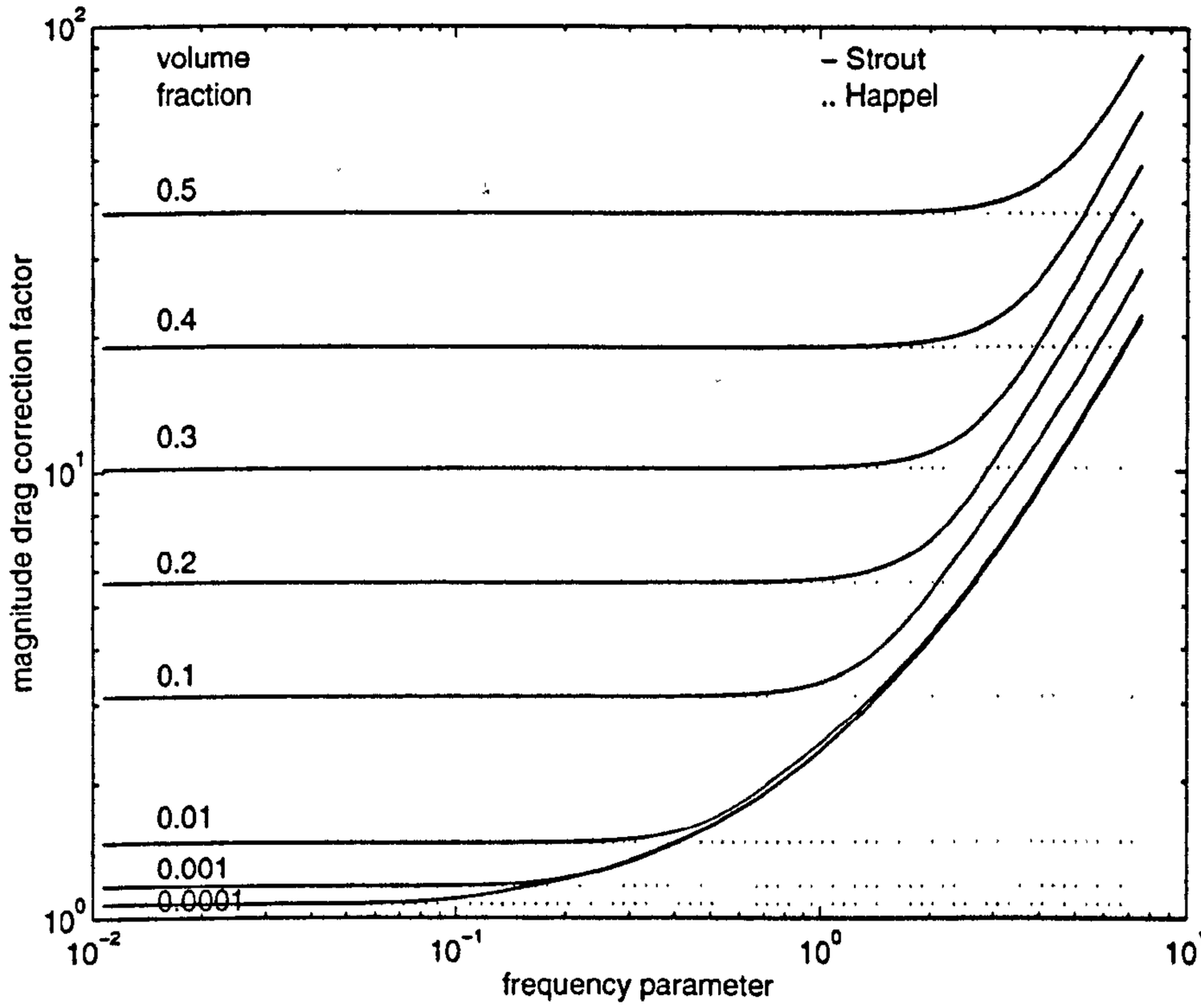

Figure 6. 3 Magnitude of Strout drag correction factor versus frequency parameter a/δ for volume fractions between 10^{-4} and 0.5. Dotted lines indicate steady state values.

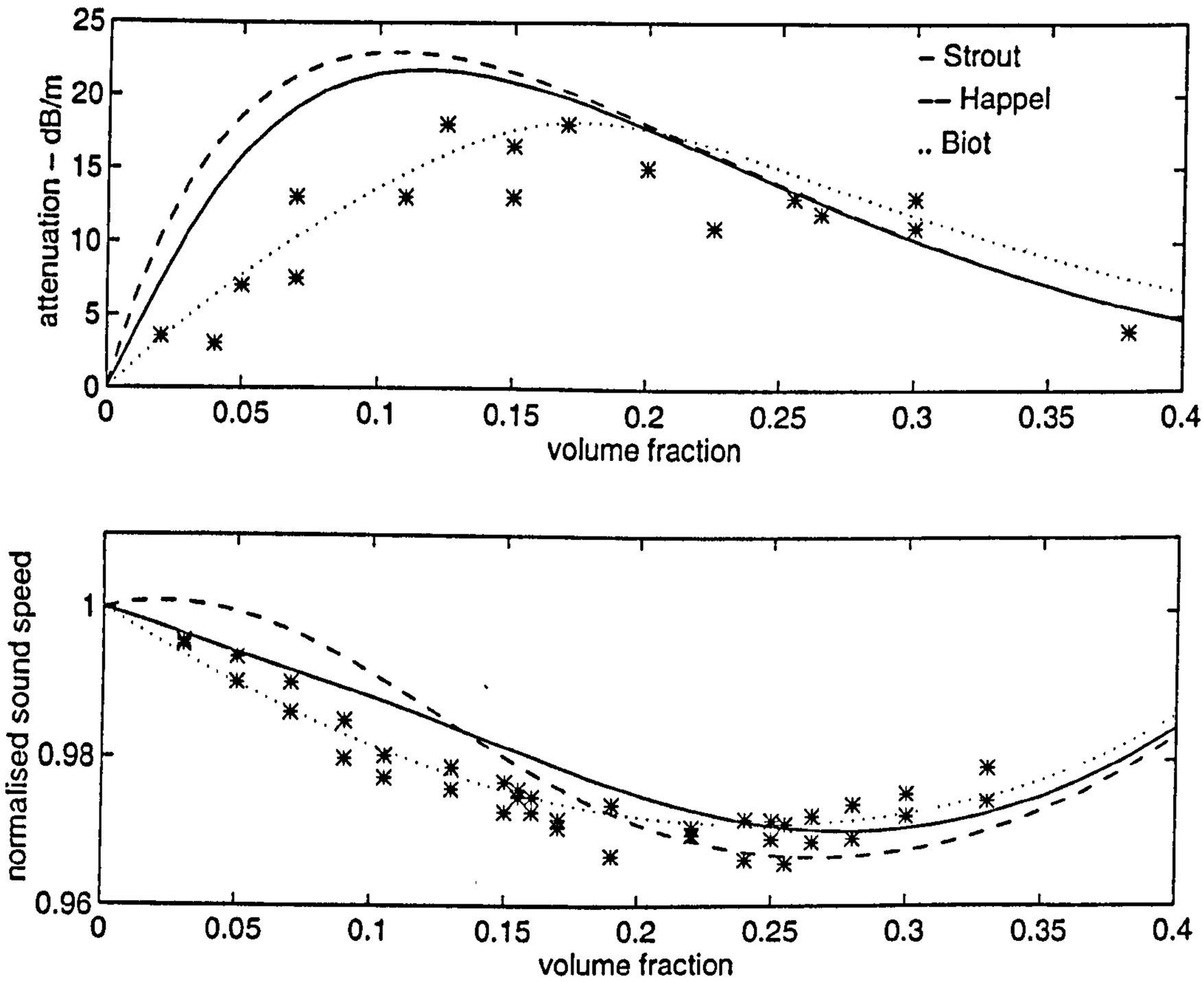

Figure 6. 4 Attenuation at 100 kHz and normalised sound speed at 600 kHz versus volume fraction for an aqueous suspension of kaolinite particles of radius 1.2 μm. Comparison of data of Hampton and predictions of frameless Biot theory and HT theory with Happel and Strout drag correction factors.

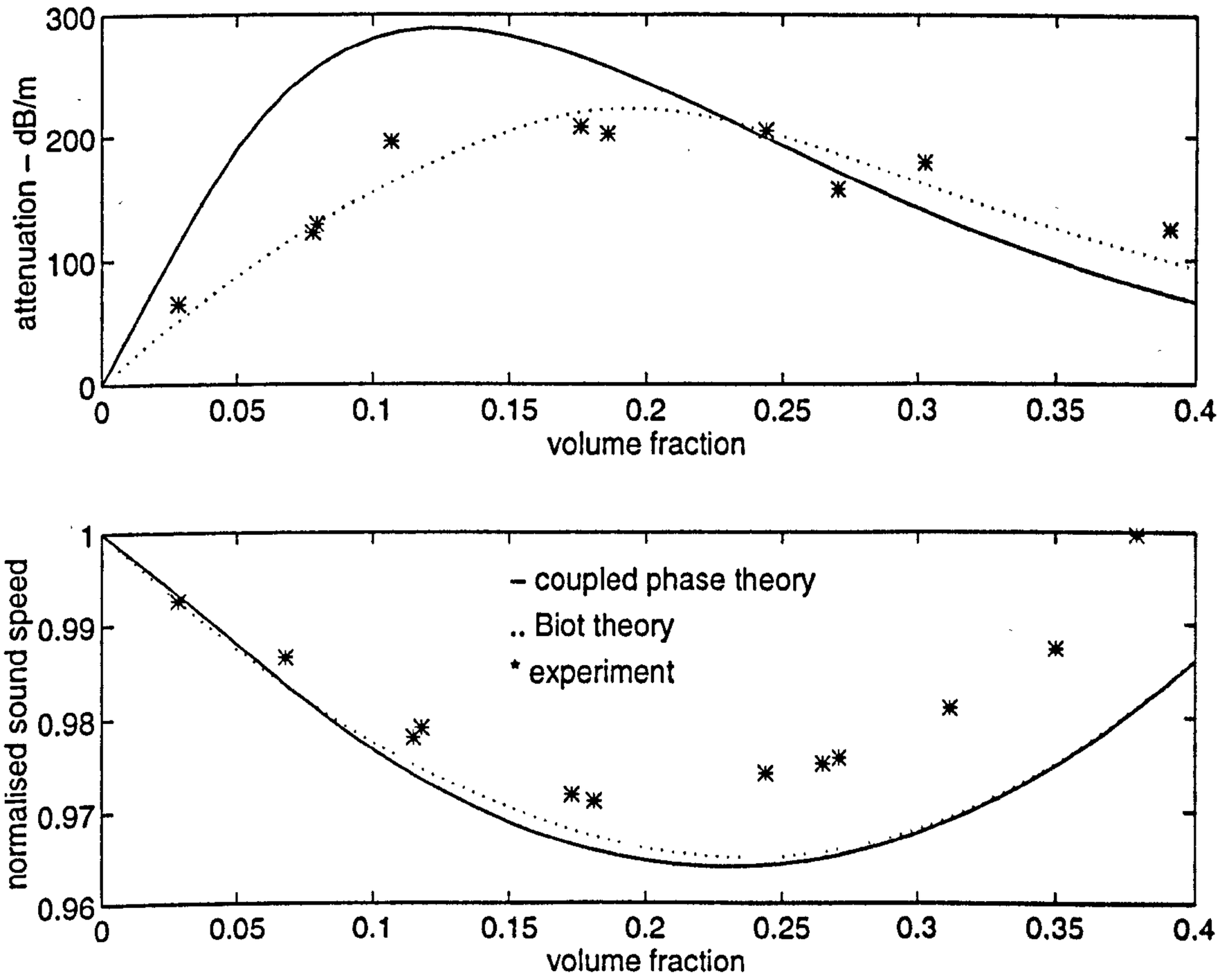

Figure 6. 5 Attenuation and normalised sound speed versus volume fraction for an aqueous suspension of kaolinite particles of radius 1.2 μm at 1 MHz. Comparison of predictions of HT theory with Strout drag correction factor and data of Urick.

6. 1. 3 Induced mass

The induced mass coefficient C for an isolated sphere is ½ from equation (4.13). Zuber [153] took account of the relative motion of spheres in a suspension and obtained

$$C = \frac{1+2\phi}{2(1-\phi)} \tag{6.9}$$

for the induced mass coefficient of a single sphere in a suspension. This is the expression used by Harker and Temple [65]. Equation (6.9) is similar to the expression of both van Wijngaarden and Geurst as quoted by Kytomaa and Atkinson [112]

$$C = \frac{1+3.2\phi}{2}. \tag{6.10}$$

Kytomaa and Atkinson derived the expression

$$C = \frac{1-\phi}{2} \tag{6.11}$$

by analogy with the electrical conductivity problem. This expression is valid for random distributions of monodisperse spheres. C given by (6.11) decreases with ϕ, whereas that given by (6.9) and (6.10) increases with ϕ. Atkinson and Kytomaa used equation (6.10), not equation (6.11), in their calculations.

The induced mass coefficients given by equations (6.9) to (6.11) and the isolated sphere value are compared in figure 6. 6.

As discussed by Kytomaa [25], the inertial momentum transfer, which is caused by the induced mass force, controls the sound speed at high frequencies.

Kytomaa measured the attenuation in an aqueous suspension of lead glass beads in the region where the effect of the Basset force begins to dominate. 50% of the beads had radii within 24 ±6 μm. The density of the glass is 2830 kgm^{-3} and its compressibility is 2×10^{10} Nm^{-2} [13]. The data is shown in figure 6. 7 for frequencies between 200 kHz and 600 kHz and at volume fractions of 0.26 and 0.58. The slope of the attenuation data versus frequency changes from slightly less than 2 (the Stokes drag region) to slightly less than ½ (the Basset force region). The frequency at which the slope changes is known as the transition frequency. As can be seen from the figure, the transition actually takes place gradually over a range of frequencies.

The maximum $k_f a$ for the Kytomaa data is 0.13. This indicates that scattering should be small and the assumptions of coupled phase theory are valid. The

solid lines in figure 6. 7 are the predictions of the HT model given by equation (4.53), using the momentum transfer term for isolated particles (4.13) with C given by (6.11). This theory was used in preference to the Strout theory from section 6. 1. 2. The Strout theory predicted that the attenuation of the 0.58 volume fraction suspension was less than the attenuation of the 0.26 volume fraction suspension. This is contrary to the evidence of the experimental data. The alternative expressions for C given by equations (6.9) and (6.10) gave similar predictions to the Strout theory. The Biot theory gave a similar prediction to the HT theory with C given by (6.11).

Figure 6. 7 shows that the theory agrees with the 0.26 volume fraction data at the higher frequencies, where it has moved to the Basset force region. The slope of the theoretical curves, slightly greater than $\frac{1}{2}$, indicates that, according to the theory, the frequency range 10^5 to 10^6 Hz is in the Basset force region. This implies that the transition frequency must be below 10^5 Hz. The transition region predicted by the theories is actually between 10^2 and 10^4 Hz. As well as being in a lower frequency range, the transition region predicted by the theory covers a wider range of frequencies than the measured transition region. To bring the theoretical transition region into this range of frequencies it is necessary to assume that a large volume fraction of the particles have radii of the order 1-5 μm. Although there is some uncertainty about the size distribution of the beads it is not wide enough to accommodate this correction.

Porous media theory also makes use of the induced mass coefficient for a sphere, as discussed in section 5. 1. 5. For materials comprised of spherical grains Berryman [124] showed that the tortuosity must depend on C as in equation (5.27) and C was assumed to be $\frac{1}{2}$, the value for an isolated sphere. More generally, porous media are assumed to be constructed of tube-like pores and the tortuosity is related to the increased path length through the pores. Here there is no connection with the induced mass coefficient for single grains since the individual grains are not considered.

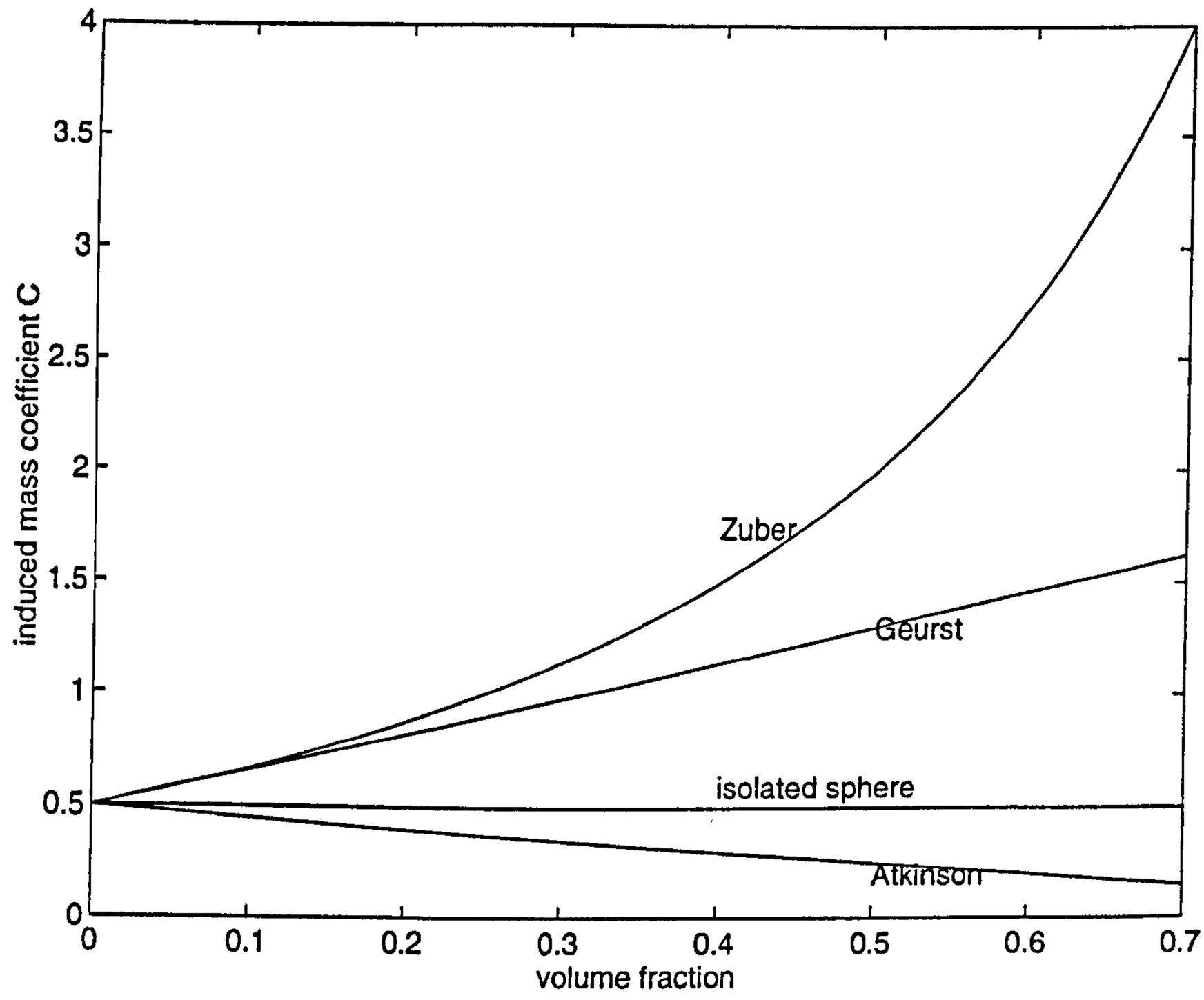

Figure 6. 6 Single sphere induced mass coefficient versus volume fraction. Comparison of isolated sphere result and results for a suspension of Zuber, Geurst and Atkinson.

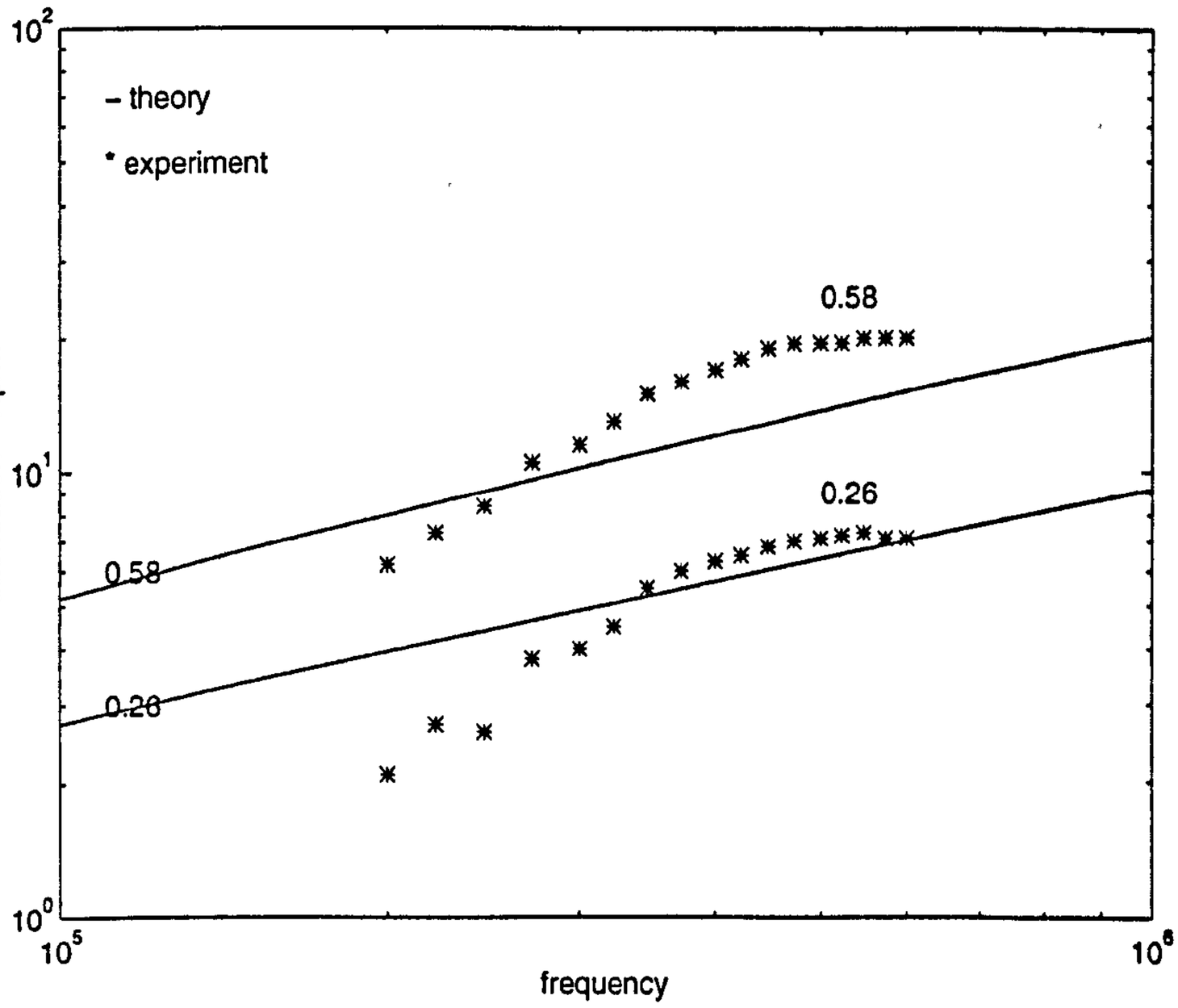

Figure 6. 7 Attenuation versus frequency for an aqueous suspension of lead glass beads of mean radius 24 μm with volume fraction 0.26 and 0.58. Comparison of data of Kytomaa and predictions of HT theory with Kytomaa and Atkinson induced mass coefficient.

6. 2 Particle size distribution

6. 2. 1 Coupled phase theory

Using the method of Harker *et al* [106], the theory from section 4. 1 can be extended to include a particulate phase with particles of different radii. Each set of particles with radius a_n is treated as a separate phase with a volume fraction ϕ_n, a momentum transfer term S_n, a heat transfer term S_{hn}, a velocity u_{sn} and a temperature T_{sn}. The solid phases have the same density ρ_s. If there are M solid phases then there will be $M+1$ momentum equations and $M+1$ energy equations. The total volume fraction ϕ will be given by

$$\phi = \sum_{n=1}^{M} \phi_n .$$

The set of equations at the beginning of section 4. 1. 14 become

$$\frac{\alpha \rho_f'}{K \rho_f{}^0} = \alpha u_f' + \sum_{n=1}^{M} \phi_n{}^0 u_{sn}' \tag{6.12}$$

$$\left(\rho_s{}^0 + \rho_f{}^0 S_n\right) u_{sn}' = \rho_f{}^0 S_n u_f' + K p' \tag{6.13}$$

$$\rho_f{}^0 \left(\alpha + \sum_{n=1}^{M} \phi_n{}^0 S_n\right) u_f' = \rho_f{}^0 \sum_{n=1}^{M} \phi_n{}^0 S_n u_{sn}' + \alpha K p' \tag{6.14}$$

$$p' = RT\rho_f' + \rho_f{}^0 R T_f' \tag{6.15}$$

$$T_{sn}' = T_f' \left(1 + \frac{\rho_s{}^0 C_s}{\rho_f{}^0 S_{hn}}\right)^{-1} \tag{6.16}$$

$$\rho_f{}^0 \sum_{n=1}^{M} \phi_n{}^0 S_{hn} T_{sn}' = \rho_f{}^0 \left(\alpha C_{pf} + \sum_{n=1}^{M} \phi_n{}^0 S_{hn}\right) T_f' - \alpha p' \tag{6.17}$$

where $T = T_f{}^0 = T_s{}^0$. From this point onwards the superscript zeros will be dropped.

Eliminating T_s' between equations (6.16) and (6.17) gives

$$\rho_f C_{vf} \left(\gamma_f + \sum_{n=1}^{M} F_{hn}\right) T_f' - p' = 0 \tag{6.18}$$

where

$$F_{hn} = \frac{\phi_n \rho_s C_s S_{hn}}{\alpha C_{vf} \left(\rho_s C_s + \rho_f S_{hn}\right)} .$$

Rewriting (6.13) gives

$$u_{sn}' = \frac{\rho_f S_n}{\rho_s + \rho_f S_n} u_f' + K \frac{1}{\rho_s + \rho_f S_n} p' , \tag{6.19}$$

and eliminating S_n between (6.13) and (6.14) gives the total momentum equation

$$\rho_s \sum_{n=1}^{M} \phi_n u'_{sn} + \alpha \rho_f u'_f = K p' . \tag{6.20}$$

Eliminating u'_{sn} between equations (6.19) and (6.20) gives

$$u'_f = K p' \frac{1 - \rho_s \sum_{n=1}^{M} \frac{\phi_n}{\rho_s + \rho_f S_n}}{\rho_{va} - \rho_s{}^2 \sum_{n=1}^{M} \frac{\phi_n}{\rho_s + \rho_f S_n}} \tag{6.21}$$

where

$$\rho_{va} = \alpha \rho_f + \rho_s \sum_{n=1}^{M} \phi_n = \alpha \rho_f + \phi \rho_s .$$

When $M = 1$, $\phi_1 = \phi$, $S_1 = S$ and equation (6.21) becomes equation (4.19).

Equations (6.19) to (6.21) can now be used to eliminate u'_f and u'_{sn} in equation (6.12), which gives

$$\rho_f K^2 p' = \alpha \rho'_f \rho(\omega) \tag{6.22}$$

where $\rho(\omega)$, the effective density, is given by

$$\rho(\omega) = \frac{\rho_{va} - \rho_s{}^2 \sum_{n=1}^{M} \frac{\phi_n}{\rho_s + \rho_f S_n}}{1 + (\rho_{va} - 2\rho_s) \sum_{n=1}^{M} \frac{\phi_n}{\rho_s + \rho_f S_n}} \tag{6.23}$$

or

$$\rho(\omega) = \rho_{va} - \frac{\alpha^2 (\rho_s - \rho_f)^2 \sum_{n=1}^{M} \frac{\phi_n}{\rho_s + \rho_f S_n}}{\frac{1}{\phi} \sum_{n=1}^{M} \phi_n \frac{\rho_f S_n + \alpha(\alpha \rho_s + \phi \rho_f)}{\rho_s + \rho_f S_n}}$$

because

$$1 = \frac{1}{\phi} \sum_{n=1}^{M} \phi_n .$$

When $M = 1$

$$\rho(\omega) = \frac{S \rho_{va} + \alpha \rho_s}{S + \alpha \rho_s \rho_b}$$

which is the momentum transfer term of the complex wavenumber from equation (4.44).

The three equations (6.15), (6.18) and (6.22) can be rewritten as the matrix equation

$$\begin{pmatrix} RT & -1 & \rho_f R \\ 0 & 1-\gamma_f & \rho_f R\left(\gamma_f + \sum_{n=1}^{M} F_{hn}\right) \\ -\alpha\rho(\omega) & \rho_f K^2 & 0 \end{pmatrix} \begin{pmatrix} \rho_f' \\ p' \\ T_f' \end{pmatrix} = 0 . \tag{6.24}$$

Setting the determinant of the matrix in (6.24) to zero gives

$$K^2 = \left(\frac{k}{\omega}\right)^2 = \alpha\kappa_f \rho(\omega) \frac{1+\sum F_{hn}}{1+\gamma_f{}^{-1}\sum F_{hn}} . \tag{6.25}$$

The heat transfer term in (6.25) is of the same form as the single particle size version (4.44) with F_h replaced with a sum over the F_{hn}. Since F_{hn} contains a ϕ_n factor this is akin to volume averaging the F_{hn}. The momentum transfer term $\rho(\omega)$ given by (6.23) is a more complicated function of S_n.

6. 2. 2 Scattering theory

McClements [64] included a distribution of particles sizes in the Allegra and Hawley long wavelength scattering theory. The scattering coefficients to insert in the formulae for the complex wavenumber are given by the volume average of the scattering coefficients of each particle size, which are given by equations (3.52) and (3.54), thus

$$A_0 = \frac{1}{\phi} \sum_{n=1}^{M} \phi_n A_{0n}(a_n) \tag{6.26}$$

$$A_1 = \frac{1}{\phi} \sum_{n=1}^{M} \phi_n A_{1n}(a_n) . \tag{6.27}$$

In order to represent a particle size distribution with a single radius, McClements made use of the Sauter mean radius a_{32} which is given by

$$a_{32} = \frac{\sum_{n=1}^{M} N_n a_n{}^3}{\sum_{n=1}^{M} N_n a_n{}^2} \tag{6.28}$$

where N_n is the number of particles of radius a_n. The Sauter mean radius will be employed in the following section.

6. 2. 3 Alumina dust in air

Moss [11] [12] has measured the sound speed and attenuation in suspensions of alumina dust in air. The frequency range was 200 Hz to 2 kHz and the volume fraction range was 10^{-6} to 10^{-5}; the physical parameters are given in appendix 1. The size distribution of the dust particles, measured with a

photosedimentometer, is shown in figure 6. 8. The radii are obtained from the settling velocities of the particles assuming they are spheres and are therefore effective radii. This is an acceptable assumption if the particles are approximately spherical [142]. The relative volume fractions are obtained by light scattering from the sedimenting particles in the horizontal plane. This assumes that the projected area of the particles is closely related to the volume fraction. This will be an acceptable assumption for small, approximately spherical particles. The Sauter mean (effective) radius from equation (6.28) is 2.8 μm.

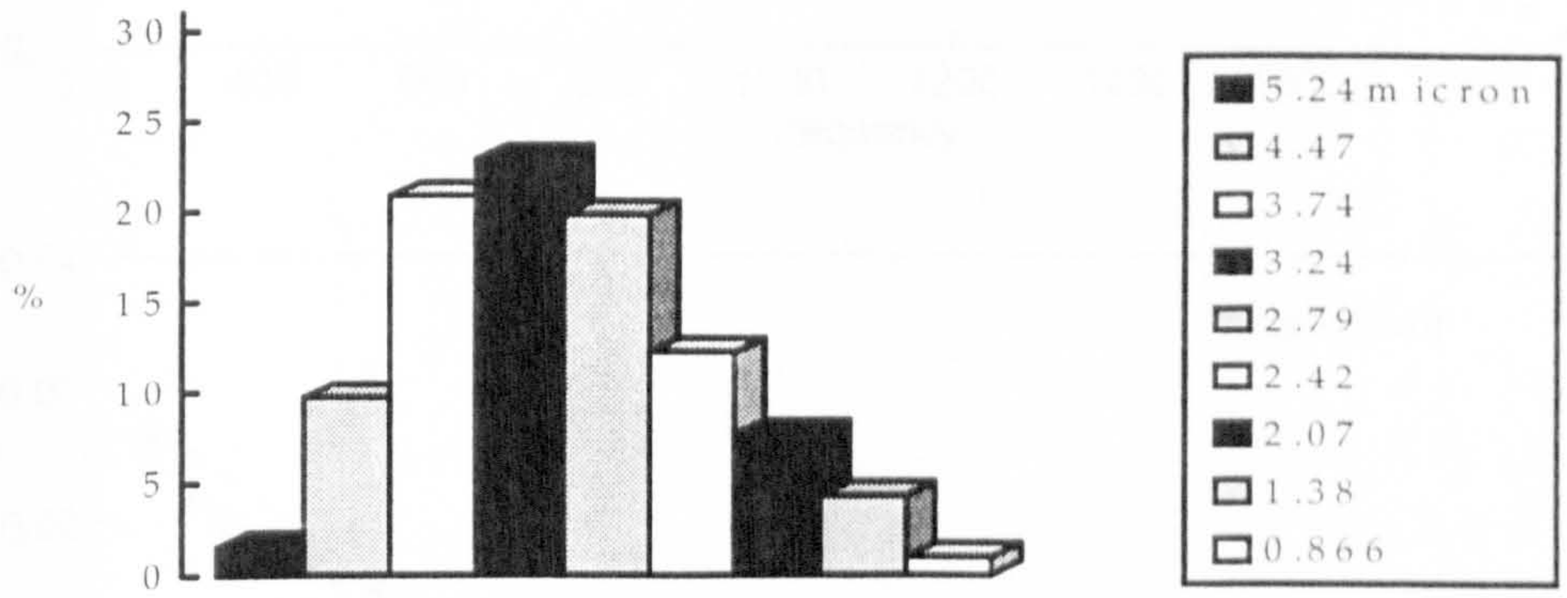

Figure 6. 8 Volume fraction as % of total volume fraction versus effective particle radius for alumina dust.

Figure 6. 9 plots the measured attenuation ξ times the wavelength λ and the measured 'dispersion', which is defined as

$$\left(\frac{c_f}{c}\right)^2 - 1,$$

versus frequency.

Also shown in figure 6. 9 are the predictions of the monodisperse coupled phase theory from equation (4.44), using a_{32}, and the theory including the size distribution (6.25). Because the volume fraction is very low the Temkin and Dobbins (TD) [98] expression for the effective density

$$\rho(\omega) = \rho_f \left(1 + \sum \phi_n \frac{\rho_s S_n}{\rho_s + \rho_f S_n}\right)$$

has been used in the place of equation (6.23). The prediction of the scattering theory from section 6. 2. 2 is very close to that of the coupled phase theory and

is not shown here. The total volume fraction was measured by settling out of the dust after the propagation experiment. It was estimated that this technique overpredicts the volume fraction by about 7% [12]. The data shown in figure 6. 9 is the average of data at three different volume fractions normalised to a volume fraction of 10^{-5}. Using this value in the theory overpredicts the attenuation. A good overall fit to the attenuation and dispersion data is obtained here by using $\phi = 9 \times 10^{-6}$. Including the particle size distribution brings the theoretical prediction into closer agreement with the measured data.

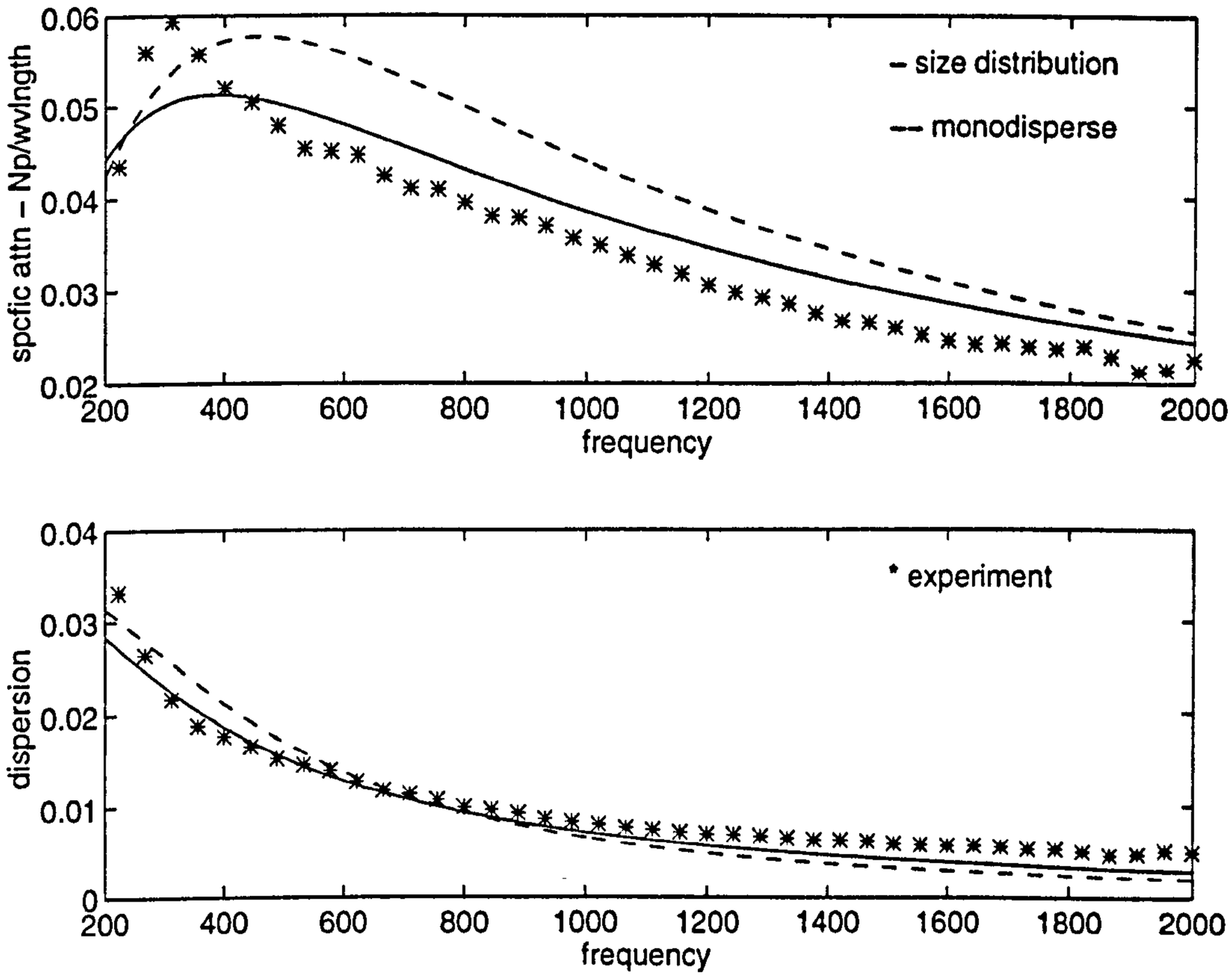

Figure 6. 9 Specific attenuation and dispersion versus frequency for an air suspension of alumina particles of Sauter mean radius 2.8 μm with volume fraction 10^{-5}. Comparison of data of Moss and predictions of coupled phase theory including size distribution and theory with monodisperse particle size distribution. Theory uses volume fraction 9×10^{-6}.

6. 3 Non-spherical particles

This section investigates the influence of particle shape on the complex wavenumber of the alumina dust suspension from section 6. 2. 3. The alumina particles were photographed with a scanning electron microscope and were seen to have irregular shapes [11].

The terms governing drag and heat transfer for spheroids and cubes in a fluid can be found in Clift *et al* [142]. Here only the steady state terms will be considered. Numerical work has shown that, for the alumina dust in air suspension at the range of frequencies shown in figure 6. 9, the unsteady terms can be neglected.

Table 6. 1 shows the steady state drag terms for spheres (the Stokes drag), cubes and spheroids. The drag is given for both oblate and prolate spheroids with their axes of symmetry either parallel or perpendicular to the flow. Also shown is the mean drag on a spheroid obtained by averaging the drag of a large number of identical spheroids with random orientations.

particle shape	drag
sphere, radius a	$6\pi\mu a$
oblate spheroid, semimajor axis a_{ob}, semiminor axis b, orientation axial, $h = b/a_{ob}$, $q = \left(1-h^2\right)^{\frac{1}{2}}$	$\dfrac{8\pi\mu a_{ob} q^2}{\dfrac{\left(1-2h^2\right)\arccos h}{q} + h}$
oblate spheroid, orientation normal	$\dfrac{16\pi\mu a_{ob} q^2}{\dfrac{\left(3-2h^2\right)\arccos h}{q} - h}$
oblate spheroid, mean of random orientations	$\dfrac{6\pi\mu a_{ob} q}{\arccos h}$
prolate spheroid, semimajor axis b, semiminor axis a_{pr}, axial orientation	$\dfrac{8\pi\mu a_{pr}\left(h^2-1\right)}{\dfrac{\left(2h^2-1\right)\ln\left(h+\sqrt{h^2-1}\right)}{\sqrt{h^2-1}} - h}$
prolate spheroid, normal orientation	$\dfrac{16\pi\mu a_{pr}\left(h^2-1\right)}{\dfrac{\left(2h^2-3\right)\ln\left(h+\sqrt{h^2-1}\right)}{\sqrt{h^2-1}} + h}$

prolate spheroid, mean of random orientations	$\dfrac{6\pi\mu a_{pr}\sqrt{h^2-1}}{\ln\left(h+\sqrt{h^2-1}\right)}$
cube, side l	$4\pi\mu l$

Table 6. 1 Drag on sphere, cube and spheroids.

The drag terms given in table 6. 1 can all be written in the form of the sphere drag $6\pi\mu a$, with an effective radius a_v. For example, the mean drag for oblate spheroids of random orientations is

$$6\pi\mu\left(\frac{a_{ob}q}{\arccos h}\right)$$

where a_{ob} is the semimajor axis, so

$$a_v=\frac{a_{ob}q}{\arccos h}.$$

The size distribution for the alumina particles is given in Figure 6. 8. This gives an effective radius for the particles assuming they are spheres. From this radius a the volume of the particles can be obtained. If it is now assumed that the particles are non-spherical but with the same volume then a_v can be calculated in terms of a. The volume of an oblate spheroid is $\frac{4}{3}\pi h a_{ob}{}^3$, so for equivalent volumes

$$a_{ob}=h^{-\frac{1}{3}}a\,.$$

The effective radii a_v for particles of the same volume are given in table 6. 2, the oblate spheroids have $h=0.1$ and the prolate spheroids have $h=10$. These h values have been set large deliberately, to show the effect on the drag.

particle shape	a_v/a
sphere	1
oblate spheroid, axial orientation, $h=0.1$	1.8365
oblate spheroid, normal orientation, $h=0.1$	1.3213
oblate spheroid, mean of random orientations, $h=0.1$	1.4576
prolate spheroid, axial orientation, $h=10$	1.2278
prolate spheroid, normal orientation, $h=10$	1.7692
prolate spheroid, mean of random orientations	1.5429

cube	1.0747

Table 6. 2 Effective radii for drag on spheres, cubes and spheroids of the same volume.

It is seen from table 6. 2 that the non-spherical particles have a greater drag than a sphere of the same volume. Hill and Power [142] showed that the Stokes drag on an arbitrarily shaped particle is less than or equal to that on a body which encloses it and greater than or equal to that on a body contained within it. The Stokes drag of a particle is not significantly affected by sharp edges or surface roughness [142].

Table 6. 3 gives the conductance multiplied by the thermal conductivity for the differently shaped particles in a stagnant medium, also from reference [142]. The symbols are the same as in table 6. 1. The conductance controls the heat transfer terms in the energy equations.

particle shape	conductance×τ
sphere	$4\pi\tau a$
oblate spheroid	$\frac{4\pi\tau a_{ob} q}{\arccos q}$
prolate spheroid	$\frac{4\pi\tau a_{pr}\left(h^2-1\right)}{\ln\left(h+\sqrt{h^2-1}\right)}$
cube	$0.656(4\pi\tau l)$

Table 6. 3 Conductances for sphere, cube and spheroids.

The heat transfer terms can be written in terms of the conductance for a sphere $4\pi a$ of the same volume using another effective radius a_h. The ratios of these radii to the sphere radius a are given in table 6. 4.

particle shape	a_h/a
sphere	1
oblate spheroid, $h=0.1$	1.4576
prolate spheroid, $h=10$	1.5429

cube	1.0575

Table 6. 4 Effective radii for conductances of spheres, cubes and spheroids of the same volume.

Comparison of tables 6. 2 and 6. 4 shows that a_h for the spheroids has the same value as that of a_v for the spheroids averaged over random orientations. The conductances of the non-spherical particles are greater than that for a sphere of the same volume for all the shapes. The conductance of a sphere of the same volume can be used as a lower bound for the conductance of a particle of arbitrary shape. An upper bound is given by the conductance of a shape circumscribing the particle [142]. For steady state heat transfer the conductance will not be significantly affected by surface roughness [142].

Figure 6. 10 plots the predictions of the coupled phase theory used in section 6. 2. 3, assuming the particles are cubes or oblate spheroids at different orientations. Also shown is the prediction of the spherical particle theory and the experimental data from figure 6. 9. The particle size distribution has been included. The oblate spheroids have $h = 0.1$. The prediction of the theory assuming the particles are prolate spheroids with $h = 10$ is shown in figure 6. 11. For all the shapes, the drag and heat transfer are increased relative to the sphere and this increases the dispersion and the attenuation over most of the frequency range.

Figure 6. 10 shows that the complex wavenumber would not be significantly altered if the particles were cubes of the same volume. The change in the complex wavenumber is significant if the particles are spheroids with $h = 10$ or 0.1. However, these are unrealistically large values of h. These values indicate that the greatest dimension of the particle is 10 times greater than the smallest, which is unlikely to be the case in practice. The photographs of the alumina dust particles showed that, for most of the particles, the greatest dimension was similar to the smallest. It can be concluded that, for this type of suspension, in the steady state region, the influence of particle shape on the complex wavenumber is not as important as that of particle size and volume fraction.

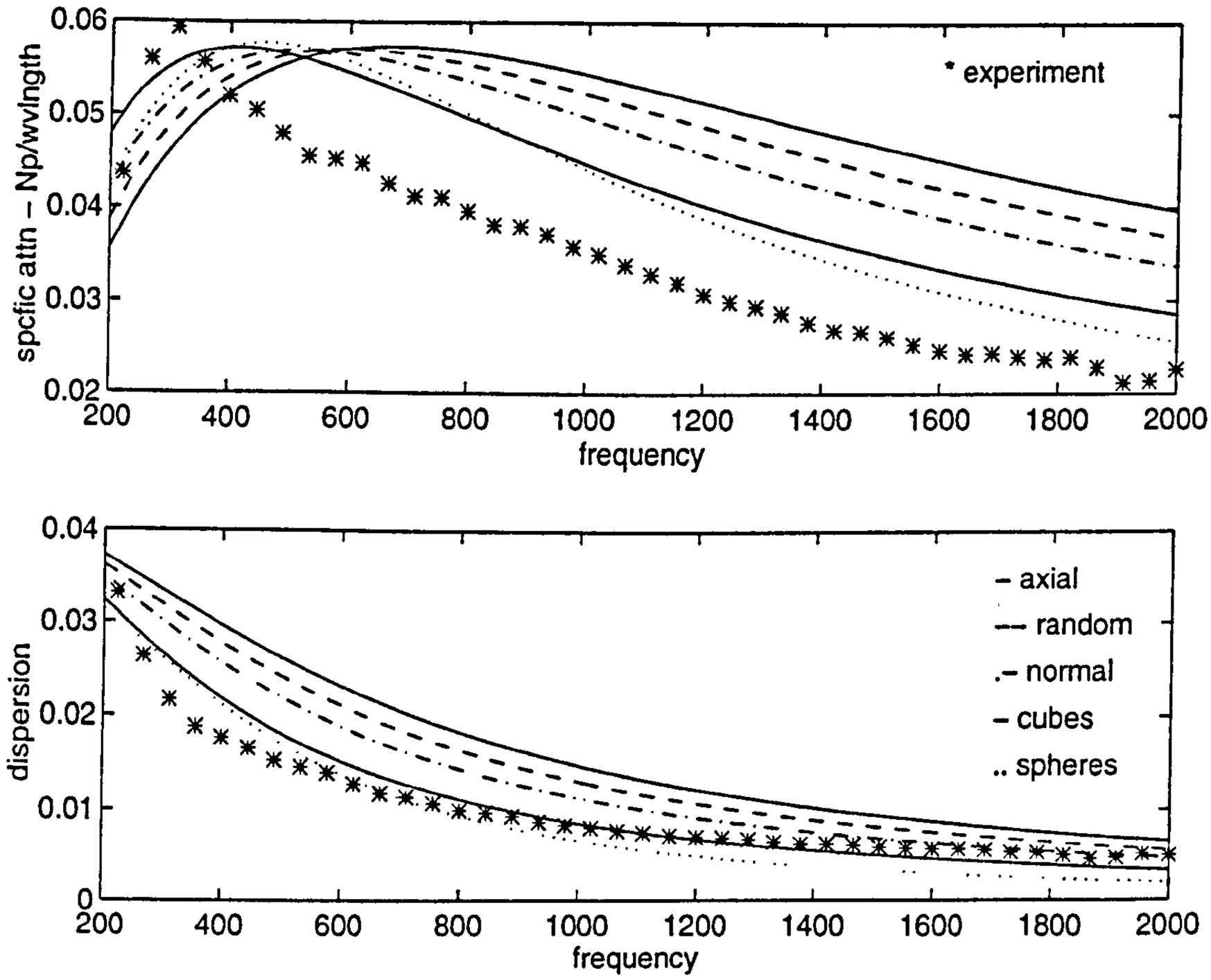

Figure 6. 10 Specific attenuation and dispersion versus frequency for an air suspension of alumina particles of Sauter mean radius 2.8 μm with volume fraction 10^{-5}. Comparison of data of Moss and predictions of coupled phase theory with oblate spheroidal particles of different orientations, spherical particles and cubic particles. Theory uses volume fraction 9×10^{-6} (see section 6. 2. 3).

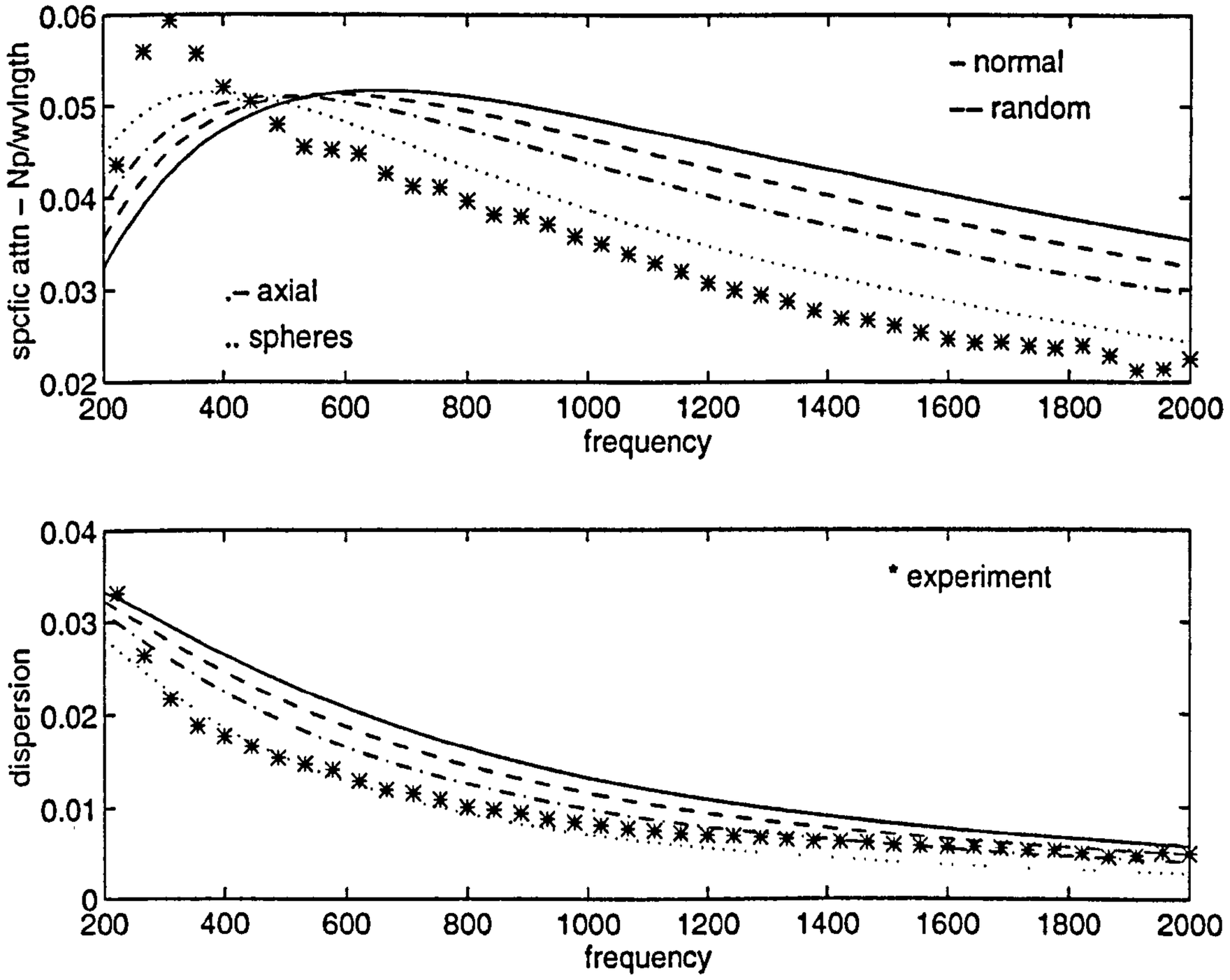

Figure 6. 11 Specific attenuation and dispersion versus frequency for an air suspension of alumina particles of Sauter mean radius 2.8 μm with volume fraction 10^{-5}. Comparison of data of Moss and predictions of coupled phase theory with prolate spheroidal particles of different orientations and spherical particles. Theory uses volume fraction 9×10^{-6}.

6. 4 Reverberation

Measuring the attenuation and sound speed of plane waves propagating in a suspension is one method of characterising it. Another possible method is to look at the reverberant modes in an enclosure containing the suspension. The frequency of the mode when the enclosure contains air will be different to that when the enclosure contains a suspension. Assuming that the sound speed in the suspension is lower than that in air, since the wavelength must remain the same the frequency must also be lower because $f = c/\lambda$. When the suspension is added to the enclosure there is a 'frequency shift' downwards. This could be obtained from the suspension sound speed predicted by the theories discussed earlier. In certain situations resonance frequency measurements can have advantages over propagation measurements for signal processing [15] [108].

A formal analysis of frequency shifts has been given by Culick [5] [6] [7] [8] [9]. His method is followed below. It is shown in section 6. 4. 6 that the predictions it gives are similar to those obtained using the sound speed given by coupled phase theory. However, Culick's method is more general in that it can be used for finite amplitudes and can include sources in the enclosure.

Reverberation time measurements have been used in the past to determine air absorption due to humidity [177] [178] [179] [180]. Most of the work used the decay in bands of modes. For frequencies below 1000 Hz, Harris and Tempest [178] looked at five modes in a spherical chamber of diameter 1.68 m. The frequency shift effect was not considered in this work.

6. 4. 1 Governing equations

Culick 1971 [6] used a simplified coupled phase theory. The conservation of mass equations are

$$\frac{\partial \overline{\rho}_s}{\partial t} + \nabla \cdot (\overline{\rho}_s \mathbf{u}_s) = 0 \text{ and} \tag{6.29}$$

$$\frac{\partial \overline{\rho}_f}{\partial t} + \nabla \cdot (\overline{\rho}_f \mathbf{u}_f) = 0. \tag{6.30}$$

The total conservation of momentum equation is

$$\frac{\partial}{\partial t}(\overline{\rho}_s \mathbf{u}_s + \overline{\rho}_f \mathbf{u}_f) + \nabla p = 0.$$

The linearised fluid momentum equation is

$$\overline{\rho}_f{}^0 \frac{\partial \mathbf{u}_f}{\partial t} + \nabla p = \mathbf{F} \tag{6.31}$$

where

$$-\mathbf{F} = \bar{\rho}_s{}^0 \frac{\partial \mathbf{u}_s}{\partial t}$$

is the linearised particulate phase momentum equation. Equation (6.31) can be obtained from equations (4.16) and (4.17) by assuming $\phi^0 \to 0$ and $\alpha \to 1$ in the pressure gradient terms, this is the low volume fraction limit. F represents momentum transfer and is proportional to $S(\mathbf{u}_f - \mathbf{u}_s)$. The velocities are of the form of equation (4.1) with zero equilibrium component.

The total conservation of energy equation is

$$\frac{\partial}{\partial t}\left(\bar{\rho}_s C_s T_s + \bar{\rho}_f C_{vf} T_f\right) + \nabla \cdot \left(p\mathbf{u}_f\right) = 0.$$

The linearised fluid energy equation is

$$\bar{\rho}_f{}^0 C_{vf} \frac{\partial T_f}{\partial t} + p^0 \nabla \cdot \mathbf{u}_f = Q \tag{6.32}$$

where

$$-Q = \bar{\rho}_s{}^0 C_s \frac{\partial T_s}{\partial t}$$

is the linearised particulate phase energy equation. Equation (6.32) has the low ϕ limit of the velocity term in equation (4.35). Q is the heat transfer term.

Adding $\bar{\rho}_s{}^0 \frac{\partial \mathbf{u}_f}{\partial t}$ to both sides of (6.31) gives

$$\left(\bar{\rho}_s{}^0 + \bar{\rho}_f{}^0\right)\frac{\partial \mathbf{u}_f}{\partial t} + \nabla p = \mathbf{F} + \bar{\rho}_s{}^0 \frac{\partial \mathbf{u}_f}{\partial t} = \bar{\rho}_s{}^0 \frac{\partial}{\partial t}\left(\mathbf{u}_f - \mathbf{u}_s\right) = \delta\mathbf{F}. \tag{6.33}$$

This defines the quantity $\delta\mathbf{F}$. Equation (6.33) is equation (2.1) in Culick 1976 [8] neglecting the nonlinear term and the mass source term.

Adding $\bar{\rho}_s{}^0 C_s \frac{\partial T_f}{\partial t}$ to both sides of (6.32) gives

$$\begin{aligned}\left(\bar{\rho}_s{}^0 C_s + \bar{\rho}_f{}^0 C_{vf}\right)\frac{\partial T_f}{\partial t} + p^0 \nabla \cdot \mathbf{u}_f &= Q + \bar{\rho}_s{}^0 C_s \frac{\partial T_f}{\partial t} \\ = \bar{\rho}_s{}^0 C_s \frac{\partial}{\partial t}\left(T_f - T_s\right) &= \delta Q\end{aligned}. \tag{6.34}$$

This defines δQ.

Using the low volume fraction limit, $\bar{\rho}_f \equiv \rho_f$, the fluid state equation is $p = R\bar{\rho}_f T_f$.

Thus

$$p^0 = R\bar{\rho}_f{}^0 T_f{}^0$$

and

$$p' = RT_f{}^0\overline{\rho}_f' + R\overline{\rho}_f{}^0T_f' .$$

As this point Culick defines a useful set of volume averaged constants, these will be indicated by an accent. The equation for the pressure fluctuation becomes

$$p' = (1+l)\hat{R}T_f{}^0\overline{\rho}_f' + (1+l)\hat{R}\overline{\rho}_f{}^0T_f' . \tag{6.35}$$

Here l is the 'loading'

$$l = \frac{\overline{\rho}_s{}^0}{\overline{\rho}_f{}^0} = \frac{\phi^0\rho_s{}^0}{\alpha\rho_f{}^0}$$

and

$$\hat{R} = \hat{C}_p - \hat{C}_v = \frac{R}{1+l}$$

where

$$\hat{C}_p = \frac{C_{pf} + lC_s}{1+l} = \frac{(\rho C_p)_{va}}{\rho_{va}} \text{ and } \hat{C}_v = \frac{C_{vf} + lC_s}{1+l} = \frac{(\rho C_v)_{va}}{\rho_{va}}.$$

Using (6.30) and (6.35), (6.34) can be rewritten as

$$\frac{\partial p}{\partial t} + \hat{\gamma}p^0\nabla\cdot\mathbf{u}_f = (\hat{\gamma}-1)\delta Q \tag{6.36}$$

where

$$\hat{\gamma} = \frac{\hat{C}_p}{\hat{C}_v}.$$

Equation (6.36) is a simplification of equation (2.2) in Culick 1976.

6. 4. 2 Inhomogeneous wave equation

Eliminating $\mathbf{u}_f$ between equations (6.33) and (6.36) gives the inhomogeneous wave equation

$$\nabla^2 p - \frac{1}{\hat{c}^2}\frac{\partial^2 p}{\partial t^2} = \nabla\cdot\delta\mathbf{F} - \frac{\hat{\gamma}-1}{\hat{c}^2}\frac{\partial\delta Q}{\partial t}, \tag{6.37}$$

where

$$\hat{c}^2 = \frac{\hat{\gamma}p^0}{\rho_{va}} = \hat{\gamma}\hat{R}T_f{}^0 = \hat{\gamma}\left(\hat{C}_p - \hat{C}_v\right)T_f{}^0 = \frac{\hat{\gamma}RT_f{}^0}{1+l}.$$

This sound speed is the same as the MH equilibrium sound speed given by equation (4.45) if $\alpha \to 1$.

The LHS of equation (6.37) is the wave equation for propagation in a medium with sound speed $\hat{c}$.

Taking the components of (6.33) normal to the boundaries of the enclosure gives the boundary condition

$$\mathbf{n}\cdot\nabla p = -\rho_{va}\frac{\partial \mathbf{u}_f}{\partial t}\cdot\mathbf{n} + \delta\mathbf{F}\cdot\mathbf{n} \tag{6.38}$$

where **n** is the unit normal for the surface of the enclosure.

6. 4. 3 Modal representation

Let h represent the right hand side of (6.37) and f represent the RHS of (6.38):

$$\nabla^2 p - \frac{1}{\hat{c}^2}\frac{\partial^2 p}{\partial t^2} = h \tag{6.39}$$

$$\mathbf{n}\cdot\nabla p = f\,. \tag{6.40}$$

The space and time dependence of the pressure and fluid particle velocity is assumed to be given by

$$\frac{p'}{p^0} = \sum_{i=0}^{\infty}\eta_i(t)\psi_i(\mathbf{r}) \text{ and} \tag{6.41}$$

$$\mathbf{u}_f = \mathbf{u}_f' = \sum_{i=1}^{\infty}\frac{\dot{\eta}_i(t)}{\hat{\gamma}\hat{k}_i^{\,2}}\nabla\psi_i(\mathbf{r})\,. \tag{6.42}$$

Here $\hat{k} = \omega/\hat{c}$. ψ_i are the mode shapes for the enclosure. The $i = 0$ term represents a shift in the average pressure and thus there is no corresponding term for the particle velocity.

Multiplying (6.39) by ψ_n and integrating over the volume of the enclosure gives

$$\int_V \psi_n \nabla^2 p\,dV - \frac{1}{\hat{c}^2}\int_V \psi_n \frac{\partial^2 p}{\partial t^2}dV = \int_V \psi_n h\,dV\,.$$

Using the identity

$$\psi_n\nabla^2 p = \nabla\cdot(\psi_n\nabla p) - \nabla p\cdot\nabla\psi_n \tag{6.43}$$

and the divergence theorem gives

$$\int_V \psi_n \frac{\partial^2 p}{\partial t^2}dV + \hat{c}^2\int_V \nabla p\cdot\nabla\psi_n dV = -\hat{c}^2\int_V \psi_n h\,dV + \hat{c}^2\int_S \psi_n f\,dS\,.$$

Using (6.43) with p and ψ_n interchanged, the condition

$$\mathbf{n}\cdot\nabla\psi_n = 0 \tag{6.44}$$

and the fact that the mode shapes satisfy the Helmholtz equation

$$\nabla^2\psi_n + \hat{k}_n{}^2\psi_n = 0$$

gives

$$\int_V \psi_n \frac{\partial^2 p}{\partial t^2} dV + \omega_n{}^2 \int_V p\psi_n dV = -\hat{c}^2 \int_V \psi_n h dV + \hat{c}^2 \int_S \psi_n f dS\,.$$

The mode shapes are orthogonal

$$\int \psi_i \psi_n dV = \delta_{ni} E_n{}^2\,,$$

where δ_{ni} is the Kronecker delta and

$$E_n{}^2 = \int \psi_n{}^2 dV\,,$$

thus substituting for the pressure from (6.41) gives

$$p^0 E_n{}^2 \left[\ddot{\eta}_n + \omega_n{}^2 \eta_n\right] = -\hat{c}^2 \int_V \psi_n h dV + \hat{c}^2 \int_S \psi_n f dS\,, \tag{6.45}$$

where the dots indicate differentiation with respect to time.

Dividing by $p^0 E_n{}^2$ gives

$$\ddot{\eta}_n + \omega_n{}^2 \eta_n = F_n \tag{6.46}$$

where

$$F_n = \frac{\hat{c}^2}{p^0 E_n{}^2}\left[-\int_V \psi_n h dV + \int_S \psi_n f dS\right]. \tag{6.47}$$

This is the equation for a simple harmonic oscillator with a forcing term F_n.

Substituting for h in (6.47) and using the identity

$$\psi_n \nabla\cdot\delta\mathbf{F} = \nabla\cdot\psi_n\delta\mathbf{F} - \nabla\psi_n\cdot\delta\mathbf{F}\,,$$

the volume integral gives

$$-\int_V \left[\nabla\cdot\psi_n\delta\mathbf{F} - \nabla\psi_n\cdot\delta\mathbf{F} - \frac{\hat{\gamma}-1}{\hat{c}^2}\psi_n\frac{\partial\delta Q}{\partial t}\right]dV.$$

Substituting for f in the surface integral gives

$$\int_S \left[-\rho_{va}\psi_n \frac{\partial \mathbf{u}_f}{\partial t}\cdot\mathbf{n} + \psi_n\delta\mathbf{F}\cdot\mathbf{n}\right]dS\,.$$

Since from (6.42) and (6.44) $\mathbf{n}\cdot\nabla\mathbf{u}_f = 0$ the first term in this surface integral can be neglected. Applying the divergence theorem to the remaining integral gives

$$\int_V \nabla\cdot\psi_n\delta\mathbf{F} dV$$

and so the forcing term is given by

$$F_n = \frac{\hat{\gamma}}{\rho_{va} E_n{}^2} \int_V \left[\frac{\hat{\gamma} - 1}{\hat{c}^2} \psi_n \frac{\partial \delta Q}{\partial t} + \delta \mathbf{F} \cdot \nabla \psi_n \right] dV \,. \tag{6.48}$$

6. 4. 4 Steady state momentum and heat transfer

For simplicity it is assumed that either the frequency or the particle radius is low enough such that only the steady state terms are important in the S and S_h momentum and heat transfer terms. This is the approximation used by Culick and Temkin and Dobbins [98]. Rearranging the particulate phase momentum and energy equations (6.31) and (6.32) gives

$$\frac{\partial \mathbf{u}_s}{\partial t} = -\frac{1}{\bar{\rho}_s{}^0} \mathbf{F} = -\frac{9\mu}{2\rho_s{}^0 a^2} \left(\mathbf{u}_s - \mathbf{u}_f \right) = -\frac{\left(\mathbf{u}_s - \mathbf{u}_f \right)}{\tau_d} \tag{6.49}$$

$$\frac{\partial T_s}{\partial t} = -\frac{1}{\bar{\rho}_s{}^0} Q = -\frac{3\tau}{C_s \rho_s{}^0 a^2} \left(T_s - T_f \right) = -\frac{\left(T_s - T_f \right)}{\tau_t} \,. \tag{6.50}$$

τ_d and τ_t are the viscous and thermal relaxation times that were previously defined by Temkin and Dobbins.

Since the velocities and temperatures depend on space and time as in equation (4.1), the space dependence can be cancelled in (6.49) and (6.50) and the partial derivatives become total derivatives. Subtracting $d\mathbf{u}_f/dt$ from (6.49) and dT_f/dt from (6.50) gives

$$\frac{d\delta \mathbf{u}}{dt} + \frac{\delta \mathbf{u}}{\tau_d} = -\frac{d\mathbf{u}_f}{dt} \text{ and} \tag{6.51}$$

$$\frac{d\delta T}{dt} + \frac{\delta T}{\tau_t} = -\frac{dT_f}{dt} \,. \tag{6.52}$$

Here $\delta \mathbf{u} = \mathbf{u}_s - \mathbf{u}_f$ and $\delta T = T_s - T_f$.

Using the definitions of $\delta \mathbf{F}$ and δQ from equations (6.31) and (6.32), neglecting spatial variations, with (6.51) and (6.52) gives

$$\delta \mathbf{F} = -\bar{\rho}_s{}^0 \frac{d\delta \mathbf{u}}{dt} = \bar{\rho}_s{}^0 \left(\frac{\delta \mathbf{u}}{\tau_d} + \frac{d\mathbf{u}_f}{dt} \right) \text{ and} \tag{6.53}$$

$$\delta Q = -\bar{\rho}_s{}^0 C_s \frac{d\delta T}{dt} = \bar{\rho}_s{}^0 C_s \left(\frac{\delta T}{\tau_t} + \frac{dT_f}{dt} \right) . \tag{6.54}$$

The differential equations (6.53) and (6.54) can be solved for $\delta \mathbf{u}$ in terms of $\mathbf{u}_f$ and δT in terms of T_f. The initial conditions are that when $t = t_0$, $\delta \mathbf{u} = \delta \mathbf{u}_0$ and $\delta T = \delta T_0$. The solutions of (6.53) and (6.54) are

$$\delta \mathbf{u} = \left[\frac{1}{\tau_d} e^{-t/\tau_d} \int_{t_0}^{t} e^{t'/\tau_d} \mathbf{u}_f(t') dt' - \mathbf{u}_f(t) \right] - \left[\delta \mathbf{u}_0 - \mathbf{u}_f(t_0) \right] e^{-(t-t_0)/\tau_d} \text{ and} \tag{6.55}$$

$$\delta T = \left[\frac{1}{\tau_t} e^{-t/\tau_t} \int_{t_0}^{t} e^{t/\tau_t} T_f(t')dt' - T_f(t)\right] - \left[\delta T_0 - T_f(t_0)\right] e^{-(t-t_0)/\tau_t} . \qquad (6.56)$$

The second terms are transients arising from the initial conditions. These are negligible when $t - t_0 \gg \tau_{d,t}$. These transients will be neglected in the following. This approximation is valid if the periods of the modes of interest are much greater than τ_d and τ_t.

The velocity fluctuation for the nth mode is given by (6.42) and the temperature fluctuation can be obtained from the pressure fluctuation (6.41):

$$T_f' = \frac{\hat{\gamma} - 1}{\hat{\gamma}} T_f{}^0 \eta_n \psi_n .$$

Using these expressions in (6.55) and (6.56) gives

$$\delta u = X_1 (\eta_n - \tau_d \dot{\eta}_n) \frac{1}{\hat{\gamma} \hat{k}_n{}^2} \nabla \psi_n \text{ and} \qquad (6.57)$$

$$\delta T = -\frac{X_2}{\omega_n} \left(\omega_n \tau_t \eta_n + \frac{\dot{\eta}_n}{\omega_n}\right) \frac{\hat{\gamma} - 1}{\hat{\gamma}} T_f{}^0 \psi_n . \qquad (6.58)$$

Here

$$X_1 = \frac{\omega_n \Omega_d}{1 + \Omega_d{}^2}$$

$$X_2 = \frac{\omega_n \Omega_t}{1 + \Omega_t{}^2}$$

$$\Omega_d = \omega_n \tau_d$$

$$\Omega_t = \omega_n \tau_t .$$

Using (6.57) and (6.58) in (6.53) and (6.54) gives

$$\delta F = \frac{\bar{\rho}_s{}^0 \omega_n}{\hat{\gamma} \hat{k}_n{}^2} \left[\left(\frac{X_1}{\omega_n \tau_d} - \omega_n\right) \eta_n - \frac{X_1}{\omega_n} \dot{\eta}_n\right] \nabla \psi_n \text{ and} \qquad (6.59)$$

$$\delta Q = \frac{\bar{\rho}_s{}^0 \omega_n}{\hat{\gamma}} C_s T_f{}^0 (\hat{\gamma} - 1) \left[-\frac{X_2}{\omega_n} \eta_n - \left(\frac{X_2}{\omega_n \tau_t} - \omega_n\right) \frac{1}{\omega_n{}^2} \dot{\eta}_n\right] \psi_n . \qquad (6.60)$$

Equations (6.59) and (6.60) are substituted in (6.48) to give

$$F_n = -\frac{l}{1+l} \left[X_1 + (\hat{\gamma} - 1) \frac{C_s}{\hat{C}_p} X_2\right] \dot{\eta}_n - \omega_n{}^2 \frac{l}{1+l} \left[\frac{\Omega_d{}^2}{1+\Omega_d{}^2} + (\hat{\gamma} - 1) \frac{C_s}{\hat{C}_p} \frac{\Omega_t{}^2}{1+\Omega_t{}^2}\right] \eta_n . \qquad (6.61)$$

6. 4. 5 The method of averaging

The modal time dependence is assumed to be

$$\eta_n(t) = \mathrm{A}_n(t)\sin\left(\omega_n t + \phi_n(t)\right) = A_n \sin\omega_n t + B_n \cos\omega_n t \tag{6.62}$$

where

$$\mathrm{A}_n = \left(A_n{}^2 + B_n{}^2\right)^{\frac{1}{2}} \text{ and} \tag{6.63}$$

$$\phi_n = \arctan\left(B_n / A_n\right). \tag{6.64}$$

The frequency of the mode when it is perturbed from that having frequency ω_n is, from (6.62),

$$\omega = \frac{d}{dt}\left(\omega_n t + \phi_n\right) = \omega_n + \dot{\phi}_n. \tag{6.65}$$

Equation (6.46) represents a forced oscillator, the energy of the oscillator is

$$\mathrm{E}_n = \tfrac{1}{2}\omega_n{}^2\eta_n{}^2 + \tfrac{1}{2}\dot{\eta}_n{}^2$$

and the energy time averaged over the interval τ at time t is

$$\langle \mathrm{E}_n \rangle = \int_t^{t+\tau} \mathrm{E}_n dt'$$

where the angled brackets indicate time averaging.

The rate at which work is done on the oscillator is $\dot{\eta}_n F_n$. Conservation of energy requires that

$$\frac{d}{dt}\langle \mathrm{E}_n \rangle = \langle \dot{\eta}_n F_n \rangle. \tag{6.66}$$

It is assumed that the change in A_n and ϕ_n over the interval τ is small, thus

$$\dot{\mathrm{A}}_n \tau \ll 1 \text{ and } \dot{\phi}_n \tau \ll 2\pi. \tag{6.67}$$

The derivative of η_n is given by

$$\dot{\eta}_n = \omega_n \mathrm{A}_n \cos\left(\omega_n t + \phi_n\right) + \left[\dot{\phi}_n \mathrm{A}_n \cos\left(\omega_n t + \phi_n\right) + \dot{\mathrm{A}}_n \sin\left(\omega_n t + \phi_n\right)\right].$$

Due to the conditions (6.67) the term in square brackets can be neglected and so

$$\dot{\eta}_n = \omega_n \mathrm{A}_n \cos\left(\omega_n t + \phi_n\right) \text{ and } \mathrm{E}_n = \omega_n{}^2 \mathrm{A}_n{}^2.$$

From (6.67) A_n and ϕ_n may be assumed to be constant in the time averaging integrals and thus (6.66) becomes

$$\frac{d\mathrm{A}_n}{dt} = \frac{1}{\omega_n \tau}\int_t^{t+\tau} F_n \cos\left(\omega_n t' + \phi_n\right) dt'. \tag{6.68}$$

A similar equation can be obtained for ϕ_n :

$$\frac{d\phi_n}{dt} = \frac{-1}{\omega_n \tau A_n} \int_t^{t+\tau} F_n \sin(\omega_n t' + \phi_n) dt'. \tag{6.69}$$

Equations (6.68) and (6.69) can be converted into expressions for A_n and B_n:

$$\frac{dA_n}{dt} = \frac{1}{\omega_n \tau} \int_t^{t+\tau} F_n \cos \omega_n t' dt' \text{ and} \tag{6.70}$$

$$\frac{dB_n}{dt} = \frac{-1}{\omega_n \tau} \int_t^{t+\tau} F_n \sin \omega_n t' dt'. \tag{6.71}$$

If there is coupling between the modes F_n has the general form

$$F_n = -\sum_{i=1}^{\infty} [D_{ni}\dot{\eta}_i + E_{ni}\eta_i] \tag{6.72}$$

and (6.70) and (6.71) give

$$\begin{aligned} \frac{dA_n}{dt} = &-\tfrac{1}{2} D_{nn} A_n - \tfrac{1}{2} \frac{E_{nn}}{\omega_n} B_n - \frac{1}{2\omega_n} \sum_{n \neq i} \{\omega_i D_{ni} [(f_{ni} + h_{ni}) A_i - (g_{ni} + l_{ni}) B_i]\} \\ &- \frac{1}{2\omega_n} \sum_{n \neq i} \{E_{ni} [(g_{ni} - l_{ni}) B_i - (f_{ni} - h_{ni}) A_i]\} \end{aligned} \tag{6.73}$$

$$\begin{aligned} \frac{dB_n}{dt} = &-\tfrac{1}{2} D_{nn} B_n + \tfrac{1}{2} \frac{E_{nn}}{\omega_n} A_n + \frac{1}{2\omega_n} \sum_{n \neq i} \{\omega_i D_{ni} [(f_{ni} - h_{ni}) B_i + (g_{ni} - l_{ni}) A_i]\} \\ &+ \frac{1}{2\omega_n} \sum_{n \neq i} \{E_{ni} [(g_{ni} - l_{ni}) B_i - (f_{ni} - h_{ni}) A_i]\}. \end{aligned} \tag{6.74}$$

The coupling terms in (6.73) and (6.74) are given by

$$f_{ni}, l_{ni} = \frac{\sin(\omega_i \pm \omega_n)\frac{\tau}{2}}{(\omega_i \pm \omega_n)\frac{\tau}{2}} \cos(\omega_i \pm \omega_n)\left(t + \frac{\tau}{2}\right) \text{ and} \tag{6.75}$$

$$g_{ni}, l_{ni} = \frac{\sin(\omega_i \pm \omega_n)\frac{\tau}{2}}{(\omega_i \pm \omega_n)\frac{\tau}{2}} \sin(\omega_i \pm \omega_n)\left(t + \frac{\tau}{2}\right). \tag{6.76}$$

With F_n given by (6.61) the only non-zero D_{ni} and E_{ni} are D_{nn} and E_{nn}. Since there is no coupling (6.73) and (6.74) give

$$\frac{dA_n}{dt} = -\tfrac{1}{2} D_n A_n - \tfrac{1}{2} \frac{E_n}{\omega_n} B_n \tag{6.77}$$

$$\frac{dB_n}{dt} = -\tfrac{1}{2} D_n B_n + \tfrac{1}{2} \frac{E_n}{\omega_n} A_n. \tag{6.78}$$

Culick [7] [9] has looked at nonlinear particle motions which result in mode coupling.

6. 4. 6 Frequency shifts

Eliminating D_n between (6.77) and (6.78) and comparing with the definition of ϕ_n in terms of A_n and B_n (6.64) gives

$$\dot{\phi}_n = \frac{E_n}{2\omega_n}.$$

This is the frequency shift $\omega - \omega_n$. In Hz this is given by

$$f - f_n = \delta f_n = \frac{E_n}{4\pi\omega_n}. \tag{6.79}$$

f is the actual frequency of the mode in the suspension while f_n is the frequency of the mode at equilibrium conditions where the sound speed is $\hat{c}$. If f_{air} is the modal frequency when the enclosure contains pure air then

$$\delta f = f_{\text{air}} - f$$

is the shift in frequency when the particles are added.

In terms of δf_n

$$\delta f = f_{\text{air}} - (\delta f_n + f_n). \tag{6.80}$$

From (6.72), E_n is the coefficient of η_n in F_n so from (6.61) and (6.79)

$$\delta f_n = \frac{f_n}{2}\frac{l}{1+l}\left[\frac{\Omega_d{}^2}{1+\Omega_d{}^2} + (\hat{\gamma}-1)\frac{C_s}{\hat{C}_p}\frac{\Omega_t{}^2}{1+\Omega_t{}^2}\right]. \tag{6.81}$$

The shift δf_n can be calculated using an iterative procedure. The procedure starts with f_n in equation (6.81). In the next step f_n is replaced with the shifted frequency $\delta f_n + f_n$ in equation (6.81), to calculate a new δf_n. This step is then repeated until convergence.

Figure 6. 12 plots the percentage frequency shifts $100\delta f/f_{\text{air}}$ using equation (6.80) for the lowest transverse resonance in a pipe of radius 0.25 m. When the pipe contains pure air the frequency is 402 Hz. The physical parameters used are those for alumina particles in air and the loading l varies between 0.034 and 1.

The curves indicated by a dotted line in figure 6. 12 are the predictions of the frequency shift using the Temkin and Dobbins (TD) [98] theory. The percentage frequency shift is given by

$$100\left(1 - c/c_f\right)$$

where c is the sound speed predicted by the TD theory

$$c = c_f \left[1 + l \left(\frac{1}{1+\Omega_d{}^2} + (\gamma - 1) \frac{C_s}{C_{pf}} \frac{1}{1+\Omega_t{}^2} \right) \right]^{-\frac{1}{2}} . \tag{6.82}$$

As can be seen from the figure, the two predictions do not have the same low radius (or low frequency) behaviour. As Ω_d and $\Omega_t \to 0$ $\delta f_n \to 0$ so from (6.80) the percentage frequency shift at low Ω from the Culick theory is $100\left(1 - \hat{c}/c_f\right)$. The corresponding result from the TD theory is given by the same expression with $\hat{c}$ replaced with the low Ω limit of equation (6.82). The largest frequency shifts for a given loading occur in this low Ω region.

At the high radii the TD curves all tend to zero while the Culick curves tend to constant finite values. Because of the low Ω assumptions made in deriving equations (6.57) and (6.58) the Culick theory is not valid for values of the radius larger than those shown in figure 6. 12. The range of validity of the theory can be increased by including extra terms in the expressions for the momentum and heat transfer [7] [9].

For alumina particles a loading l of 0.034 corresponds to a volume fraction ϕ of 10^{-5} and $l = 1$ corresponds to $\phi = 3 \times 10^{-4}$. These values are in the low ϕ range required for the validity of the Culick and TD theories.

Vetter and Culick [15] [108] have shown that the frequency shift method in useful for low order modes in enclosures containing suspensions with moderate volume fractions in the low Ω regime.

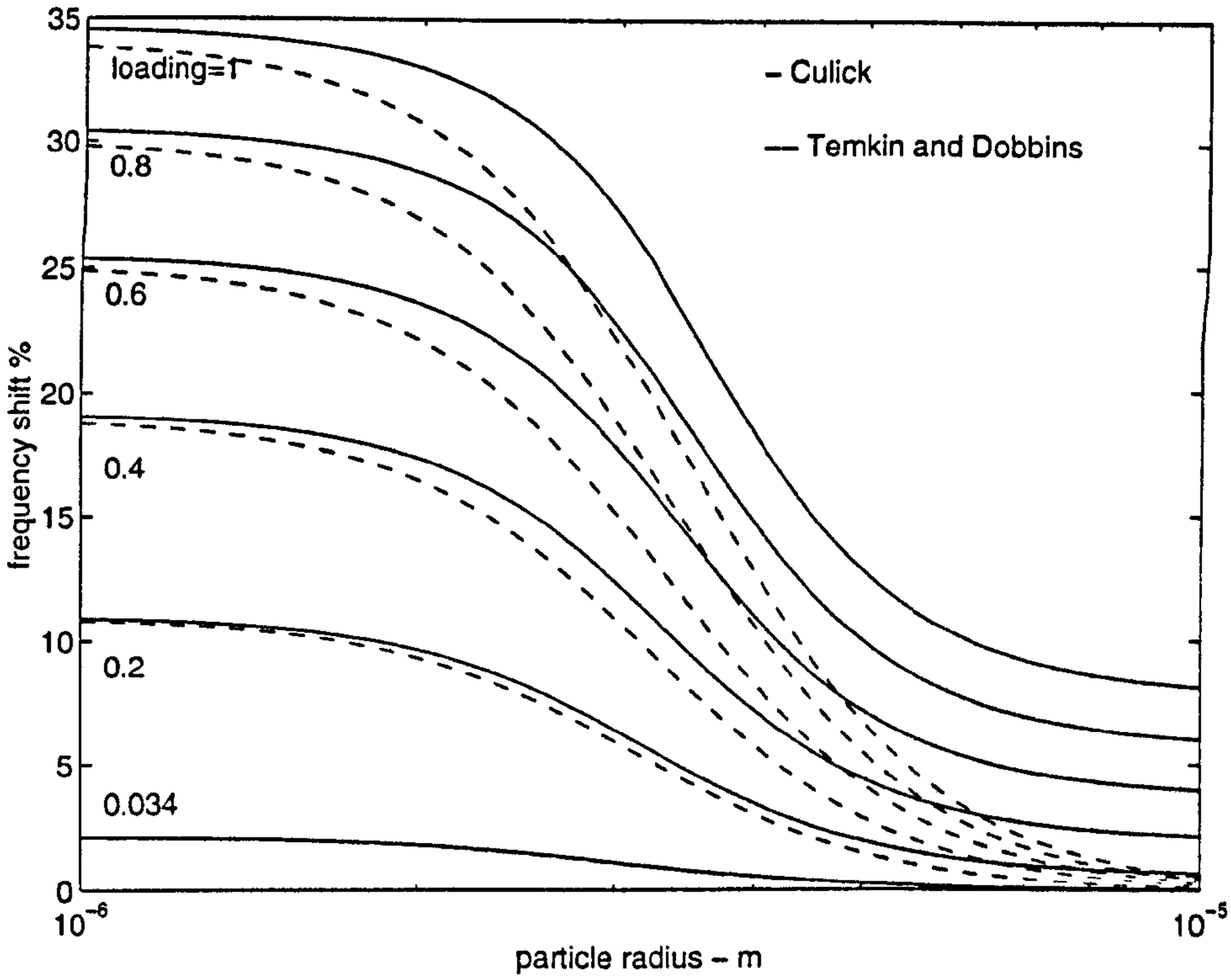

Figure 6. 12 Percentage frequency shift versus particle radius for first transverse mode in a 0.25 m radius pipe containing an alumina in air suspension with loading between 0.034 and 1. Comparison of predictions of Culick theory and calculations from Temkin and Dobbins sound speed.

6. 4. 7 Decay constants

To obtain decay constants for the modes, it is assumed

$$A_n(t) = A_n(0)\exp(\alpha_n t) \tag{6.83}$$

where $A_n(0)$ is the initial amplitude of the mode.

Eliminating E_n between (6.77) and (6.78) gives

$$\tfrac{1}{2}\frac{d}{dt}\left(A_n{}^2 + B_n{}^2\right) = -\tfrac{1}{2}D_n\left(A_n{}^2 + B_n{}^2\right)$$

or, from (6.63),

$$\frac{dA_n{}^2}{dt} = -D_n A_n{}^2. \tag{6.84}$$

The solution of (6.84) is

$$A_n = \exp\left(-\tfrac{1}{2}D_n t\right)$$

and thus, from (6.83),

$$\alpha_n = -\tfrac{1}{2}D_n$$

which is, from (6.61),

$$\alpha_n = -\tfrac{1}{2}\frac{l}{1+l}\left[X_1 + (\hat{\gamma}-1)\frac{C_s}{\hat{C}_p}X_2\right]. \tag{6.85}$$

The (spatial) plane wave attenuation coefficient is obtained from the (temporal) decay constant by dividing by c_f. (6.85) is then identical to the low mass concentration expression for the plane wave attenuation coefficient derived by Temkin and Dobbins (equation (39) in reference [98]).

6. 5 Diffusion

Margulies and Schwartz (MS) [2] [4] used overall (total) and relative (diffusive) conservation equations instead of writing an equation for each phase. The diffusive momentum equation is related to the generalised Fick's law. Fick's law states that the rate of diffusion (spreading of particles) is proportional to the concentration gradient. The generalised Fick's law also includes phoretic effects. Phoresis refers to the phenomena whereby particles are transported by gradients of temperature (thermophoresis), gradients of pressure (barophoresis), gradients of concentration (pcynophoresis) or external forces (e.g. electrophoresis).

6. 5. 1 Theory

The MS total mass balance equation is obtained by adding the individual phase mass balance equations

$$\frac{\partial \overline{\rho}}{\partial t} + \frac{\partial}{\partial z}(\overline{\rho} u) = 0 . \tag{6.86}$$

Here $\overline{\rho}$ is the total volume averaged density $\overline{\rho}_f + \overline{\rho}_s$ and u is the total velocity given by

$$u = \frac{\rho_f u_f + \rho_s u_s}{\overline{\rho}} . \tag{6.87}$$

It will be assumed that the properties of the phases are spatially uniform, this means that the phase and mass averaging operations defined by Margulies and Schwartz are not necessary.

In terms of the mass concentration m, where $m_f = \overline{\rho}_f / \overline{\rho}$ and $m_s = \overline{\rho}_s / \overline{\rho}$,

$u = m_f u_f + m_s u_s$.

It is also necessary to define relative velocities v where

$v_f = u_f - u$

$v_s = u_s - u$

and thus

$v = v_s - v_f = u_s - u_f$

which is called the diffusive velocity.

The MS diffusive mass balance equation is given by equation (2) in reference [2], neglecting the mass production term. The flux of particles is given by $\overline{\rho}_s v_s = \overline{\rho} m_s m_f v$ which gives

$$\bar{\rho}\frac{\partial m_s}{\partial t}+\frac{\partial}{\partial z}\left(\bar{\rho}m_s m_f v\right)=0. \tag{6.88}$$

The total momentum balance is given by equation (3a) in reference [2]. It is assumed that the sum of the momentum supplies to each phase is zero, that there are no body forces and that viscous effects can be neglected except in the boundary layer region of the particles. This gives

$$\bar{\rho}\frac{\partial u}{\partial t}+\frac{\partial p}{\partial z}=0 \tag{6.89}$$

where p is the total pressure p_f+p_s, the sum of the pressures of each phase.

The diffusive momentum balance is obtained from the generalised linear form of Fick's equation given by equation (10) in reference [2]. Neglecting the thermophoresis, pcynophoresis and phoresis due to external forces terms gives

$$v+\frac{\bar{\rho}m_s m_f}{P_D}\frac{\partial v}{\partial t}=-\frac{\beta_C}{P_D}\frac{\partial p}{\partial z}. \tag{6.90}$$

The second term in equation (6.90) represents inertial diffusion. The pressure gradient term on the RHS of equation (6.90) represents barophoresis.

β_C is the coefficient of expansion with respect to the concentration of particles defined as

$$\beta_C=-\frac{1}{\bar{\rho}}\frac{\partial\bar{\rho}}{\partial m_s}=\bar{\rho}\left(\frac{1}{\rho_s}-\frac{1}{\rho_f}\right)$$

and P_D is the frictional coefficient. For a low concentration of particles $m_s \ll 1$ and considering only Stokes drag, P_D is N, the number of particles, times the drag on a single particle i.e.

$$P_D=N(6\pi\mu a)=\tfrac{9}{4}\phi\rho_f\omega\frac{\delta^2}{a^2}.$$

The total energy equation is

$$\bar{\rho}\frac{\partial U}{\partial t}=0 \tag{6.91}$$

where U, the total specific internal energy, is of the form

$$U=U(\bar{\rho},m_s,T)$$

and T is the temperature, which is the same for both phases. This is a single temperature model and so neglects heat transfer. To include heat transfer it would necessary to have two temperatures. This would either be a temperature for each phase as in chapter 4 or a total, volume averaged temperature and a

temperature difference analogous to the total and diffusive velocities in the momentum equations above.

Writing p, the total pressure, as a power series in the variables $(\overline{\rho}, m_s, T)$, differentiating with respect to z, and retaining only the first order terms gives

$$\frac{\partial p}{\partial z} = \frac{{c_0}^2}{\gamma}\left(\frac{\partial \overline{\rho}}{\partial z} + \overline{\rho}\beta_C \frac{\partial m_s}{\partial z} + \overline{\rho}\beta \frac{\partial T}{\partial z}\right). \tag{6.92}$$

c_0, β and γ are the total thermodynamic parameters for the two phase medium. Inserting (6.92) into (6.89) gives

$$\overline{\rho}\frac{\partial u}{\partial t} + \frac{{c_0}^2}{\gamma}\left(\frac{\partial \overline{\rho}}{\partial z} + \overline{\rho}\beta_C \frac{\partial m_s}{\partial z} + \overline{\rho}\beta \frac{\partial T}{\partial z}\right) = 0. \tag{6.93}$$

Writing U as a power series in $(\overline{\rho}, m_s, T)$, differentiating with respect to time and neglecting the terms above first order makes (6.91)

$$\overline{\rho}C_v \frac{\partial T}{\partial t} - \frac{C_p - C_v}{\beta}\frac{\partial \overline{\rho}}{\partial t} - \frac{\overline{\rho}(\gamma - 1)\beta_C C_v}{\beta}\frac{\partial m_s}{\partial t} = 0. \tag{6.94}$$

C_p and C_v are the total specific heats for the two phase medium.

Equation (6.92) can also be inserted into (6.90) to eliminate p from the set of equations. This leaves 5 equations in the variables $(\overline{\rho}, m_s, T, u, v)$. Assuming these variables are of the form (4.1), the set of equations can be linearised and the differentials replaced by the transformations (4.2). As in section 4. 1. 13 the set of equations are written as a matrix equation $\mathbf{A}y = 0$ and setting $\det \mathbf{A} = 0$ gives a solution for k, the complex wavenumber. The MS theory gives

$$\left(\frac{kc_0}{\omega}\right)^2 = \frac{m_f J + 1}{m_f J\left(\beta_C{}^2 m_s m_f + 1\right) + 1} \tag{6.95}$$

where

$$J = \frac{-i\overline{\rho}\omega m_s}{P_D} = \frac{\rho_s}{\rho_f S}.$$

S is the momentum transfer term given by equation (4.13), here it only includes the Stokes drag term. The mass concentrations here are the constant equilibrium components of the corresponding variables.

For solid particles in a gas $\rho_s/\rho_f \gg 1$ and for low concentrations $m_s \ll 1$

$\beta_C \approx -(1 + m_s)$.

Substituting this approximation into (6.95), retaining terms of order m_s only, dividing by $m_s(1+J)$, using $m_f \approx 1$ and $m_s/m_f \ll 1$ gives

$$\left(\frac{kc_0}{\omega}\right)^2 = 1 + \frac{m_s}{1+J}.$$

Since $m_s{}^0 \equiv \phi\rho_s/\alpha\rho_f$ this can be rewritten as

$$\left(\frac{kc_0}{\omega}\right)^2 = \frac{S\left(\phi\rho_s + \rho_f\right) + \rho_s}{S\rho_f + \rho_s} \tag{6.96}$$

in the notation employed in chapter 4. This result for the effect of viscous drag on the complex wavenumber has been obtained by Temkin and Dobbins [98]. It is of the same form as the Harker and Temple result (equation (4.50)).

6. 5. 2 Discussion

Margulies and Schwartz write their equations in terms of the total field variables p, U and T and the total thermodynamic quantities c_0, γ, β, C_p and C_v, defined for the two phase medium. They do not, however, give complete information of how these are related to known quantities. Apart from c_0, which appears in the final expression (6.95), this information was not necessary for the above derivation. If the MS method is to be compared to the theory developed in chapter 4 it will be necessary to define completely these quantities.

The total pressure in the MS theory is defined as the sum of the partial pressures i.e. the pressures of the individual phases. Mecredy and Hamilton [18] obtained the partial pressures by volume averaging the total pressure (see equations (4.16) and (4.17)).

In their 1994 paper Margulies and Schwartz use the total U and T in their equations to derive the complex wavenumber but later use the individual phase temperatures to obtain their thermal transfer function. It is not explained how the total and individual temperatures are related.

In deriving (6.95) only one of the total thermodynamic quantities, c_0, remains in the expression for k. Margulies and Schwartz defined the quantity $\left(\gamma/c_0{}^2\right)$ in terms of $\left(\gamma_f/c_f{}^2\right)$ and $\left(\gamma_s/c_s{}^2\right)$ but this is not sufficient to find c_0 since γ is not given. Volume averaged quantities for c_0, γ, C_p and C_v such as those used by Culick shown in equations (6.35) to (6.37) could be used.

Chapter 7
Conclusions and future work

This thesis has reviewed and extended the theoretical and experimental work on sound propagation in suspensions and emulsions. Scattering theory, coupled phase theory and porous media theory and related work were reviewed in chapter 2. The thesis has shown the wide range of applications for coupled phase theory and how it relates to scattering theory and porous media theory. The most important result is the extension of coupled phase theory to model sound propagation in emulsions. Coupled phase theory has advantages over scattering theory for modelling sound propagation in suspensions and emulsions that behave as continua. However, when $k_f a$ is near 1 the coupled phase method is not valid and scattering theory must be used. It has been shown that coupled phase theory and the theories used for modelling porous media are very closely related. Chapter 6 has shown that the coupled phase approach is readily extendible. Comparisons with experimental data in the low $k_f a$, high volume fraction regime are encouraging but not entirely satisfactory and more experimental data is required to say whether the theories successfully model sound propagation in this regime.

7. 1 Scattering theory (chapter 3)

The important regimes of scattering theory as it applies to sound propagation in suspensions and emulsions have been identified in chapter 3. Results in the lossless and viscothermal scattering and single and multiple scattering regimes, and the prototypic model of incoherent scattering in the single scattering regime presented by Morse and Ingard [10], were discussed.

Viscothermal scattering is important when $k_f a \leq 1$ and is neglected when $k_f a \gg 1$ and compressional wave or lossless scattering is dominant. The value of $k_f a$ indicates how many A_n scattering coefficients will be required. The work of Allegra and Hawley [49] and Lin and Raptis [52] on viscothermal scattering in the long wavelength regime with thermoelastic solid and viscothermal liquid particles was reviewed in section 3. 2.

Multiple scattering is important unless the acoustic depth $N\sigma_0 L$ is very small. The acoustic depth is a function of the volume fraction ϕ and $k_f a$. The most often used multiple scattering results for coherent wave propagation have been compared numerically for viscothermal scattering and analytically for lossless scattering. The data of Atkinson and Kytomaa [13] for high volume fraction suspensions at $k_f a$ near 1 has been used to corroborate the Ma *et al* [75] lossless multiple scattering theory. The long wavelength theory was used and it is expected that closer agreement with the experimental data would be obtained if higher order scattering coefficients were included. Multiple scattering theory for coherent wave propagation has been shown to work for $k_f a \geq 1$ and low volume fractions but there is very little experimental data in the intermediate and high volume fraction range.

Only the most common multiple scattering theories have been studied in this thesis. There are now alternatives to the Twersky style approach such as the diagram method (Ye and Ding [27], Walden [181]) for coherent waves and the random field method (Liu [93]) for incoherent scattering. Incoherent scattering of ultrasound in the very strong scattering region is known as ultrasound diffusion and is an important area of current research [31] [32] [43] [97]. Page *et al* [31] have pointed out that acoustic work will be important in the study of the multiple scattering of classical waves as it avoids some of the limitations inherent in light scattering experiments.

7. 2 Coupled phase theory and extensions (chapters 4 and 6)

Coupled phase theory is more general and versatile than scattering theory for modelling sound propagation in suspensions and emulsions in the continuum regime.

Previous coupled phase theories belong to one of two categories: (i) those that include heat transfer between the phases and assume incompressible particles or (ii) those that include compressibility in the particulate phase but neglect heat transfer. The two major models in category (i) are the Mecredy and Hamilton (MH) model [18] and the Gumerov, Ivandaev and Nigmatulin (GIN) [102] model. By neglecting mass transfer an analytical solution has been

obtained for the MH model. It has been shown that the MH and GIN models are formally identical, a minor difference in the momentum equations of the two models proves to be unimportant in practice. Numerical and analytical comparisons with the Allegra and Hawley long wavelength scattering theory showed that, in the low $k_f a$ and low volume fraction regime, the two approaches give similar predictions. There are important differences between the approaches in the steady state limit.

The most important form of category (ii) models has been obtained by Harker and Temple (HT) [65] and Atkinson and Kytomaa [113]. The category (i) and (ii) models have been compared analytically. A new theory incorporating categories (i) and (ii), i.e. heat transfer and a compressible particulate phase, was developed in section 4. 3. The new theory is the only alternative to scattering theory for modelling sound propagation in emulsions. Predictions of the theory compare favourably to McClements' [64] [71] experimental data on emulsions at low $k_f a$ in the high volume fraction regime. Numerical comparisons with multiple scattering theory and experimental data suggest that the theory may be a better model for the volume fraction dependence of the complex wavenumber in the low $k_f a$, or continuum, regime. Comparisons between the two theories and experimental data are not, however, definitive enough to say whether the theories successfully model sound propagation in emulsions. More experimental data on emulsions in the continuum regime up to high volume fractions is required.

Work on the effect of particle hydrodynamic interactions on momentum transfer was reviewed in section 6. 1. A correction factor for these effects has been included in the HT coupled phase theory by Strout [42]. Strout tried similar corrections in scattering theory but these were not particularly successful. Interactions between the particles also have an effect on heat transfer (Sangani and Acrivos [151]). It would be possible to develop a correction factor for the heat transfer term, analogous to the correction factor of Strout, to model these effects in coupled phase theory.

Predictions of the Strout model have been compared to the experimental data of Hampton [131] and Urick [104] [105], who measured sound speed and attenuation in suspensions at low $k_f a$ and high volume fractions. The predictions were also compared to predictions of the frameless Biot porous media theory [131]. The frameless Biot theory gives better agreement with the experimental data but this requires the use of an adjustable parameter. The relationship between coupled phase theory and the frameless Biot theory is

discussed in the following section. Both the theories give better agreement with the data than multiple scattering theory. As was said above for emulsions, more data is required for suspensions in the low $k_f a$ and high volume fraction regime to confirm that the theories are satisfactory. The pneumatic conveying of suspensions in pipes is one method of forming air suspensions at high volume fractions, on which propagation experiments can be performed.

Several workers have derived volume fraction dependent expressions for the induced mass force at high volume fractions. The influence of the induced mass becomes important at higher $k_f a$ in the region where the Bassett force controls the frequency dependence of the attenuation. Kytomaa [25] measured attenuation in suspensions in the 'transition region' where the Bassett force begins to dominate. Coupled phase theory predictions using the various expressions for the induced mass were compared to this data in section 6. 1. 3 (see figure 6. 7). The theoretical predictions do not agree particularly well with the experimental data. More experimental work on the induced mass force in concentrated suspensions will be required to determine which is the best model.

Harker and Temple [106] modified their coupled phase theory to allow for a range of particle sizes. Their approach has been used to include a size distribution in the MH model. Predictions of coupled phase theory including a size distribution have been compared to the experimental data of Moss [12], who measured attenuation and sound speed in alumina suspensions with a known size distribution. The prediction of the theory including the size distribution was in better agreement with the experimental data than the prediction using a monodisperse distribution based on the Sauter mean radius. Pendse and Sharma [19] used attenuation data measured over a wide frequency range to calculate the particle size distribution of a slurry. The size distribution was obtained by inverting an integral equation which relates it to the attenuation.

The effect of particle shape on the complex wavenumber has been investigated by including the steady state drag and heat transfer terms for spheroidal and cubic particles in a coupled phase theory. Predictions of the theory were compared to Moss' data. In the very low $k_f a$ regime, the influence of particle shape is unimportant relative to the effect of volume fraction and size distribution.

The method of Culick [8] [9] has been used to calculate frequency shifts for the lowest transverse mode in a pipe into which suspensions are introduced. The

results were compared to the predictions of an intuitive approach using the modified sound speed of the suspension. Both methods are only valid in the very low $k_f a$ regime, but it would be possible to extend them. The range of validity of the Culick method can be extended by numerical solution. Compared to the intuitive approach the Culick method is rather involved. However, it has the advantages that it is valid for finite amplitudes and can be used to model sources in the enclosure. Vetter and Culick [108] have measured frequency shifts and concluded that the technique only works well for small particles and low order modes in large enclosures.

Section 6. 5 studied the method of Margulies and Schwartz [2] for modelling the effect of particle diffusion on sound propagation. Margulies and Schwartz have considered other influences on sound propagation such as fluid flow, radiation, viscoelasticity, chemical reactions between the phases, the Dufour effect (where heat is transported by diffusing particles) and phoresis. Phoresis refers to the diffusion of particles by gradients of temperature (thermophoresis), by gradients of pressure (barophoresis) by gradients of concentration of particles (pcynophoresis) or by external forces e.g. electrophoresis. Extension to finite amplitudes was discussed by Benharbit, Margulies and Schwartz [3].

7. 3 Porous media theory and coupled phase theory (chapter 5)

It has been demonstrated how the frameless Biot theory and rigid frame theory arise as special cases of the general Biot theory. Making use of Berryman's expression for the inertial force in terms of the induced mass of a single sphere [124], it has been shown that, apart from the expression for the viscous force, the frameless Biot theory is identical to the HT coupled phase theory. The expression for the viscous force usually used in the Biot theory is derived from a tube model of the pores between the particles. The expression usually used in coupled phase theory is derived from the forces on the particles. Predictions of the theory using the pore model for the viscous force give better agreement with the data of Hampton [131] than predictions using the particle model. This is partly because the pore model has an adjustable parameter. The pore model also gives better agreement than the improved particle model which includes hydrodynamic interactions, as was described above. Further experimental work is needed to establish which is the most suitable model for sound propagation in suspensions in the continuum regime at high volume fractions.

The Biot-Allard [46] rigid frame theory, which includes an effective compressibility to model heat transfer, has been used to predict the reflection

coefficient for air saturated stacked glass beads. Agreement with measurements was achieved by specifying a range of values for the Biot shape factor. Section 5. 2. 7 studied the water suction method for estimating the pore size distribution of porous materials. Measurements of the pore size distribution of stacked glass beads of various sizes were used in the Attenborough [121] rigid frame theory as an alternative to the Biot-Allard theory for predicting the reflection coefficient. The theory assumes a log normal distribution of pore sizes: agreement with the reflection coefficient measurements was obtained by specifying a range of values for the standard deviation. Estimates of the flow resistivity using the pore size distribution measurements were compared to direct measurements of the flow resitivity obtained using air flow apparatus.

7. 4 Porous media theory and scattering theory

Schwartz and Johnson [82] discussed the Biot formula for the effective density, neglecting viscous effects, in relation to multiple scattering. In general, the Biot formula, characterising the suspension by one geometrical parameter, the tortuosity, is only rigorously applicable for ordered suspensions. For disordered suspensions the tortuosity will depend on the densities of the two phases as well as the geometry.

Nagy [32] used the general Biot theory to model slow wave propagation in low permeability porous plates. The theory successfully predicted the slow wave speed but not its attenuation. An energy balance of the coherent and incoherent scattering indicated that the observed excess attenuation is caused by viscous losses greater than those predicted by the theory. It would be interesting to compare Nagy's results to the work on ultrasound diffusion discussed in section 2. 1. 6.

References

[1] T. S. Margulies and W. H. Schwartz, "Acoustic wave propagation in fluids," in *Frontiers in Fluid Mechanics*, ed. S. H. Davis and J. L. Lumley (Springer-Verlag, New York, 1985), pp. 219-280.

[2] W. H. Schwartz and T. S. Margulies, "Sound wave propagation through emulsions, colloids and suspensions using a generalized Fick's law," J. Acoust. Soc. Am. 90, 3209-3217 (1991).

[3] A. Benharbit, T. S. Margulies and W. H. Schwartz, "Finite-amplitude wave propagation through a two-phase system of particles in a viscothermal fluid," J. Acoust. Soc. Am. 91, 2556-2568 (1992).

[4] T. S. Margulies and W. H. Schwartz, "A multiphase continuum theory for sound wave propagation through dilute suspensions of particles," J. Acoust. Soc. Am. 96, 319-331 (1994).

[5] F. E. C. Culick, "Some recent result for nonlinear acoustics in combustion chambers," AIAA Journal 32, 146-169 (1994).

[6] F. E. C. Culick, "Non-linear growth and limiting amplitude of acoustic oscillations in combustion chambers," Combustion Science and Technology 3, 1-16 (1971).

[7] F. E. C. Culick, "Nonlinear behaviour of acoustic waves in combustion chambers," Daniel and Florence Guggenheim Jet Propulsion Center, California Institute of Technology, Pasadena, California (1975).

[8] F. E. C. Culick, "Nonlinear behaviour of acoustic waves in combustion chambers I," Acta Astronautica 3, 715-734 (1976).

[9] F. E. C. Culick, "Nonlinear behaviour of acoustic waves in combustion chambers II," Acta Astronautica 3, 735-757 (1976).

[10] P. M. Morse and K. U. Ingard, *Theoretical Acoustics* (McGraw-Hill, New York, 1968).

[11] S. H. O. Moss and K. Attenborough, "Measurements of attenuation and dispersion in an airborne suspension of dust," Applied Acoustics 42, 187-196 (1994).

[12] S. H. O. Moss, unpublished work.

[13] C. M. Atkinson and H. K. Kytomaa, "Acoustic properties of solid-liquid mixtures and the limits of ultrasound diagnostics I: experiments," J. Fluids Eng. 115, 665-675 (1993).

[14] K. Froyse and O. Nesse, "Ultrasonic wave propagation in dispersions," Proceedings 15th International Congress on Acoustics, 349-352 (1995).

[15] A. A. Vetter and F. E. C. Culick, "Evaluation of the Acoustical Resonance Measurement of particle loading in two-phase flow," U. S. Department of Energy report DOE/ER/80193-1 (1985).

[16] A. E. Hay, "Sound scattering from a particle-laden turbulent jet," J. Acoust. Soc. Am. 90, 2055-2074 (1991).

[17] D. L. Johnson and T. J. Plona, "Acoustic slow waves and the consolidation transition," J. Acoust. Soc. Am. 72, 556-565 (1982).

[18] R. C. Mecredy and L. J. Hamilton, "The effects of nonequilibrium heat, mass and momentum transfer on two-phase sound speed," Int. J. Heat Mass Transfer 15, 61-72 (1972).

[19] H. P. Pendse and A. Sharma, "Particle size distribution analysis of industrial colloidal slurries using ultrasonic spectroscopy," Part. Part. Syst. Charact. 10, 229-233 (1993).

[20] R. A. Roy and R. E. Apfel, "Mechanical characterization of microparticles by scattered ultrasound," J. Acoust. Soc. Am. 87, 2332-2341 (1990).

[21] K. K. Shung, Y. W. Yuan and D. Y. Fei, "Effect of flow disturbance on ultrasonic backscatter from blood," J. Acoust. Soc. Am. 75, 1265-1272

(1984).

[22] A. Gronningsaeter, B. A. J. Angelsen, A. Gresli, H. G. Torp and D. T. Linker, "Blood noise reduction in intravascular ultrasound imaging," IEEE Transactions on Ultrasonics, Ferroelectrics and Frequency Control 42, 200-209 (1995).

[23] M. O'Donnell, E. T. Jaynes and J. G. Miller, "Kramers-Kronig relationship between ultrasonic attenuation and phase velocity," J. Acoust. Soc. Am. 69, 696-701 (1981).

[24] R. C. Chivers, "Ultrasound propagation in heterogeneous systems" in *Developments in Acoustics and Ultrasonics* ed. M. Povey and J. McClements (Institute of Physics Publishing Ltd., 1992).

[25] H. K. Kytomaa, "Theory of sound propagation in suspensions: a guide to particle size and concentration characterization," Powder Technology 82, 115-121 (1995).

[26] P. D. Thorne, C. Manley and J. Brimelow, "Measurements of the form function and total scattering cross section for a suspension of spheres," J. Acoust. Soc. Am. 93, 243-248 (1993).

[27] Z. Ye and L. Ding, "Acoustic dispersion and attenuation relations in bubbly mixture," J. Acoust. Soc. Am. 98, 1629-1636 (1995).

[28] G. A. Davidson, "A Burgers' equation for finite amplitude acoustics in fog," J. Sound Vib. 45, 473-485 (1976).

[29] D. J. McClements, "Characterisation of emulsions using a frequency scanning ultrasonic pulse echo reflectometer," Proceedings of the Institute of Acoustics 13 (2), 71-78 (1991).

[30] V. J. Pinfield, M. J. W. Povey and E. Dickinson, "The application of modified forms of the Urick equation to the interpretation of ultrasound velocity in scattering systems," Ultrasonics 33, 243-251 (1995).

[31] J. H. Page, H. P. Schriemer, A. E. Bailey and D. A. Weitz, "Experimental test of the diffusion approximation for multiply scattered sound," Phys. Rev. E 52, 3106-3114 (1995).

[32] P. B. Nagy, "Local variations of slow wave attenuation in air-filled permeable materials," to be published.

[33] R. Ishii and H. Matsuhisa, "Steady reflection, absorption and

transmission of small disturbances by a screen of dusty gas," J. Fluid Mech. 130, 259-277 (1983).

[34] J. F. Vignola, Y. H. Berthelot, S. Jones and J. Jarzynski, "Equation of motion of microparticles in suspension in an insonified medium," J. Acoust. Soc. Am 92, 332-334 (1992).

[35] J. A. Gallego-Juarez, "Nonlinear effects in ultrasonic processing applications," Proceedings 15th International Congress on Acoustics, 41-44 (1995).

[36] P. D. McCormack and L. Crane, *Physical Fluid Dynamics*, (Academic Press, New York 1973).

[37] J. Happel and H. Brenner, *Low Reynolds Number Hydrodynamics - with special applications to particulate media* (Prentice-Hall, Englewood Cliffs, N. J. 1965).

[38] A. S. Sangani and A. Acrivos, "Slow flow through a periodic array of spheres," Int. J. Multiphase Flow 8, 343-360 (1982).

[39] G. D. Scott, "Packing of spheres," Nature 188, 908-910 (1988).

[40] J. D. Bernal and J. Mason, "Co-ordination of randomly packed spheres," Nature 188, 910-911 (1988).

[41] A. D. Pierce, *Acoustics: An Introduction to Its Physical Principles and Applications* (McGraw-Hill Book Company, New York 1991).

[42] T. A. Strout, "Attenuation of sound in high-concentration suspensions: Development and Application of an Oscillatory Cell Model," Ph. D. Thesis, University of Maine 1991.

[43] R. C. Chivers, "Measurement of ultrasonic attenuation in inhomogeneous media," Acustica 74, 8-15 (1991).

[44] E. E. Michaelides and Z. Feng, "Heat transfer from a rigid sphere in a nonuniform flow and temperature field," Int. J. Heat Mass Transfer 37, 2069-2076 (1994).

[45] J. L. Leander, "Sound propagation in dilute gas-liquid suspensions: definition of the regime of noninteracting bubbles via scattering theory and the causality approach," J. Acoust. Soc. Am. 97, 1974-1977 (1995).

[46] J. F. Allard, *Propagation of sound in porous media* (Elsevier Science Publishing, Essex, 1993).

[47] P. S. Epstein and R. R. Cahart, "The absorption of sound in suspensions and emulsions. I. Water fog in air," J. Acoust. Soc. Am. 25, 553-564 (1953).

[48] J. W. Zink and L. P. Delsasso, "Attenuation and dispersion of sound by solid particles suspended in a gas," J. Acoust. Soc. Am. 30, 765-771 (1958).

[49] J. R. Allegra and S. A. Hawley, "Attenuation of sound in suspensions and emulsions: theory and experiments," J. Acoust. Soc. Am. 51, 1545-1564 (1972).

[50] W. H. Lin and A. C. Raptis, "Viscous effects on acoustic scattering by elastic solid cylinders and spheres," Tech. Memo. ANL-CT-82-X, Argonne National Laboratory (1982).

[51] W. H. Lin and A. C. Raptis, "Acoustic scattering by elastic solid cylinders and spheres in viscous fluids," J. Acoust. Soc. Am. 73, 736-748 (1983).

[52] W. H. Lin and A. C. Raptis, "Thermoviscous effects on acoustic scattering by thermoelastic solid cylinders and spheres," J. Acoust. Soc. Am. 74, 1542-1554 (1983).

[53] L. W. Anson and R. C. Chivers, "Thermal effects in the attenuation of ultrasound in dilute suspensions for low values of acoustic radius," Ultrasonics 28, 16-26 (1990).

[54] V. M. Ayres and G. C. Gaunaurd, "Acoustic resonance scattering by viscoelastic objects," J. Acoust. Soc. Am. 81, 301-311 (1987).

[55] L. W. Anson and R. C. Chivers, "Ultrasonic scattering from spherical shells including viscous and thermal effects," J. Acoust. Soc. Am. 93, 1687-1699 (1993).

[56] P. C. Waterman, "New formulation for acoustic scattering," J. Acoust. Soc. Am. 45, 1417-1429 (1969).

[57] P. Jansson, "Acoustic scattering from a rough sphere," J. Acoust. Soc. Am. 93, 3032-3042 (1993).

[58] H. S. Kim, J. S. Kim and H. J. Kang, "Acoustic wave scattering from axisymmetric bodies," J. Sound Vib. 163, 385-396 (1993).

[59] K. Attenborough and L. A. Walker, "Sound dissipation by a small cylindrical obstacle," J. Acoust. Soc. Am. 51, 192-196 (1972).

[60] T. K. Stanton, "Simple approximate formulas for backscattering of sound by spherical and elongated objects," J. Acoust. Soc. Am. 86, 1499-1510 (1989).

[61] A. Ishimaru, *Wave propagation and scattering in random media. Volume 1. Single scattering and transport theory*, Academic Press Inc., London (1978).

[62] A. Ishimaru, *Wave propagation and scattering in random media. Volume 2. Multiple scattering, turbulence, rough surfaces and remote sensing*, Academic Press Inc., London (1978).

[63] V. Twersky, "On scattering of waves by random distributions. I. Free space scatterer formalism," J. Math. Phys. 3, 700-715 (1962).

[64] D. J. McClements, "Comparison of multiple scattering theories with experimental measurements in emulsions," J. Acoust. Soc. Am. 91, 849-853 (1992).

[65] A. H. Harker and J. A. G. Temple, "Velocity and attenuation of ultrasound in suspensions of particles in fluids," J. Phys D: Appl. Phys. 21, 1576-1588 (1988).

[66] V. Twersky, "On a general class of scattering problems," J. Math. Phys. 3, 716-723 (1962).

[67] V. Twersky, "On scattering of waves by random distributions. II. Two space scatterer formalism," J. Math. Phys. 3, 724-734 (1962).

[68] C. Javanaud and A. Thomas, "Multiple scattering using the Foldy-Twersky integral equation," Ultrasonics 26, 341-343 (1988).

[69] V. Twersky, "Coherent scalar field in pair-correlated random distributions of aligned scatterers," J. Math. Phys. 18, 2468-2486 (1977).

[70] V. Twersky, "Acoustic bulk parameters in distributions of pair-correlated scatterers," J. Acoust. Soc. Am. 64, 1710-1719 (1978).

[71] D. J. McClements and M. J. W. Povey, "Scattering of ultrasound by emulsions," J. Phys. D: Appl. Phys. 22, 38-47 (1989).

[72] D. J. McClements, M. J. W. Povey, M. Jury and E. Betsanis, "Ultrasonic characterization of a food emulsion," Ultrasonics 28, 266-272 (1990).

[73] P. C. Waterman and R. Truell, "Multiple scattering of waves," J.

Math. Phys. 2, 512-537 (1961).

[74] P. Lloyd and M. V. Berry, "Wave propagation through an assembly of spheres IV. Relations between different multiple scattering theories," Proc. Phys. Soc. 91, 678-688 (1967).

[75] Y. Ma, V. K. Varadan and V. V. Varadan, "Comments on ultrasonic propagation in suspensions," J. Acoust. Soc. Am. 87,2779-2782 (1990).

[76] A. K. Holmes, R. E. Challis and D. J. Wedlock, "A wide bandwidth study of ultrasound velocity and attenuation in suspensions: comparison of theory with experimental measurements," J. Colloid Int. Sci. 156, 261-268 (1993).

[77] J. S. Tebbutt and R. E. Challis, "On the physical acoustics of colloidal mixtures," Acoustics Bulletin July / August 1995, 5-10.

[78] I. Alig and D. Lellinger, "Frequency dependence of ultrasonic velocity and attenuation in two-phase composite systems with spherical scatterers," J. Appl. Phys. 72, 5565-5570 (1992).

[79] D. Wu, Z. W. Qian and D. Shao, "Sound attenuation in a course granular material," J. Sound Vib. 162, 529-535 (1993).

[80] K. Attenborough and L. A. Walker, "Scattering theory for sound absorption in fibrous media," J. Acoust. Soc. Am. 49, 1331-1338 (1971).

[81] L. Schwartz and T. J. Plona, "Ultrasonic propagation in close-packed disordered suspensions," J. Appl. Phys. 55, 3971-3977 (1984).

[82] L. M. Schwartz and D. L. Johnson, "Long-wavelength acoustic propagation in ordered and disordered suspensions," Phys. Rev. B 30, 4302-4313 (1984).

[83] G. M. Romack and R. L. Weaver, "Monte Carlo studies of multiple scattering of waves in one-dimensional random media," J. Acoust. Soc. Am. 87, 487-494 (1990).

[84] C. M. Sayers, "On the propagation of ultrasound in highly concentrated mixtures and suspensions," J. Phys. D: Appl. Phys. 13, 179-184 (1980).

[85] C. M. Sayers and R. L. Smith, "The propagation of ultrasound in porous media," Ultrasonics 20, 201-205 (1982).

[86] J. G. Berryman, "Long-wavelength propagation in composite elastic

media I. Spherical inclusions," J. Acoust. Soc. Am. 68, 1809-1819 (1980).

[87] J. G. Berryman, "Long-wavelength propagation in composite elastic media II. Ellipsoidal inclusions," J. Acoust. Soc. Am. 68, 1820-1831 (1980).

[88] L. W. Anson and R. C. Chivers, "Ultrasonic velocity in suspensions of solids in solids - a comparison of theory and experiment," J. Phys. D: Appl. Phys. 26, 1566-1575 (1993).

[89] J. Adach, R. C. Chivers and L. W. Anson, "Ultrasonic propagation, scattering and defocusing in suspensions," J. Acoust. Soc. Am. 93, 3208-3219 (1993).

[90] V. Twersky, "Low-frequency scattering by correlated distributions of randomly oriented particles," J. Acoust. Soc. Am. 81, 1609-1618 (1987).

[91] R. J. Lucas and V. Twersky, "Inversion of ultrasonic scattering data for red blood cell suspensions under different flow conditions," J. Acoust. Soc. Am. 82, 794-799 (1987).

[92] V. Twersky, "Low-frequency scattering by mixtures of correlated nonspherical particles," J. Acoust. Soc. Am. 84, 409-415 (1988).

[93] K. C. Liu, "Wave scattering in discrete random media by the discontinuous stochastic field method, I: Basic method and theory," J. Sound Vib. 147, 301-311 (1991).

[94] K. C. Liu, "Wave scattering in discrete random media by the discontinuous stochastic field method, II: Contribution of the second order moment of the β-field," J. Sound Vib. 147, 313-321 (1991).

[95] K. C. Liu, "Wave scattering in discrete random media by the discontinuous stochastic field method, III: Contribution of the third order moment of the β-field," J. Sound Vib. 147, 323-334 (1991).

[96] I. Tolstoy, "Superresonant systems of scatterers. I," J. Acoust. Soc. Am. 80, 282-294 (1986).

[97] R. L. Weaver and W. Sachse, "Diffusion of ultrasound in a glass bead slurry," J. Acoust. Soc. Am. 97, 2094-2102 (1995).

[98] S. Temkin and R. A. Dobbins, "Attenuation and dispersion of sound by particulate-relaxation processes," J. Acoust. Soc. Am. 40, 317-324

(1966).

[99] S. Temkin and R. A. Dobbins, "Measurements of attenuation and dispersion of sound by an aerosol," J. Acoust. Soc. Am. 40, 1016-1024 (1966).

[100] E. P. Mednikov, "Absorption and dispersion of sound in aerosols at large particle velocity amplitudes," Soviet Physics - Acoustics 15, 507-510 (1970).

[101] R. C. Mecredy and L. J. Hamilton, " Speed and attenuation of acoustic waves in two-phase two-component media," Proc. Sixth Southeastern Seminar Thermal Sciences (April 1990).

[102] N. A. Gumerov, A. I. Ivandaev and R. I. Nigmatulin, "Sound waves in monodisperse gas-particle or vapour-droplet mixtures," J. Fluid Mech. 193, 53-74 (1988).

[103] R. Wei, Y. Tian and Q. Lu, "Absorption of sound in water fog composed of submicron droplets," J. Acoust. Soc. Am. 81, 1350-1354 (1987).

[104] R. J. Urick, "A sound velocity method for determining the compressibility of finely divided substances," J. Appl. Phys. 18, 983-987 (1947).

[105] R. J. Urick, "The absorption of sound in suspensions of irregular particles," J. Acoust. Soc. Am 20, 283-289 (1948).

[106] A. H. Harker, P. Schofield, B. P. Stimpson, R. G. Taylor and J. A. G. Temple, "Ultrasonic propagation in slurries," Ultrasonics 29, 427-438 (1991).

[107] S. L. Soo, *Fluid dynamics of multiphase systems* (Blaisdell, Waltham, MA, 1967).

[108] A. A. Vetter and F. E. C. Culick, "Acoustical Resonance Measurement of particle loading in gas-solid flows," Journal of Engineering for Gas Turbines and Power 109, 331-335 (1987).

[109] A. A. Vetter, "Sensitivity of the Acoustical Resonance Measurement of particle loading in gas-solid flows," Journal of Engineering for Gas Turbines and Power 110, 197-200 (1988).

[110] A. S. Ahuja, "Wave equation and propagation parameters for sound propagation in suspensions," J. Appl. Phys. 44, 4863-4868 (1973).

[111] A. S. Ahuja and W. R. Hendee, "Effects of particle shape and orientation on propagation of sound in suspensions," J. Acoust. Soc. Am. 63, 1074-1080 (1978).

[112] H. K. Kytomaa and C. M. Atkinson, "Sound propagation in suspensions and acoustic imaging of their microstructure," Mechanics of Materials 16, 189-197 (1993).

[113] C. M. Atkinson and H. K. Kytomaa, "Acoustic wave speed and attenuation in suspensions," Int. J. Multiphase Flow 18, 577-592 (1992).

[114] G. Kirchhoff, "Ueber der Einflufs der Warmeleitung in einem Gase auf die Schallbewegung," Annalen der Physik and Chemie 134, 177-193 (1868).

[115] D. E. Weston, "The theory of the propagation of plane sound waves in tubes," Proc. Phys. Soc. London Sec. B 66, 695-709 (1953).

[116] C. Zwikker and C. W. Kosten, *Sound absorbing materials* (Elsevier, New York, 1949).

[117] M. R. Stinson, "The propagation of plane sound waves in narrow and wide circular tubes, and generalization to uniform tubes of arbitrary cross-sectional shape," J. Acoust. Soc. Am. 89, 550-558 (1991).

[118] A. Craggs and J. G. Hildebrandt, "Effective densities and resistivities for acoustic propagation in narrow tubes," J. Sound and Vib. 92, 321-331 (1984).

[119] A. Craggs and J. G. Hildebrandt, "The normal incidence absorption coefficient of a matrix of narrow tubes with constant cross-section," J. Sound and Vib. 105, 101-107 (1986).

[120] M. A. Biot, "Theory of propagation of elastic waves in a fluid-saturated porous solid. II. Higher frequency range," J. Acoust. Soc. Am 28, 179-191 (1956).

[121] K. Attenborough, "Models for acoustical properties of air-saturated granular media," Acta Acustica 1, 213-226 (1993).

[122] T. Yamamoto and A. Turgut, "Acoustic wave propagation through porous media with arbitrary pore size distributions," J. Acoust. Soc. Am. 83, 1744-1751 (1988).

[123] A. W. J. Heijs and C. P. Lowe, "Numerical evaluation of the

permeability and the Kozeny constant for two types of porous media," Phys. Rev. E 51, 4346-4352 (1995).

[124] J. G. Berryman, "Confirmation of Biot's theory," Appl. Phys. Lett. 37, 382-384 (1980).

[125] P. Leclaire, F. Cohen-Tenoudji and J. Aguirre-Puente, "Extension of Biot's theory of wave propagation to frozen porous media," J. Acoust. Soc. Am. 96, 3753-3768 (1994).

[126] P. B. Nagy, "Slow wave propagation in air-filled permeable solids," J. Acoust. Soc. Am. 93, 3224-3234 (1993).

[127] K. Attenborough, "Acoustical characteristics of rigid fibrous absorbents and granular materials," J. Acoust. Soc. Am. 73, 785-799 (1983).

[128] K. Attenborough, "On the acoustic slow wave in air-filled granular materials," J. Acoust. Soc. Am. 81, 93-102 (1987).

[129] C. W. Kosten and J. H. Janssen, "Acoustic properties of flexible and porous materials," Acustica 7, 372-378 (1957).

[130] P. R. Ogushwitz, "Applicability of the Biot theory. I. Low-porosity materials," J. Acoust. Soc. Am. 77, 429-440 (1985).

[131] P. R. Ogushwitz, "Applicability of the Biot theory. II. Suspensions," J. Acoust. Soc. Am. 77, 441-452 (1985).

[132] J. M. Hovem, "Viscous attenuation of sound in suspensions and high-porosity marine sediments," J. Acoust. Soc. Am. 67, 1559-1531 (1980).

[133] J. M. Hovem and G. D. Ingram, "Viscous attenuation of sound in saturated sand," J. Acoust. Soc. Am. 66, 1807-1812 (1979).

[134] R. L. Gibson and M. N. Toksoz, "Viscous attenuation of acoustic waves in suspensions," J. Acoust. Soc. Am. 85, 1925-1934 (1989).

[135] R. L. Weaver and Y. Pao, "Dispersion relations for linear wave propagation in homogeneous and inhomogeneous media," J. Math. Phys. 22, 1909-1918 (1981).

[136] M. O'Donnell, E. T. Jaynes and J. G. Miller, "General relationships between ultrasonic attenuation and dispersion," J. Acoust. Soc. Am. 63, 1935-1937 (1978).

[137] S. Temkin, "Attenuation and dispersion of sound in bubbly fluids via the Kramers-Kronig relations," J. Fluid. Mech. 211, 61-72 (1990).

[138] N. Brauner and A. I. Beltzer, "Linear waves in bubbly liquids via the Kramers-Kronig relations," J. Vib. Acoust. 113, 417-419 (1991).

[139] C. L. Morfey and G. P. Howell, "Speed of sound in air as a function of frequency and humidity," J. Acoust. Soc. Am. 68, 1525-1527 (1980).

[140] A. I. Nachman, J. F. Smith and R. C. Waag, "An equation for acoustic propagation in inhomogeneous media with relaxation losses," J. Acoust. Soc. Am. 88, 1584-1595 (1990).

[141] R. L. Weaver, "Causality and theories of multiple scattering in random media," Wave Motion 8, 473-483 (1986).

[142] R. Clift, J. R. Grace and M. E. Weber, Bubbles, Drops and Particles, Academic Press, New York 1978.

[143] L. D. Landau and E. M. Lifshitz, *Fluid Mechanics* (Pergamon Press, New York, 1959).

[144] P. Mazur and D. Bedeaux, "A generalisation of Faxen's theorem to nonsteady motion of a sphere through an incompressible fluid in arbitrary flow," Physica 76, 235-246 (1974).

[145] H. Brenner, "The Oseen resistance of a particle of arbitrary shape," J. Fluid. Mech. 11, 604-610 (1961).

[146] H. Brenner and R. G. Cox, "The resistance to a particle of arbitrary shape in translational motion at small Reynolds numbers," J. Fluid. Mech. 17, 561-595 (1963).

[147] R. P. Kanwal, "Drag on an axially symmetric body vibrating slowly along its axis in a viscous fluid," J. Fluid. Mech. 19, 631-636 (1964).

[148] R. Y. S. Lai and L. F. Mockros, "The Stokes-flow drag on prolate and oblate spheroids during axial translatory accelerations," J. Fluid. Mech. 52, 1-15 (1972).

[149] E. Achenbach, "The effects of surface roughness and tunnel blockage on the flow past spheres," J. Fluid. Mech. 65, 113-125 (1974).

[150] S. Kuwabara, "The forces experienced by randomly distributed parallel circular cylinders or spheres in a viscous flow at small Reynolds number," J. Phys. Soc. Japan 14, 527-532 (1959).

[151] A. S. Sangani and A. Acrivos, "Slow flow past periodic arrays of cylinders with application to heat transfer," Int. J. Multiphase Flow 8, 193-206 (1982).

[152] A. Acrivos, E. J. Hinch and D. J. Jeffrey, "Heat transfer to a slowly moving fluid from a dilute fixed bed of heated spheres," J. Fluid Mech. 101, 403-421 (1980).

[153] N. Zuber, "On the dispersed two-phase flow in the laminar flow regime," Chem. Eng. Sci. 19, 897-917 (1964).

[154] G. K. Batchelor, "Transport properties of two-phase materials with random structure," Annual Rev. Fluid Mech. 6, 227-255 (1974).

[155] G. Mo and A. S. Sangani, "A method for computing Stokes flow interactions among spherical objects and its application to suspensions of drops and porous particles," Phys. Fluids 6, 1637-1652 (1994).

[156] J. O. Hinze, "Momentum and mechanical-energy balance equations for a flowing homogeneous suspension with slip between the two phases," Appl. Sci. Res. 11, 33-46.

[157] R. G. Cox and S. G. Mason, "Suspensed particles in fluid flow through tubes," Annual Rev. Fluid Mech. 3, 291-316 (1971).

[158] C. T. Crowe, "On the relative importance of particle-particle collisions in gas-particle flows," Paper C78-81, Conf. on gas-borne particles, Inst. of Mech. Engr., Oxford, England, 1981, pp. 135-137.

[159] C. T. Crowe, "Review - Numerical models for dilute gas-particle flows," J. Fluids Eng. 104, 297-303 (1982).

[160] M. Di Giacinto, F. Sabetta and R. Piva, "Two-way coupling effects in dilute gas-particle flows," J. Fluids Eng. 104, 304-312 (1982).

[161] Y. D. Choi and M. K. Chung, "Analysis of turbulent gas-solid suspension flow in a pipe," J. Fluids Eng. 105, 329-334 (1983).

[162] V. Kumaran and D. L. Koch, "Properties of a bidisperse particle-gas suspension Part 1. Collision time small compared with viscous relaxation time," J. Fluid Mech. 247, 623-641 (1993).

[163] V. Kumaran and D. L. Koch, "Properties of a bidisperse particle-gas suspension Part 2. Viscous relaxation time small compared with collision time," J. Fluid Mech. 247, 643-660 (1993).

[164] L. Tsang, J. A. Kong and T. Habashy, "Multiple scattering of acoustic waves by random distribution of discrete spherical scatterers with the quasicrystalline and Percus-Yervick approximation," J. Acoust. Soc. Am. 71, 552-558 (1982).

[165] Thurston, in *Physical Acoustics*, edited by W. P. Mason (Academic Press, 1964), Volume 1, part A, p. 9.

[166] J. M. Evans and K. Attenborough, "A coupled phase theory for sound propagation in an emulsion of heat-conducting, compressible liquids," Proceedings 15th International Conference on Acoustics, Trondheim, Norway, 345-348 (1995).

[167] R. J. S. Brown, "Connection between formation factor for electrical resistivity and fluid-solid coupling factor in Biot's equations for acoustic waves in fluid-filled porous media," Geophysics 45, 152-159 (1980).

[168] S. Teuber, "Schallausbreitung in porosen Absorben," PhD thesis, Carl von Ossietzky Universitat, Oldenburg, Germany (1995).

[169] C. Howorth, "Sound propagation over rigid porous layers," PhD thesis, The Open University 1991.

[170] T. J. Marshall and J. W. Holmes, *Soil Physics*, (Cambridge University Press 1979).

[171] M. Th. van Genuchten, "Calculating the hydraulic conductivity with a new closed form analytical model," Res. Rep. no. 78-WR-08, Princetown University, Princetown, NJ (1978).

[172] M. Th. van Genuchten, "A closed form equation for predicting the hydraulic conductivity of unsaturated soils," Soil. Sci. Soc. Amer. J. 44, 892-898 (1980).

[173] V. Vand, "Viscosity of solutions and suspensions. I, II and III," J. Phy. Colloid Chem. 52, 277-321 (1948).

[174] H. Hasimoto, "On the periodic fundamental solutions of the Stokes equation and their application to viscous flow past a cubic array of spheres," J. Fluid. Mech. 5, 317-328 (1959).

[175] J. Happel, "Viscous flow in multiparticle systems: slow motion of fluids relative to beds of spherical particles," AICHE J. 4, 197-201 (1958).

[176] M. S. Greenwood, J. L. Mai and M. S. Good, "Attenuation measurements of ultrasound in a kaolin-water slurry: A linear dependence on frequency," *J. Acoust. Soc. Am.* 94, 908-916 (1993).

[177] C. M. Harris, "Absorption of sound in air in the audio-frequency range," J. Acoust. Soc. Am. 35, 11-17 (1963).

[178] C. M. Harris and W. Tempest, "Absorption of sound in air below 1000 cps," J. Acoust. Soc. Am. 36, 2390-2394 (1964).

[179] R. G. Monk, "Thermal relaxation in humid air," J. Acoust. Soc. Am. 46, 580-586 (1969).

[180] E. N. Bazley, "Sound absorption in air at frequencies up to 100 kHz," NPL Acoustics Report AC 74, February 1976.

[181] C. J. Walden, "Multiple scattering of classical waves in systems with liquidlike correlations: formulation as a liquid-state theory," Phys. Rev. E 52, 3115-3126 (1995).

[182] *An Engineering Data Book* ed A. J. Munday and R. A. Farrar (MacMillan Education Ltd. 1986).

[183] From suppliers: Washington Mills Electro Minerals Ltd., Mosely Road, Trafford Park, Manchester M17 1NR.

[184] D. C. Ginnings and R. J. Corruccini, "Enthalpy, specific heat and entropy of aluminum oxide from 0°C to 900°C," J. Research Nat. Bur. Standards 38, 593-600 (1947).

Appendix 1
Physical properties

Alumina dust in air suspension

The physical properties of air at 20°C and 10^5 Pa are [182]

property	value	units
density	1.19	kgm^{-3}
specific heat at constant pressure	1005	$Jkg^{-1}K^{-1}$
ratio of specific heats	1.4	1
dynamic viscosity	1.82×10^{-5}	Nsm^{-2}
thermal conductivity	0.026	$Wm^{-1}K^{-1}$
coefficient of thermal (volume) expansion	1/273.15	K^{-1}

The speed of sound in dry air at 20°C is from Pierce [41] equation (1-9.4) $343\ m\ s^{-1}$.

The physical properties of alumina at room temperature and pressure are

property	value	units	reference
density	3.8×10^3	kgm^{-3}	[183]

specific heat	760	$Jkg^{-1}K^{-1}$	[184]
thermal conductivity	19.5	$Wm^{-1}K^{-1}$	[183]

Sunflower oil in water emulsion

The following data are taken from McClements and Povey [71]. The properties are all at 293.1°K. The water is actually a solution of Tween 20 in water. The density and sound speed of this solution were measured and the other properties were assumed to be the same as for distilled water.

property	water/Tween 20	sunflower oil	units
speed of sound	1488.9	1469.9	$m\ s^{-1}$
density	1000.9	920.6	kgm^{-3}
dynamic viscosity	0.001	0.054	Nsm^{-2}
specific heat at constant pressure	4182	*1980*	$Jkg^{-1}K^{-1}$
thermal conductivity	0.591	0.170	$Wm^{-1}K^{-1}$
coefficient of thermal (volume) expansion	2.1×10^{-4}	7.1×10^{-4}	K^{-1}

Hexadecane in water emulsion

The following data are taken from McClements [29]. The properties are all at 293.15°K. The water is actually a solution of Tween 20 in water. The density and sound speed of this solution were measured and the other properties were assumed to be the same as for distilled water.

property	water/Tween 20	hexadecane	units
speed of sound	1485.7	1357.5	$m\ s^{-1}$
density	999.6	773.0	kgm^{-3}
dynamic viscosity	0.001	0.0034	Nsm^{-2}

specific heat at constant pressure	4183	2201	$Jkg^{-1}K^{-1}$
thermal conductivity	0.59	0.14	$Wm^{-1}K^{-1}$
coefficient of thermal (volume) expansion	2.1×10^{-4}	9.4×10^{-4}	K^{-1}

Aqueous suspension of polystyrene particles

The following data are taken from Allegra and Hawley [49]. The properties are all at 293.15°K. The dynamic viscosity of the water is 1.005×10^{-3} Nsm^{-2}. The shear rigidity Lame constant of the polystyrene μ_{es} is 1.27×10^{9} Nm^{-2}. The Lame constant λ_{es} can be obtained from the sound speed because

$$c^2=\frac{\lambda_e+2\mu_e}{\rho}.$$

The bulk modulus (or κ^{-1}) is then

$$\lambda_e+\tfrac{2}{3}\mu_e.$$

The coefficients of thermal volume expansion were obtained from Table I in reference [49].

property	water	polystyrene	units
speed of sound	1482.7	2320	$m\ s^{-1}$
density	996.4	1055	kgm^{-3}
specific heat at constant pressure	4181	1194	$Jkg^{-1}K^{-1}$
thermal conductivity	0.587	0.115	$Wm^{-1}K^{-1}$
coefficient of thermal (volume) expansion	2.0×10^{-4}	1.9×10^{-4}	K^{-1}

Kaolinite in water suspension

The physical properties used by Hovem [132] are

property	value	units
density water	1.00×10^{3}	kgm^{-3}
density kaolinite	2.65×10^{3}	kgm^{-3}

bulk modulus water	2.15×10^{9}	Nm^{-2}
bulk modulus kaolinite	3.6×10^{10}	Nm^{-2}
dynamic viscosity water	10^{-3}	Nsm^{-2}

These values were also used by Urick [104] [105] and Hampton [131], except the density of kaolinite used by Hampton was 2.71×10^{3} kgm^{-3} and the bulk modulus of kaolinite used by Urick was 4.37×10^{10} Nm^{-2}.

Appendix 2
Mathematica and Mathcad listings

mecred.mcd
Mecredy and Hamilton coupled phase theory

Variables

$\rho f := 1 \quad \rho s := 1 \quad S := 1 \quad K := 1 \quad \phi := 1 \quad Fh := 1 \quad \gamma := 1 \quad R := 1 \quad T := 1$

Matrix

$$m := \begin{bmatrix} \rho f \cdot S & -(\rho s + \rho f \cdot S) & K & 0 \\ -\rho f \cdot (1 - \phi + \phi \cdot S) & \phi \cdot \rho f \cdot S & K \cdot (1 - \phi) & 0 \\ 0 & 0 & 1 - \gamma & \rho f \cdot R \cdot (\gamma + Fh) \\ (1 - \phi) \cdot R \cdot T \cdot K \cdot \rho f & \phi \cdot R \cdot T \cdot K \cdot \rho f & -(1 - \phi) & (1 - \phi) \cdot R \cdot \rho f \end{bmatrix}$$

Determinant

$$m := -\rho s \cdot \rho f^2 \cdot R - \rho f^3 \cdot S \cdot R + 2 \cdot \phi \cdot \rho f^3 \cdot S \cdot R \cdot Fh - \phi^2 \cdot \rho f^3 \cdot S \cdot R \cdot Fh - \phi^2 \cdot R^2 \cdot T \cdot K^2 \cdot \rho f$$

Factor

$$m := \rho f^2 \cdot R \cdot (\phi^2 \cdot S \cdot \rho s - \phi \cdot S \cdot \rho s - \rho f \cdot \phi^2 \cdot S - \rho f \cdot S - \rho s + 2 \cdot \phi \cdot \rho f \cdot S - 2 \cdot R \cdot T \cdot K^2 \cdot \rho$$

Pick out factor

$$(\phi^2 \cdot S \cdot \rho s - \phi \cdot S \cdot \rho s - \rho f \cdot \phi^2 \cdot S - \rho f \cdot S - \rho s + 2 \cdot \phi \cdot \rho f \cdot S - 2 \cdot R \cdot T \cdot K^2 \cdot \rho s \cdot \phi \cdot \gamma + R$$

Collect on K

$$(R \cdot T \cdot \rho s \cdot \gamma + R \cdot T \cdot \rho s \cdot Fh + R \cdot T \cdot \rho s \cdot \phi^2 \cdot \gamma - 2 \cdot R \cdot T \cdot \rho s \cdot \phi \cdot \gamma - 2 \cdot R \cdot T \cdot \rho s \cdot \phi \cdot Fh - \rho$$

Factor K coefficient

$$R \cdot T \cdot (\gamma + Fh) \cdot (\rho s + \rho s \cdot \phi^2 + \phi \cdot \rho f + \rho f \cdot S - \rho f \cdot \phi^2 - 2 \cdot \rho s \cdot \phi) \cdot K^2 + (\phi^2 \cdot S \cdot \rho s -$$

Factor non-K terms

$$R \cdot T \cdot (\gamma + Fh) \cdot (\rho s + \rho s \cdot \phi^2 + \phi \cdot \rho f + \rho f \cdot S - \rho f \cdot \phi^2 - 2 \cdot \rho s \cdot \phi) \cdot K^2 + (1 + Fh) \cdot (-$$

Simplify K coefficient

$$R \cdot T \cdot (\gamma + Fh) \cdot ((-1 + \phi)^2 \cdot \rho s + (\phi + S - \phi^2) \cdot \rho f) \cdot K^2 + (1 + Fh) \cdot (-1 + \phi) \cdot (-\rho$$

Simplify non-K terms

$$R \cdot T \cdot (\gamma + Fh) \cdot ((-1 + \phi)^2 \cdot \rho s + (\phi + S - \phi^2) \cdot \rho f) \cdot K^2 + (1 + Fh) \cdot (-1 + \phi) \cdot (((

couple.ma
Coupled phase theory for emulsions

```
Clear[ph];
```

Data given

```
rs=920.6 ;al=1-ph; rf=1000.9; cps=1980;
cpf=4182; bs=7.1 10^-4; bf=2.1 10^-4; ss=1469.9;
sf=1488.9; ms=0.054; mf=10^-3 ; ts=0.17; tf=0.591;
fr=1.25 10^6; te=293.1; ra=7.4 10^-7;
```

Calculate other variables

```
ks=(rs ss^2)^-1; kf=(rf sf^2)^-1;
gs=(((ss bs)^2) te)/cps)+1;
gf=(((sf bf)^2) te)/cpf)+1;
cs=cps/gs; cf=cpf/gf; om=2 Pi fr;
dv=(((2 mf)/(rf om))^0.5)/ra;
dts=(((2 ts)/(rs cps om))^0.5)/ra;
dtf=(((2 tf)/(rf cpf om))^0.5)/ra;
sv=(1/2)+((9/4) dv)+(((9 I)/4) (dv+dv^2));
zs=(1+I)/dts;
zf=(1+I)/dtf;
shs0=Tan[zs]+(3/zs)-((3 Tan[zs])/zs^2);
shs=shs0/(Tan[zs]-zs);
shf=1/(1-I zf);
sh0=(shf-((tf/ts) shs))^-1;
(* sh0=1-I zf; *)
sh=((3 tf)/(-I ra^2 rf om)) sh0;
```

Matrix

```
m={{0,ph,0,-k*ph*rs,0,0,0,rs},
{-al,0,k*al*rf,0,0,0,0,rf},
{0,0,rf*sv,-(rs+rf*sv),0,0,k,0},
{0,0,-rf(al+ph*sv),ph*rf*sv,0,0,k*al,0},
{0,0,0,(k*rs*cs*(gs-1))/bs,rf*sh,
-(rs*cs+rf*sh),0,0},
{0,0,(k*al*rf*cf*(gf-1))/bf,0,
-rf*(al*cf+ph*sh),rf*ph*sh,0,0},
{0,1,0,0,0,rs*bs,-gs*rs*ks,0},
{1,0,0,0,rf*bf,0,-gf*rf*kf,0}};
```

Solve for K in terms of phi

```
Solve[Det[m]==0,k];
```

Find attenuation and sound speed in terms of phi

```
at=8.7*om*Im[k] /.%;
ss=1/Re[k] /.%%;
```

Evaluate attenuation and sound speed

```
ph={1 10^-6,0.05,0.1,0.15,0.2,0.25,0.3,\
0.35,0.4,0.45,0.5,.55,.6,.65,.7};
N[at] // TableForm
```

```
-0.000691172   -33.7959   -66.0276   -96.6252   -1
   499   -152.536   -177.588   -200.467   -220.927
     -238.645   -253.193   -264.001   -270.295   -
   .019   -264.719
```

```
0.000691172    33.7959    66.0276    96.6252
  125.499    152.536    177.588    200.467
  220.927    238.645    253.193    264.001
  270.295    271.019    264.719
```

couplf.ma
Coupled phase theory for emulsions

```
Clear[sv,sh,at,ss];
```

Data given

```
rs=920.6 ;ph=.1084; al=1-ph; rf=1000.9; cps=1980;
cpf=4182; bs=7.1 10^-4; bf=2.1 10^-4; ss=1469.9;
sf=1488.9; ms=0.054; mf=10^-3 ; ts=0.17; tf=0.591;
te=293.1; ra=7.4 10^-7;
```

Calculate other variables

```
ks=(rs ss^2)^-1; kf=(rf sf^2)^-1;
gs=(((ss bs)^2) te)/cps)+1;
gf=(((sf bf)^2) te)/cpf)+1;
cs=cps/gs; cf=cpf/gf; om=2 Pi fr;
```

Matrix

```
m={{0,ph,0,-k*ph*rs,0,0,0,rs},
{-al,0,k*al*rf,0,0,0,0,rf},
{0,0,rf*sv,-(rs+rf*sv),0,0,k,0},
{0,0,-rf(al+ph*sv),ph*rf*sv,0,0,k*al,0},
{0,0,0,(k*rs*cs*(gs-1))/bs,rf*sh,
-(rs*cs+rf*sh),0,0},
{0,0,(k*al*rf*cf*(gf-1))/bf,0,
-rf*(al*cf+ph*sh),rf*ph*sh,0,0},
{0,1,0,0,0,rs*bs,-gs*rs*ks,0},
{1,0,0,0,rf*bf,0,-gf*rf*kf,0}};
```

Solve for K in terms of Sv, Sh

```
Solve[Det[m]==0,k];
```

Find attenuation and sound speed in terms of Sv, Sh

```
at=(8.7*2*Pi*sf)*Im[k] /.%;
ss=1/(sf*Re[k]) /.%%;
```

Evaluate Sv and Sh

```
rrf=10^-3 {.1,.2,.3,.4,.5,.6,.7,.8,.9,1,\
1.5,2,2.5,3,3.5,4,4.5,5,6,7,8,9,10};
dv=((mf/(Pi rf))^0.5)/rrf;
dts=((ts/(Pi rs cps))^0.5)/rrf;
dtf=((tf/(Pi rf cpf))^0.5)/rrf;
sv=(1/2)+((9/4) dv)+(((9 I)/4) (dv+dv^2));
Clear[dv];
zs=(1+I)/dts;
zf=(1+I)/dtf;
Clear[dts,dtf];
shs0=Tan[zs]+(3/zs)-((3 Tan[zs])/zs^2);
shs=shs0/(Tan[zs]-zs);
Clear[zs];
shf=1/(1-I zf);
Clear[zf];
sh0=(shf-((tf/ts) shs))^-1;
Clear[shs,shf];
sh=((3 tf)/(-2 Pi I rrf^2 rf)) sh0;
Clear[sh0];
```

Evaluate attenuation and sound speed

```
N[ss] // TableForm
```

```
-0.991205    -0.99171    -0.992663    -0.993684    -0.
   452    -0.994972    -0.995342    -0.995623    -0.99
    47    -0.996031    -0.996608    -0.996915    -0.997
    07    -0.997237    -0.997332    -0.997404    -0.997
    46    -0.997505    -0.997573    -0.997622    -0.997
    59    -0.997688    -0.997711
0.991205     0.99171     0.992663     0.993684
  0.994452     0.994972     0.995342     0.995623
     0.995847     0.996031     0.996608     0.996915
     0.997107     0.997237     0.997332     0.997404
      0.99746     0.997505     0.997573     0.997622
     0.997659     0.997688     0.997711
```

porous.ma
Pore size distribution theory

```
Clear;
```

Data given

```
mu=1.82 10^(-5); rho=1.19; s=0.05; alp=0.378;
sig=13000;
tort=alp^(-0.5);
(* tort=1; *)
cp=1005; t=.026;
gam=1.4; c=343;
```

Calculate other variables

```
bm=rho*(c^2);
npr=((mu*cp)/t)^(0.5);
mean=((3*mu*tort)/(alp*sig))^(0.5);
mean=mean*Exp[-((s*Log[2])^2)];
mean=(-Log[mean])/Log[2];
low=mean-(3*s); high=mean+(3*s);
fl={}; flh={}; oml={};
f0=Exp[(-((p-mean)^2))/(2*(s^2))];
f0=f0/(s*((2*Pi)^(0.5)));
```

Calculate size dependent functions fl and flh

```
Do[

om=2*Pi*(10^indic);
oml=Append[oml,om];
l=((-I*om*rho)/mu)^(0.5);
l=(2^(-p))*l;
lh=l*npr;
f=(2^p)*f0*Tanh[l];
fh=(2^p)*f0*Tanh[lh];
n=NIntegrate[f,{p,low,high}];
nh=NIntegrate[fh,{p,low,high}];
f=f0*(1-((Tanh[l])/l));
fh=f0*(1-((Tanh[lh])/lh));
d=NIntegrate[f,{p,low,high}];
dh=NIntegrate[fh,{p,low,high}];
f=(((-I*mu*om*rho)^(0.5))*n*tort)/((alp*sig)*d);
fl=Append[fl,f];
fh=((-I*mu*om*rho)^(0.5))*nh*tort;
fh=fh/((alp*sig)*dh);
flh=Append[flh,fh];

,{indic,2,4,.05}];
```

Calculate acoustical properties

```
cd=(I*sig)*(fl/oml);
cd=(cd)+((rho*tort)/alp);
```

```
cd=cd*alp;
ch=(I*sig)*(flh/oml);
ch=ch+((rho*tort)/alp);
ch=ch*alp;
bulk=(gam-(((gam-1)*rho*tort)/ch))^(-1);
bulk=bulk*bm;
k=(oml)*((cd/bulk)^(0.5));
imp=((bulk*cd)^(0.5))/(alp*rho*c);
imp=(imp)*Coth[-I*k*0.05];
imp=(imp-1)/(imp+1);
```

Output reflection coefficient data

```
N[(180/Pi)*Arg[imp]] // TableForm
(* N[Abs[imp]] // TableForm *)
```

5.49578

6.15097

6.88073

7.69257

8.59471

9.59627

10.7076

11.9412

13.3121

14.8404

16.5525

18.4848

20.6876

23.2308

26.2113

29.763

34.0693

39.3718

45.9484

53.9393